Exploitation de séries temporelles d'images multi-sources pour la cartographie des surfaces en eau

Filsa Bioresita

Université de Strasbourg

UNIVERSITÉ DE STRASBOURG

ÉCOLE DOCTORALE DES SCIENCES DE LA TERRE ET DE L'ENVIRONNEMENT - ED413

Laboratoire Image, Ville, Environnement UMR 7362 CNRS

THÈSE présentée par :

Filsa BIORESITA

soutenue le : **07 mars 2019**

pour obtenir le grade de : **Docteur de l'université de Strasbourg**

Discipline/ Spécialité : Géographie / Géomatique

EXPLOITATION DE SERIES TEMPORELLES D'IMAGES MULTI-SOURCES POUR LA CARTOGRAPHIE DES SURFACES EN EAU

Use of Multi-Source Image Time Series for Surface Water Mapping

THÈSE dirigée par :

Mme. PUISSANT Anne	Professeure, université de Strasbourg

RAPPORTEURS :

M. CORGNE Samuel	Professeur, université Rennes 2
M. ROBIN Marc	Professeur, université de Nantes

AUTRES MEMBRES DU JURY :

Mme. DE JONG Carmen	Professeure, université de Strasbourg

Université de Strasbourg

UNIVERSITY OF STRASBOURG

ÉCOLE DOCTORALE DES SCIENCES DE LA TERRE
ET DE L'ENVIRONNEMENT - ED413

Laboratoire Image, Ville, Environnement UMR 7362 CNRS

PhD Thesis presented by :

Filsa BIORESITA

Public defence on **March 7th , 2019**

For obtaining the degree : **Doctor of the University of Strasbourg**

Discipline/ Speciality : Geography / Geomatics

USE OF MULTI-SOURCE IMAGE TIME SERIES FOR SURFACE WATER MAPPING

THESIS directed by :

Mrs. Anne PUISSANT	Professor, University of Strasbourg

REVIEWER :

Mr. Samuel CORGNE	Professor, University of Rennes 2
Mr. Marc ROBIN	Professor, University of Nantes

OTHER JURY MEMBERS :

Mrs. Carmen DE JONG	Professor, University of Strasbourg

Abstract

Surface waters are important resources for the biosphere and the anthroposphere. Surface waters preserve diverse habitat, support biodiversity and provide ecosystem service by controlling nutrient cycles and global carbon. Surface waters are essential for human's everyday life, such as for irrigation, drinking-water and/or the production of energy (power plants, hydro-electricity). Further, surface waters through flooding can pose hazards to human, settlements and infrastructures. Monitoring the dynamic changes of surface waters is crucial for decision making process and policy.

Remote sensing data can provide information on surface waters. Nowadays, satellite remote sensing has gone through a revolution with the launch of the Sentinel-1 SAR data and Sentinel-2 optical data with high revisit time at medium to high spatial resolution. Those data can provide time series and multi-source data which are essential in providing more information to upgrade ability in observing surface water. Analyzing such massive datasets is challenging in terms of knowledge extraction and processing as nearly fully automated processing chains are needed to enable systematic detection of water surfaces.

In this context, the objectives of the work are to propose new (e.g. fully automated) approaches for surface water detection and flood extents detection by exploring the single and combined used of Sentinel-1 and Sentinel-2 data.

We presents the Water-S1 method developed for Sentinel-1 image processing. The method is tested and validated on several flood events that occurred in Central Ireland, Northern England and Northwest Italy. For all test cases, the results show that surface water are estimated with an average F-measure about 0.8. However, omission of permanent river beds are observed for the three experiments. Thus, further improvements of the processing chain could include the analysis of SAR time-series to amplify the signal of permanent riverbeds through spatio-temporal averaging.

We propose a methodology for surface waters detection by combining Sentinel-1 and Sentinel-2 data time series based on image fusion approach in decision-level with a Bayesian sum for the operator. The method is experimented for surface water over Ireland. The proposed methodology allows reducing the noise and increasing the accuracy of the detection of the permanent surface water. Moreover, the analysis of image time series allows a better monitoring of temporary surface water.

Another methods are tested, such as: (i) the use of SAR polarimetry for surface water classification and (ii) feature-level image fusion for comparison and assessment of the best fusion approach. Validation of proposed methods on different thematic context is presented through two different experiments of massive processing.

Although the use of remote sensing data as operational source of information for surface water and flood observations still requires development, the methods and tests proposed in this PhD thesis are promising.

Résumé

Les eaux de surface sont des ressources importantes pour la biosphère et l'anthroposphère. Elles favorisent la préservation des habitats, le développement de la biodiversité et le maintien des services écosystémiques en contrôlant le cycle des nutriments et le carbone à l'échelle mondiale. Elles sont essentielles à la vie quotidienne de l'homme, notamment pour l'irrigation, la consommation d'eau potable, la production hydro-électrique, etc. Par ailleurs, lors des inondations, elles peuvent présenter des dangers pour l'homme, les habitations et les infrastructures. La surveillance des changements dynamiques des eaux de surface a donc un rôle primordial pour guider les choix des gestionnaires dans le processus d'aide à la décision.

L'imagerie satellitaire constitue une source de données adaptée permettant de fournir des informations sur les eaux de surface. De nos jours, la télédétection satellitaire a connu une révolution avec le lancement des satellites Sentinel-1 (Radar) et Sentinel-2 (Optique) qui disposent d'une haute fréquence de revisite et d'une résolution spatiale moyenne à élevée. Ces données peuvent fournir des séries temporelles essentielles pour apporter davantage d'informations afin d'améliorer la capacité d'observation des eaux de surface. L'exploitation de telles données massives et multi-sources pose des défis en termes d'extraction de connaissances et de processus de traitement d'images car les chaines de traitement doivent être le plus automatiques possibles.

Dans ce contexte, l'objectif de ce travail de thèse est de proposer de nouvelles approches permettant de cartographier l'extension spatiales des eaux de surface et des inondations, en explorant l'utilisation unique et combinée des données Sentinel-1 et Sentinel-2.

Nous présentons une méthode Water-S1 qui est développée pour le traitement automatique d'image Sentinel-1. La méthode est testée et validée pour trois zones d'étude affectées par des inondations survenues dans la partie centrale de l'Irlande, dans le nord de l'Angleterre et dans le nord-ouest de l'Italie. Pour tous les cas d'étude, les résultats montrent une bonne estimation des eaux de surface avec une moyenne de F-measure d'environ 0,8. Cependant, des erreurs d'omissions sur les lits de rivière permanents sont observées quel que soit le site d'étude. Ainsi, de nouvelles améliorations de la chaîne de traitement pourraient inclure l'analyse de séries temporelles d'images Sentinel-1 afin d'améliorer la détection des eaux de surface permanentes localisées dans les lits de rivières.

Nous proposons une méthodologie pour la détection des eaux de surface en combinant les séries temporelles de données Sentinel-1 et Sentinel-2 basées sur l'approche de fusion d'images au « niveau décision » fondée sur la théorie bayésienne. La méthode est expérimentée pour les eaux de surfaces en Irlande. Les résultats indiquent une réduction du bruit et une augmentation de la précision de la détection des

eaux de surfaces permanentes. De plus, l'analyse des séries temporelles d'images permet un meilleur suivi des eaux de surface temporaires.

Les autres méthodes de détection sont ensuite testées, telles que: (i) l'utilisation de la polarimétrie RSO pour la classification des eaux de surface et (ii) la fusion d'images au « niveau des attributs » pour la comparaison et l'évaluation de la meilleure approche de fusion. La validation des méthodes proposées sur différents contextes thématiques est ensuite présentée à travers deux expériences différentes de traitement massif.

Bien que l'utilisation de données de télédétection comme outils opérationnels pour l'observation des surfaces en eau (permanentes et temporaires) reste à finaliser, les résultats proposés dans cette thèse sont très prometteurs.

Acknowledgements

Alhamdulillah, all praises to Allah for the strengths and His blessing in completing this PhD thesis.

I would like to offer great appreciation to my supervisor Mme. Anne Puissant for her supervision and constant support. Her invaluable help of the useful comments, remarks, suggestions throughout the experimental and thesis works have contributed to the success of this research. Furthermore, I would like to thank M. André Stumpf for valuable guidance, help me in programming and the support on the way. I am also very grateful to M. Jean-Philippe Malet for writing assistance and suggestions.

To defend this thesis I have invited M. Marc Robin, M. Samuel Corgne, Mme. Carmen De Jong, M. Bernard Allenbach, and M. Muhammad Taufik and I am indebted to them for kindly accepting this invitation and dedicating time to review the manuscript.

I thank David Eschbach for help me filling the gaps in my knowledge on hydrography aspect and also help me write in french. I thank Nicolas Debonnaire and Benoit Ribon for help me learn programming language. I thank Theodorus Arnadi Murtiyoso for scientific discussion, language editing, and proofreading. I thank Anita Thea Saraswati for proofreading.

I was lucky to share the last four years with many amicable colleagues. I thank Aurelia, Nishi, Cecile, Corina, Fang-fang, Jana, Wachim, Caline, Pierre, Johan, and Valentin for all the laughters. I thank all students in PPI Alsace who become my family in France.

I would like to express my gratitude for the Indonesia Endowment Fund for Education (LPDP), Ministry of Finance, Republic of Indonesia and the French funded program ANR TIMES who support my PhD research. I would like to express my very profound gratitude to my alma mater, Geomatics Engineering, Sepuluh Nopember Institute of Technology, and all colleagues there for all the support.

My deepest gratitude goes to all my family who always encouraged me to reach my dream. This thesis is dedicated to my mother who always trust me that I can do many things and never forget to pray for me wherever I am. My father who always support

me from behind and encouraged me to explore more. My sister who always listen to my story, my brother who always make me smile, and my nephew who always makes my day. Last but not least, for my husband Faisal, thank you for your support and love, you always believe that I am strong enough to do many things. This accomplishment would not have been possible without them. I will be grateful forever for your love. Thank you.

Contents

List of figures

List of tables

Chapter 1

Introduction, research questions and objectives

Contents

1.1 Importance of surface water

About 71% of the Earth's surface is covered by water. Only 3% of water is classified as fresh water and only 0.3% of this category is labelled as surface water distributed into lakes, rivers, wetland areas, and the other surface water table (Perlman, 1998). It corresponds to **surface water on inland bodies** (Figure 1. 1). Despite this repartition, surface water is important resource for the biosphere and the anthroposphere. It remains the most abundant natural resource and the major driving force on our planet which supports numerous ecosystems, commercial and cultural services. It becomes a critical parameter for climate changes analysis (GCOS, 2011 in Pekel et al., 2014), diverse habitat preservation and biodiversity support (Brönmark and Hansson, 2002; Duker and Bore, 2001; Palmer et al., 2015). On a global scale, surface water is significant component of nutrient cycles and global carbon (Bastviken et al., 2011; Tranvik et al., 2009 in Palmer et al., 2015). In the human's daily life, surface water is used for irrigation, drinking-water, power plant, recreation, fisheries, ecotourism, transport, religious uses, etc.

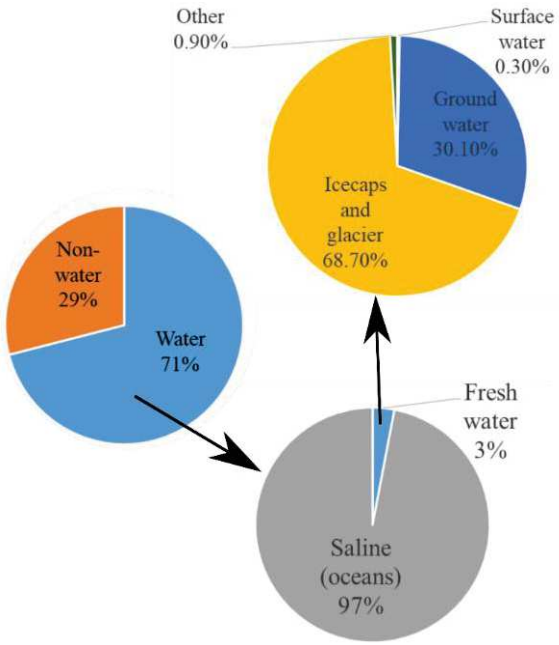

Figure 1. 1. Earth's water distribution (modified from Perlman, 1998).

The pressure on surface water will continue to increase in the coming years because of increased frequency of drought, urbanization, urban population growth, deforestation, increased use of fertilizers and pesticides, and spread of invasive species. It is expected

that the quality of surface water will deteriorate with continued warming due to global climate change.

Surface water on inland bodies can classically categorizes in two thematic classes: (1) permanent surface water and (2) temporary surface water.

Permanent surface water is defined as surface water areas which retaining most of their volumes over the year and that do not dry up. Its variations are mostly dependent on the hydro-meteorological cycle with rainfall, evaporation and possible overtopping of streams. Permanent surface water is usually in the form of rivers or lakes. River is identified as water courses, which may be a waterway (Wetzel, 2001), whereas lake is non-flowing, enclosed water bodies filled with water within a lake basin not directly linked with the sea (Anderson et al., 1976). At times when there is little or no rain, the water level of permanent surface water is maintained by groundwater contributions. The extent and distribution of the permanent surface water are yet poorly and unevenly known at the global scale, since their size varies from small (i.e., ponds) to very large (i.e., Great Lakes) often creating inconsistencies in detection and inventory over broad geographic scale (Ogashawara et al., 2017). Moreover, mapping permanent surface water is also valuable in the context of severe drought response and for water resources management. They can also serve for the validation of hydraulic models (Matgen et al., 2010; Pappenberger et al., 2007; Schumann et al., 2009).

Temporary surface water is part of surface water areas which experiences a recurrent dry phase of varying duration, such as small ponds, puddles and wetlands, or correspond to surfaces frequently affected by **flooding**. Floods can cover various events based on their size, duration, and causes. Three types of floods can be generally distinguished based on these criteria (Figure 1. 2).

Figure 1. 2. Examples of floods: (a) Plain floods; (b) Flash floods; (c) Coastal floods.

- *Plain floods* take place mainly in a plain area (Figure 1. 2a). They are caused by rains occur in long time or melting snow and ice, that also depend on soil saturation. Usually, when the dikes along rivers unable to resist flood discharge, it leads to wide areas flooding (Menne and Murray, 2013). This type of flood can affect wide areas for long-lasting period.
- *Flash floods* are caused by heavy or intense rainfall (Figure 1. 2b). This type of floods can also be referred to as local and sudden floods which affect small area. Normally they occur in small catchments in mountainous areas due to intensive precipitation, thin soils, and high run off velocities (Menne and Murray, 2013). The duration of flash floods is short but causes great damage. In some areas next to a volcano, flash floods can be caused by a mixture of lahar (cold lava) and high rainfall.
- *Coastal floods* are one type of floods caused by sea level rise, high tides, tsunami and land subsidence (Figure 1. 2c). It is identified as coastal areas inundation that covers a larger area than the one caused by normal tides. This type of flood last for long time period and can affect wide areas, however the extent depends on topography, erosion conditions and the barriers on the coast (natural or man-made) (Cwik, 2017).

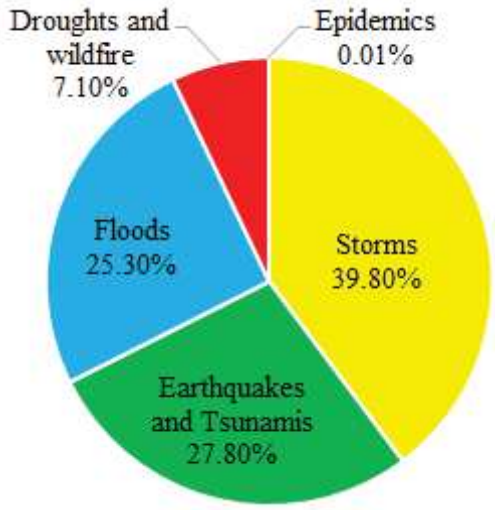

Figure 1. 3. Percentage of damages caused by each type of natural disasters (modified from Duggar et al., 2016).

Surface waters through flooding can pose hazards to human, settlements and infrastructures (Feyisa et al., 2014). Floods become a representation of the most

common type in natural disaster which have led to losses of lives and property, as well as internal displacement and lack of resources (Schlaffer et al., 2012). Floods can affect residential areas, buildings, or farm areas, also contaminate waters and lead to diseases. From 1980 to 2015, Duggar et al. (2016) highlights that 25.3% of global damage caused by natural hazards are due to flooding (Figure 1. 3). Floods can be considered as the most costly type of hazard in terms of property damage and fatalities (Martinis, 2010).

Since it is impossible to avoid flood risks or prevent their occurrence, flood disaster management is important to reduce their effects. Flood mapping to identify sites in high hazard zones is one of the powerful tools for this purpose (Voigt et al., 2007). Mapping floods will be beneficial to urban and infrastructure planners, risk managers and disaster response, insurance and emergency services during extreme and intense rainfall events.

For the both study cases (permanent and temporary surface water), Earth Observation (EO) data from optical or Synthetic Aperture Radar (SAR) sensors offers a relevant alternative for mapping and monitoring surface water resources.

1.2 Remote sensing of surface water

The information of surface water can be retrieved from remote sensing data. The main advantage of remote sensing is its capability to perform frequent large-scale synoptic. The data provides first order information which are dynamic, real-time and low-cost compared with in-situ observation data (Du et al., 2016). Remote sensing observes Earth's surface objects by measurement of electromagnetic (EM) energy (Janssen and Huurneman, 2001). The general concept of remote sensing explained that EM radiation from Earth's surface objects are measured and translated to information about those objects (De Jong and Van der Meer, 2004).

Based on its system, remote sensing can be divided into two types (Figure 1. 4):

- **Passive remote sensing** uses the sun energy as its source and detects reflected energy from Earth's surface objects. This system also detects emitted energy from the Earth's surface itself.

- **Active remote sensing** produces EM radiation itself and transmitted it to Earth's objects. The system captures the backscattering energy from those objects (Janssen and Huurneman, 2001).

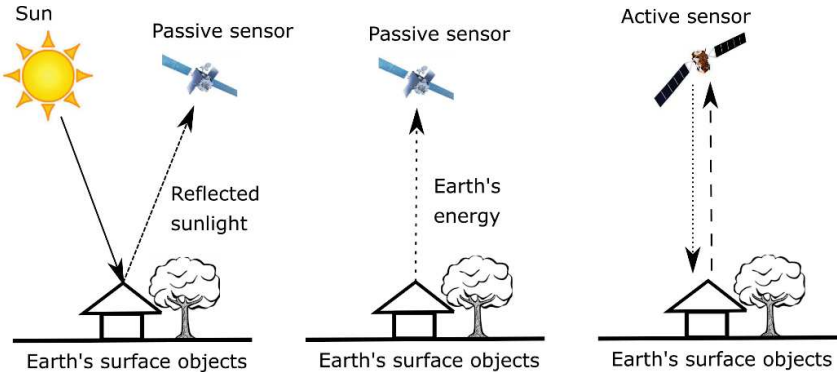

Figure 1. 4. Remote sensing system (active and passive) (modified from Janssen and Huurneman, 2001).

1.2.1 Optical remote sensing characteristics (passive)

Passive or optical remote sensing relies on sunlight reflection, can only works during daylight. Optical remote sensing needs to handle atmospheric conditions, as an effect of various illumination conditions of the sun (Janssen and Huurneman, 2001). In the electromagnetic spectrum, optical remote sensing domain extends from the visible range to the infrared range. Visible has 400 – 700 nm wavelengths while infrared has a wavelength around 700 nm – 1 mm. Visible region of spectrum take only small portion of EM spectrum. Infrared has longer wavelength compared to visible spectrum. It can be used for many applications such as calculate surface temperature (3 – 14 μm for Thermal Infrared) or vegetation condition. In the Thermal Infrared (TIR) remote sensing, sensor captures directly emitted energy from the earth, thus it can operate day or night (Janssen and Huurneman, 2001).

Table 1. 1. Examples of several types of sensors in optical remote sensing.

Type	Examples			
	Sensors	Spatial coverage	Temporal resolution	Spatial resolution
Panchromatic	Landsat	~ 185 km	16 days	15 m
	SPOT	60 to 80 km	1 to 5 days	1.5 to 10 m
Multispectral	Landsat	~ 185 km	16 days	30 to 120 m
	SPOT	60 to 80 km	1 to 5 days	6 to 20 m
	Sentinel-2	290 km	2 to 10 days	10 to 60 m
Super-spectral	MODIS	2330 km	1 to 2 days	250 m – 1 km
	WorldView-3	13.1 km	<1 to 5 days	1.24 – 30 m
Hyperspectral	AVIRIS	12 km	1 year	20 m
	EO-1 Hyperion	7.75 km	16 days	30 m

There are several types of sensors in optical remote sensing (Table 1. 1):

(1) *Panchromatic* imagery consists of a single spectral band or broad band (Schowengerdt, 2007). Panchromatic imaging combines the information from the visible bands. Instead of partitioning information into different spectra, panchromatic is established by using the total energy in the visible spectrum. It provides a single intensity value per pixel and is visualized in a greyscale image. Panchromatic image usually has higher spatial resolution than multispectral images. Most of satellites such as Landsat, Digital Globe's range of satellites and SPOT constellation produce panchromatic image in addition to multispectral image.

(2) *Multispectral* imagery consists of multiple bands or multiple numbers of wave bands, typically 3 to 10 spectral bands. Most optical remote sensing systems acquire images in this mode (e.g., Landsat, SPOT). Multispectral mode is often more valuable than panchromatic because it supplies rich spectral information (Schowengerdt, 2007).

(3) *Super-spectral* imagery consists of more than ten spectral bands, with bandwiths narrower than multispectral (e.g. Worldview-3 with 28 bands and MODIS with 36 bands). Short-Wave Infrared bands (SWIR) add spectral coverage to the invisible range with the advantage to penetrate haze, fog, smog, dust and smoke.

(4) *Hyperspectral* imagery collects information as a series of narrow and contiguous wavelength bands at 10 to 20 nm intervals. Hyperspectral can contain as many as 200 (or more) spectral bands (e.g., AVIRIS, EO-1 Hyperion) (Lillesand et al., 2015). The numerous bands of hyperspectral provide more sensitive to subtle variations in reflected energy, thus have a greater potential to detect differences among land and water features.

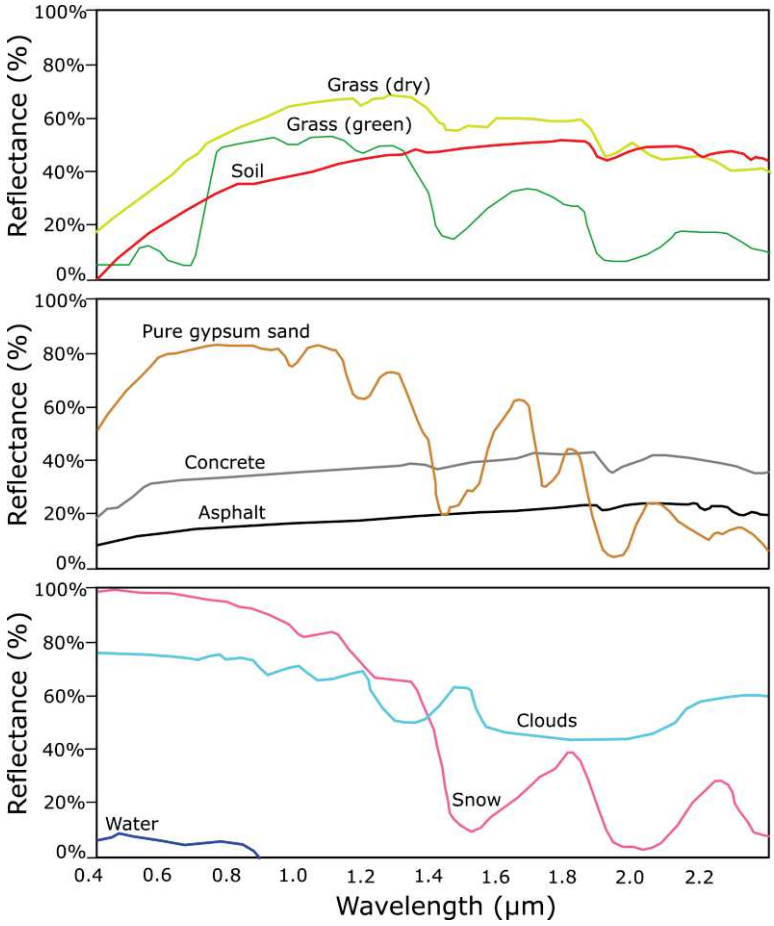

Figure 1. 5. Spectral reflectance for different types of land cover (modified from Lillesand et al., 2015).

Figure 1. 5 shows average spectral reflectance for various types of land cover. Each land cover type reflects different energy which result different unique curve from each

other. The spectral reflectance of water is small due to energy absorption by water bodies. Thus in the passive remote sensing image, surface water will appear dark or with low pixel values. However, surface water reflectance also depends on turbidity of water, which is caused by organic or inorganic materials in the waters. Water with suspended sediments normally will have higher reflectance than water without suspended sediments (Lillesand et al., 2015).

Optical multispectral imagery is then frequently used for surface water mapping (Verpoorter et al., 2012). It provides good delineation of surface water areas if clouds, trees and floating vegetations do not obscure the water surface. The most commonly used spectral bands for vegetation and water mapping are green, red and near-infrared. Near-infrared can strongly absorbed by water, but reflected by land. Thus they are mainly effective for mapping water area (Klemas, 2015).

During a flood, waters will inundate vegetation, urban areas, etc. Their reflectance will be different from surface water area. In urban areas, artificial surfaces may have very low reflectance mistakenly labelled as flooded areas. At the opposite, flooded areas can have very high reflectance due to, for example, specular reflections of surrounding buildings or a shallow water layer over a bright pavement. Urban area is recognized as a highly complicated type of land cover in the remote sensing applications context including floods monitoring (Refice et al., 2017).

Some previous researches provide successful use of optical data in surface water mapping. Quite a few studies use MODIS for waters mapping (Lee et al., 2015; Ottinger et al., 2013). This imagery has coarse spatial resolution (250m, 500m and 1000m) and 36 spectral bands. This image is free for all users and available via a simple self-registration at Earth Explorer USGS (United States Geological Survey) (USGS, n.d.) Landsat image (Figure 1. 13a), with medium spatial resolution (30 meters) and 11 bands (Figure 1. 6), has been used on many studies related to surface water mapping (Brakenridge and Anderson, 2006; Feyisa et al., 2014; Frazier and Page, 2000; Jiang et al., 2014; Ogilvie et al., 2018). SPOT is another optical sensor providing also useful imagery in surface water delineation (e.g., Blasco et al., 1992; Davranche et al., 2010; Fisher and Danaher, 2013; Musa et al., 2015), with a higher spatial resolution (10 to 20 m) than Landsat imagery and 5 bands (Figure 1. 6). Landsat imagery is also freely available since the beginning of the mission (1976) at Earth Explorer USGS. For SPOT

imagery, even if the archive of Spot World Heritage (SWH) become available for the community (1986-2010) through the data and services THEIA infrastructure, these images are not completely available with a user-friendly access.

Optical imagery with very high spatial resolution (metric and sub-metric) can be used to detect small-sized water bodies (Du et al., 2016; C. Huang et al., 2018). However, the presence of shadows in the image can affect water detection and these images are often unsuitable for mapping large water bodies due to their small scene coverage. In addition, the revisit frequency for most of these sensors, and the availability of most of their images, is also largely limited due to their access are not freely distributed for all users (Huang et al., 2018). Despite these limitations, there are quite many applications based on IKONOS, Pléiades or WorldView-2 imagery (Figure 1. 6) to detect surface water (Huang et al., 2015; Liew et al., 2011; Marcus and Fonstad, 2008; Sidle et al., 2007; Yesou et al., 2015)

As a continuation of the Global Monitoring for Environment and Security (GMES) program, the European Commission (EC) and the European Space Agency (ESA) initiate Copernicus program. This Earth observation program provides freely distributed data to all users. As part of this program, the Sentinel constellation has been launched. The optical component is composed of two satellites: Sentinel 2A and 2B. These data products are available in the Open Access Hub (https://scihub.copernicus.eu/) (ESA, 2014). Sentinel-2 (A and B) provides high spatial resolution and high temporal resolution (10 days at the equator with one satellite, and 5 days with 2 satellites under cloud-free conditions which results in 2-3 days at mid-latitudes).

Sentinel-2 carries an optical instrument with 13 spectral bands (Figure 1. 6). The four bands at 10 meter resolution and six bands at 20 meter resolution satisfy requirements for enhanced land-cover classification and for the retrieval of geophysical parameters. These six bands include three bands in the ‘red edge', provide key information on the vegetation state. Bands at 60 meter are dedicated mainly to atmospheric corrections and cirrus-cloud screening.

Optical data are very sensitive to cloud cover. In some European Countries, the cloud cover percentage average is varying from 30 to 70% (Direction de la Climatologie, 2009). The acquisition of exploitable optical time series data is almost impossible. In

winter and spring period, cloud cover appears more often, when they are precisely the crucial period for monitoring hydrological dynamics. In conclusion, the arrival of optical imagery with a high temporal resolution would be benefit but active remote sensing remains actually, the best acquisition mode due to its independence to the atmospheric condition.

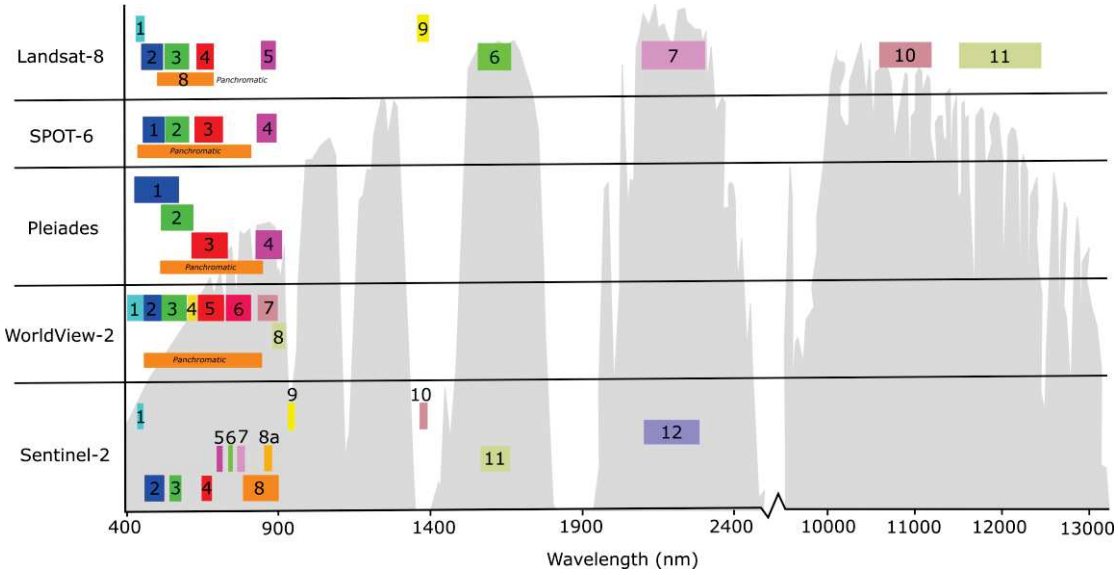

Figure 1. 6. Bands and their wavelength from several optical remote sensing data.

1.2.2 Active remote sensing characteristics

There are some types of instrument in active remote sensing system where the most useful for surface water are LIDAR and RADAR (EOSDIS, 2018). LIDAR (Light Detection and Ranging) instrument measures distance to a target by illuminating the target with pulsed laser light and measuring the reflected pulses with a sensor. Differences in laser return times and wavelengths can then be used to make digital 3-D representations of the target. LIDAR is often used for surface water mapping (e.g., Morsy et al., 2018; Schlaffer et al., 2015) but its use implies significant cost, especially for mapping large area (Cazals, 2017).

Radar is particularly adapted to the mapping and monitoring of surface water for several reasons. First, radar can supply their own illumination, thus it can capture image of Earth's surface in day or night. Second, radar can penetrate cloud cover, light rain, or

fog. It can overcome optical data limitation related to cloud cover. Third, radar is sensitive to the presence of smooth open surface water. Radar data usually have a high contrast of backscatter energy between smooth open water bodies and dry land areas (Schumann, 2017).

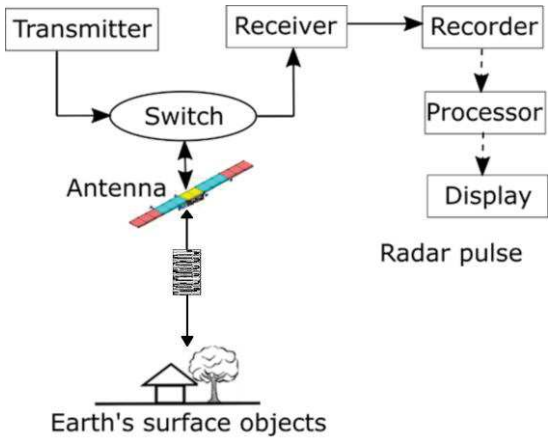

Figure 1. 7. Radar system illustrated in block diagram (modified from Chan and Koo, 2008).

Radar works in microwaves range of EM spectrum with radio frequency. Generally, radar system consists of transmitter to generate a high power of electromagnetic wave, switch to direct signal to antenna and return echo to receiver, antenna to transmit EM pulse towards object of study and collects returned echoes, receiver to convert returned signal to digital number, then recorder to store data values (Figure 1. 7) (Chan and Koo, 2008).

One type of radar for water mapping is altimeter. This instrument measures the distance between the Earth and the satellite and is generally used to estimate the topography of oceans's surface. This instrument is also used to measure the water level elevation of continental waters such as large lakes or rivers (Calmant et al., 2008).

SAR (Synthetic Aperture Radar) is also one type of Radar used very often for surface water mapping. Aperture, one of the words from SAR abbreviation, means the antenna collects the reflected energy and form an image. SAR principle is to take advantage of Doppler history from radar echoes generated by the forward motion of the satellite to synthesize a large antenna. Thus, it is called "synthetic aperture". This allows high azimuth resolution in the resulting image despite a physically small antenna (Sarmap, 2009).

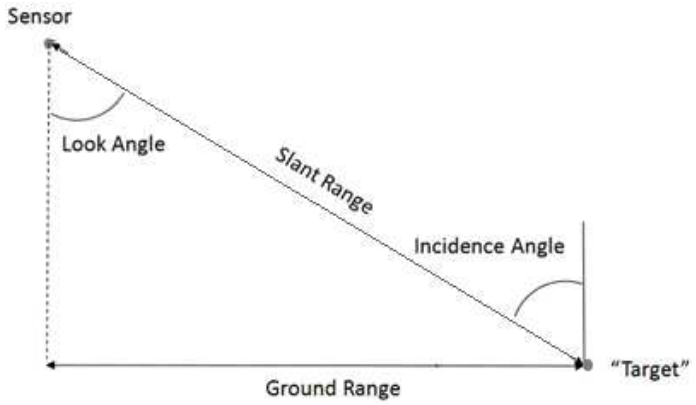

Figure 1. 8. Illustration of slant range and ground range (modified from Van Zyl and Kim, 2010).

SAR transmits signal in a side-looking direction towards the Earth's surface objects with a look angle and an incidence angle. Different from optical imagery, spatial resolution in SAR image is defined by range and azimuth resolution. Azimuth resolution is the ability of SAR system to separate two objects targets in the along-track direction of the sensor (Martinis, 2010). The azimuth increases with increasing distance from the SAR satellite. Range (across-track) resolution is dependent on length of SAR system pulsed (Sarmap, 2009). Range resolution consists of slant-range and ground-range resolutions. Slant range is the length between the sensor and the target. Ground range is the length between the sensor ground track and the target (Figure 1. 8) (Van Zyl and Kim, 2010).

SAR imagery can have different wavelengths (Table 1. 2). The longer the wavelength (shorter frequency), the stronger is the penetration into Earth's surface object. For example, in the Figure 1. 9, L band with longer wavelength than X and C band can penetrate more into the vegetation and, on dry conditions, to some extent, into the soil (for instance dry snow or sand).

Table 1. 2. Band types of SAR (modified from Sarmap, 2009).

Band types	Wavelength	SAR		
		Sensors	Temporal resolution	Spatial resolution
P-band	~ 65 cm	AIRSAR	-	60 cm
L-band	~ 23 cm	JERS-1 SAR	44 days	18 m
		ALOS- 1/2 PALSAR	14 to 46 days	3 to 100 m
		SEASAT-1	17 days	25 m
		SIR-A/B/C/X-SAR	-	13 to 58 m
S-band	~ 10 cm	Almaz-1	-	10 to 15 m
C-band	~ 5 cm	ERS-1/2 SAR	35 days	25 m
		SIR-C/X-SAR	-	26 m
		ENVISAT	35 days	30 m to 1 km
		RADARSAT-1/2	24 days	3 to 100 m
		RISAT-1	25 days	1 to 50 m
		Sentinel-1	6 to 12 days	1.7 to 93 m
X-band	~ 3 cm	SIR-C/X-SAR	-	10 to 20 m
		SRTM	-	30 to 90 m
		TerraSAR-X/TanDEM-X	11 days	25 cm to 40 m
		COSMO-SkyMed	16 days	1 to 100 m
K-band	~ 1.2 cm	Military domain	-	-

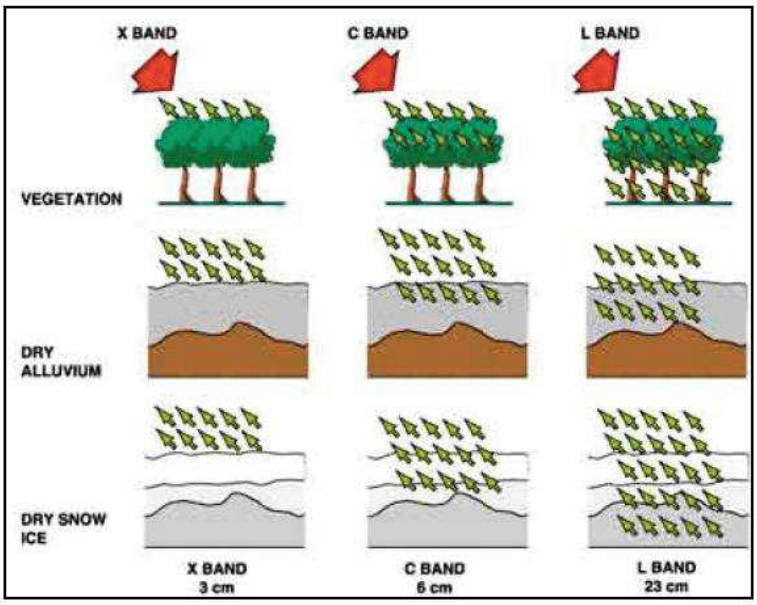

Figure 1. 9. Penetration of SAR signals from some bands (X, C and L band) (Sarmap, 2009).

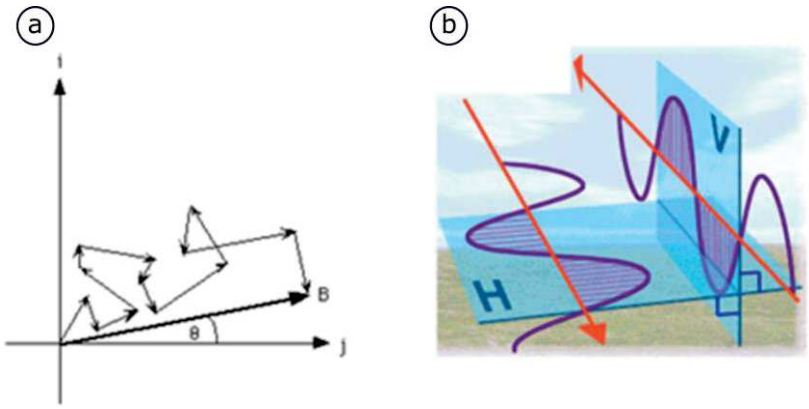

Figure 1. 10. (a) Illustration of random walks in speckle effect; (b) Horizontal and vertical polarizations (Sarmap, 2009).

Brightness variation in SAR image is not smooth. It has granular texture called speckle (Van Zyl and Kim, 2010). Speckle is produced by the interference of EM waves scattered from Earth's surface objects. Each target contributes backscatter energy when illuminated by SAR, which is then coherently added to all scatterers called random walks (Figure 1. 10a) (Sarmap, 2009). The wavelength of SAR signals can transmit and receive either horizontal (H) or vertical (V) electric field vectors (Figure 1. 10b). This term called polarization and normally there are four types of polarization (HH, HV, VV and VH).

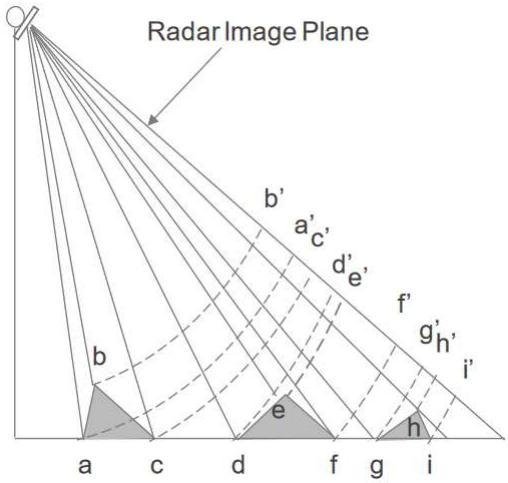

Figure 1. 11. SAR geometric effects: Layover, b' appears closer than a' in SAR image; Foreshortening, d' and e' are closer together in SAR image; Shadowing, h' to i' not illuminated by the SAR (Van Zyl and Kim, 2010).

Due to geometric properties of SAR data in range and azimuth direction there are some effects in SAR image. First effect is foreshortening which makes areas that slope toward the sensor look shorter in the image and areas that slope away from the sensor look longer in the image than in horizontal areas. Second effect, layover, appears in the extreme case where the slope is larger than the incidence angle. Mountainous area would look as if it is projected over the region in front of it. Shadowing, as the third effect, occurs when radar waves cannot illuminate steep slope which facing away from the radar, thus the area on that slope cannot be imaged (Figure 1. 11) (Van Zyl and Kim, 2010).

Interaction between SAR signals with water bodies depends on water surface condition (Figure 1. 12). For smooth open water, specular backscattering will generally occur because its smooth surface acts like a mirror for SAR signals. In this case, only very little energy will be scattered back to the SAR sensor. Therefore, in the image, it will appear dark (Figure 1. 13 c and d). Opposed to smooth open water, rough open water reflects SAR pulse in all directions, called diffuse surface backscattering, and a portion of the energy is scattered back to the radar sensor. Thus, in the image, it will appear brighter than smooth open water (Martinis, 2010; Yuan et al., 2015).

Considering flooded vegetation areas, SAR pulse will penetrate vegetation and generate double-bounce backscattering, the enhanced one, and diffuse volume backscattering. Double-bounce backscattering occurs when SAR signals bounce twice off water surface and vegetation, then most of the energy is reflected back to the SAR sensor. The enhanced double-bounce backscattering will occur when SAR pulse bounces more than twice off water surface and several parts of vegetation. Diffuse volume backscattering will occur when SAR signal cannot penetrate vegetation canopy, thus the pulse will scatter because of the rough surface on vegetation canopy. Double-bounce backscattering and diffuse volume backscattering will make object appear brighter in the SAR image.

Double-bounce backscattering and the enhanced one can be occurred also in the flooded urban areas. SAR signal will bounce to the existing buildings and flood waters. Double backscattering strengths make flooded areas appear brighter. On the other hand, smooth artificial surfaces in the urban areas will act like a mirror and thus resulting in a dark apparition because of specular backscattering (Martinis, 2010). Those two things will

cause errors in image interpretation, especially in separating flooded and not-flooded areas in the zone of urban.

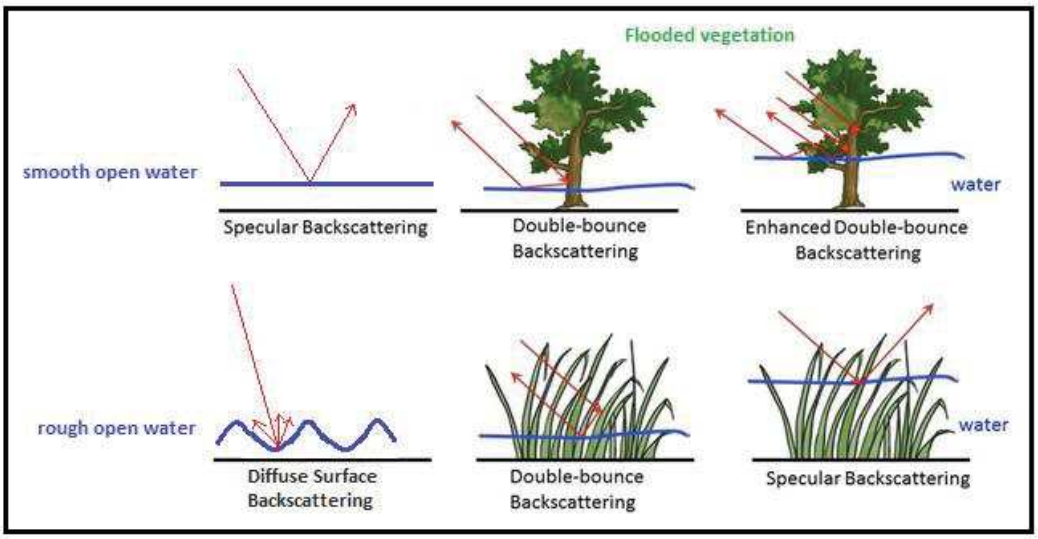

Figure 1. 12 Backscattering types related to surface water areas (modified from Martinis, 2010; Yuan et al., 2015).

Since almost 20 years, SAR sensors have increasingly been used for large-scale surface water mapping mainly at medium spatial resolutions, using X-band (SIR-C/X-SAR, SRTM), C-band (ERS-1/2 AMI, Envisat ASAR, RADARSAT-1, RISAT-1, SIR-C/X-SAR) (Baghdadi et al., 2001; Manjusree et al., 2012), and L-band (SEASAT-1, JERS-1, ALOS PALSAR, SIR-A/B/C/X-SAR). The launch of the X-band TerraSAR-X/TanDEM-X and COSMO-SkyMed (CSK) constellations with very high spatial resolutions (up to 0.24 m for the TerraSAR-X Staring SpotLight mode) increased capabilities for estimating flood extent and for flood monitoring in the case of complex, small-scale and operational scenarios are available. The potential of this new generation X-band data has already been demonstrated by several use cases in flood emergency situations (e.g., Martinis et al., 2015a; Martinis and Twele, 2010; Pierdicca et al., 2013). Unfortunately, those very high resolution of SAR data are not accessible for all users.

The first of the five missions that ESA is developing for the Copernicus initiative is Sentinel 1, a constellation of two polar-orbiting satellites (ESA, 2014). The satellites carry a C-band synthetic-aperture radar instrument which is within the 4–8 GHz frequency range (7.5–3.75 cm wavelength). Sentinel-1 provides high spatial resolution (about 20 meters in Interferometric Wide swath (IW) mode) and high temporal

resolution (a 12-day repeat cycle for one satellite, and 6-day for the pair). The data products are freely access in the scihub (https://scihub.copernicus.eu/). The potential of Sentinel-1 in mapping water bodies has been provided in some papers (e.g., Huang et al., 2018; Martinis, 2017; Twele et al., 2016).

In the future, the National Aeronautics and Space Administration (NASA) and CNES, the French space agency, in partnership with Canadian Space Agency (CSA) and UK Space Agency (UKSA) developed the Surface Water Ocean Topography (SWOT) mission. This mission carries a Ka-band radar interferometer sensor. This mission is planned for launch in 2021 and intends to provide a major improvement in the availability of surface extent and storage change for surface water bodies such as lakes, reservoirs, wetlands, and rivers globally, also give information about water levels (Cazals, 2017).

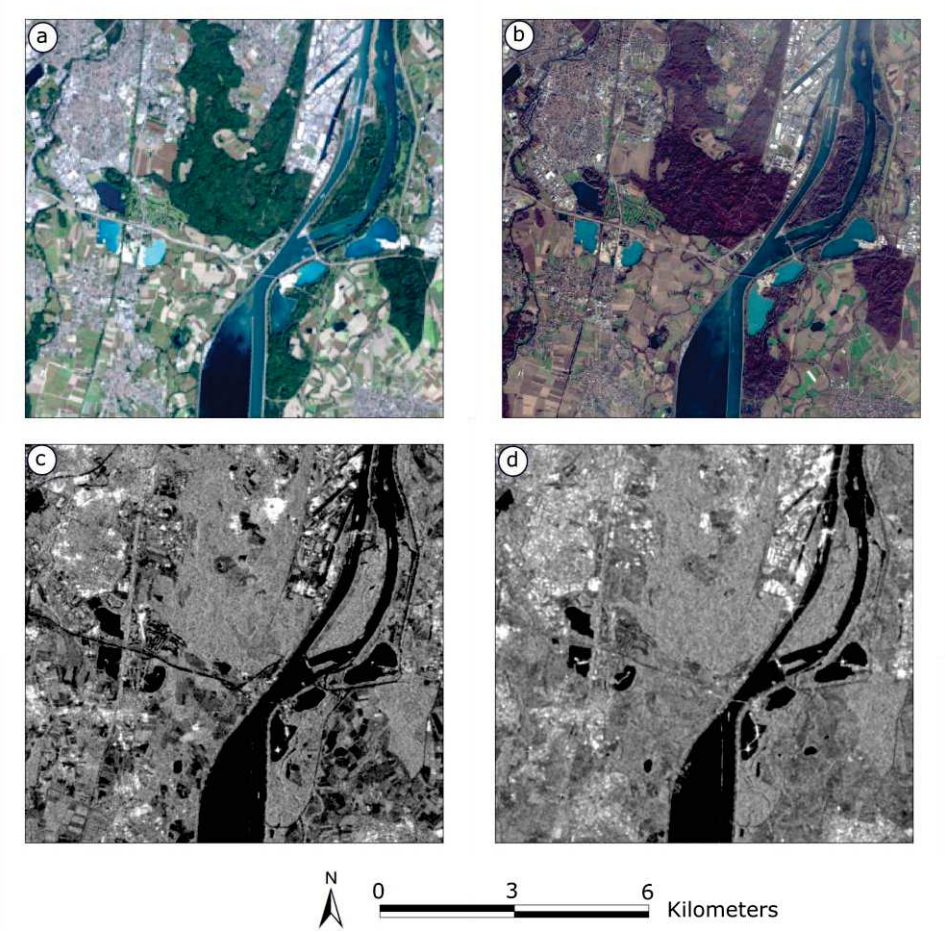

Figure 1. 13. Surface water in Grand-Est, France, seen by different sensors: (a) Landsat 8 image (natural color composite), (b) Sentinel-2 image (natural color composite), (c) ALOS-2 image (Sigma-nought HH), (d) Sentinel-2 image (Sigma-nought VV).

1.3 Research questions, hypotheses and structure of the manuscript

The availability of the Sentinel constellation in providing open data with optical and SAR imagery leads to the explosive growth of remote sensing data. The launch of that constellation can provide multi-source data and give unprecedented type of information. High temporal resolution provided from Sentinel leads to the availability of time series data and offer new opportunities for better understanding in Earth's surface changes. This deluge of satellite data correspond to "Satellite Image Time Series (SITS)" and provide a larger data series with short time interval between two images. Related to surface water mapping and monitoring, the SITS will give a new tools in observing surface water changes for either long or short time period. In addition, the availability of multi-source data can offer complementary information for surface water mapping.

Sentinel-1 mission can provide SAR data with various spatial resolution, various polarizations and the most important, it support high temporal resolution (up to 6-day for the pair of two polar-orbiting satellites). The high quality data of Sentinel-1 provided on an open and free basis are an attractive source of information for researchers. With their high temporal resolution, Sentinel-1 data can offer new opportunity for more understanding hydrological dynamics and phenomenon. They can increase capabilities for estimating flood extent and for flood monitoring. There's has been little research done to investigate the usefulness of Sentinel-1 for surface water mapping, while the design of this mission for operating in a pre-programmed conflict-free mode ensuring consistent long-term data archives (Torres et al., 2012) and the possibility of fully-automated surface water services (Twele et al., 2016) have been studied. It is important to address this gap by investigating thoroughly the potential of Sentinel-1 data for the efficient and reliable surface water mapping.

Sentinel-2 mission can bring systematic global acquisitions of fine spatial resolution multispectral images with a fine revisit frequency, which is important for the next generation of operational products, such as surface water monitoring. The Sentinel-2 images would surely be of great significance for surface water mapping, due to its

appealing properties (the four bands at 10 meter resolution and up to 2 days revisit time) and the free access (Du et al., 2016).

With this evolution in term of data to process, some challenges appear. The first one is the high temporal frequency caused high volume of data which implies to propose new methods for data processing and analysis, as conventional method will not be sufficient to take into account of this temporal dimension and to manage massive data. The other one is manual or supervised processing methods which are not adapted with SITS and multi-source data. That is because, manual processing method used the expert intervention which must be reduced through the automation in the processing chain in order to obtain information rapidly and efficiently, also to improve results' realibility and precision.

In this context, the main objective of this PhD thesis is to propose new (e.g. fully automated) approaches for surface water detection by exploring the single and combined used of Sentinel-1 and Sentinel-2 data, with the first focus on SAR data. In order to achieve this objective, several thematical and methodological research questions related to the enhancement of surface water mapping are listed:

- *What is the suitability and which methods are adapted and robust for an operational exploitation of Sentinel-1 data ?*
- *What is the contribution of Sentinel-1 times series ?*
- *What is the contribution of multi-sensor data ?*

In this context, the proposed research is focus on the development of operational methods for surface water mapping based on Sentinel 1&2 times series. The objective is to map permanent and temporary surface water with a high accuracy assessment at the 1:25 000 scale.

Based on these research questions, three hypotheses are addressed:

1. Satellite Image Time Series data can enhance surface water mapping.
2. Multi-sensor images are useful and relevant for surface water mapping and monitoring.
3. The proposed methods can be successfully applied for another thematic application.

In order to answer the research questions and to check the hypotheses, this PhD thesis has following structure:

Chapter 2 presents the state-of-the-art methods for the detection of surface water successively in radar imagery, in optical imagery, and by combining both sources of information.

Chapter 3 provides the datasets and study areas use to develop and validate the proposed methods. This chapter presents existing database or web-services of surface water. Pre-processing step of Sentinel 1&2 imagery is also detailed.

Chapter 4 will focus on the detection of surface water by SAR data, due to its capability to acquire observations during periods of persistent cloud cover, when flood events often occur. The usefulness of the C-band Sentinel-1 sensor mission for surface water mapping purposes will be thoroughly investigated. To the best of our knowledge, several semi-automatic and automatic tools already exist for surface water mapping from SAR data (Huth et al., 2015; Martinis et al., 2015b; Schlaffer et al., 2012; Westerhoff et al., 2013), but currently only a few scientific references present a fully automatic water detection method, especially tuned for Sentinel-1 imagery (Twele et al., 2016). The literature proposes a large number of methods for detecting surface waters from SAR data. We aim to find the best configurations in order to map surface waters automatically and rapidly using Sentinel-1 imagery. Thus, this chapter will present the Water-S1 method (detection of surface waters) developed for Sentinel-1 image.

Chapter 5 explores the contribution of Sentinel-1 time series data for the detection of permanent surface water. In order to explore the potentialities of the temporal information, we explore also how to take into account of this temporal analysis in the processing chain. This chapter also investigates Sentinel-2 as new optical data for surface water mapping. In this context, we decide to explore the potentialities of multi-source sensor (passive and active such as Sentinel-1 and Sentinel-2) to improve surface water mapping.

Chapter 6 presents some experiments in order to observe another methods for surface water detection. Sentinel-1 polarimetric data for surface water mapping are

investigated. We will evaluate also another approach of image fusion, classically tested in the literature. Finally, to support the demonstration of our proposed methods and to qualify their reproducibility to other thematic context, some experiments related to very different thematic applications are performed.

Finally, **Chapter 7** concludes the manuscript by summarizing the results and by presenting some perspectives.

During this study, operational methods are developed by maximizing the use of free software or free programming language. Sentinel-1 pre-processing is performed in Sentinel Application Platform (SNAP)[1] provided by European Space Agency (ESA). Polarimetric processing of Sentinel-1 is performed also in SNAP. With the help of Sen2Cor[2] plugin, Sentinel-2 pre-processing is also carried out in SNAP. Algorithmic developments and statistical analysis are executed in R[3] and Python[4]. Geographical treatments and accuracy assessments of results are performed using QGIS[5].

The PhD work has been supported by the Indonesia Endowment Fund for Education (LPDP), Ministry of Finance, Republic of Indonesia and the French funded program ANR TIMES (ANR-17-CE23-0015-01). It is a continuation of the various works carried out at LIVE and EOST on satellite image time series processing for the analysis of environmental processes. It is a contribution to the program A2S—Alsace Aval Sentinel of University of Strasbourg on the development of innovative processing chains for Sentinel data.

1. http ://step.esa.int/main/toolboxes/snap/
2. http://step.esa.int/main/third-party-plugins-2/sen2cor/
3. https://www.r-project.org/
4. https://www.python.org/
5. https://www.qgis.org/en/site/

Chapter 2

The state of the art

Contents

The previous chapter allowed us to understand surface water as our object of study, its definition and importance. It also provided us with the characteristics of surface water in the remote sensing data. This chapter aims to discussing the state of the art of surface water mapping methods based on remote sensing techniques and presents existing surface water products. The purpose is not to present an exhaustive review of the large amount of published works, but to give an overview of the methods existing for surface water mapping.

This chapter presents the existing methods using single-date optical (section 2.1) and SAR remote sensing data (section 2.2) allowing surface water mapping. In the section 2.3, a review of methods based on time series (2.3.1) and multisource (2.3.2) data is presented. These methods allow improving surface water mapping. They are also used for surface water monitoring. The last section (section 2.4) summarizes existing services, tools and products or database of surface water derived from massive processing of remote sensing data.

2.1 Optical remote sensing for surface water detection

In case of favorable weather conditions, optical Earth Observation (EO) sensors are the preferred information source for the detection of surface water due to their straightforward interpretability. Numerous single-date methods have been developed in the literature to mapping surface water with optical imagery.

Many methods are derived based on the low reflectance return from surface water bodies:

- Density slicing method (Figure 2. 1) is a simple way which has been reported successfully extracting surface water from single band or multispectral optical imagery (Frazier and Page, 2000). This method is simple and effective to distinguish water from the other areas. However, in this method, result depends on the selection of threshold value. Errors are common because of the mixing of water pixels with different land cover types.

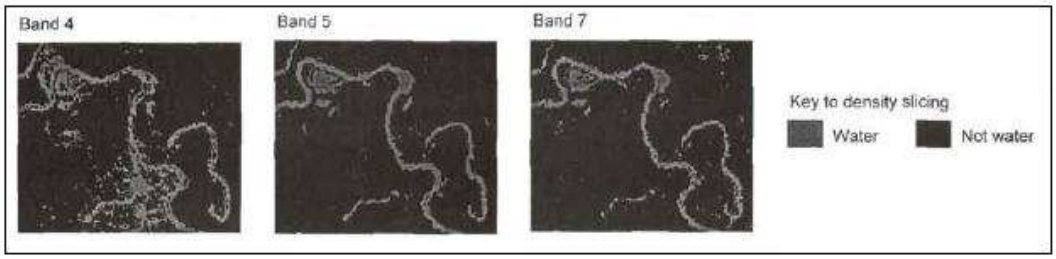

Figure 2. 1. Example of density slicing results in Landsat TM bands (Frazier and Page, 2000).

- Edge detection is also a simple method to delineate surface water (Shah et al., 2011). As the previous method, the selection of appropriate threshold value is important for this method.
- Classification methods, either unsupervised or supervised (Figure 2. 2) are also classically used to extract water bodies from multispectral imagery (Banukumar et al., 2011; Chen et al., 2014; Frazier and Page, 2000; Kingsford et al., 1997; Taylor and Mosiman, 2003). Unsupervised classification can minimize human error because it does not use any user-defined training classes. Yet, unsupervised classification relies purely on spectral and statistical information to clusters pixels in a dataset in order to determine classes that may not necessarily correspond to the informational categories of interest. Supervised classification has more control over the type of classes defined within a geographic area. However the training data selected for a given class does not account for the variation in environmental conditions throughout the study area.
- Decision tree for surface water delineation can also be built from multispectral imagery (Acharya et al., 2016; Sun et al., 2011). However, this method makes use of classification rules which are difficult to build and sometimes can not be applied universally.

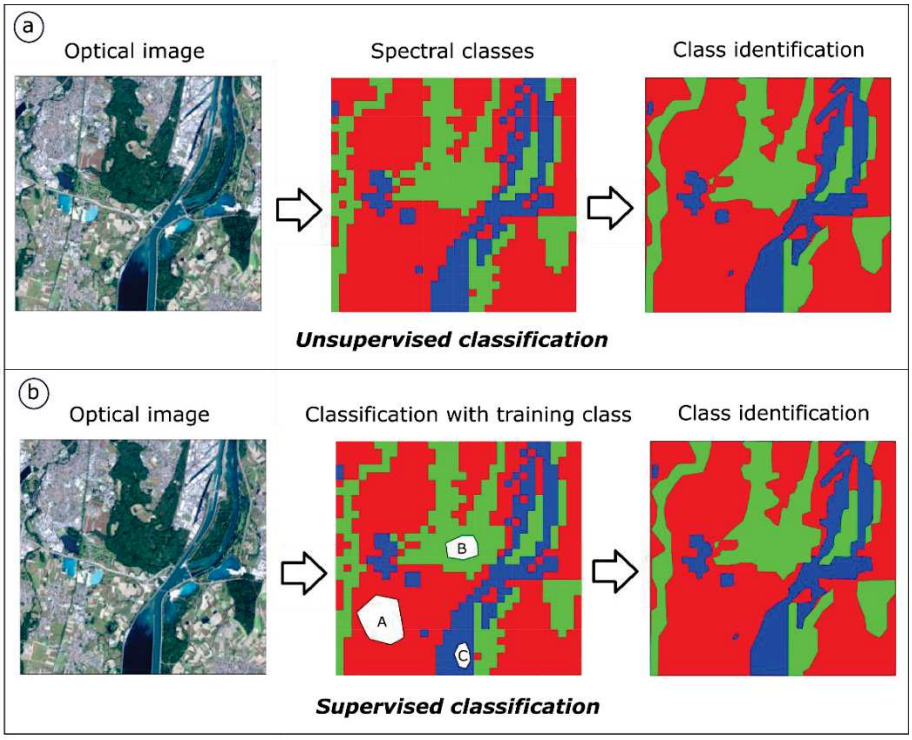

Figure 2. 2. Illustration of (a) unsupervised and (b) supervised classification method.

The easy and effective way to distinguish water and non-water areas is to use water indices. This method combines spectral bands using various algebraic operations to increase the difference between water bodies and land. Many indices have been developed to extract surface water areas or flood inundation extent (Huang et al., 2018):

- The Tasseled Cap Wetness Index (TCW) is developed by Crist (1985) to separate water and non-water objects. This index is derived from six bands of surface reflectance data and set a threshold of 0. The comparison performed by Zhou et al. (2017) shows many non-water pixels that were mistakenly classified into water pixels in the result using TCW.
- The Normalized Difference Vegetation Index (NDVI) is known to show small values for water body, thus surface water areas are easily observed by low NDVI values (e.g., Khand et al., 2017). Nevertheless, this index is more appropriate to extract vegetation area because it does not directly provide information about surface water area.
- The Normalized Difference Water Index (NDWI) is the first generation of water index (McFeeters, 1996). This index makes use of Near Infrared (NIR) band to reflect water's characteristics. NDWI proved to work well in separating water

body and vegetation but has limitations when it comes to soil and built up area (Figure 2. 3 a).

- The Modified Normalized Difference Water Index (MNDWI) is developed by replacing the NIR band in NDWI with the Short-Wave Infrared (SWIR) band (Figure 2. 3 b). The SWIR band is less sensitive to concentration of sediments in the water than the NIR band. Thus this index is believed to be more stable than NDWI, especially in detecting water features for water regions with backgrounds dominated by built-up land areas (Gautama et al., 2015). Yet, for some optical data, the combination of the SWIR band and Green band in MNDWI can degrade image quality due to different spatial resolution of bands. MNDWI also has limitation in discriminating water and snow due to the normalized difference between Green band and SWIR band for snow is as high as that of water (Huang et al., 2018).
- The Wetness component of K-T transformation is proposed for extracting the wet areas from the optical image, not only surface water area but also humid area (Wang et al., 2013). However, this method produced the confusion of water and buildings existing in image.
- The Automated Water Extraction Index (AWEI) is a new index proposed by Feyisa et al. (2014) (Figure 2. 3-c) as an alternative and improve water index, especially in extracting water information from areas where noisy results are expected because of the presence of shadows and built-up surfaces. This index was developed for Landsat images and consists of two indices, $AWEI_{nsh}$, working well when there are no shadows, and $AWEI_{sh}$, allowing further distinguishes between water pixels and shadow pixels. AWEI is found more efficient in detecting water features in urban areas than in large open surface water (Rokni et al., 2014).
- The Water Index (WI2015) is proposed by Fisher et al. (2016) using statistical analysis of surface reflectance on Visible, NIR, and SWIR bands. This index was developed for Landsat data. Surface reflectance as an input for this index is believed to be more accurate than the used of digital number (DN or top of atmosphere (ToA) reflectance. However, conversion process from DN to surface relectance is usually requires a lot of computation and time-consuming (Huang et al., 2018).

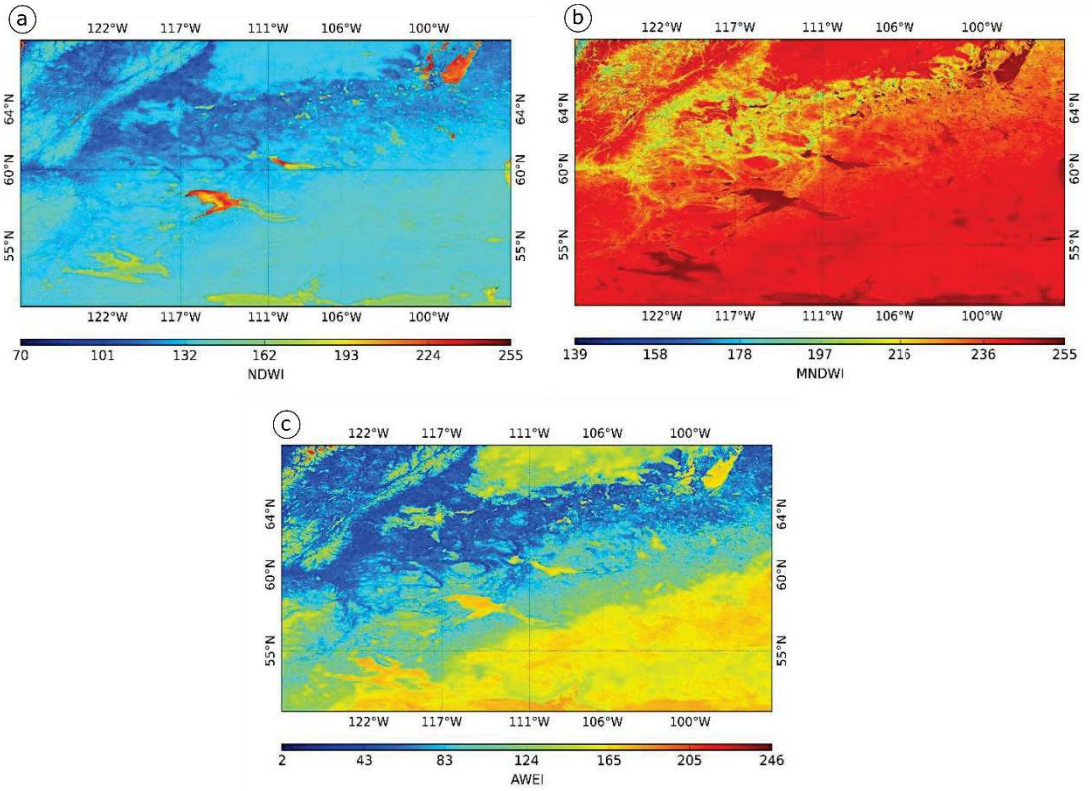

Figure 2. 3. Example of water indices results (a) Normalized Difference Water Index (NDWI), (b) Modified Normalized Difference Water Index (MNDWI), (c) Automated Water Extraction Index (AWEI) (modified from Sharma et al., 2015).

Thresholding is one of important issues in surface water mapping. Methods, such as density slicing, edge detection and water indices are applied thresholding to extract surface water. The selection of thresholds value is tricky and sometimes difficult to be generalised due to different characteristics of surface water in each images. The results sometimes misclassify mountain shadows, urban areas or other background noise as water bodies, if a threshold is not selected appropriately. Thus, manual adjusment on the threshold is needed to achieve more accurate results. Automatic extraction can be performed by applying single threshold for all data. Huang, et al. (2014) performed this technique using Open Water Likelihood (OWL) index proposed by Guerschman et al. (2011) which was a regression model based on five variables that are relevant to surface water and has stable values. Another automatic method is proposed by Zhang et al. (2018) using Modified Histogram Bimodal Method (MHBM). This method seeks minimum values in the threshold range to achieve an automated dynamic threshold.

Automatic thresholding using Otsu algorithm is applied by Buma et al. (2018) to map surface water extent of Lake Chad.

All the methods mentioned above usually use pixel-based values to extract surface water. However, methods based on pixel values will be difficult to deal with very high spatial resolution images. When very high spatial resolution images are used, Object-Based Image Analysis (OBIA) is more appropriate. The idea is to classify objects based on their characteristic texture features (Dronova et al., 2015). But this type of method requires high processing for the segmentation step, which mostly limits the size of the processed image in dependence on the used software package (Hahmann et al., 2008). Furthermore, in order to achieve useful results it is necessary to have solid expertise on relevant features.

For many years, several efforts have been devoted to develop surface water extraction methods from optical remote sensing data, including automatic method. Although the principle of extracting surface water from optical sensors is straightforward, it is also important to accept their limitation. The most critical one is that they are easily affected by cloud obscuration. In these conditions, several methods have been developed in the literature using SAR images.

2.2 SAR remote sensing for surface water detection

Several methods can be found in the literature to map surface water from SAR imagery. Using single-date data, the methods are only able to detect surface water extension. Identification of floods areas can be obtained using integration of additional information about pre-flood condition.

Thresholding (Figure 2. 4) is one of the most common adopted methods in SAR imagery to discriminate between water and non-water area (e.g., Bartsch et al., 2012; Cazals, 2017; Muster et al., 2013; Yamazaki et al., 2013). The approach is based on the low radar return from surface water. Its advantage is represented by the computation efficiency that could make it suitable for rapid mapping purposes (Martinis, 2010). However, the choice of the threshold value is a critical aspect because it depends on environmental parameters of the study area (e.g. land cover), as well as on system

parameters (frequency band, polarization, and observation angle). Surface water can be extracted using this technique in moderate roughness conditions of the water surface, as the contrast between the water and non-water class is significant. In the case of double-bounce backscattering or the enhanced one due to flooded vegetation, rough water surfaces or flooded urban areas (see Chapter 1), thresholds value will be more difficult to determine. Therefore, thresholding method sometimes does not provide satisfactory results in vegetated, forested, and urban areas or in the presence of wind that roughens the surface water (Pulvirenti et al., 2012).

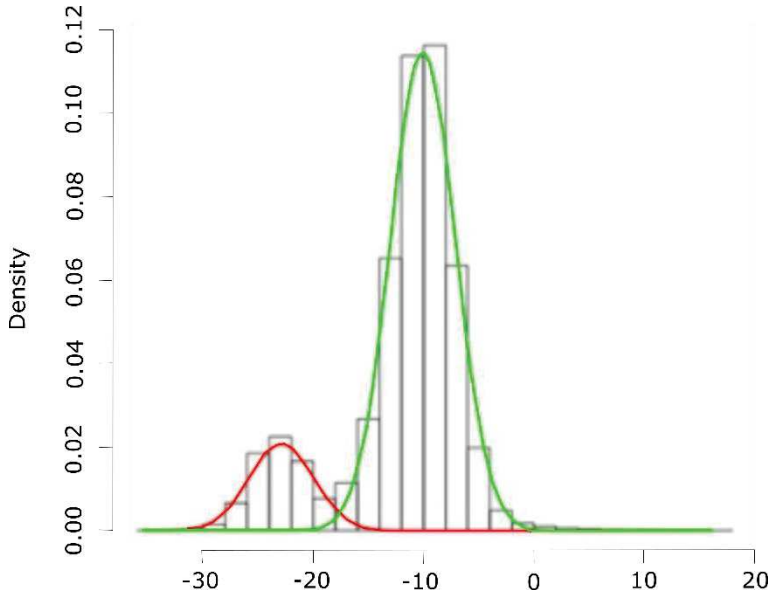

Figure 2. 4. Illustration of thresholding method.

Two approaches are existing to set a threshold for water surface detection on single-SAR image:

- *Manual* determination can be performed by visual interpretation of image histogram and trial-and-error procedures. Henry et al. (2006) applied this method to intensity image of multi polarization ENVISAT data (HH, HV and VV). Similar applications have been conducted by Lang et al. (2008) using sigma-nought image of Radarsat-1 with HH polarization and Matgen et al. (2007) using intensity image of ENVISAT data with VH polarization. This simple technique can provide interactive threshold which adapted to surface water characteristics from each images. Yet, the quality of result from this technique depends on the subjective interpretation of the operator.

- *Automatic* thresholding for surface water mapping can be based on several algorithms.
  - ✓ It can be performed using the **Otsu** algorithm. This method selects the threshold value that maximizes the between-class variances of the histogram. This is optimal for thresholding large objects from the background, which means that it is strongly depended on bimodality of histogram. Schumann et al. (2010) apply this method for sigma-nought image of ENVISAT with VV polarization.
  - ✓ One of the limitations of Otsu algorithm is the threshold value can over or underestimate the extent of surface water when the bimodality of histograms is unbalanced (Behnamian et al., 2017). To address this, a modified version of Otsu's thresholding algorithm called **valley emphasis** has been developed. It attempts to select a threshold that is closer to the valley between the two modes. Li and Wang (2015) use this method for intensity image of Radarsat-2 imagery with HV polarization.
  - ✓ Automatic thresholding can be based on statistical modeling of histograms. Matgen et al. (2011) applied this method to intensity image of RADARSAT-1 with HH polarization. Similar applications have been conducted by Martinis et al. (2009) using sigma-nought image of TerraSAR-X imagery with HH polarization. They manage to reduce user intervention, yet the method only works successful in smooth water surface due to sufficient contrast between land and smooth water surface.

Several supervised and unsupervised classification methods can also identify the surface water on SAR images. Study of De Roo et al. (1999) used a maximum likelihood classification of supervised method for separated flooded and non-flooded areas. Yet, supervised method needs user intervention for determined training sites. Unsupervised classification in ALOS PALSAR imagery in order to mapping regional inundation was presented in Chapman et al. (2015). The result shown a good performance for open water extent, but not in the regions where there may be differences in sensitivity to widespread and shallow seasonal flooding event. The disadvantage of unsupervised methods are it relies purely on spectral and statistical information, also it has less control over the type of classes.

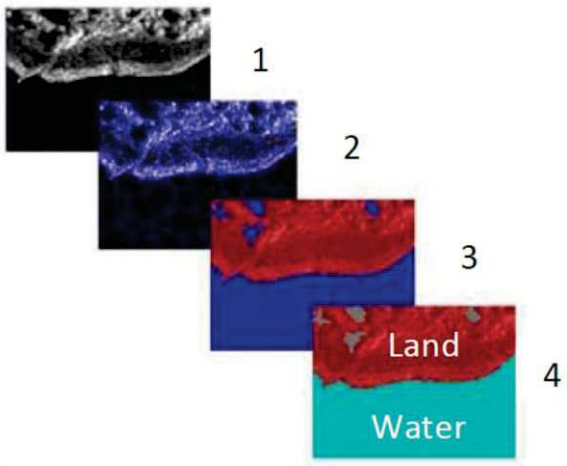

Figure 2. 5. Illustration of OBIA steps : (1) SAR data, (2) segmentation, (3) first classification, (4) second classification (modified from Simon et al., 2014)

Most of the above mentioned studies are consider pixels as smallest geometrical components of raster data (pixel-based). The surface water detection is performed without taken into account contextual information. Misclassification will often occurs due to salt-and-pepper appearance affecting result accuracy. In very high resolution of SAR data, Earth' surface objects are usally larger than the pixel size. Therefore, although the pixels represent different spectral properties, they can be the same object. OBIA (Figure 2. 5) for SAR imagery has increasingly developed in surface water mapping during recent years (e.g., Evans et al., 2010; Hahmann et al., 2008; Simon et al., 2014) to overcome this problem. This approach has advantages for improving classification with combination of spectral characteristic and contextual information. However, this method classifies image elements by segmentation phase using limited contextual information. OBIA does not consider inter-spatial relationships between different scale representations in SAR image and does not explore more the inter-spatial relationships between adjacent objects (Martinis, 2010).

Several researches use topographic data as additional information to improve surface water detection result. The purpose of integration is to detect surface water beneath vegetation by removing water-like areas based on hydrological assumption (Clement et al., 2017; Martinis, 2017). With this concept, flood mapping procedure is presented by Pierdicca et al. (2008) using fuzzy sets theory. The method integrates digital elevation model (DEM) with SAR data.

Segmentation approach such as region growing methods has been used by some studies in the past for surface water detection. The expansion of seeded regions is based on their statistical characteristics and will stop according to reached conditions. For instance, Malnes et al. (2002) presents region growing method for RADARSAT-1 data. Surface water areas are determined based on the seeded regions which growing within three standard deviations from the mean intensity value. In recent years, Active Contour Models (ACMs) or snake algorithms are popular method to extract surface water from SAR data based on region growing (e.g., De Roo et al., 1999; Matgen et al., 2007; Schumann et al., 2009). Dynamic curvilinear contour is used in these algorithms to search through image space iteratively until it founds surface water boundaries.

In conclusion, most of the surface water mapping methods based on single-date optical or SAR images and proposed in the literature require a considerable amount of user intervention. This human intervention is not practical for operational mapping and is not adapted to the new generation of optical (Sentinel 2) and SAR data (Sentinel-1), which are characterized by increased temporal resolution. Indeed, contextual information, such as the correlation among neighboring pixels must be taken into account, considering that individual pixels are not independent random variables but form a random field. Since few years, multi-temporal image analysis has proven their superiority to mono-temporal approaches in image processing to extract surface water and to monitor these surfaces.

2.3 Multi-temporal and multi-source data for surface water mapping and monitoring

2.3.1 Satellite Image Time Series: value and existing methods

Satellite Image Time Series (SITS) is defined as a set of satellite images taken from the same scene at different times. Analysis using SITS has proven producing better results and more popular than single-date approaches for surface water mapping (e.g., Martinis, 2010; Mitchell et al., 2015; Pulvirenti et al., 2012; Schlaffer et al., 2015; Zhao et al., 2014). A single-date approach is typically only able to distinguish water and non-water area. The approach uses multi-date, multi-temporal or time series analysis opens

the opportunity to be able to classify surface water; for example, distinguish permanent surface water and temporary surface water (floods). It also provides a way for surface water monitoring, floods detection, changes detection which simply cannot be done only with mono-date. With the redundancy of information provided in SITS data, the quality of surface water detection and mapping can be increased (Clement et al., 2017; Martinis, 2017).

In the case of optical data, study in Lunetta and Balogh (1999) proposed the use of SITS with Landsat 5 TM imagery for wetlands identification, as one of temporary surface water area. They use a GIS rule-based classification model in an attempt to improve the classification accuracies of the wetland classes. Limitations of this approach are related to expert intervention or reference in order to determine parameters to classify wetland land cover.

Another use of optical SITS was proposed by Mueller et al. (2016) for water observations in Australia. The method classifies permanent and temporary surface water based on their occurrence in observations. A water detection algorithm was used based on a decision tree classifier, and a comparison methodology using a logistic regression. The method shows that it is operationally feasible to apply a single algorithm over many different environmental and climatic conditions and achieve a high degree of accuracy. However, some known errors remain, mainly derived from shadow produced by clouds and steep terrain. Important additional errors also derived from data anomalies and urban structures.

As for SAR data, study in Martinez and Toan (2007) presented the use of SITS for flood dynamics and spatial distribution of vegetation based on decision rules over two decision variables. However, discrimination between open surface water, bare soils and low vegetated areas present a lower accuracy with this method. Another study of SITS using supervised classification was applied by Zhao et al. (2014) to a series of polarimetric SAR data for floodplain seasonal inundation monitoring. They have hypothesis that the interaction between radar signals and land-cover types at the different seasons can be learned further using composite polarimetric features. Unfortunately, the result shows that the intensity of the single polarization performed better than the composite features for classification predictor of the floodplain.

Unsupervised clustering method using SITS was presented by Pulvirenti et al. (2012) to map flooded areas from SAR data. The procedure is based on an automatic image segmentation technique and on the interpretation of the radar return from the segments derived from an electromagnetic model. However, the methodology needs to be further tested on different case studies because it was specifically designed to deal with multi-temporal, single channel, high resolution radar data provided by COSMOSkyMed.

Change detection and thresholding methodology has been developed using Sentinel-1 images to map floods events in Clement et al. (2017). Yet there are still misclassification of urban features and a problem in smaller scale pluvial inundation. Automatic thresholds analysis was applied by Schlaffer et al. (2015) for flood detection from multi-temporal SAR data. Harmonic analysis of a multi-temporal time series was done and classified by means of an automatic threshold optimization. Noise is reduced by using multi-temporal data and no interaction by the user is required. However, the need to calibrate the harmonic model and preprocess SAR time series data make computational cost increasing, thus it become the disadvantages of this approach.

Martinis and Twele (2010) extent their study with SITS in automatic tile-based parametric thresholding approach to extract flood using a hybrid multi-contextual Markov image model of unsupervised change detection methods. They showed that computational demands and classification error can be reduced using hybrid model. Nevertheless, this method does not flexibly react with the diversity in multi modal histogram of SAR image. Subtraction method and MNF (Minimum Noise Fraction) were applied by Mitchell et al. (2015) to multi-date SAR imagery in order to map spatial data of inundation extent. The final water result was produced using the intersection of low backscatter areas in MNF images and band difference. However, this approach needs user intervention and works in pixel-based.

2.3.2 Multi-source data: value and existing methods

The possibility to collect different kinds of observations over a same area has considerably increased with the multiplication of sensors. It can now be said that remote sensing is ‘multi-modal’ (Gómez-Chova et al., 2015) or multi-source. As described in

section 2.1 and 2.2, the sensors can be use different modalities (optic, radar, etc). Even for a same modality, they can exhibit very distinct characteristics (for instance optical sensors show different spectral configurations (number of spectral bands, position and width of the spectral bands), spatial resolutions, and revisit times). The possibility to capture genuine time series is then increased.

As a consequence, combining remote sensing data with different characteristics is a standard remote sensing problem that has been extensively investigated in the literature (Chavez, 1991). The main aim consists in fusing multi-sensor information as a means of combining the respective advantages of each sensor (Goyal and Wahla, 2015; Pohl and Van Genderen, 1998). Combining existing sensors can mitigate limitations of any one particular sensor for various land cover issues (Gamba, 2014; Joshi et al., 2016). Complementary observations can thus be exploited for land cover mapping purposes. More specifically, many case studies present methods for surface water extraction based on **multi-source (optic and SAR) image fusion**.

Fusion of heterogeneous image source has been widely investigated in the remote sensing (Benediktsson et al., 2018; Chavez, 1991; Pohl and Van Genderen, 1998; Schmitt and Zhu, 2016). Image fusion can be implemented at three different levels (Ghassemian, 2016; Liu et al., 2018a): (1) pixel level, (2) feature level and (3) decision level (Figure 2. 6).

Image fusion at pixel level combines two or more geometrically registered images of the same scene into a single image that is more easily interpreted than any of the originals. The aim is to obtain information of greater quality. For that purpose, pan-sharpening is a well-known technique that integrates the geometric details of a high resolution panchromatic image and the color information of a low spatial resolution multispectral.

Image fusion at feature level deals with data at higher processing levels than pixel level methods. At first, feature extraction procedures are applied. For instance, the extraction of objects is obtained by segmentation procedures. Then, features (spectral or spatial indices, texture-based, etc) are computed from each image sources. Examples of remote sensing fusion methods at feature level, applied to several landcover types,

can be found in Ban and Jacob (2013); Dechesne et al. (2017); Fauvel et al. (2007); Wegner et al. (2011); Xia et al. (2018).

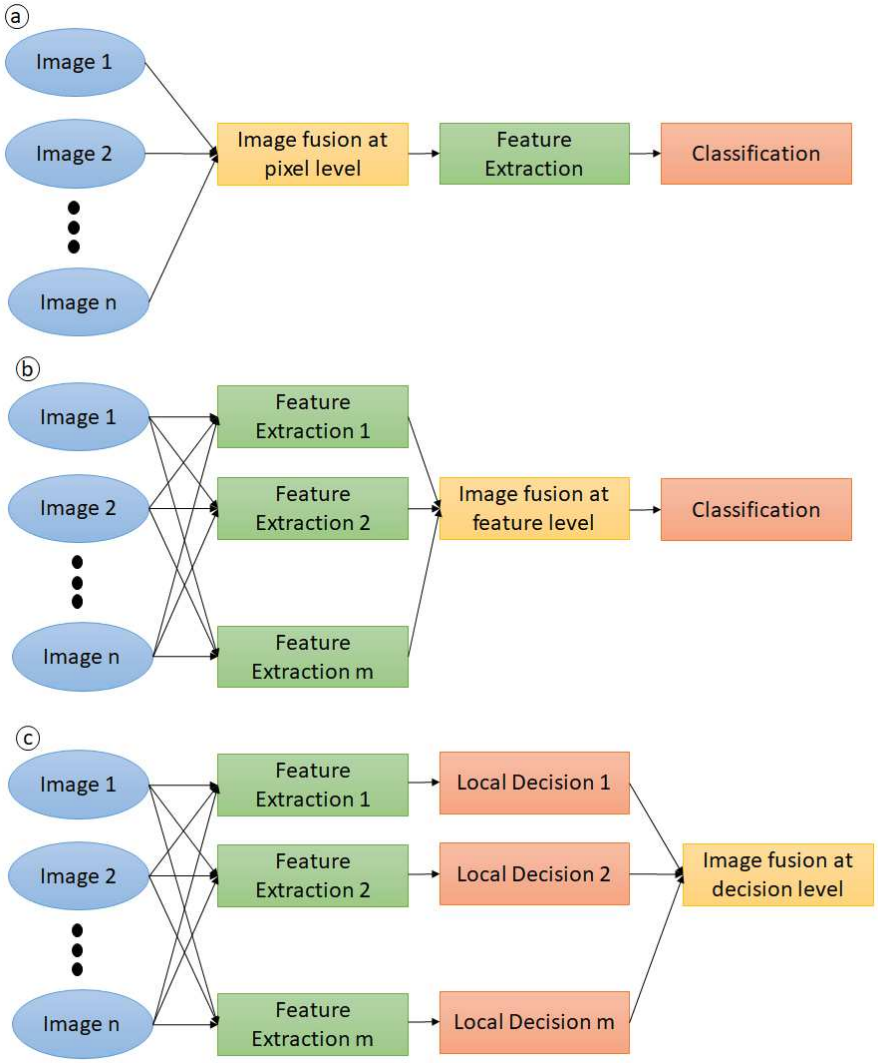

Figure 2. 6. Fusion levels: (a) pixel level, (b) feature level, (c) decision level (modified from Ghassemian, 2016).

Image fusion at decision level is the process of merging information from several individual data sources after each data source has undergone a preliminary classification. First, the input images are processed individually for information extraction. Then, the decision rules are used to combine extracted information to resolve differences and furnish a better understanding of the observed objects. Decision level fusion has great uses in the distributed and parallel processing systems.

This type of approach is commonly used for surface water extraction. When images originate from several sensors, the most relevant method for data fusion is to combine the images with the surface waters results extracted individually for each image source (Pohl and Van Genderen, 1998; Wendl et al., 2018; Zadeh, 1976). For instance, Wang et al. (2011) use RADARSAT and Landsat imagery to extract surface water information. RADARSAT images effectively extract the open water areas and a large number of small water bodies using supervised classification method. Meanwhile, Landsat imagery separated vegetation and water bodies using wetness index and vegetation index (NDVI). Then, the results were fused. The study demonstrated that the complementary information of RADARSAT SAR images and Landsat ETM+ images can achieve semi-automatic and rapid extraction of water information. However, the accuracy of this method depends on the accuracy of the surface water extraction from each image. Westerhoff et al. (2013) fuse SAR and MODIS in order to produce water imagery. Water extraction in that study uses thresholding method. Yet, there is no global threshold to make binary surface water map. The threshold values are varies, depending on the area in the world and the incidence angle. Another method from Chengquan et al. (2018) presents decision level fusion of multi-temporal and multi-source satellites data to monitoring surface water dynamics. They use machine learning (DeVries et al., 2017; Huang et al., 2018) for each satellites images then merge the results.

In conclusion, using image times series and data fusion techniques to increase the accuracy of permanent surface waters extraction is promising (Bourgeau-Chavez et al., 2009; Liu et al., 2018b; Riffler et al., 2018). Combining data of different properties and data acquired at several periods can improve image classification (Riffler et al., 2018). For instance, Aires et al. (2018) presents inundation mapping using multi-temporal and multi-source satellites data. They merge and classify features extracted from various type of satellites imagery. Approach from Riffler et al. (2018) shows decision-level fusion using multi-temporal and multi-source satellites data to produce water and wetness index. However, eventhough promising, there are only a few studies combining multi-temporal and multi-source approach.

2.4 Review of existing products, tools and services for surface water mapping

Many databases at several scales are mapping surface water areas by using massive processing of optical and/or SAR images times series.

At global scale, Landsat times series have been processed to propose the **Global Surface Water (GSW) product** (Figure 2. 7a) computed by the EC-Joint Research Centre (The European Commission's Joint Research Centre, n.d.). This product is generated from 30 m spatial resolution Landsat images with a minimum mapping unit of 10 ha. This product allows quantifying changes of surface waters over a period of 32 years (1984-2015) using expert non-parametric classifiers. It also propose a water seasonality product for 2014-2015, water occurrence and water transition maps (Pekel et al., 2016).

Another product, the **SRTM Water Body** is available at global scale by National Geospatial-Intelligence Agency (NGA) (USGS, n.d.). It is derived from radar data (SRTM Digital Terrain Elevation Data) with a minimum mapping unit of 10 ha (Figure 2. 7b). The elevation data are classified based on topographic rules to identify oceans, lakes and rivers. This product provide minimum surface area of at least 10 ha (Messager et al., 2016).

The **Global Lakes and Wetlands Database (GLWD)** of WWF and the University of Kassel is a third available product mapping water surfaces (Lehner and Döll, 2004). This is generated from various cartographic sources documenting lakes, reservoirs and wetlands on a global scale (Figure 2. 7c). The product combines the best existing global and regional maps that were aggregated at a 1 km spatial resolution using expert concepts and thresholds (WWF, n.d.). The product provides a minimum mapping unit of 10 ha.

The **Water and Wetness product** from EC-COPERNICUS (Figure 2. 7d) is produced from Landsat, Sentinel-1, ENVISAT-ASAR and ancillary GIS datasets (Copernicus, n.d.). Thresholding is used to derive surface waters from optical and SAR data before fusing the results with GIS datasets to generate the final classification. The minimum mapping unit for this product is 400 m2. The product does not map small river channels

and streams of widths less than 40 m (Langanke, 2016). Two classes of waters are categorized in this product: the "permanent water" class (e.g. rivers and lakes) corresponds to water surfaces identified in, at least, 80% of all observations; the "temporary water" class corresponds to water surfaces identified in more than 25% and less than 80% of all observations.

Figure 2. 7 presents an overview of the existing products over a study case in Ireland (see Chapter 3). Consequently, these existing surface waters products are relevant for some applications but do not fulfill all the current needs of the science and water management communities. For instance, GLWD and SRTM Water Body do not identify small surface waters of less than 10 ha and narrow water bodies such as watercourses or streams. GSW is based on Landsat imagery with gaps in the observation records because of the occurrence of clouds. The Water and Wetness product is already using Sentinel-1 data but relies on 30-m spatial resolution Landsat imagery.

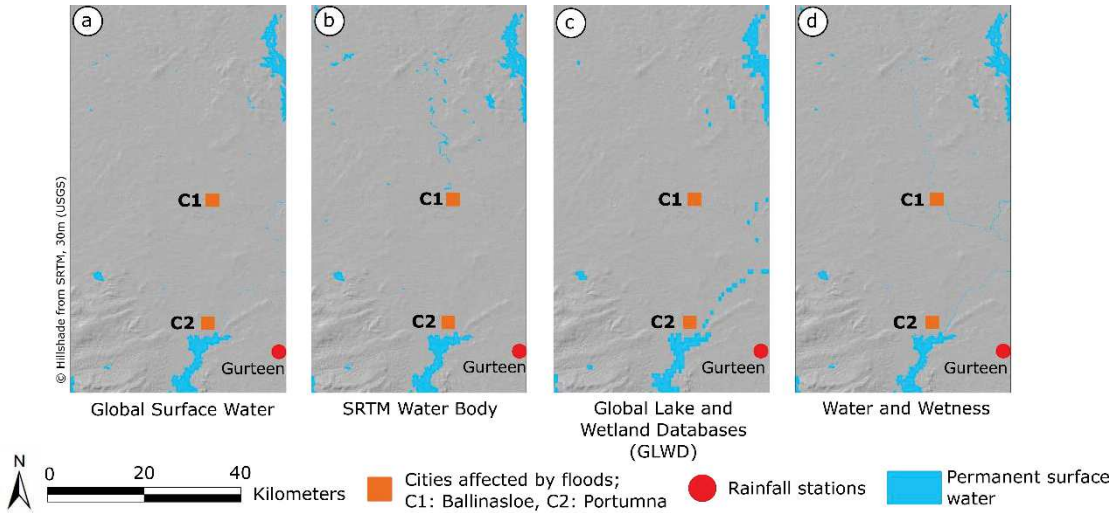

Figure 2. 7. An overview of the existing products over the study case in Ireland. (a) Global Surface Water ; (b) SRTM Water Body ; (c) GLWD ; (d) Water and Wetness.

With increased access to large or massive volumes of remotely sensed data and innovative techniques for optimizing the processing and interpretation of those data, a recent issue is to propose **online tools or services to map surface water**.

The **Surface Water Mapping** tool leverages the extensive archive of Landsat data in the Google Earth Engine archive and Google's cloud processing power to quickly

calculate past patterns of surface water extent from multiple layers of Landsat imagery. The tool consists of a Google Earth Engine application and a user friendly web interface which allows the user to specify the period evaluated and other calculation parameters that are then executed in a cloud service. Results are displayed on screen and can be downloaded for specified areas. An example of this tool is available here: *http://surface-water-servir.adpc.net/*.

Another example of tool is the **WATERS GeoViewer** which is an EPA (Environmental Protection Agency) GeoPlatform based webmapping application (*https://www.epa.gov/waterdata/waters-geoviewer*). It provides acess to data at the national level of the Unites States.

WaMaPro is also a user friendly tool for water surface derivation from SAR data developed at the German Remote Sensing Data Center (DFD) of the German Aerospace Centre (DLR). The tool is described in detail in Gstaiger et al. (2012); Huth et al. (2015); Kuenzer et al. (2013). The method uses simple thresholding and morphological filtering approach to extract water covered areas from the backscatter images. The method requires user intervention for thresholding.

RaMaFlood is tool for semi-automatic flood extent mapping developed by DFD and DLR. It is using an interactive object-based classification algorithm (Martinis et al., 2015b). **The TerraSAR-X Flood Service (TFS) and the TanDEM-X Water Indication Mask processor (TDX WAM)** are water detection tools based on a fully-automatic processing of TerraSAR-X and TanDEM-X images (Martinis, 2010; Martinis et al., 2015b). The Canada Centre for Remote Sensing has developed the **FnFCE (Forest non-Forest Class Extraction) water detection tool** for the automated extraction of water bodies, but this tool only ingests Radarsat images (Short et al., 2009).

NASA's Goddard's Office of Applied Science proposes an automated global daily surface water mapping service (*http://oas.gsfc.nasa.gov/floodmap/*). As one of the first SAR-based services, the **Fast Access to Imagery for Rapid Exploitation (FAIRE)** service hosted on the ESA's Grid Processing on Demand system (G-POD, *http://gpod.eo.esa.int/*) provides automatic SAR pre-processing and change detection capabilities which can be triggered on demand by a user via a web-interface. Automatic

algorithms for medium resolution surface water mapping have been presented by (Schlaffer et al., 2012), e.g. **Fully Automatic Aqua Processing Service/FAAPS**) and (Westerhoff et al., 2013).

Generally, in all countries, surface water database are provided in national topographic database. For instance, there are BD TOPO Hydrography (IGN, 2014) contains hydrographic networks data of France (*http://professionnels.ign.fr/bdtopo*) and the national database of the Irish Environmental Protection Agency (EPA, n.d.) provides river and lakes data of Ireland (*http://www.epa.ie/irelandsenvironment/*) (see Chapter 3).

Conclusions of Chapter 2

Remote sensing technology provides effective ways to observe surface water due to its advantages in acquiring Earth observation information at a range of spatial, temporal, and thematic scales. Optical imagery has been used for many surface water mapping applications due to its straightforward interpretability. Yet, a perfect method that works for all cases has not yet been developed, contributions to the methods are still expected in the future.

The limit in using optical imagery is related to weather conditions. This type of image is sensitive to the presence of cloud cover. Therefore, several methods have been developed in the literature using SAR images. This type of image has more benefits because of its capability to transmit and receives signals in any weather conditions. SAR image can penetrate cloud and sometimes can also penetrate vegetation. Unfortunately, most of the surface water mapping methods based on single-date optical or SAR images require a considerable amount of user intervention. It is not adapted to Sentinel-2 and Sentinel-1 as the new generation of remote sensing data with high temporal resolution. Furthermore, contextual information, such as the correlation among neighboring pixels must be taken into account.

Multi-temporal image analysis has proven their superiority to mono-temporal approaches to extract and monitor surface water. The approach opens the opportunity for surface water monitoring, floods detection, changes detection and to classify surface

water; for example, distinguish permanent surface water and temporary surface water (floods). With the increasing demand of understanding surface water over the world, multiple sources of remote sensing data with long time series can be employed to serve this purpose. However, the studies combining multi-temporal and multi-source approach are still few.

Several databases are mapping surface water areas by using massive processing of optical and/or SAR images times series. Nevertheless, the existing surface water databases are relevant for some applications but do not fulfill all the current needs of the science and water management communities. Therefore another method which can handle multi-source and time series data and provide surface water database must be developed.

The next chapter introduces the datasets, study areas, and pre-processing of Sentinel-1 and Sentinel-2 data.

Chapter 3

Study area, datasets and pre-processing of Sentinel 1&2

Contents

This chapter will provide information about the selected study areas to propose methods in exploiting the new Constellation of Sentinel-1 and Sentinel-2 times series for mapping and monitoring surface water. The **section 3.1** explains the choice of three study cases in Ireland, England and Italy submitted to extreme flooding events. Two others areas of interest are then selected to validate our developments. The satellite image times series used in this study (S1&S2) and the other data used will be presented. The **section 3.2** describes the applied pre-processing procedures for Sentinel-1 and Sentinel-2 images.

3.1 Study area and datasets

In this section, a technical description of the Sentinel 1 and 2 image products (Sub-section 3.1.1) is presented. The selected study sites with the list of remote sensing images (S1 and S2) used and their coverage areas are also presented (Sub-section 3.1.2).

3.1.1 The Sentinel Constellation: Sentinel-1 and Sentinel-2 products

Sentinel-1 is the first of the Copernicus program by the European Commission (EC) and the European Space Agency (ESA). The mission is composed of a constellation of two satellites, Sentinel-1A and Sentinel-1B, placed in the same orbit, with sun-synchronous, near-polar, circular orbit at a height of 693 km. Sentinel-1 offers a C-SAR instrument (see Chapter 1) and it operates in four acquisition modes with ascending and descending geometry:

- Stripmap (SM) provides coverage with a 5 m by 5 m resolution over a narrow swath width of 80 km;
- Interferometric Wide swath (IW) mode combining a large swath width (250 km) with a moderate geometric resolution (5 m by 20 m);
- Extra Wide swath (EW) mode has five sub-swaths and a lower resolution (20 m by 40 m);
- Wave mode (WV) acquisitions are composed of stripmap (20 km by 20 km), acquired alternately on two different incidence angles.

Sentinel-1 in each mode can provide Level-0, Level-1 SLC, Level-1 GRD, and Level-2 OCN data. The SAR Level-0 products consist of compressed unfocused SAR raw data. The product intended for most data users is Level-1 data, which consists of two types, i.e., Single Look Complex (SLC) and Ground Range Detected (GRD). Level-1 SLC products consist of focused SAR data, geo-referenced using orbit and altitude data from the satellite, and provided in slant-range geometry. The products include a single look in each dimension using the full available signal bandwidth and complex samples (real and imaginary). The products consist of amplitude and phase information.

Level-1 GRD products consist of focused SAR data that has been detected, multi-looked and projected to ground range using a terrestrial ellipsoid model. Pixel values represent detected magnitude, while phase information is lost. The resulting product has approximately square resolution pixels and square pixel spacing with reduced speckle, and with thermal noise removed. GRD products can be in one of three resolutions: Full Resolution (FR), High Resolution (HR) and Medium Resolution (MR). The resolution is dependent upon the amount of multi-looking performed. Level-1 GRD products are available in MR and HR for IW and EW modes, MR for WV mode and MR, HR and FR for SM mode.

Level-2 OCN products include components for Ocean Swell spectra (OSW) providing continuity with ERS and ASAR WV and two new components: Ocean Wind Fields (OWI) and Surface Radial Velocities (RVL).

Sentinel-1 instruments supports operation in single polarization (HH or VV) and dual polarization (HH+HV or VV+VH). Wave mode is available in single polarization, while SM, IW, and EW modes in single and dual polarization. (Bourbigot et al., 2016; Cwik, 2017; ESA, 2012). After the literature review about surface water and methods to extract its area (see Chapter 1 and 2), only the data products from **Sentinel-1 Level-1 in IW** mode are used and only high resolution products in **double polarization** (VV+VH) are used. In order to assess the potentialities of the finest spatial resolution images, only the **GRD products** are used for proposed method. In the case of SAR polarimetry experiment, SLC products are used. The spatial resolution of range by azimuth is 2.7×22 m to 3.5×22 m for SLC product while for GRD product, spatial resolution is 20×22 m.

Sentinel-2 mission comprises a constellation of two polar-orbiting satellites (Sentinel-2A and Sentinel-2B) placed in the same orbit, phased at 180° to each other. The coverage limits are from between latitudes 56° south and 84° north. It is wide-swath (290 km), high-resolution and multispectral imaging mission. Its optical instrument samples 13 spectral bands:

- Four bands of Sentinel-2 with 10 m spatial resolution: Band 2 (490 nm), Band 3 (560 nm), Band 4 (665 nm) and B8 (842 nm);
- Six bands at 20 m: Band 5 (705 nm), Band 6 (740 nm), Band 7 (783 nm), Band 8a (865 nm), Band 11 (1610 nm) and Band 12 (2190 nm);
- Three bands at 60 m: Band 1 (443 nm), Band 9 (940 nm) and Band 10 (1375 nm).

The products are available in Level-1C (Top Of Atmosphere (TOA) reflectances). The products at Level-2A (Bottom Of Atmosphere (BOA) reflectance images) can be obtained using the ground segment or by the Sentinel-2 Toolbox. In some areas, Sentinel-2 Level-2A are directly available and can be downloaded from the THEIA - Land Data Center (Theia, 2018). In this research, Sentinel-2 data are used to assess the contribution of high spatial resolution optical data in mapping surface water. In order to utilize the finest spatial resolution, only the **four spectral bands with 10 m** spatial resolution are used (B2, B3, B4 and B8).

3.1.2 Study sites, images used and reference data

Three test areas in Ireland, England and Italy are chosen as the first study areas based on our main research objective, to propose an operational and fully automatic methodology to extract temporary surface water (flooding), detailed in Chapter 4. The selection of these three areas of interest are also based on the availability of reference data (part 3.1.2.1). Test area of Ireland is selected also for mapping permanent surface water, detailed in Chapter 5. The other two sites in Grand-Est and Indonesia are chosen to validate the application of our methodology in some different thematic case study (part 3.1.2.2).

3.1.2.1 Sites of interest for testing developed methodology

In order to assess the results of our proposed method (Chapter 4) in extracting temporary surface water (flooding), we have selected three sites in Europe where the COPERNICUS Emergency Management (EM) Service has been activated during the period 2015 and 2016 (corresponding to the beginning of our research). This service produces flood maps of those sites using ESRI World Imagery, COSMO-SkyMed, Radarsat-2, and other images other than Sentinel imagery. Those flood maps are used in this study for reference data. The data can be downloaded freely from the website: https://emergency.copernicus.eu/mapping/map-of-activations (Figure 3. 1).

Figure 3. 1. Copernicus website to access floods maps.

During the winter 2015 – 2016, three extreme floods events are occurred in Ireland (EMSR149 activation), in England (EMSR150 activation), and in Italy (EMSR192 activation) – Figure 3. 2. Each site is described below and the Sentinel 1 and Sentinel 2 images used are listed.

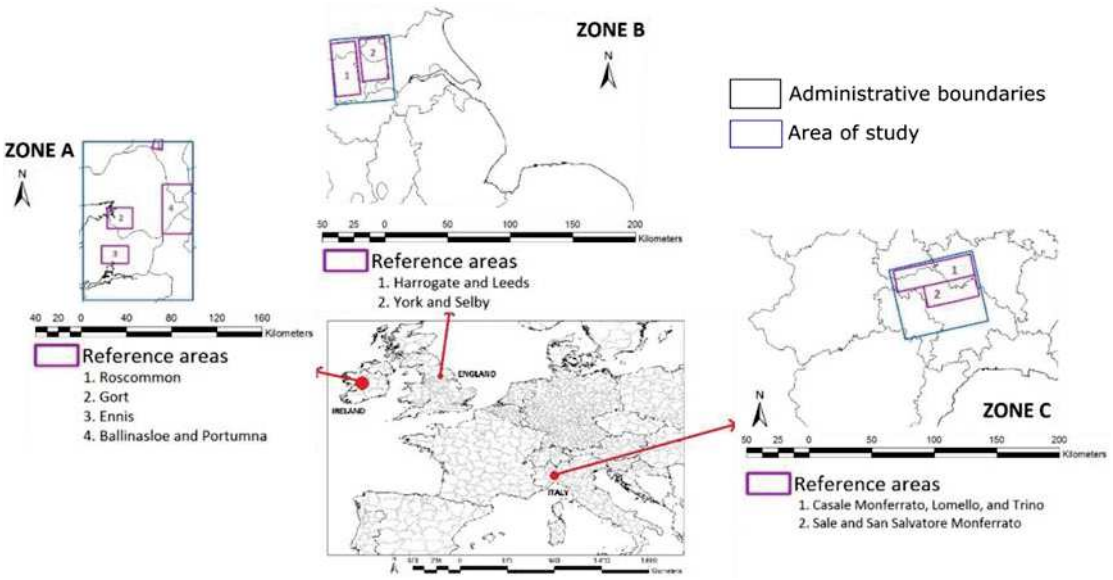

Figure 3. 2. Study areas with extreme flooding events during 2015-2016.

Zone A – Ireland, Zone B – England and Zone C – Italy.

- **Ireland (Zone A)**

The first site is located in Ireland, especially in central areas of the island (Figure 3. 4). During Storm Desmond on the 4th December 2015, heavy rain with a 24 h total precipitation of 160.8 mm was reported at Keenagh Beg (County Mayo, Ireland) (Éireann, 2015). The storm led to a severe flooding event during winter 2015-2016, altering the spatial extent of surface waters for some days. This 100-year record flood event particularly affects the catchment of the Shannon River (Figure 3. 4). Areas such as Ennis, Gort, Roscommon, Ballinasloe, and Portumna had been severely affected. Road networks, grasslands and croplands were submerged during the flooding (National Directorate for Fire and Emergency Management, 2016) (Figure 3. 3). Therefore those areas are of specific interest in our study.

Figure 3. 3. Photos of flood in central area of Ireland (Pollak, 2016).

Figure 3. 4 and Table 3. 1 present Sentinel-1 & 2 coverage areas and the list of images used in Ireland between the end of 2015 and 2016. All Sentinel-1 images are in ascending mode.

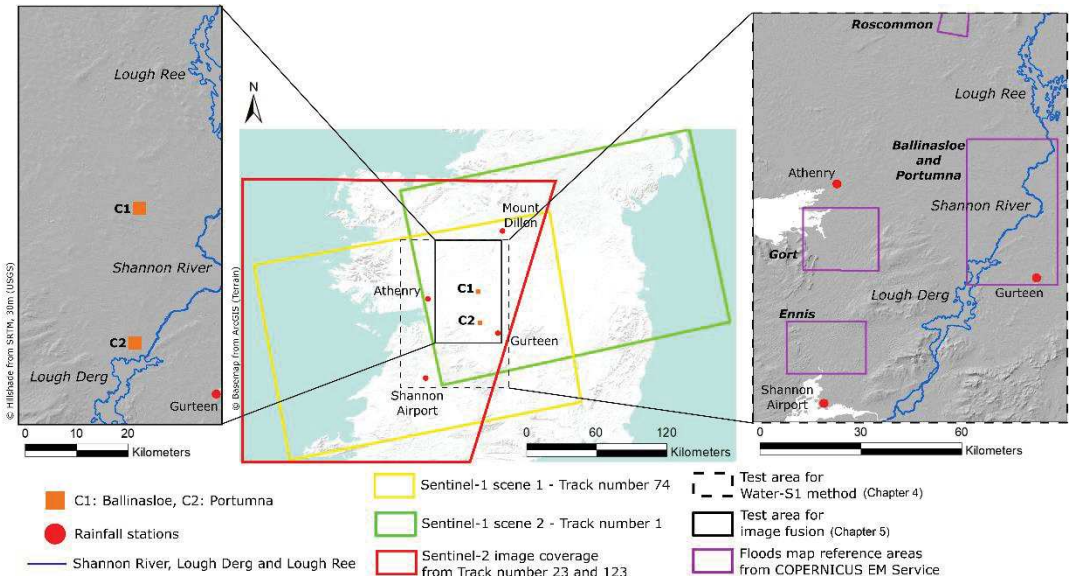

Figure 3. 4. Study area in Ireland with Sentinel-1 & 2 coverage areas.

Table 3. 1. Images used for the Ireland study area.

Track number	Levels	Sentinel-1 acquisition	Time series	Information	Track number	Sentinel-2 acquisition	Cloud cover
74	L1 GRD	22/11/2015	t1	Dry	/	/	/
74	L1 GRD	16/12/2015	t2	Flooding	23	22/12/2015	5.6%
74	L1 GRD	28/12/2015	t3	Dry			
74	L1 GRD	09/01/2016	t4	Flooding	/	/	/
74	L1 GRD	14/02/2016	t5	Dry	/	/	/
74	L1 GRD	26/02/2016	t6	Dry			
74	L1 GRD	09/03/2016	t7	Dry	/	/	/
74	L1 GRD	21/03/2016	t8	Dry			
74	L1 GRD	14/04/2016	t9	Dry	/	/	/
74	L1 GRD	08/05/2016	t10	Dry	/	/	/
1	L1 GRD	08/06/2016	t11	Dry	/	/	/
1	L1 GRD	14/07/2016	t12	Dry	23	18/07/2016	6.6%
1	L1 GRD	19/08/2016	t13	Dry	/	/	/
1	L1 GRD	12/09/2016	t14	Dry	/	/	/
1	L1 GRD	18/10/2016	t15	Dry	/	/	/
1	L1 GRD	30/10/2016	t16	Dry			
					23	06/11/2016	4.5%
74	L1 SLC	16/12/2015	-	Flooding			
74	L1 SLC	09/01/2016	-	Flooding			

For Chapter 4, Sentinel-1 scene 1 (track number 74) images are used in order to process a large area including Roscommon, Ennis, Gort, Ballinasloe and Portumna (Figure 3. 4). Since Chapter 4 is only focused on flooding events, four images of Sentinel-1 IW GRD are used (Sentinel-1 22/11/2015, 16/12/2015, 09/01/2016 and 14/02/2016). Those images include pre-event, during event and post-event images of floods.

This first site is also interesting for testing the methodology as (1) the density of permanent surface waters (e.g. lakes and rivers) is high and (2) the variation in spatial extents over the season is moderated because of the oceanic temperate climate. For those reasons, this study case has been selected to answer our second main research questions related to the potentialities of times series to improve permanent surface water extraction and to monitor flooding. All listed images of Sentinel-1 IW GRD (Table 3. 1) have been used for Chapter 5.

For analysis of multi-source images in Chapter 5, only three cloud-free Sentinel 2 images are available (cloud cover less than 15%). For SAR polarimetry analysis presented in Chapter 6, Sentinel-1 SLC mode is used during the flooding events (16/12 and 09/01/2015).

- **England (Zone B)**

For the second test site, an area in England (activations n ° 150) has been selected. On 22nd December 2015, around three weeks after Storm Desmond, Storm Eva occurred and caused heavy rainfalls (about 215 mm 24h rainfall) in the Yorkshire area (British Geological Survey, 2015). A series of downpours leading to extensive flooding which particularly affected a large zone of West Yorkshire including the city of Leeds was observed (Figure 3. 5). Related to the flooding event, this area become the second area of interest in this study. Figure 3. 6 and Table 3. 2 present coverage areas of England and images used (Sentinel-1 IW image in descending mode and Sentinel-2 image). This study area is used only for Chapter 4.

Figure 3. 5. Photos of flood in England site area (Etherington-Smith, 2015; York Press, 2016).

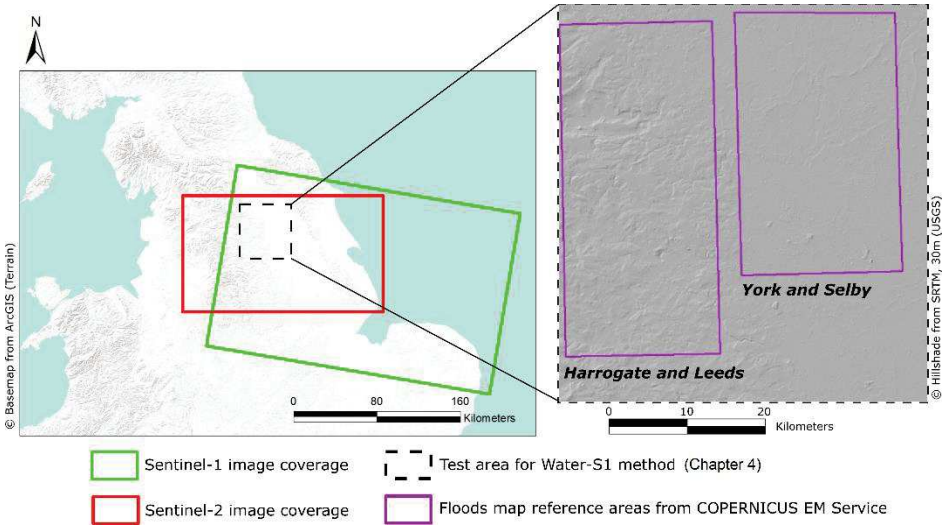

Figure 3. 6. Study area of England with Sentinel-1 & 2 coverage areas.

Table 3. 2. Images used for England.

Track number	Levels	Sentinel-1 acquisition	Information	Track number	Sentinel-2 acquisition	Cloud cover
81	L1 GRD	29/12/2015	Flooding	137	29/12/2015	11%

- **Italy (Zone C)**

In order to validate the methods developments in Chapter 4, a third study case submitted to flooding event has been selected. Starting on 21st November 2016, persistent rainfalls with levels of up to 200 mm in around 12 hours were recorded in some areas of north west Italy (Figure 3. 8). Those areas reported to be facing some of the worst flooding in 20 years. Floods that arise have caused damages and difficulties such as mud deposits, vehicle destruction and road cut-offs. Two deaths were reported and hundreds

of people were evacuated (Copernicus, 2016). Table 3. 3 shows Sentinel-1 IW in descending mode and Sentinel-2 images used in this study.

Figure 3. 7. Photos of flood in Italy site area (euronews, 2016).

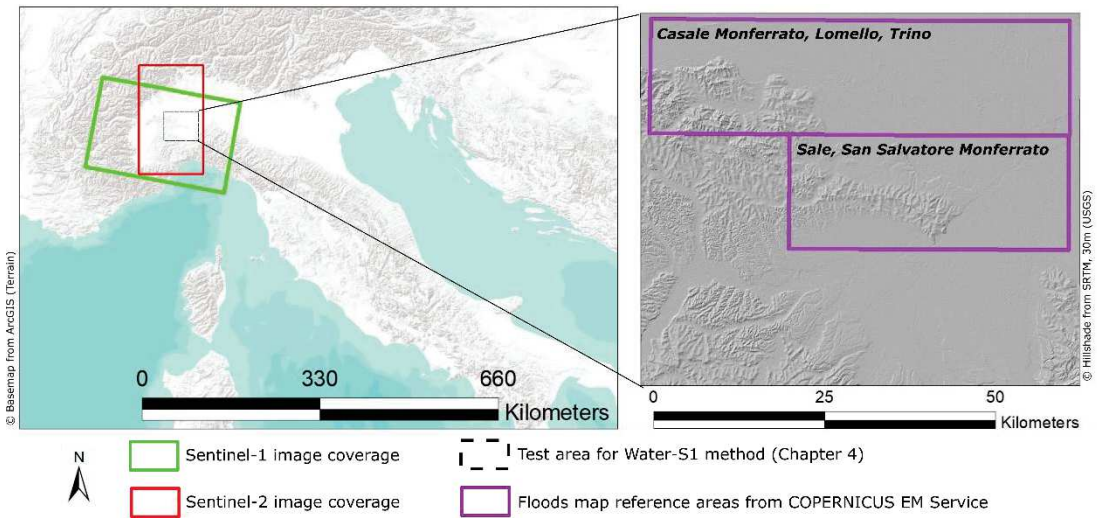

Figure 3. 8. Study area of Italy with Sentinel-1 & 2 coverage areas.

Table 3. 3. Images used for Italy.

Track number	Levels	Sentinel-1 acquisition	Information	Track number	Sentinel-2 acquisition	Cloud cover
66	L1 GRD	28/11/2016	Flooding	65	08/11/2016	3.4%

3.1.2.2 Sites of interest for validation in different thematic context

In order to validate our methodological approach, we decided to select two other areas of interest in two different countries (France and Indonesia).

- **Grand-Est, France: monitoring floods plain**

The first one is related to a recent event of flooding during the winter 2018 in the Grand-Est Region. The objective is to apply the method of Chapter 4 to produce rapidly floods maps around the catchment of the Zorn River (next to Brumath – Figure 3. 10). Another purpose is to apply the time series analysis method of Chapter 5 to extract permanent surface water.

The passage of the Storm Eleanor (Cyclone Burglind) had already brought significant amounts of rain in 2-3 January 2018 and affected Ireland, the United Kingdom, France, the Benelux, Germany, Austria and Switzerland. After the storm, heavy rainfall occurred and caused several overflowing floods in France including the Grand-Est region (CCR, 2018; Mertz, 2018). Data reported that January become unusually wet in Grand-Est region. Surplus of precipitation which is already present at the end of December increased and reached to more than 50%. The data also stated that the minimum river discharge measured in France during the month of January were above normal (eaufrance, 2018).

One of the main river in Grand-Est, the Zorn, was overwhelmed by those strong precipitations and caused inundation in its surrounding areas (Figure 3. 9). On 23 January 2018, data reported that floods occurred in Zorn watershed near to the municipalities of Brumath, Hoerdt and Hochfelden (Sertit, 2018). Zorn River lies in the Moselle and Bas-Rhin departments with 580 km of linear streams. Historically, floods are frequently occurred in the Zorn watershed area. The municipalities of Eschbourg, Brumath and Dossenheim-sur-Zinsel are the most affected floods areas (Conseil Général du Bas-Rhin, 2012).

Figure 3. 9. Photos of flood in Grand-Est site area (Aurélien Willem, 2018).

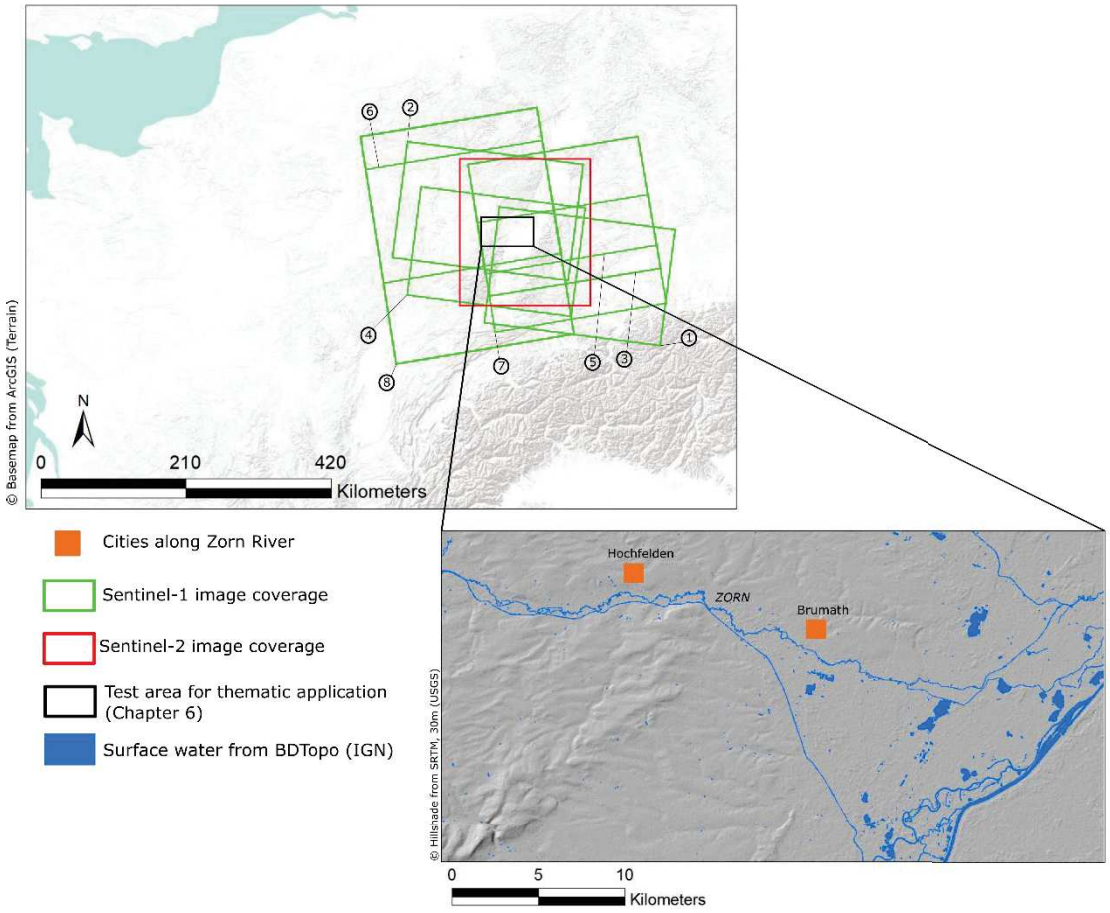

Figure 3. 10. Study area of Grand-Est with Sentinel-1 & 2 coverage areas.

For this application, 11 images of Sentinel-1 IW GRD from short-term periods in 2017 and 2018, with short range intervals, minimum interval is 1 day and maximum interval is 22 days have been downloaded (Table 3. 4). Coverage areas of images used can be seen in Figure 3. 10 with their ID number. Post-events images of Sentinel-2 are only used for qualitative assessment due to no images are available during the floods events.

For quantitative assessment, flood reference map produced by ICUBE-SERTIT is used (Sertit, 2018). The map is produced within the framework of the EUGENIUS H2020 project (European Group of Enterprises for a Network of Information Using Space). The project provides regional (local) small and mid-size flood monitoring service based on the combined exploitation of Copernicus satellite data (especially Sentinel-1 and Sentinel-2) and local data (eugenius, 2018).

Table 3. 4. Images used for Grand-Est.

ID	Track number	Levels	Sentinel-1 acquisition	SAR Acquisition Mode	Information	Track number	Sentinel-2 acquisition	Cloud cover
1	66	L1 GRD	10/10/2014	Descending	Dry	/	/	/
1	66	L1 GRD	15/03/2015	Descending	Dry	/	/	/
2	139	L1 GRD	04/12/2017	Descending	Dry	/	/	/
2	139	L1 GRD	16/12/2017	Descending	Dry	/	/	/
3	15	L1 GRD	19/12/2017	Ascending	Dry	/	/	/
4	139	L1 GRD	22/12/2017	Descending	Dry	/	/	/
5	15	L1 GRD	31/12/2017	Ascending	Dry	/	/	/
6	88	L1 GRD	05/01/2018	Ascending	Flooding	/	/	/
7	15	L1 GRD	06/01/2018	Ascending	Flooding	/	/	/
8	88	L1 GRD	11/01/2018	Ascending	Dry	/	/	/
8	88	L1 GRD	23/01/2018	Ascending	Flooding	/	/	/
6	88	L1 GRD	29/01/2018	Ascending	Dry	/	/	/
4	139	L1 GRD	20/02/2018	Descending	Dry	/	/	/
/	/	/	/	/	/	108	24/07/2018	0.72%
/	/	/	/	/	/	108	03/08/2018	0.64%
/	/	/	/	/	/	108	28/08/2018	4.05%

- **Bengawan Solo (East Java – Indonesia): monitoring river changes**

The last area of interest is located in the Bengawan Solo watershed, especially in the downstream area. This area is situated in East Java, Indonesia and covers the Bojonegoro, Tuban and Lamongan districts. Bengawan Solo River is recorded as the longest and the largest river on Java Island, Indonesia (Figure 3. 11). Thus, this river becomes one of the biggest water resources in Java, Indonesia. Flood occurred almost annually in the Bengawan Solo watershed (Rahmawaty, 2015). On the other hand, based on water resource balances, Bengawan Solo watershed also showed a water deficit (Anna et al., 2017).

The downstream area of Bengawan Solo River is a meeting place of water flow from two sources of the river (sources come from Wonogiri and Ponorogo). That is why this area has the highest flood risk. Another reason is due to erosion in the upstream area of Bengawan Solo River which created sedimentation in the Bengawan Solo downstream.

In addition, damage on the catchment area leads to a decrease in groundwater and increase in surface flow, therefore causing flooding during the rainy season and drought during the dry season. Based on those reasons, this area is specifically interesting in this study for thematic application.

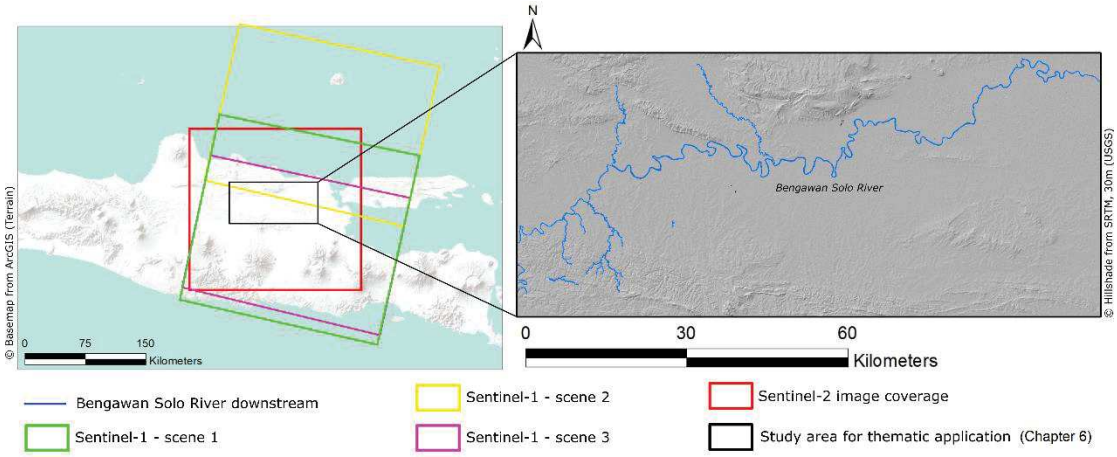

Figure 3. 11. Study area of Bengawan Solo River downstream with Sentinel-1 & 2 coverage areas.

Table 3. 5. Images used for Bengawan Solo.

Scene	Track number	Levels	Sentinel-1 acquisition	SAR Acquisition Mode	Track number	Sentinel-2 acquisition	Cloud cover
1	3	L1 GRD	22/01/2017	Descending	/	/	/
2	3	L1 GRD	15/02/2017	Descending	/	/	/
3	3	L1 GRD	11/03/2017	Descending	/	/	/
3	3	L1 GRD	04/04/2017	Descending	/	/	/
3	3	L1 GRD	10/05/2017	Descending	/	/	/
3	3	L1 GRD	15/06/2017	Descending	/	/	/
3	3	L1 GRD	09/07/2017	Descending	/	/	/
3	3	L1 GRD	14/08/2017	Descending	89	07/08/2017	0.08%
3	3	L1 GRD	07/09/2017	Descending	/	/	/
3	3	L1 GRD	13/10/2017	Descending	/	/	/
3	3	L1 GRD	18/11/2017	Descending	/	/	/
3	3	L1 GRD	12/12/2107	Descending	/	/	/

For Bengawan Solo River downstream, 12 images of Sentinel-1 IW GRD are used. Those images were obtained in a one year period (2017), with one image for each month (Table 3. 5). Coverage areas of the images used can be seen in Figure 3. 11. The test areas are also represented in Figure 3. 11. For the study area of Bengawan Solo, Sentinel-2 image is used only for qualitative assessment.

3.1.3 Other reference data

Some other reference data are used in this research as complementary data to explore or sample surface water and to improve our methods. Usually, these data come from National Reference Structure such as IGN for France or Environmental Protection Agency (EPA) for Ireland. Two types of data have been used: (1) national topographic database and (2) Digital Elevation Model (DEM), rainfall and in-situ data.

3.1.3.1 National Topographic database

The BD TOPO (thematic – Hydrography) (IGN, 2014) serves as reference data for preliminary statistical analysis in surface water detection (Section 3.2). The data contain hydrographic networks such as streams, water bodies, reservoirs and water points. BD TOPO is exploitable at scales ranging from 1: 5,000 to 1: 50,000 and has maximum accuracy 0.5 m. The data are used for making training sample classes and also for accuracy assessment.

The national database of the Irish Environmental Protection Agency (EPA, n.d.) provides water data such us river networks and lakes in Ireland with scale either be 1:250,000 or 1:1,000,000. This data are used for visual comparison with another surface water products and surface water extracted from proposed method in Chapter 5.

Topographical map from the Indonesian Geospatial Information Agency (BIG, 2017) is used for the thematic application in Indonesia. This map provides land use classes with a map scale of 1: 25,000. Water class and irrigation croplands class from this map are needed to assess and analyze the result.

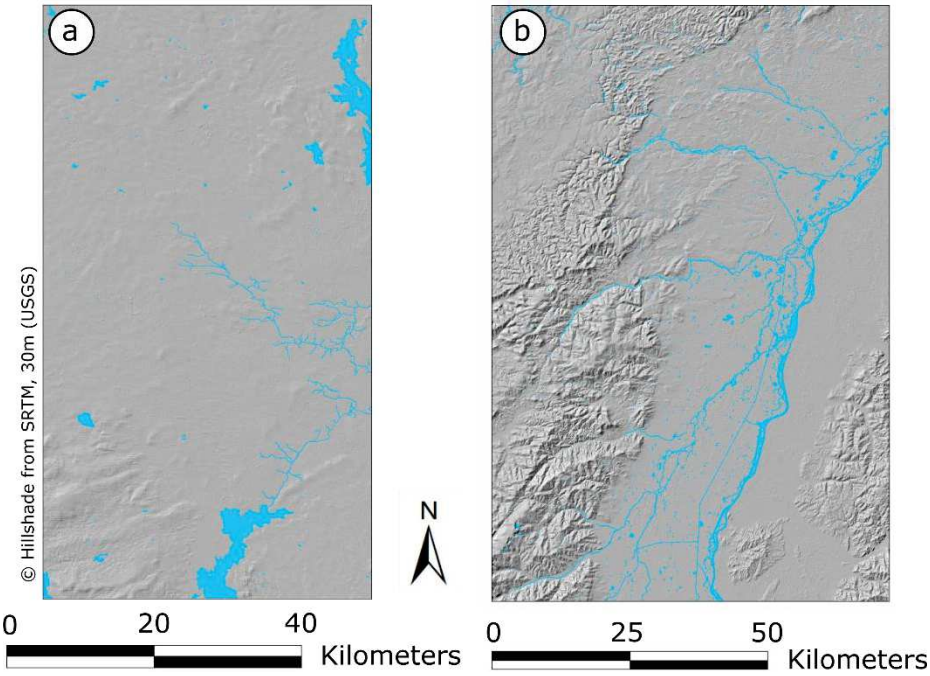

Figure 3. 12. Examples of national database of surface water: (a) River and lakes from Irish EPA in Ireland study area, (b) Surface water database from BD TOPO IGN in Grand-Est study area.

3.1.3.2 Global Topographic database of surface water

For the evaluation of permanent water result, the Water and Wetness product by EC-COPERNICUS is used as the reference (see Chapter 2 – Section 2.4). The Water and Wetness product derived permanent water class for the 2015 reference year. The class consists of permanent inland lakes (natural), artificial ponds (permanent fish ponds, reservoir), natural ponds (permanent open surface waters), rivers, channels (permanently with water), liquid dump sites (permanent) and surface waters with floating vegetation which are detectable using remote sensing techniques (Langanke, 2016).

3.1.3.3 SRTM 30-meter Digital Elevation Model

SRTM (Shuttle Radar Topography Mission) version 3, 1 Arc-Second Global is used in this study. This SRTM data is a type of Digital Elevation Model (DEM) which can be downloaded for free in (USGS, n.d.). SRTM data are generated from SIR-C/X-SAR

instruments which has an approximate altitude of 233 km. The specifications of SRTM version 3 are 30 m x 30 m of spatial resolution with ≤ 16 m absolute vertical height accuracy, ≤ 10 m relative vertical height accuracy and ≤ 20 m absolute horizontal circular accuracy.

From SRTM data, Height above Nearest Drainage (HAND) can be generated. HAND is a new quantitative topographic algorithm in the form of terrain index based on the drainage network (Donchyts et al., 2016; Nobre et al., 2011; Rennó et al., 2008). HAND is used to account for limitation of surface waters area. With HAND, false positive of surface water detections which are located high above the nearest drainage line can potentially be removed.

3.1.3.4 Other statistical data

For the temporal analysis in Chapter 5, **rainfall data** is collected. It was taken from four stations (Shannon airport, Gurteen, Athenry, and Mount Dillon) in Ireland at November 2015 until October 2016 (Éireann, n.d.). Those stations were chosen because they are located in and around the Ireland study area. The rainfall data can be downloaded freely in Met éireann, The Irish Meteorological Service (https://www.met.ie/climate/ available-data/monthly-data).

In Chapter 6, river discharge estimation is performed for the Bengawan Solo river, especially in the downstream area. For the result validation and comparison, **in-situ measured data** from PUSDATARU Central Java Indonesia (PUSTADARU, 2017) is used. This in-situ data can be accessed on Open Data - PUSTADARU (https://pusdataru.jatengprov.go.id/).

3.2 Pre-processing of Sentinel-1&2 data

The objective of this section is first to explore the potential of Sentinel-1 image related to surface water detection (**Sub-section 3.2.1**). Sentinel-1 is free available satellite images in C-band which has higher revisit time than the other free SAR images.

Potentially, it can increase capabilities to detect surface waters and flood, also monitoring their change. However, only a few studies investigate the usefulness of the C-band Sentinel-1 sensor mission for surface water extraction (Huang et al., 2018; Martinis, 2017). In this context, we made some evaluations to explore and define:

(a) The Minimum Unit Area
(b) The optimal polarization mode
(c) The optimal feature
(d) The influence of speckle filtering

Based on these results, pre-processing steps will be applied on Sentinel 1 amplitude data (**Sub-section 3.2.2**). Finally, pre-processing steps for Sentinel 2 is detailed (**Sub-section 3.2.3**).

3.2.1 Analysis / Parameters of Sentinel-1 data

a. Identification of the Minimum Unit Area (MUA)

Surface water in Sentinel-1 images cannot be extracted if the area is too small. The area of one pixel on Sentinel-1 IW GRD high resolution image is approximately 440 m2. One pixel is not enough to label it as surface waters. Water areas can be detected from Sentinel-1 images in the form of pixel sets. In this research, using some sample classes, the spatial ability of Sentinel-1 to detect surface water will be tested in order to define MUA. These tests have been performed on the study area of Grand-Est with Sentinel-1 IW GRD in 2014 and 2015 (Table 3. 4) because it constitutes a well-documented area in term of existing topographic database (see part 3.1.2.1).

Three sample classes of surface water are defined based on their area or number of pixels:

1) Surface water with area of less than 0.5 ha. The value of 0.5 ha is determined based on area estimation of 10 pixels;
2) Surface water with area of more than or equal to 0.5 ha but less than 1 ha. This class is determined based on area estimation of more than 10 pixels to ± 25 pixels;

3) Surface water with area of more than or equal to 1 ha but less than 1.5 ha. This class is determined in order to test if area of 1 ha or more can be extracted from Sentinel-1 image.

One sample class of non-surface water (land) is created in order to observe its separability with sample classes of surface water. All samples are created using BD TOPO IGN as mask to extract pixel values from the sigma-nought image of Sentinel-1 (10/10/2014) VV polarization (see **part b** below). Pixels' values distribution from the extraction results are then compared based on their type of classes (Figure 3. 13).

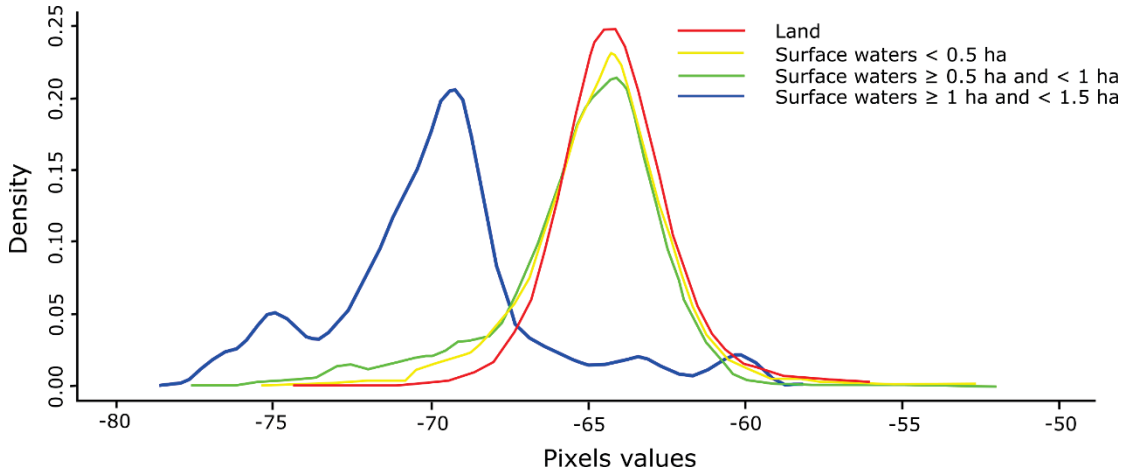

Figure 3. 13. Comparison of pixel values distribution from each sample class.

From those graphs, it can be seen that two sample classes of surface water with area of less than 1 ha have a distribution range value of almost the same as the land sample class. Only the surface water class with area of more than or equal to 1 ha but less than 1.5 ha has separate distribution from the land sample class. Thus, it can be concluded that with the spatial resolution of Sentinel-1 image, detection of surface water with area of less than 1 ha will be difficult. Consequently, for quantitative assessment of surface water mapping results, only **areas greater than or equal to 1 ha** will be retained in the reference maps.

b. Comparison between VV and VH polarizations

Polarization choice plays a role in detecting surface water. In general, HH polarization provides the most obvious discrimination between surface water and other types of land cover classes (Henry, 2004; Pulvirenti et al., 2012; Yamazaki et al., 2013). Low

scattering of the horizontal component signal from the open water made vivid separability between water and non-water area. HH and VV as co-polarizations lead to nearly identical separability of class distributions over a smooth open water area. However, an increase in surface roughness reduces the ability to discriminate between water and land in VV more than in HH polarization. Over smooth open water area, co-polarization offers improved class separability in comparison to cross-polarization (Martinis, 2010).

Several researches denote the superiority of the cross-polarization of HV and VH (Henry, 2004; Solbø and Solheim, 2005) over co-polarization VV in terms of a rough open water. That is why a VV polarized signal is more sensitive to ripples and waves. Combining backscatter variations in different polarizations could potentially improve the accuracy of surface waters mapping. However, multi-polarization can cause a reduction in resolution and coverage.

The Sentinel-1 IW used in this study consists of two polarizations, i.e. VV and VH. With the intention of focusing in temporal observation in the next discussion, we will limit our study in just one type. Consequently, it is necessary to analyze both VV and VH polarizations in order to determine which polarization type will be used in this study for water and non-water separation.

In order to compare between VV and VH polarization, two Sentinel-1 GRD images acquired in 10/10/2014 and 15/03/2015 are used. Preliminary test is done by performing manual thresholding method to extract surface water from sigma-nought of those images. Water model and land model were calculated from sigma nought images using finite mixture model (Benaglia et al., 2009). Afterwards, the threshold is determined based on the intersected values between the two models. In this process, the histogram of pixel distribution values become important in relation to model building in finite mixture models. Therefore, in the selection of the polarization type, the histogram and models are the main things to be considered.

Table 3. 6 presents the histograms of pixel value distributions from sigma-nought images VV and VH in two different dates. Those histograms and blue lines showed bimodal distribution which is very important in creating the two different models. Table

3. 6 also denotes water and land fitted models in a density distribution. Water model is showed in red density line while land model is in green lines.

Table 3. 6. Histograms and fitted models of sigma-nought images.

Sigma-nought	Histograms	Fitted Models
10/10/2014 VV	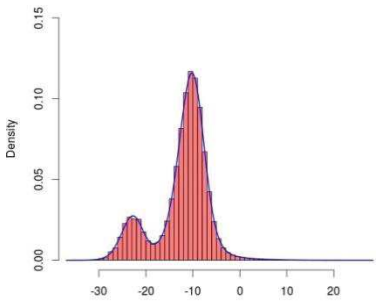	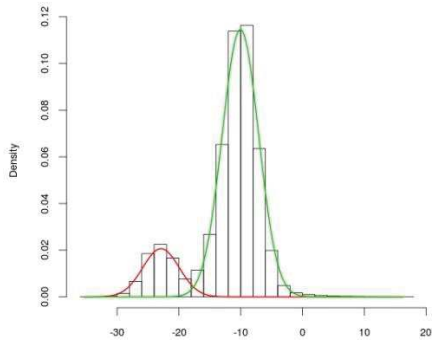
10/10/2014 VH	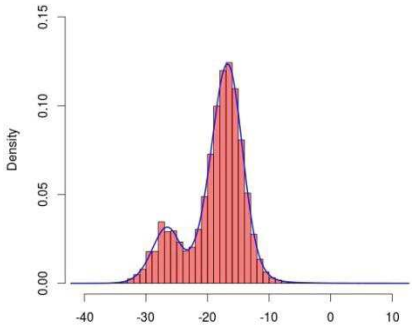	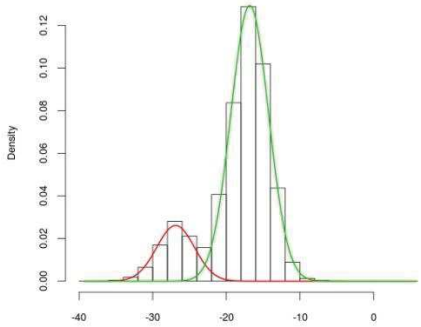
15/03/2015 VV	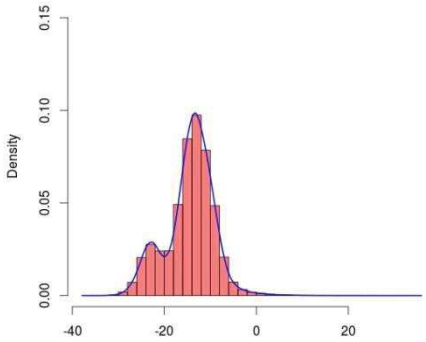	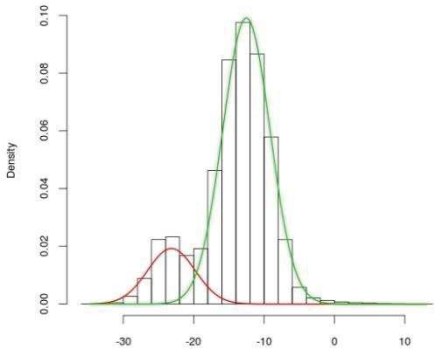
15/03/2015 VH	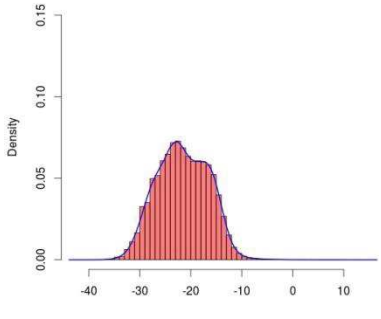	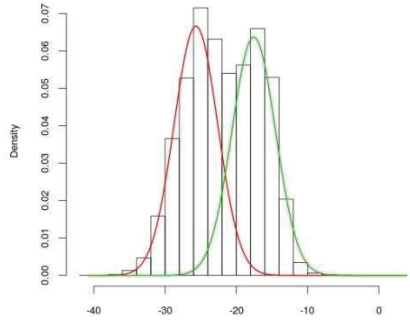

The histogram of sigma-nought VH 15/03/2015 has a different pattern with the other histograms. Another histograms indicated very clear bimodal distribution, while this histogram looks almost like unimodal distribution. Two peaks of the histogram are very close. The different patterns of the histograms made different patterns in fitted models. The histogram from sigma-nought VH 15/03/2015 make it difficult to create two models. Difficulty in creating two models will affect the determination of the threshold value. In the case of sigma-nought VH 15/03/2015, the separability between two classes would produce many errors, because the histogram distribution did not show a separation in its pattern.

Quantitative analysis to compare VV and VH polarizations can be done using ROC (Receiver Operating Characteristic) calculation (Fawcett, 2006). The results can be seen Table 3. 7. ROC calculations produce two parameters, namely the True Positive Rate (TPR) and the False Positive Rate (FPR). ROC shows better result than the others if it has higher True Positive Rate and lower False Positive Rate (Fawcett, 2006).

Table 3. 7. ROC calculation results.

Sigma-nought images	Threshold	FPR	TPR
10/10/2014 VV	≤ -17.8	1.45%	89.22%
10/10/2014 VH	≤ -23	1.93%	91.52%
15/03/2015 VV	≤ -19.8	0.97%	89.55%
15/03/2015 VH	≤ -21.8	43.88%	94.66%

From Table 3. 7, it can be seen that VH polarization tends to have higher TPR. However, we can notice the percentage of FPR value for sigma-nought VH 15/03/2015 is very high compared to another images (about 44%), while the difference in TPR values are only about one until three percent between VV and VH. VH polarization also tends to have an irregular histogram which make it difficult to build models which subsequently causes errors in the surface water extraction results. Accordingly, in this study, **VV polarization is selected** as data input for subsequent processes.

c. Selection of optimal feature for surface water mapping

Some features can be extracted from Sentinel-1 (10/10/2014) GRD image in VV polarization. In this section, five features are extracted. Two features are calculated directly from raw data of Sentinel-1 GRD image (1- amplitude and 2- intensity images). Three others features are produced by radiometric calibration: 3- sigma-nought, 4- beta-nought and 5- gamma images (Figure 3. 14).

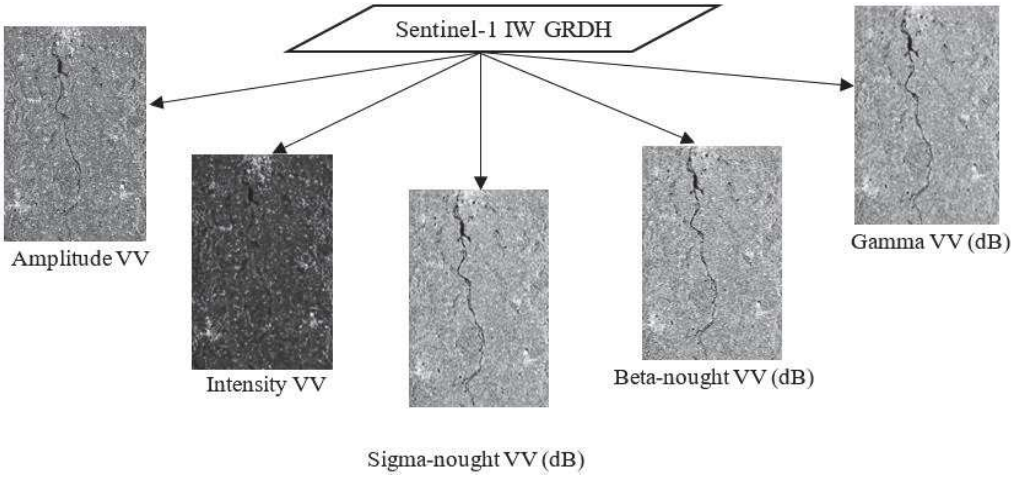

Figure 3. 14. Original and calibrated products from Sentinel-1 IW GRDH image.

Correlation analysis (Gogtay and Thatte, 2017) which describes the connection (strength and direction) between variables (two by two) is then computed in order to observe the relationship between features (Table 3. 8). High values in correlation analysis result mean strong connection between both variables. If the features within have high correlation between each other, use of all features will be useless, because the features will not have unique values which can completed with each other. However, if there are features with low correlation values between each other, those features can be used for next processing.

The results show very high correlation values between features. There are no low values of correlation between features. As a consequence of this condition, it would be more effective if only one feature is used. In this case, **sigma-nought is chosen** because it is the power returned to the antenna from the horizontal (ground) plane and is thus in the realm of ground range (Sarmap, 2009). That condition is very appropriate with the type of Sentinel-1 data used in this study (GRD products). Furthermore, the sigma-nought is a calibrated product which is better than non-calibrated products (in terms of amplitude and intensity). Many studies used sigma-nought for surface water mapping

from SAR data and described the capabilities of this feature (Lee et al., 2015; Matgen et al., 2010; Pulvirenti et al., 2012; Schlaffer et al., 2012).

Table 3. 8. Correlation between features observed from water and land sample classes.

Parameters	Correlation	
	Water	Land
Sigma - Beta	0.9999954	0.9999493
Sigma - Gamma	0.9999958	0.9999496
Sigma - Amplitude	0.9999818	0.9997938
Sigma - Intensity	0.9999818	0.9997938
Beta - Gamma	0.9999824	0.9997977
Beta - Amplitude	0.9999955	0.9999476
Beta - Intensity	0.9999955	0.9999476
Gamma - Amplitude	0.9999601	0.9995395
Gamma - Intensity	0.9999601	0.9995395
Amplitude - Intensity	1	1

d. Influence of speckle filtering in surface water areas

One common problem of SAR data is the appearance of speckle noise. It appears as random spots of images with bright and dark spots which can degrade the image quality and reduce its potential for interpretation (Lee and Pottier, 2009). Sentinel-1 imagery also has speckle noise in their raw data. One of the approaches to reduce speckle noise is speckle filtering. In speckle filtering, there are many methods, for example mean, median, Lee, etc.

Some of speckle filtering methods have been analyzed in order to understand the best method which can be used in the pre-processing procedure (Sub-section 3.3.2). Analysis is performed by calculating the filter evaluation index (ENL and speckle index) of surface water areas after filtering (Huang and Genderen, 1996; Wang et al., 2012). In this evaluation, sample class is used as a mask to determine the boundary of surface water areas. The observation is conducted with two different values of parameters for each spatial filtering method (Table 3. 9).

Table 3. 9. Statistical characteristics and filter evaluation index of filtered images in surface water area.

Method	Windows Size / Description	Mean	Standard deviation	ENL	Speckle Index
Mean	3x3	-73.7116	4.2255	304.3100	-0,0573
	5x5	-73.2597	4.3316	286.0402	-0,0591
Median	3x3	-74.1611	3.9887	345.6955	-0,0538
	5x5	-74.1693	3.6993	401.9880	-0,0499
Gamma Map	3x3	-73.7129	4.2233	304.6343	-0,0573
	5x5	-73.1263	4.4423	287.5962	-0,0607
Lee	3x3	-73.7123	4.2243	304.4844	-0,0573
	5x5	-73.2643	4.3251	286.9367	-0,0590
Frost (k:2)	3x3	-73.8231	4.1135	322.0718	-0,0557
	5x5	-73.7409	4.0095	338.2488	-0,0544
Refined Lee	3000	-73.5072	4.1872	308.1866	-0,0569
	5000	-73.5069	4.1889	307.9346	-0,0570

Table 3. 9 describes the statistical characteristics (mean, standard deviation) and filter evaluation index (ENL, speckle index) of the filtered images of the surface water area. The higher value of ENL (Equivalent Number of Looks) for a filter means the higher the efficiency is in smoothing speckle noise over homogeneous areas. The smaller the speckle index means the less speckle noise is left in the images. From Table 3. 9, the median method using a window of 5x5 pixels has the higher ENL value and smaller speckle index value. Therefore, **Median 5x5** will be used as the speckle filtering method in this study.

Speckle filter with median method is one of the filtering methods using kernel. It replaced the pixel value with the median value of the neighboring pixels. The median value is calculated by sorting pixel values from the surrounding neighborhood into numerical order and replacing the pixel value with the center pixel value. If neighboring pixels consist of an even number, the median value will be determined by the average of two central pixel values. Because of its robustness, if there is one single pixel in the neighborhood with an unrepresentative value, it will not affect median value. The median filter did not create any new pixel values; as it uses the pixel value from one of

the neighboring pixels, it will not produce unrealistic values when filtering around the edges. Consequently, the median filter is better at preserving sharp edges than the mean filter (Saxena and Rathore, 2013).

For summarizing, the analysis performed in this sub-section allows us to define some parameters of the Sentinel 1 amplitude data. The VV polarization, with the sigma-nought features from Sentinel-1 GRD images will be used to assess the potentiality of Sentinel-1 in extracting surface water areas around 1 ha. For the next section, in the pre-processing procedure, the median filter with a 5x5 size will be used for spekle filtering.

3.2.2 Pre-processing steps of Sentinel-1 amplitude data

Image pre-processing is applied to each Sentinel-1 IW GRD dataset in order to reduce **orbital errors, speckle noise, and geometric distortion** (Figure 3. 15).

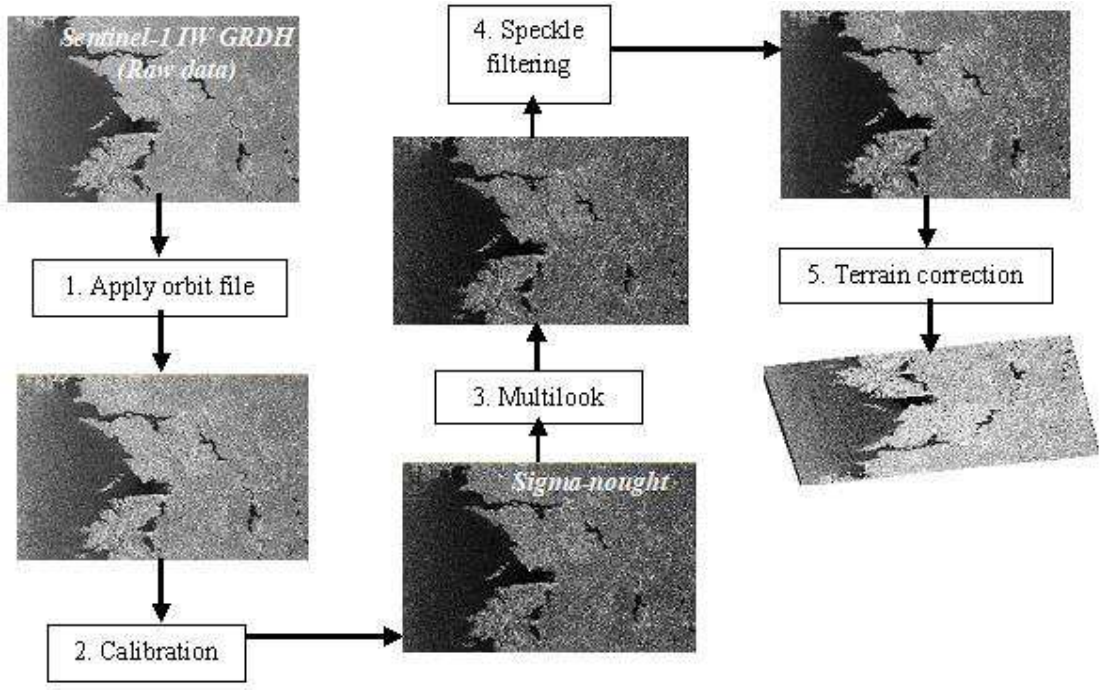

Figure 3. 15. Step by step in pre-processing of Sentinel-1 GRD (amplitude data) and their results visualization.

The **first processing step** comprises the application of precise Sentinel orbits, which can be obtained from SNAP (Sentinel Application Platform) (Foumelis, 2015; Stewart,

2016) and considerably improve the geolocation accuracy. Sentinel-1 data actually have some problems with their orbit information in metadata. This problem caused a non-accurate effect when they are superimposed. Thus to be able to overcome this problem, orbit data of Sentinel-1 images must be updated with available orbit file data. This step called **apply orbit file**.

In the **second step**, to transform raw amplitude images to **calibrated products** for the quantitative use of SAR images, we used also SNAP software. Based on discussion above (Sub-section 3.2.1) sigma-nought was selected among available calibrated products from SNAP, such as amplitude, intensity, beta-nought, and gamma.

In the **third and fourth steps**, in order to reduce speckle noise, **multilook and speckle filtering** with a Median filter and window size of 5 × 5 pixels were used based on discussion above (Sub-section 3.2.1).

Subsequently, in the **fifth step**, **Range Doppler Terrain Correction** is applied to geocode the images. Some reasons can cause distortion of distance in SAR images. For example diverse topographic in scene from satellite's sensors which produce SAR effects (e.g. layover, shadow, foreshortening). The other reason is the tilt of the satellite sensor. Those are the examples of causes in image distortion, generally where image data lie not directly at the sensor's nadir location. In order to solve these distortions, terrain corrections are performed (Mahapatra and Hanssen, 2011).

In the terrain correction step, radiometric normalization is done in order to minimize the influence of the local incident angle on the image (Warner et al., 1996). It is important, because local incident angle can affect the value of backscattering image. The same object, if the value of local incident angle is different, it can create different backscattering value. Thus, radiometric normalization is carried out. Radiometric normalization applied in this study is based on method proposed by (Kellndorfer et al., 1998) with equation as shown below.

$$\sigma^0_{NORM} = \sigma^0_{ELLIPSOID} \frac{\sin \theta_{DEM}}{\sin \theta_{ELLIPSOID}} \qquad (3.1)$$

Where θ_{DEM} is described as the angle between the incoming radiation vector and the projected surface normal vector into range plane. In the implementation, it is the local incidence angle projected into the range plane (Schreier, 1993).

In the Figure 3. 15, SAR image will appear upside down before terrain correction process. The geometry provided in that image is represented by a collection of backscattering ordered in time, both in azimuth and range. SAR image presented in Figure 3. 15 is in ascending mode, thus it appears north-south flipped. If SAR image is in descending mode, it will appears east-west flipped. Terrain correction make image projected geographically correct and fix that orientation issue.

3.2.3 Pre-processing steps of Sentinel-2 data

Image pre-processing is applied to each Sentinel-2 data in order to obtain **Bottom of Atmosphere (BoA) values, remove cloud and shadow areas and obtaining water index** (Figure 3. 16).

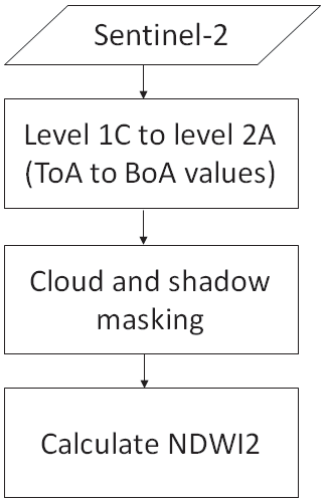

Figure 3. 16. Pre-processing steps of Sentinel-2 data.

In the **first step**, the Sentinel-2 **level 1C (Top of Atmosphere (ToA) values) are corrected to level 2A (BoA values)** using Sen2Cor tools available in SNAP (Louis et al., 2016). The correction must be done to remove the effects of all gaseous and aerosols properties of the atmosphere from the image. The result has BoA and can be used to extract accurate spectral information from features on the Earth's surface.

The **second step** is **cloud and shadow masking**. As been stated before, optical data are sensitive to cloud cover which can also produce shadow area in the image. Cloud and shadow masks can be obtained from Scene Classification product resulted in Sentinel-2 level 2A. Those masks can be used to remove cloud and shadow areas from image in order to get accurate result.

The **third step** consists of **NDWI2 calculation**. Normalized Difference Water Index (NDWI) may refer to one of at least two remote sensing-derived indexes related to liquid water. The first one is used to monitor changes in water content of leaves, using near-infrared (NIR) and short-wave infrared (SWIR) wavelengths. The second one is used to monitor changes related to water content in water bodies, using green and NIR wavelengths. NDWI2 (Equation 3.2) is the name in SNAP sofware which calculate water index using the second combination. This index classically used to extract surface water (Du et al., 2016; McFeeters, 1996), calculated at 10 m spatial resolution and is used for feature extraction.

$$\text{NDWI2} = \frac{(B3 - B8)}{(B3 + B8)} \tag{3.2}$$

where B3 is the green band and B8 is the near-infrared band.

This chapter presented the datasets necessary for performing surface water mapping in this study. The technical description of the datasets were presented. The study areas were described and the background about the selected study areas were provided. Lists of Sentinel-1 and 2 used in this study were presented. Their coverage areas were also provided. The pre-processing of Sentinel-1 image including its exploratory analysis were presented. The pre-processing of Sentinel-2 imagery was also detailed. The next chapter will introduce the Water-S1 method developed for Sentinel-1.

Chapter 4

Detection of surface water area using mono-date Sentinel-1 amplitude data

Contents

The previous chapter provided information about the datasets necessary for performing surface water mapping. It described the selected study areas and presented lists of Sentinel-1 and 2 images used in this study. It also presented softwares used and pre-processing of Sentinel-1 amplitude data. This chapter will present the automatic mapping of surface water (the Water-S1 method) developed for Sentinel-1 image processing.

This chapter was written based on an article published in the Remote Sensing MDPI journal 2018 volume 10, issues 2*: A Method for Automatic and Rapid Mapping of Water Surfaces from Sentinel-1 Imagery (Bioresita, F., Puissant, A., Stumpf, A., and Malet J.P., 2018)*. Some redundancies can then appear in this chapter.

4.1 Introduction

Several SAR-based water detection algorithms have been proposed in the literature (see Chapter 2). Among the methods, thresholding is the most commonly adopted method for SAR image analysis to discriminate water and non-water areas. However, based on discussion in Chapter 2, it is difficult to determine the optimal threshold value for a scene/landscape, which implies the need for user intervention.

The number of SAR-based water detection algorithms and automatic flood mapping services has increased in the last years (see Chapter 2). In most cases, a certain amount of user interaction is needed for data collection, pre-processing, and integration of auxiliary data in the processing pipelines. Hence, while several semi-automatic and automatic tools already exist, there are, to the best of our knowledge, currently only a few scientific references which present a fully automatic water detection processor for surface water mapping from Sentinel-1 imagery (Clement et al., 2017; Martinis, 2017; Twele et al., 2016). This method uses thresholding on individual pixels ignoring the correlation among neighboring pixels. Considering that individual pixels are not independent random variables but form a random field (Schindler, 2012), the potential to improve the accuracy of the flood extent maps exists.

The objectives of this chapter are thus (1) to investigate the use of bilateral filtering as a smooth labeling method for defining the thresholds; (2) to integrate hydrologic/topographic information in the detection using the 'Height above nearest drainage' (HAND) index (Rennó et al., 2008); and (3) to quantitatively evaluate the accuracy of our proposed fully-automated SAR-based water detection algorithm for Sentinel-1 data.

4.2 Methods

Three test areas are used in this chapter i.e., Ireland, England and Italy. Lists of images used have been detailed in Chapter 3. In order to assess our results, floods maps from COPERNICUS EM Service (Copernicus, n.d.) are used.

The automatic processing chain proposed in this chapter is described in Figure 4. 1. It includes five components: (i) pre-processing of raw Sentinel-1 data which has been detailed in Chapter 3, (ii) a tiling approach in order to focus on water surface areas automatically, (iii) class modeling with Finite Mixture Models (Benaglia et al., 2009) to produce probability map based on established class models, (iv) bilateral filtering (Schindler, 2012) for smooth labelling, and (v) post-processing and accuracy assessment.

In this chapter, we try to compare two scenarios of the processing chain based on the use of the HAND map. In the first scenario, the HAND index is applied in the pre-processing step to limit the considered area for the next processing step in order to avoid misclassification. In the second scenario, the HAND index is used as a final post-processing step for the amount of misclassified areas in the surface water maps. Moreover, we also perform a sensibility analysis of tile size used for the tiling approach in order to find a suitable tile size to be used in the processing.

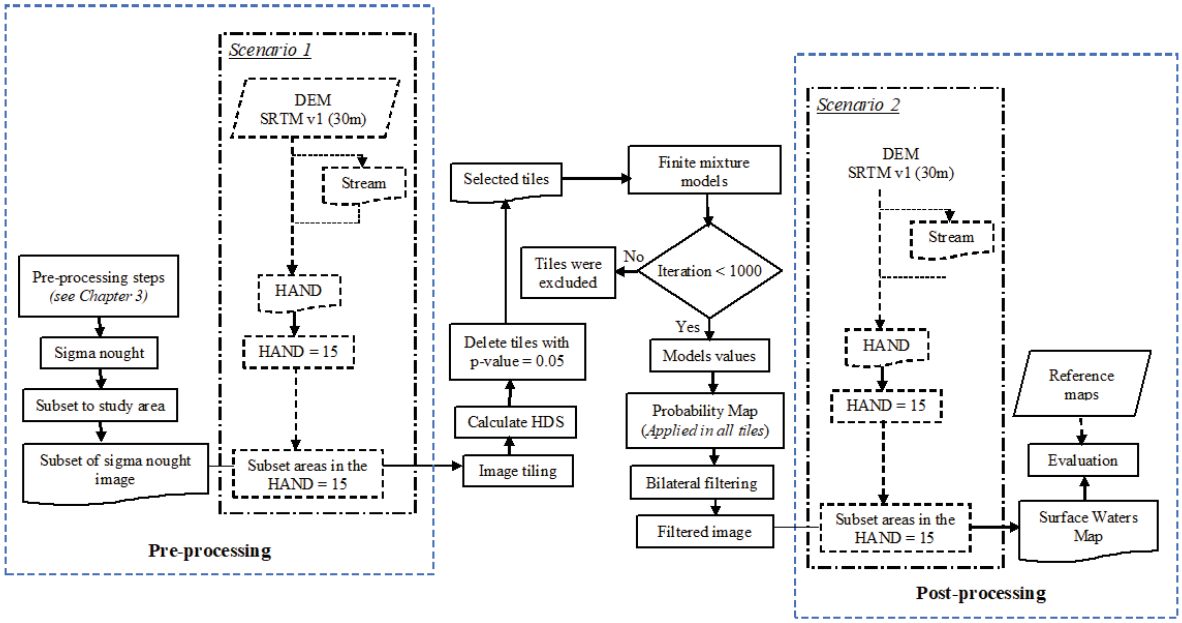

Figure 4. 1. Flowchart showing the overall proposed methods.

4.2.1 Processing chain

4.2.1.1. Image tiling using a Modified Split-Based Approach (MSBA)

A Split-Based Approach (SBA) was originally proposed by (Bovolo and Bruzzone, 2007) for flood detection with Radarsat images. This approach comprises a tiling of the satellite imagery into smaller sub scenes of a user-defined size and a successive local thresholding analysis. The approach's performance has been confirmed in many studies for automatic mapping in remote sensing, (e.g., Chini et al., 2015; Martinis et al., 2009). The original SBA approach relies on the coefficient of variation to pre-select tiles for further processing and a global thresholding method to produce binary maps of surface water coverage. As noted by the authors, global thresholding methods are well adapted for small scene extents but face problems for the larger scene extents of Sentinel-1 with higher backscatter variances resulting from variations in the incidence angle.

To address this issue, we proposed a modified split-based approach which only applied pre-selection tiles for class modelling. Images are first automatically tiled into squared non-overlapping blocks. The tiles selection is then performed to choose only image tiles, which contain some portion of surface waters. This selection is based on

Hartigan's dip statistic (HDS) value (Freeman and Dale, 2013). The underlying hypothesis is that tiles with surface waters and land areas have bimodal grey-value distributions. HDS is used to distinguish between tiles with unimodal and bimodal distributions. P-values resulting from the HDS test are considered with values less than 0.05, indicating statistically significant bimodality (Freeman and Dale, 2013). Thus, only tiles with a p-value of less than 0.05 will be used for the subsequent class modelling with finite mixture models. In this context, it is important to note that this processing step only concerns the pre-selection for the class modeling, whereas the entire image is processed for the generation of the final water surface maps.

4.2.1.2. Class modelling with Finite Mixture Models (FMM)

The Finite Mixture Models represent the existence of subclass diversity with a limited number of distributions. They allow the decomposition of probability distributions into subgroups assuming that the observed distribution is the result of a mixture of sub-populations which are distributed according to a particular form (i.e., Gaussian). A popular method for modeling the parameters of the probability distributions contributing to the mixture is Expectation-Maximization (EM) (Benaglia et al., 2009). The experimental results presented in this chapter rely on the assumption of a mixture of two Gaussian components, whereas the underlying implementation also allows the use of skewed distributions such as the Gamma function. Their initial means are determined automatically from the binned histograms and the standard deviation is set as 3 for the respective tile. The probability of surface waters is set as 0.1 in accordance with previous works (Bazi et al., 2007; Martinis et al., 2009), suggesting that a minimum amount of 10% of each class is sufficient for accurate threshold detection. Sensitivity tests of these parameters are performed to quantify the influence of standard deviation and probability parameters in this process. The EM-based distribution fitting is performed over a maximum of 1000 iterations and tiles for which convergence is not reached within this number of iterations are excluded only for the calculation of the threshold value. Instead of directly determining the threshold value, this process is used to compute posterior probabilities to generate surface water probability maps.

The standard EM algorithm for normal mixtures is based on a first step called the E-step (Equation 4.1) and followed by a second step called the M-step (Equation 4.2) (Benaglia et al., 2009). In the E-step, it searches for the expected value *p* of the complete likelihood for all *i* = 1, . . . , *n* and *j* = 1, . . . , *m* at iteration *t*, from a given parameterization (λ, $\phi(x)$).

$$\boldsymbol{p}_{ij}^{(t)} = \left[\mathbf{1} + \sum_{j' \neq j} \frac{\lambda_{j'}^{(t)} \phi_{j'}^{(t)}(x_i)}{\lambda_j^{(t)} \phi_j^{(t)}(x_i)}\right]^{-1} \quad (4.1)$$

In the M-step, it finds the model parameters λ that maximize the conditional expected values from the E-step.

$$\boldsymbol{\lambda}_j^{(t+1)} = \frac{1}{n} \sum_{i=1}^{n} \boldsymbol{p}_{ij}^{(t)}, \text{ for j = 1, . . . , m.} \quad (4.2)$$

After computing the model parameters for each tile, we calculate the average of those parameters to derive a global set of parameters. Then, using the global parameters, posterior probabilities (Equation 4.1) are computed for each pixel of the entire image.

4.2.1.3. Smooth labelling using a Bilateral Filtering approach

Binary thresholding methods commonly treat each pixel independently to assign class labels such as land and surface water areas. However, considering the spatial auto-correlations among nearby pixels, it can be assumed that nearby pixels tend to have the same class label (smoothness assumption) (Schindler, 2012).

Based on this assumption, bilateral filtering is used as a strategy for smooth labelling and the suppression of small spurious detection. This filter is a non-linear, edge-preserving, and noise-reducing smoothing filter commonly used in image processing. The intensity value at each pixel in an image is replaced by a weighted average of intensity values from nearby pixels. The resulting image is subsequently transformed into a binary image assigning all pixels with a probability of surface water greater than 0.9 as water surface.

4.2.1.4. Post-processing

In the post-processing step, the accuracy of final binary maps is assessed by calculating classical measures (overall accuracy, F-measure (van Rijsbergen, 1979), true positive rates, false positive rates, omission and commission errors) obtained by a comparison with very-high resolution Copernicus products (Copernicus, n.d.).

4.2.2 Comparison of two scenarios using HAND maps

A previous study showed the advantages of using HAND maps for flood mapping (Clement et al., 2017; Twele et al., 2016) to remove false positive surface water detections which are located high above the nearest drainage line. In order to create HAND maps, stream networks are defined with a 10 ha threshold (Montgomery and Dietrich, 1988). For this study, a HAND threshold of 15 m (Nobre et al., 2011; Twele et al., 2016) is used.

In this chapter, we performed two approaches to improve the accuracy of the surface water mapping. The first approach is using the HAND map in the pre-processing step, while the second approach employs the HAND map in the post-processing step. A comparison of the results will determine the best scenario for this study. A tile size of 10 km will be used in both of the scenarios.

4.2.2.1 Scenario 1: Use of HAND maps in Pre-processing

For the first scenario, we use a HAND map in the pre-processing step, after subsetting the sigma-nought image in the study area boundary. All areas with a HAND index of >15 m are excluded from all further processing steps including the computation of the HDS, finite mixture modelling, the generation of the probability maps, bilateral filtering, and the generation of the final maps. In this scenario, potential false positives are removed in the initial stage of the processing chain and will thus not impact the statistical analysis. A further advantage of this scenario is the reduction of the amount of data and hence faster processing.

4.2.2.2 Scenario 2: Use of HAND maps in Post-processing

In the second scenario, we use a HAND map only in the post-processing step after labeling the surface water class. In order to reduce misclassification, we subset surface water areas in the HAND ≤ 15 m boundaries and produced the final surface waters map. In this scenario, all previous processing steps are based on the entire input image.

4.2.3 Sensitivity analysis of tile size used in tilling approach

It is a known issue that statistical thresholding methods applied to subsets of the image are sensitive to the size of the individual tiles (Martinis et al., 2009). The default tile size used in this study is 10 × 10 km due to the spatial extent of a Sentinel-1 image (250 km swath), but it cannot be excluded that increasing or reducing the tile size might improve or degrade the accuracy of the final maps. Using the first processing scenario, tile sizes of 2.5 km and 5 km are also evaluated and compared for the three study areas.

4.3 Results

4.3.1 Influence of FMM parameters values

Given that FMMs are sensitive to the initial values set for standard deviations and prior class probabilities, the impact of variations in the initial parameter settings on the final class model is examined. The influence of FMM parameter values is assessed for the Sentinel-1 image (9 January 2016). This analysis is performed for three tiles in the Ireland study area, which are deemed representative for different proportions of land and surface waters (Figure 4. 2). In Tile (a), surface waters cover more than 70% of the area, while in Tile (b), land and surface waters cover the same proportion of areas. In Tile (c), the majority is land surface. FMMs are initialized on these three tiles testing initialization values from 1 to 9 and from 0.1 to 0.9 for the standard deviation and prior class probabilities, respectively.

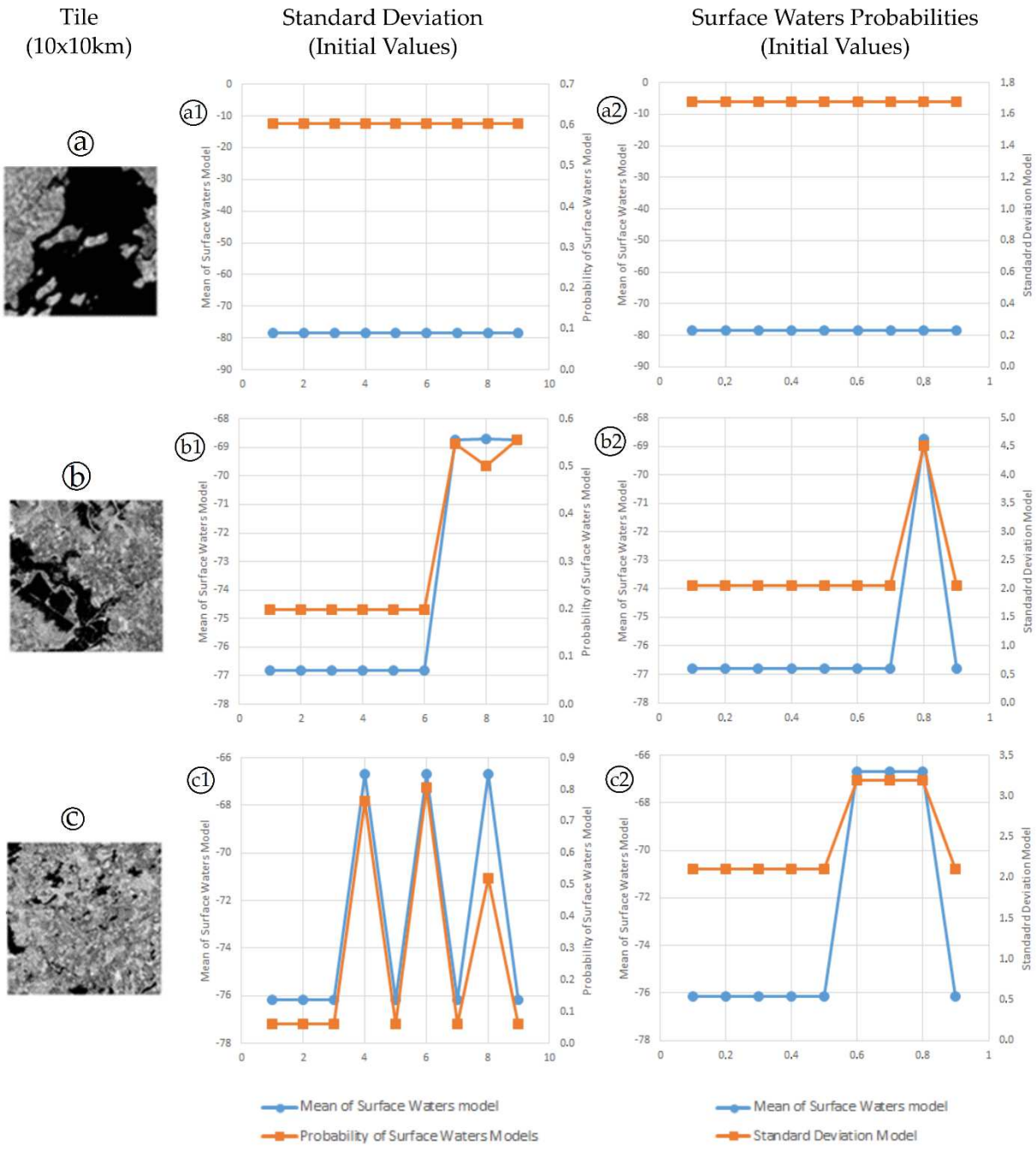

Figure 4. 2. Variation of standard deviation (**a1, b1, c1**) and surface water probabilities (**a2, b2, c2**) in the initial values of FMM parameters to output models for different proportions of land and surface waters in tiles.

The results of this evaluation are presented in Figure 4. 2. In the standard deviation column, we give various values of standard deviation as initial values and observe mean and probability values of the model. The graphs indicate the mean and probability values of the model associated with initial values of the standard deviation. Subsequently, in the column with surface water probabilities, we give various values

of probability as initial values and observed the mean and standard deviation values of the model. Figure 4. 2 shows that image tiles with large portions of surface water areas converge to the same stable output model no matter which initial values are selected. Contrarily, Tile (c), which includes rather small portions of surface water area, tends to generate marginal solutions with standard deviations above 3 or prior probabilities for the surface water class above 0.5. For Tile (b), which presents an intermediate contribution of water surfaces, the FMMs converge to a stable solution below standard deviations of 7 and water class probabilities of 0.7. Considering the result of this analysis, the use of a standard deviation of 3 and prior probability of 0.1 was considered as sufficiently low to assure that the FMMs will generally converge to stable solutions with a good approximation of the bimodal distributions.

4.3.2 Sensitivity of Bilateral Filtering parameter

The size of the filtering window and its influence on the results is also analyzed. The sensitivity of the classification accuracy to changes in these parameters is evaluated empirically for the image Sentinel-1 scene recorded on 9 January 2016 over the Gort area in Ireland study area.

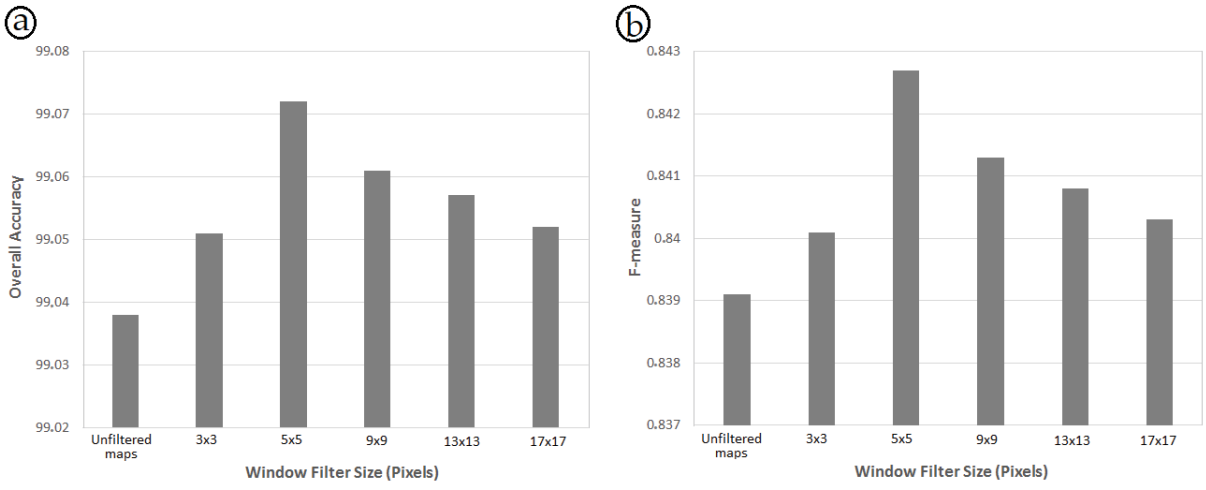

Figure 4. 3. Dependence of classification result on bilateral filter window size indicated (a) by overall accuracy and (b) F-measure value.

Figure 4. 3 represents the dependence of overall accuracy and F-measure on changes in the window size. It can be seen that a window size of 5 × 5 pixels yields the optimal

result with the overall accuracy reaching 99.07% and F-measure at 0.84. Therefore, for all experiments, the bilateral filtering window was fixed to 5 × 5 pixels.

Figure 4. 3 also shows that bilateral filtering yields higher overall accuracies when compared to unfiltered maps over a wide range of window sizes between 3 × 3 pixels and 17 × 17 pixels. This clearly justifies the use of bilateral filter as a smooth labeling method in this study.

4.3.3 Results comparison between Scenario 1 and Scenario 2

Based on a comparison of quantitative evaluation results from scenario 1 and 2, there are no significant differences in all evaluation parameter values between the two scenarios. However, compared to scenario 2, scenario 1 gives slightly better evaluation results. This can be seen in Figure 4. 4, which displays the F-measure values from all images. In the F-measure graph, the higher the value signifies the better the results. Figure 4. 4 shows higher values for scenario 1 for two images and the same values for the other images. Thus, the use of scenario 1 is recommended and will be applied for this study.

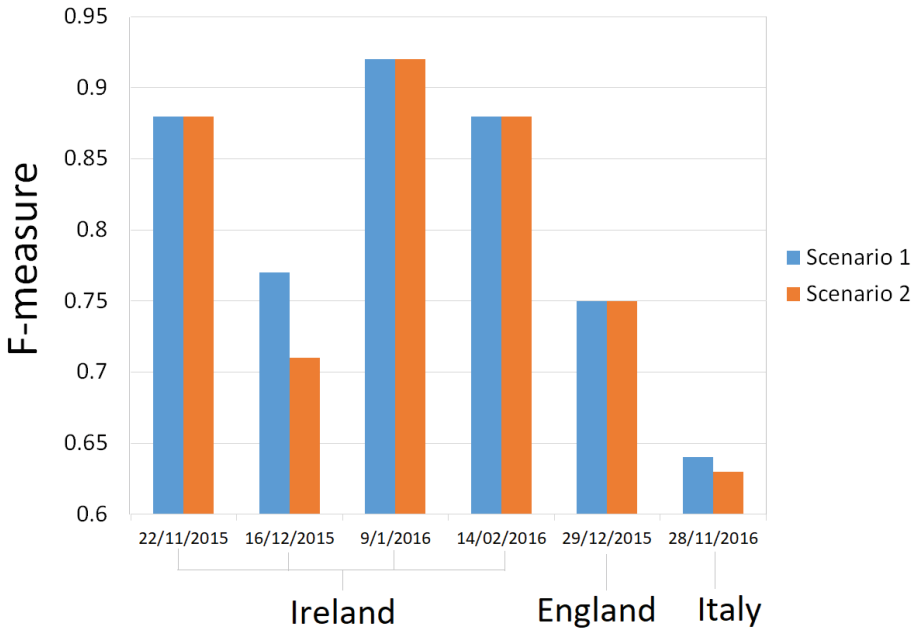

Figure 4. 4. Comparison of F-measure between scenarios 1 and 2.

4.3.4 Sensitivity of tile size in MSBA and FMM steps

A sensitivity analysis is carried out in all three study areas through a quantitative assessment of the results with different tile sizes. Using scenario 1 and all further processing steps as explained above, only the tile size used in the MSBA and FMM steps is changed to values of 10 km, 5 km, and 2.5 km. A quantitative comparison against the available reference maps in Ireland study area is presented in Table 4. 1 and indicates only subtle differences between three tile sizes. While small variations exist regarding the tradeoff between TPR and FPR, the F-measures are indistinguishable.

Table 4. 1. Result assessment for three different tile sizes in the study area of Ireland.

Evaluation	22/11/2015			16/12/2015			9/1/2016			14/02/2016		
	10 km	5 km	2.5 km	10 km	5 km	2.5 km	10 km	5 km	2.5 km	10 km	5 km	2.5 km
Overall accuracy	99.41%	99.40%	99.40%	98.68%	98.68%	98.68%	98.68%	98.67%	98.66%	99.35%	99.36%	99.38%
F-measure	0.88	0.88	0.88	0.77	0.77	0.78	0.92	0.92	0.92	0.88	0.88	0.88
TPR	81.27%	81.65%	81.44%	66.96%	67.04%	67.83%	89.67%	89.42%	89.18%	86.42%	86.26%	86.51%
FPR	0.09%	0.10%	0.10%	0.22%	0.22%	0.24%	0.47%	0.45%	0.44%	0.29%	0.27%	0.31%
Omission error	18.73%	18.35%	18.56%	33.04%	32.96%	32.17%	10.32%	10.58%	10.82%	13.58%	13.74%	13.49%
Commission error	3.79%	4.29%	4.06%	8.54%	8.60%	9.31%	5.26%	5.10%	4.96%	10.80%	10.22%	11.29%

Table 4. 2. Result assessment for three different tile sizes in the study areas of England and Italy.

Evaluation	England 29 December 2015	Italy 28 November 2016				
	10 km	10 km	5 km	2.5 km	5 km	2.5 km
Overall accuracy	98.40%	98.68%	98.75%	98.75%	98.42%	98.40%
F-measure	0.75	0.64	0.66	0.7	0.76	0.76
TPR	62.44%	48.51%	52.11%	61.05%	66.13%	67.36%
FPR	0.15%	0.10%	0.11%	0.33%	0.28%	0.36%
Omission error	37.56%	51.49%	47.89%	38.95%	33.87%	32.64%
Commission error	5.72%	7.50%	8.15%	18.17%	9.57%	11.64%

Similarly, in study area of England, a smaller tile size seems to favor both a higher TPR and a higher FPR, whereas the F-measure remains rather stable among all tested tile sizes (Table 4. 2). On the other hand, the results for study area of Italy indicate a significant improvement from an F-measure of 0.64 towards 0.7 when using smaller tile sizes (Table 4. 2). This might be due to smaller water surfaces in study area of Italy, which are less likely to be omitted at smaller tile sizes.

4.4 Discussion

Generally, the accuracy assessment shows very high overall accuracies of about 98% for each of the study sites. Moreover, the commission error remains below 20% for all test zones. The final quantitative evaluation of surface water extraction results is presented in Table 4. 3. The presented results are obtained fully automatically using scenario 1 and a tile size of 10 km. As shown in the previous section, further improvements can be expected through an adaptation of the tile size, whereas we prefer to present here the results obtained with a default value that is more realistic for an operational scenario.

For each zone, a map depicting the extent of surface waters is presented and several zooms overlaying Sentinel-2 imagery allow a better visualization of results. The surface water detection in study area of Ireland shows results with F-measures ranging from 0.77 to 0.92. Figure 4. 5a–d show that false negatives occur mainly along the borders of surface water bodies, where most of the false positives are also located. In the Ennis area, the narrow river with a width of around 50 m cannot be detected. This is probably due to vegetation along the river banks and increased turbulence along the permanent riverbed which leads to increased backscattering in those areas (see Figure 4. 5d). Flooded areas are detected in wetland areas along Shannon River (Figure 4. 5b).

The evaluation of study area of England shows an adequate performance of the automatic detection with an F-measure value of 0.75. The study area of England comprises numerous narrow river sections which, even during flooding events, do not exceed 100 m in width and are consequently difficult to detect with Sentinel-1 (see Figure 4. 6d). Similar to study area of Ireland, the detection of these sections is further

complicated by tree-and hedge lines along the river banks, as well as greater turbulence and hence water surface roughness along the permanent riverbed.

Study area of Italy comprises several narrow river sections in Sale regions, which similarly leads to omission errors of about 51%. Some false negatives are visible along the borders of Po River (see Figure 4. 7a,b) and mostly appear in the bar or river bank areas (see Figure 4. 7c,d). In particular, it seems that several bar and river banks already reemerged after the main flooding event on 25 and 26 November 2016. The omission is hence due to the acquisition delay of Sentinel-1 because, at the time of imaging, these areas where not submerged.

Table 4. 3. Quantitative evaluation of surface water extraction results (using scenario 1 and tile size 10 km).

Study Area	Image Date	Event	Overall Accuracy	F-measure	True Positive Rate	False Positive Rate	Omission error	Commission error
Ireland	22/11/2015	Before floods	99.41%	0.88	81.27%	0.09%	18.73%	3.79%
	16/12/2015	Floods occurred	98.68%	0.77	66.96%	0.22%	33.04%	8.54%
	09/01/2016	Floods occurred	98.68%	0.92	89.67%	0.47%	10.32%	5.26%
	14/02/2016	After floods	99.35%	0.88	86.42%	0.29%	13.58%	10.80%
England	29/12/2015	Floods occurred	98.40%	0.75	62.44%	0.15%	37.56%	5.726
Italy	28/11/2016	Floods occurred	98.68%	0.64	48.51%	0.10%	51.49%	7.50%

Given the persistent omission of permanent river beds at all three study sites, further improvements of the processing chain could include the analysis of SAR time-series to amplify the signal of permanent riverbeds through spatio-temporal averaging. Considering these results, our new automatic chain processing for floods detection and rapid surface water mapping using Sentinel-1 data appears to be efficient for mapping flood events and water surfaces. It has been applied to three major floods events in Ireland, the United Kingdom, and Italy with largely favorable results. The proposed method features a short processing time. For instance, using a computer with multiple Intel Duo processors of 1.90 GHz and 32 GB RAM, the time of processing is about 10 h per Sentinel-1 image. Multiple images can be processed easily in parallel. Rapid mapping can hence be achieved in less than half a day after the image data is made publicly available. Given the variable landscape characteristics at the investigated sites,

we consider that the processing chain can also be deployed for rapid mapping in other geographic regions. Probabilistic map products can also be derived to better guide further intervention by human operators if required.

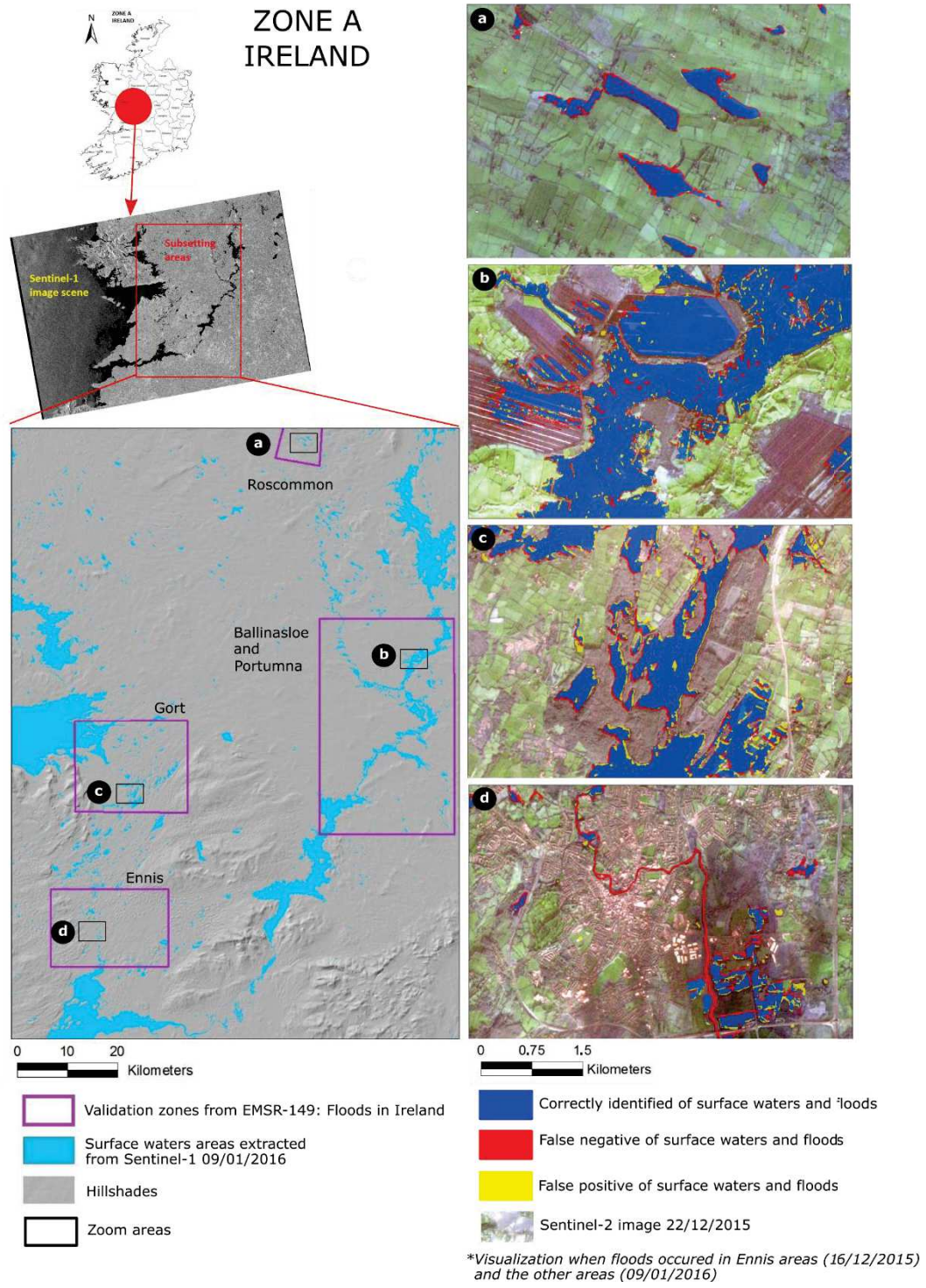

Figure 4. 5. Surface water extraction result in the study area of Ireland with several zoom areas overlaying Sentinel-2.

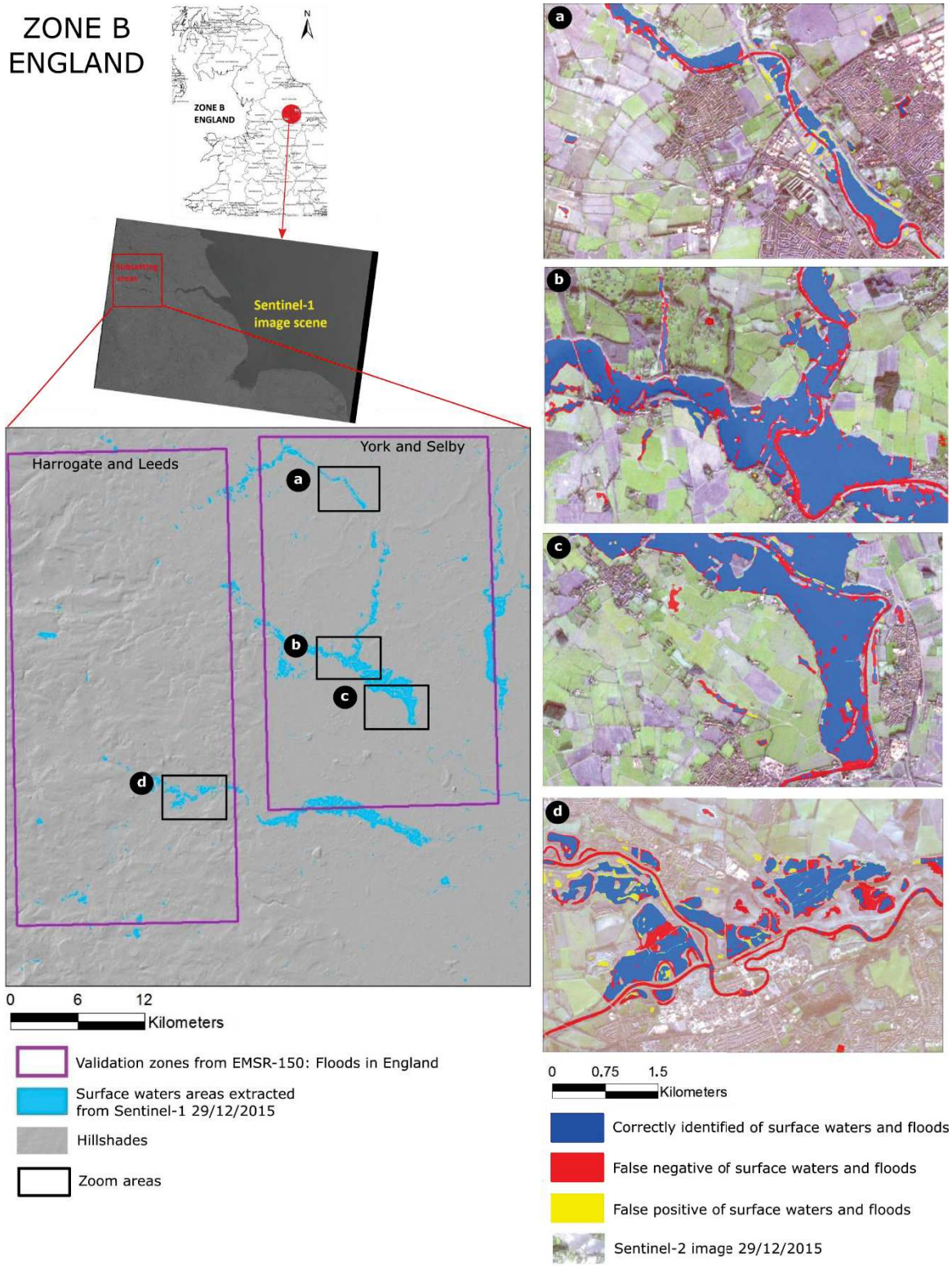

Figure 4. 6. Surface water extraction result in the study area of England with several zoom areas overlaying Sentinel-2 imagery.

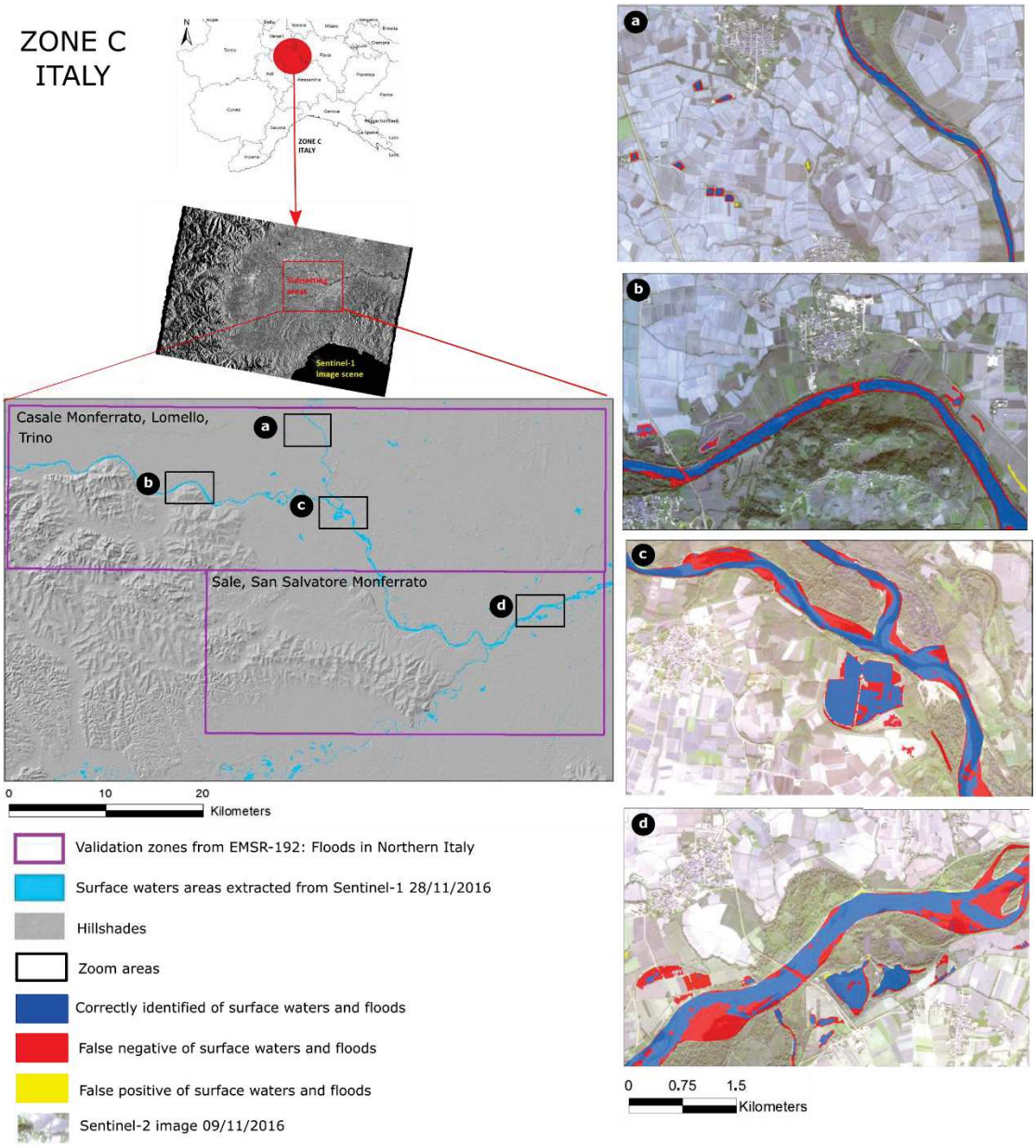

Figure 4. 7. Surface water extraction result in the study area of Italy with several zoom areas overlaying Sentinel-2 imagery.

In this study, the methodology was specifically designed for the analyses of Sentinel-1 data and the suitability of the method for rapid surface water mapping was explored. The method is adapted to the particular features of high spatial resolution Sentinel-1 data which are different from the other available automatic tools targeting the use of SAR images with a very high spatial resolution (e.g., Martinis et al., 2015; Wendleder et al., 2013). Since the required Sentinel-1 input data is publicly available without restriction, it will be easy to access unlimited data of Sentinel-1 and process it for surface water mapping.

4.5 Conclusions

The objective of the study in this chapter has been twofold. First, to assess the suitability of Sentinel-1 data for flood detection and surface waters mapping. Second, to construct automatic chain processing for surface waters extraction. To this end, we presented an approach consisting of pixels modelling, probability maps, and a smoothness assumption in order to capture floods and surface waters.

We developed a modified SBA method to facilitate focusing on surface water areas rather than the entire image scene observed. Finite Mixture Models are found to be suitable for the automatic modelling of surface water class and land. Using bilateral filtering for smooth labeling from a probability map led to more accurate results than using direct thresholding. HAND maps are used as terrain filters in order to remove potential false positives early on in the processing chain. A comparison of two procedures integrating HAND in the pre- or post-processing showed better results when used already in the pre-processing step. Sensitivity analysis of tile size pointed out the importance of surface water areas to determine tile size. Yet, a default tile size of 10 km can yield high overall accuracies. Our results show that we were able to estimate floods and surface waters in the three study areas with an average F-measure of about 0.8.

Using Sentinel-1 as free SAR data with wide area monitoring capabilities, we established a processing chain which can extract floods and surface water areas automatically. The automatic approach has been tested for three floods events in Ireland, England, and Italy, suggesting an applicability for rapid flood mapping at other sites beyond the presented study areas.

This chapter has outlined the automatic mapping of surface water (the Water-S1 method) developed for Sentinel-1 image processing and discussed the results. The next chapter will explore the contribution of multi-temporal and multi-source data for increasing the detection and mapping of surface water.

Chapter 5

Detection of surface water area using time series of Sentinel-1 amplitude data and Sentinel-2 data

Contents

The previous chapter has been explored mono-date Sentinel-1 imagery related to surface water mapping. The Water-S1 method as automatic mapping developed for Sentinel-1 image in detecting surface water has been presented. This chapter will provide the contribution's analysis of multi-source data (Sentinel-1 and Sentinel-2) for increasing the detection and mapping of surface water.

This chapter was written based on an article accepted in March 2019 to International Journal of Remote Sensing entitled *Fusion of Sentinel-1 and Sentinel-2 Image Time Series for Permanent and Temporary Surface Water Mapping (Bioresita, F., Puissant, A., Stumpf, A., and Malet J.P.)*. Some redundancies can then appear in this chapter.

5.1 Introduction

As been reminded in Chapter 2, some databases of surface water are available such as the Global Surface Water product of the EC-Joint Research Centre (The European Commission's Joint Research Centre, 2016), the SRTM Water Body product of National Geospatial-Intelligence Agency (NGA, 2005), the Global Lakes and Wetlands Database (GLWD) of WWF and the University of Kassel, Germany (Lehner and Döll, 2004), the Water and Wetness product from EC-COPERNICUS (Copernicus, 2015a) or the Landsat Level-3 Dynamic Surface Water Extent (DSWE) Science Product from Earth Resources Observation and Science (EROS) Center (EROS Center, 2018).

Consequently, these existing surface waters products are relevant for some applications but do not fulfill all the current needs of the science and water management communities. For instance, GLWD and SRTM Water Body do not identify small surface waters of less than 10 ha and narrow water bodies such as watercourses or streams. GSW and the DSWE products are based on Landsat imagery with gaps in the observation records because of the occurrence of clouds. The Water and Wetness product is already using Sentinel-1 data but relies on 30-m spatial resolution Landsat imagery.

Figure 5. 1 presents an overview of the existing products over the case study in Ireland as well as the national database of the Irish Environmental Protection Agency (EPA,

2017). Over the study area, the extension of the surface water is respectively of ± 92 km^2 in GSW, ± 120 km^2 in GLWD, ± 114 km^2 in SRTM Water Body, ± 99 km^2 in Water & Wetness, and ± 111 km^2 in the national EPA database.

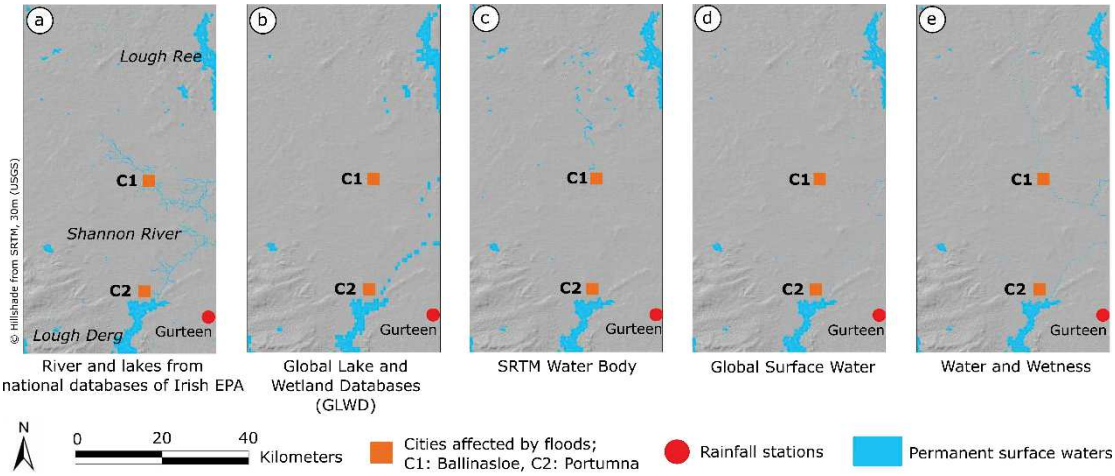

Figure 5. 1. An overview of the existing products over the study case in Ireland. (a) the national database of the Irish EPA ; (b) GLWD ; (c) SRTM Water Body ; (d) GSW ; (e) Water and Wetness.

A method for automatic and rapid mapping of water surfaces has been presented in Chapter 4 (Bioresita et al., 2018). The method uses finite mixture models and bilateral filtering as a smooth labeling for defining the thresholds. The method gives successful results in terms of water surface extraction (and in all subsequent cases) as it relies on significant contrast of pixel values between water and non-water areas. However, the method gives misclassification if non-water areas have lower backscattering values than water areas such as airport runways or some smooth agricultural fields where specular reflexion is observed.

The high revisiting time of Sentinel-1 and Sentinel-2, together with spatial resolution in the range 10 to 30 m is hypothesized to fill the gap for producing maps of permanent water bodies at monthly time scale. Methods combining SAR and optical imagery for water surface detection are seldom though they offer complementary information. Optical data provide information on the multispectral reflectivity of surface waters whereas SAR data provide information on the texture (Chaouch et al., 2012; Markert et al., 2018) of the surface waters. Using image times series and data fusion techniques to increase the accuracy of permanent surface waters extraction is promising

(Bourgeau-Chavez et al., 2009; Liu et al., 2018; Riffler et al., 2018). Combining data of different properties and data acquired at several periods can improve image classification (Riffler et al., 2018). The studies presented by (Du et al., 2016) and (Bourgeau-Chavez et al., 2009) applied this concept to extract surface waters.

The objective of our work is to investigate, quantify and measure the performance of Sentinel-1 and Sentinel-2 time series for improving surface waters mapping by applying fusion techniques. The approach is being tested on image time series over study area of Ireland (± 3657 km^2) using a time series of sixteen Sentinel-1 IW GRD images and three Sentinel-2 images (See Chapter 3).

5.2 Methodology

The general methodology is described in Figure 5. 2. The detection of the surface waters and the calculation on the probability of occurrence are carried out on the Sentinel-1 images with the Water-S1 method presented in Chapter 4. An adaptation of the Water-S1 method is used for the processing of the optical Sentinel-2 data (see Sub-section 5.2.1). The occurrence maps obtained for the two time series (Sentinel-1, Sentinel-2) are combined using decision level methods (see Sub-section 5.2.2). Finally, the fused results are evaluated for the permanent water bodies and for the temporary flooded areas for the corresponding time periods (see Sub-section 5.2.3).

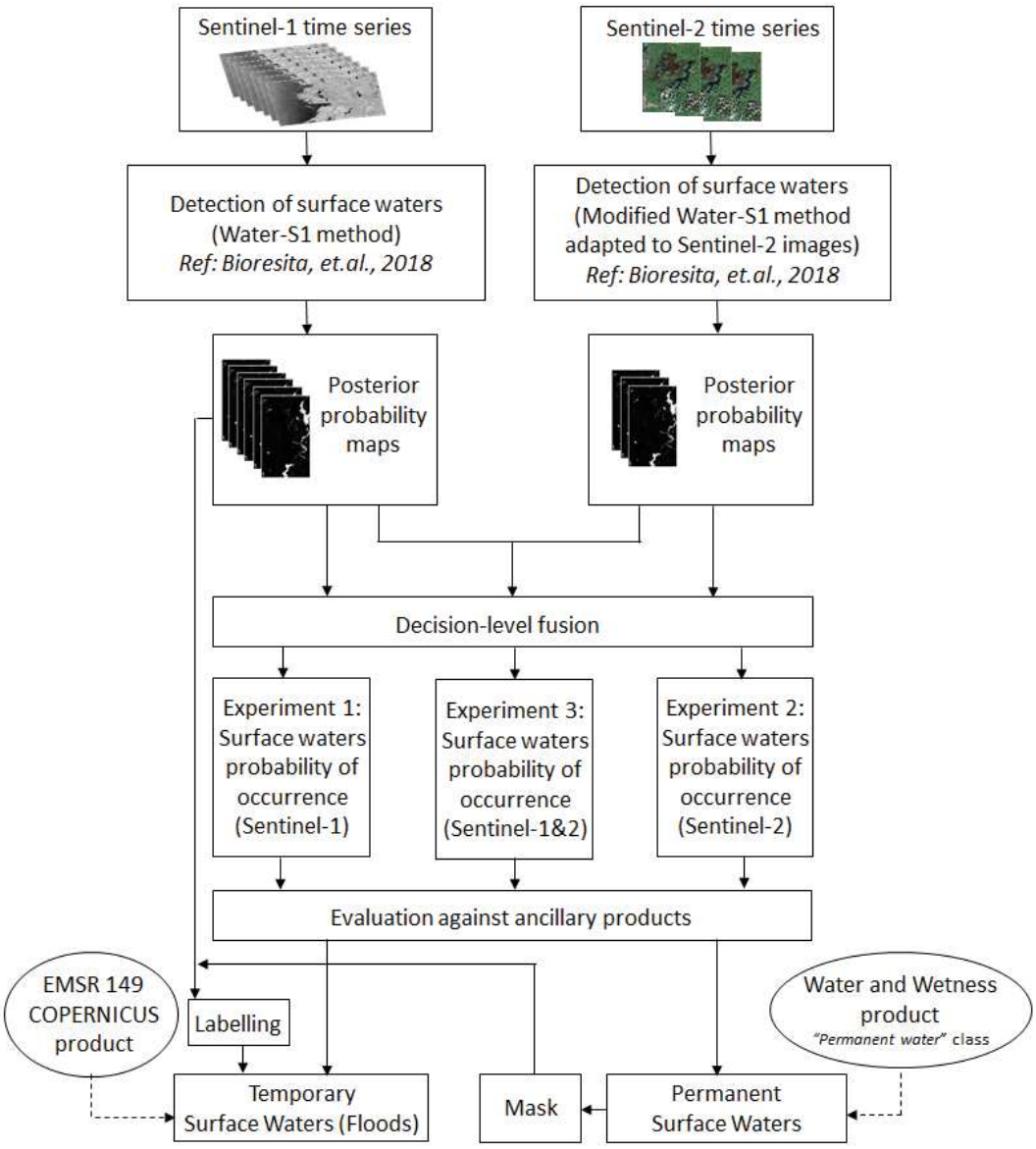

Figure 5. 2. Methodological workflow.

5.2.1 Extraction of surface waters and calculation of probability of occurrence maps from Sentinel-1 and Sentinel-2 images

The processing of Sentinel-1 IW GRDH image is based on the Water-S1 method described in Chapter 4 and summarized in Figure 5. 3. The first step consists of a correction of orbital errors, speckle noise and geometric distortion of the data. The application of precise Sentinel orbits, the radiometric calibration of the SAR images to Sigma-nought images, the multi-looking, the filtering of speckle, and terrain relief are

applied in the Sentinel Application Platform / SNAP (Foumelis, 2015; Stewart, 2016) (See Chapter 3). Then, a subset of Sigma-nought images is masked using the Height above Nearest Drainage (HAND) terrain index. This index is based on the drainage network and is used to constrain the processing area in order to avoid classification errors in topographically non-plausible water areas.

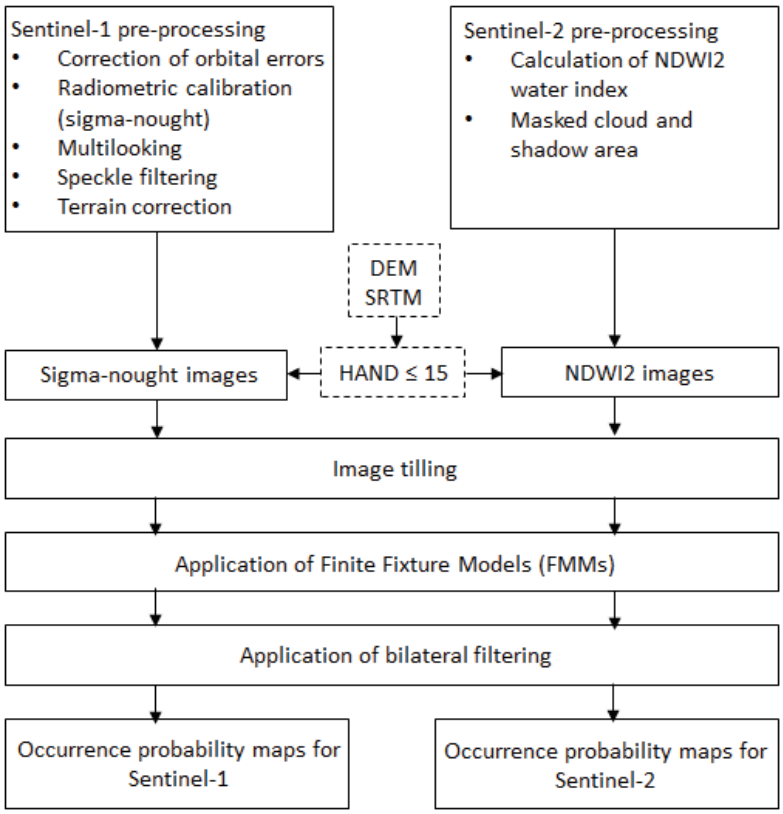

Figure 5. 3. Flowchart of surface waters extraction: Water-S1 method (for Sentinel-1) and modified Water-S1 method applied to Sentinel-2 mono-date images.

A threshold of HAND <15 m is applied in order to filter the false positives of surface waters located above the nearest drainage line. Then, a statistical modified Split-Based Approach (SBA) is used in order to tile the input images into squared non-overlapping blocks of 10x10 km size and to select the tiles for class modeling. The strategy for tile selection consists in choosing only the image tile which contain some portions of surface waters based on Hartigan's dip statistic (HDS) value (Freeman and Dale, 2013). Class modeling is performed by applying Finite Mixture Models (FMM) (Benaglia et al., 2009). The model parameters for each tile are calculated, then global sets of parameters are defined and probabilities of occurrences are computed. Finally, a

labeling using Bilateral Filtering is applied to the occurrence images (Schindler, 2012). The filtered occurrence probability images are then used as input data for image fusion.

For Sentinel-2 image processing, the general workflow of Water-S1 is applied with some adaptations. First, the Sentinel-2 level 1C (Top of Atmosphere values) are corrected to level 2A (Bottom of Atmosphere values) using Sen2Cor tools available in SNAP (Louis et al., 2016), and cloud and shadow area are masked. The NDWI2 water index (Equation 5.1), classically used to extract water surfaces (Du et al., 2016; McFeeters, 1996), is calculated at 10-m spatial resolution and is used for feature extraction.

$$\text{NDWI2} = \frac{(B3 - B8)}{(B3 + B8)} \tag{5.1}$$

where B3 is the green band and B8 is the near-infrared band.

The HAND topographic index (Nobre et al., 2011) is calculated on the SRTM topography and applied to the NDWI2 images in order to remove regions located above the nearest drainage line and avoid misclassification.

5.2.2 Methods of image fusion: decision-level fusion rules

Image fusion can be implemented at three different levels: (a) pixel, (b) feature, or (c) decision level (Liu et al., 2018). When images originate from several sensors, the most relevant method for data fusion is to combine the images with the surface waters results extracted individually for each image source (Pohl and Van Genderen, 1998; Wendl et al., 2018; Zadeh, 1976).

Several methods of decision level fusion are compared in order to identify the most suitable approach for surface waters. This information is fused in order to create value-added layers (Zadeh, 1976). Probabilities of occurrence of surface waters are calculated, first, in order to evaluate the interest of time series to enhance the mapping and, second, to evaluate the complementarity of results from the SAR and optical sensors. All calculations are performed at pixel level by combining the probabilities of occurrence of each experiment (experiment 1 = time series of Sentinel-1 data,

experiment 2 = time series of Sentinel-2 data, experiment 3 = time series of Sentinel-1 and Sentinel-2 data). The final image fusion is expressed in terms of posterior probability.

The fuzzy logic method and the Bayesian method are tested for the decision level fusion. The most powerful fusion method identified for Sentinel-1 results is then applied for the fusion of the Sentinel-2 results and for the fusion of Sentinel-1 and Sentinel-2 results (see point 5.3.1.1).

Image fusion using fuzzy logic (Wendl et al., 2018) is powerful to combine uncertain data. Considering a reference set L of classes, then a fuzzy set A in L, is a set of ordered pairs:

$$A = [(x, P_A(x) \mid x \in L)] \quad (5.2)$$

where $P_A : L \rightarrow [0, 1]$ is the membership function of A in L which range is a subset of the nonnegative real numbers whose supremum is finite. The algorithm proposed by (Wendl et al., 2018) is used for the calculation. It uses a minimum number of fuzzy logic operators (Equation 5.3). The details of the membership functions are presented in Figure 5. 4. The fuzzy logic minimum operator is used based on the accurate results obtained by (Wendl et al., 2018) for urban land use classification.

$$P_{fusion}(x) = \text{Min}\,(P_A(x), P_B(x)) \quad (5.3)$$

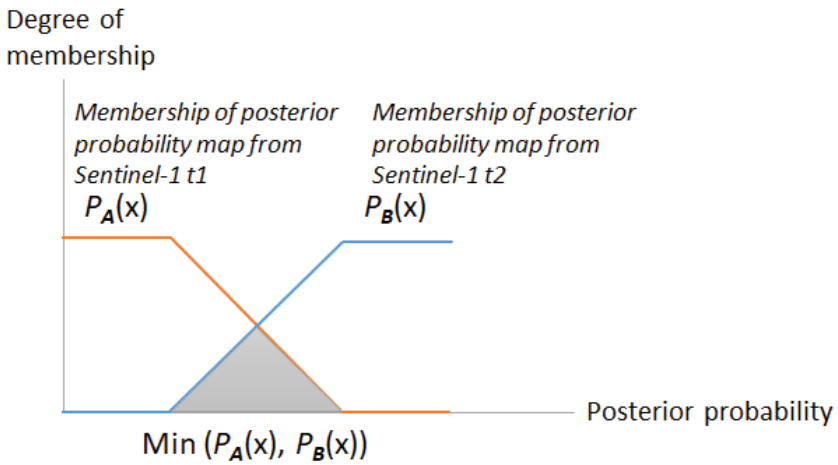

Figure 5. 4. Decision-level Fusion: Application of the fuzzy logic minimum operator, with example of combination of Sentinel-1 posterior probability maps (t1 and t2, see Table 3.1).

The second approach for data fusion is Bayesian, with algorithm proposed by (Wendl et al., 2018). Bayesian approach is also used based on the accurate results obtained by (Wendl et al., 2018) for urban land use classification. It executes image fusion based on the operator product (Equation 5.4) or operator sum (Equation 5.5).

$$P_{fusion}(x) = P_A(x) \times P_B(x) \quad (5.4)$$

$$P_{fusion}(x) = P_A(x) + P_B(x) \quad (5.5)$$

where P_A and P_B are the posterior probability maps.

5.2.3 Evaluation procedure

A threshold of 90% is used to differentiate the permanent surface water (posterior probability > 90%) from other classes (posterior probability < 90%). The "permanent water" class of the Water and Wetness product is used as the reference product for the evaluation of the "permanent surface water" class detected with our methodology. The reasons are that the Water and Wetness product is produced from Sentinel-1 (Figure 5. 1e; see Section 5.1), and has nearly the same spatial resolution as our results..

The "*temporary surface water*" class in our study was extracted from Sentinel-1 images using the "*permanent surface water*" map issued from the best fusion algorithm (Bayesian Sum S1&S2) as a mask. Due to the flooding events of December 2015 and January 2016, the "*temporary surface water*" class of the Water and Wetness product cannot be used as reference data. Therefore, for the evaluation of the "*temporary surface water*" class detected with our methodology, the Copernicus Emergency Management Service (EMS) (Copernicus, 2015b) maps are used. For the period of interest, only one EMS product is available (9 January 2016).

All the quantitative assessments are based on the calculation of confusion matrices and of indicators such as the Overall accuracy, the F-measure, the True Positive Rate (TPR), the False Positive Rate, and the Omission and Commission error. Qualitative assessment is also applied and presented in Section 5.3 for the "permanent surface water" (see Sub-section 5.3.1) and "temporary surface water" (see Sub-section 5.3.2).

5.3 Results

5.3.1 Mapping of "permanent surface water"

5.3.1.1 Mono-date detection of surface water from Sentinel-1 and Sentinel-2 images

Figure 5. 5 presents the detection of surface water over the region of Portumna (Figure 5. 1, C2) for the 16 Sentinel-1 images and the 3 Sentinel-2 images expressed in terms of occurrence probability maps. The maps are binarized in two classes (presence and absence of water) using a posterior probability threshold > 90% (Bioresita et al., 2018). The surface extents vary in the range 86 to 225 km2 over the period. In the Sentinel-1 time series, during the flooding period of Winter 2015/2016, waters are detected in the North area of Lough Derg until 14th February 2016. Extraction of surface waters in April, June and October 2016 present some errors due to roughness of the water surfaces caused by wind and turbulence effects. Roughness causes a higher backscattering signal and therefore an enhanced brightness in the SAR data.

In the Sentinel-2 image of December 2015, surface waters are clearly depicted in the north area of Lough Derg. Due to the presence of thin cirrus and dark pixels areas, surface water areas are overestimated for the Sentinel-2 image of November 2016. In order to overcome those problems, decision-level fusion is applied on the mono-date water detection.

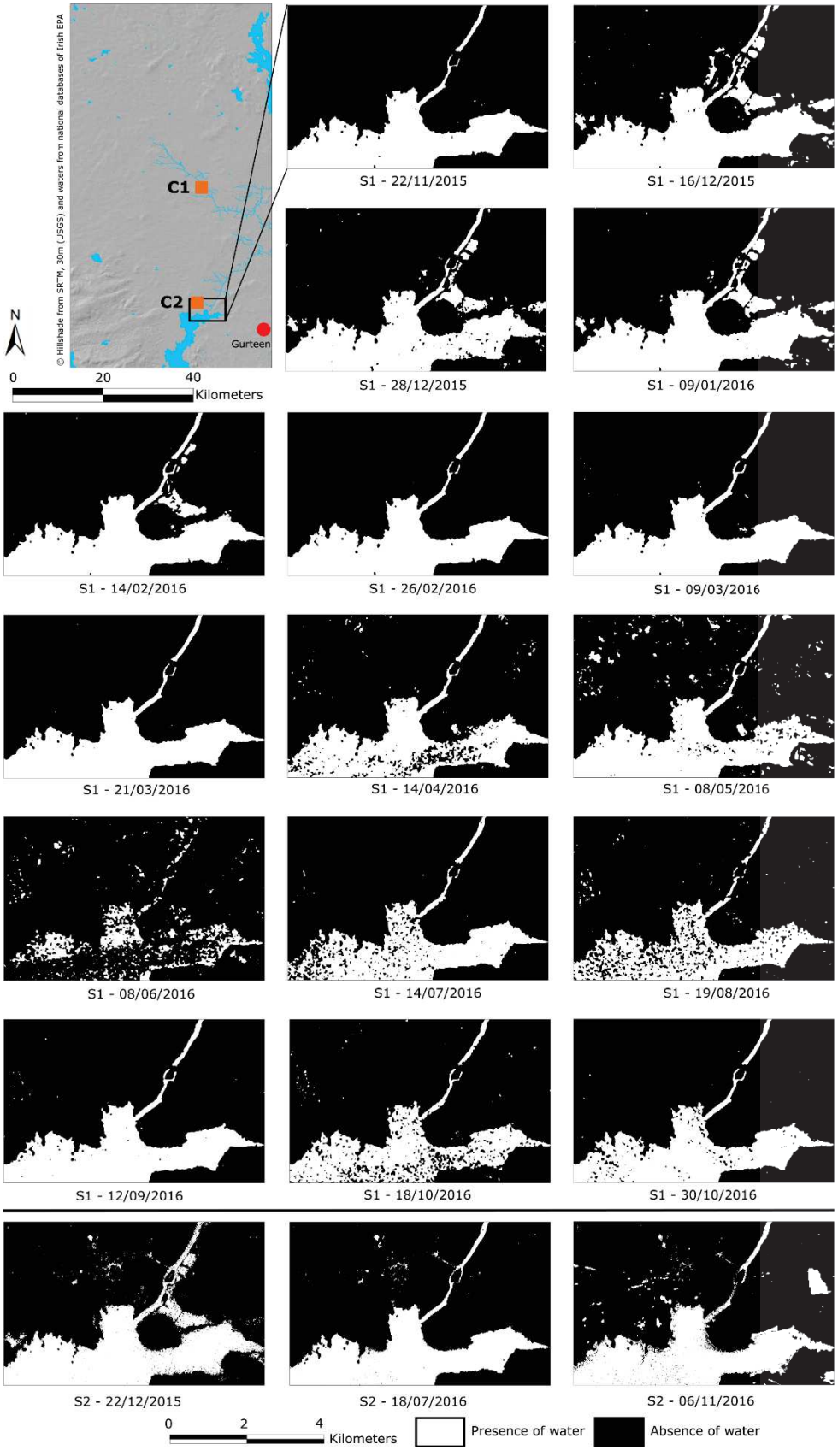

Figure 5. 5. Surface water detected for the 16 Sentinel-1 images and the 3 Sentinel-2 images in terms of occurrence probability maps, with a zoom on the region of Portumna (C2).

5.3.1.2 Multi-date detection of "permanent surface water" bodies with time series image fusion

Results of image fusion of the Sentinel-1 time series images are presented in Figure 5. 6. All fusion results present a reduction of the noise level. However, comparison with the reference product indicates different performance of the decision-level rules. Test 1 (operator fuzzy logic Min) only identifies fractions of Lough Derg and is not able to identify the permanent surface waters along Shannon River; test 2 (Bayesian operator product) does not identify Lough Derg and the Shannon River (presence of false negative); test 3 (Bayesian operator Sum) gives the best results with the identification of the Shannon River and of nearly the full area of Lough Derg.

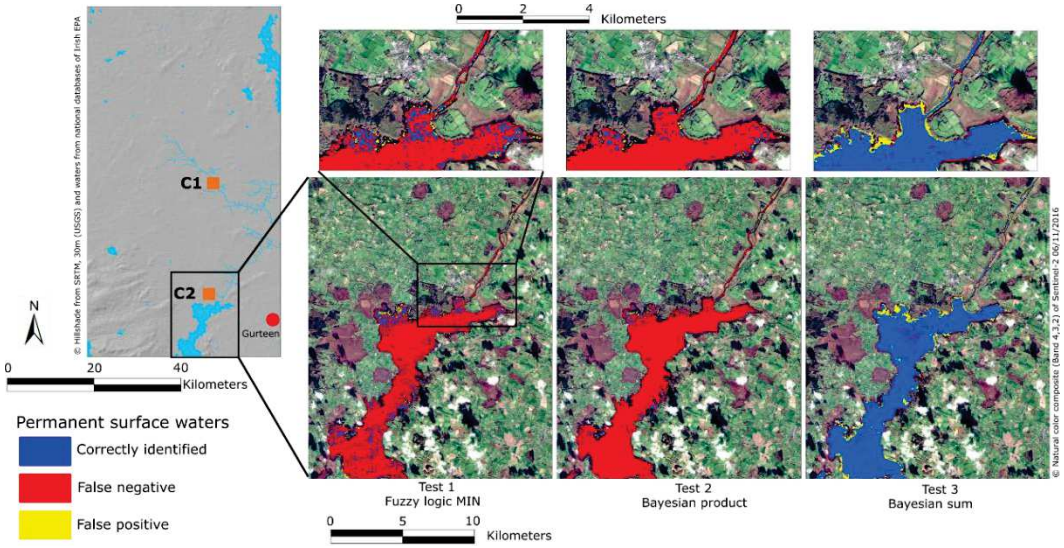

Figure 5. 6. Decision-level fusion results for the Sentinel-1 time series over the region of Portumna, with details (zoom) on the north bank of Lough Dergh and for the three methods of image fusion.

The quantitative assessment (Table 5. 1) indicates high overall accuracies of above 99%. Test 2 gives very low F-measure with a value of about 0.55 and True Positive Rate (TPR) with a value of about 38%. Omission error of Test 2 is very high reaching 61%. Test 1 gives better F-measure than Test 2 with a value of 0.77 but the TPR is low with a value of 62%. Omission error in Test 1 is also high with a value of 37%. Those measures explain the appearance of a large amount of false negatives (Figure 5. 6) for Test 1 and Test 2 even if the overall accuracies are high. Test 3 shows the highest overall accuracy and F-measure with a value of 0.99, a high TPR with a value of 98% and low

omission error with a value of 1.4%. As a consequence, the Bayesian sum operator is used and applied for the fusion of the multi-temporal Sentinel-2 images (experiment 2), and for the fusion of Sentinel-1 and Sentinel-2 times series (experiment 3).

Table 5. 2 summarizes the comparison of the three experiments of image fusion to the Water & Wetness products considered as reference data. Results of decision-level fusion from Sentinel-2 images (Experiment 2) are presented in Figure 5. 7. Experiment 2 gives the best TPR and omission error than the other experiments, but it is based only on three images with a low cloud density. Experiment 2 allows detecting both the Lough Derg and the Shannon River at high accuracy with an overall accuracy of 99%, a F-measure of 0.98 and a TPR of 99%.

Table 5. 1. Classification accuracy of Sentinel-1 time series for the three methods of decision-level fusion.

Tests	Methods	Overall Accuracy	F-measure	True Positive Rate	False Positive Rate	Omission error	Commission error
Test 1	Fuzzy MIN	99.50%	0.77	62.473%	0.002%	37.52%	0.30%
Test 2	Bayesian Product	99.32%	0.55	38.301%	0.001%	61.69%	0.26%
Test 3	Bayesian Sum	99.94%	0.99	98.602%	0.023%	1.39%	0.83%

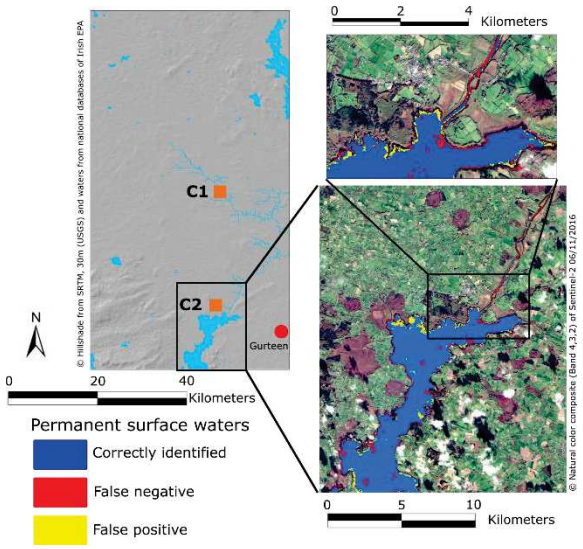

Figure 5. 7. Decision-level fusion results for the Sentinel-2 images over the region of Portumna, with details (zoom) on the north bank of Lough Dergh.

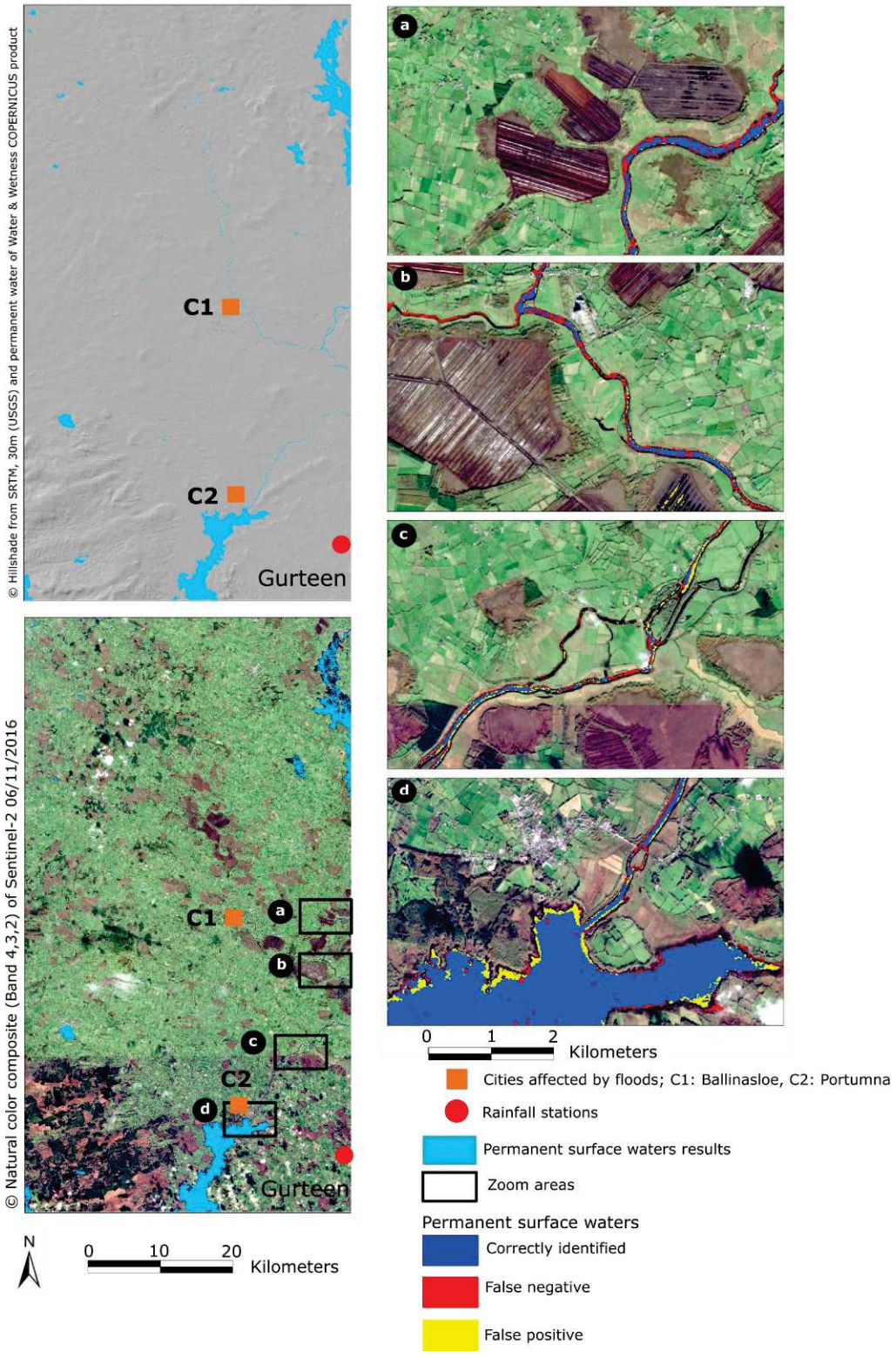

Figure 5. 8. Decision-level fusion results for the Sentinel-1 and Sentinel-2 images over the region of Portumna, with details (zoom) on the Shannon River (sector a, b, c) and the north bank of Lough Dergh (sector d).

Table 5. 2. Comparison of images fusion results with Water & Wetness reference data.

Experiments (with Bayesian operator Sum)	**Overall Accuracy**	**F-measure**	**True Positive Rate**	**False Positive Rate**	**Omission error**	**Commission error**
Experiment 1 (S1)	99.94%	0.98	98.60%	0.02%	1.40%	0.83%
Experiment 2 (S2)	99.95%	0.98	99.20%	0.04%	0.80%	1.79%
Experiment 3 (S1 & S2)	99.95%	0.99	98.31%	0.01%	1.69%	0.34%

Results of decision-level fusion from Sentinel-1 and Sentinel-2 time series (Experiment 3) are presented in Figure 5. 8. Experiment 3 gives better values in terms of F-measure (0.99), FPR (0.01%) and commission error (0.34%) than the other experiments. The surface waters are detected at very high accuracy with an overall accuracy of more than 99%. The omission error is very low (1.7%). A few false negatives are observed mainly along the borders of the surface water bodies (Figure 5. 8; sectors a, b, c). False positives are detected on the borders of Lough Derg (Figure 5. 8; sector d).

Considering all the parameters using for accuracy assessment, the best result is obtained with the fusion of Sentinel-1 and Sentinel-2 times series with the Bayesian operator sum.

5.3.2 Mapping of "temporary surface water": flooded areas

"Temporary surface water" bodies are extracted for the Sentinel-1 image of 09/01/2016 by applying the *"permanent surface water"* map resulted from experiment 3 as a mask. Table 5. 3 indicates high overall accuracy (> 98%), F-measure (0.90) and TPR (86%) for the detection of these *"temporary surface water"* bodies; the omission error is low (13.9%).

Table 5. 3. Comparison of image fusion results to the flood map of EMS Copernicus used as reference data for the date 9 January 2016.

Date	Overall Accuracy	F-measure	True Positive Rate	False Positive Rate	Omission error	Commission error
09/01/2016	98.79%	0.90	86.07%	0.35%	13.92%	5.72%

Figure 5. 9 identifies false positives along the borders of the Lough Derg lake and along the Shannon River. These false positives are related to sandbank in the course of the river or to narrow river banks identified as *"temporary surface water"* in our results while they are identified as *"permanent surface water"* in the flood map of the Copernicus Emergency Management Service (EMSR149). The image fusion method allows mapping almost all flooded areas as proven by the little amount of false negatives (Figure 5. 9).

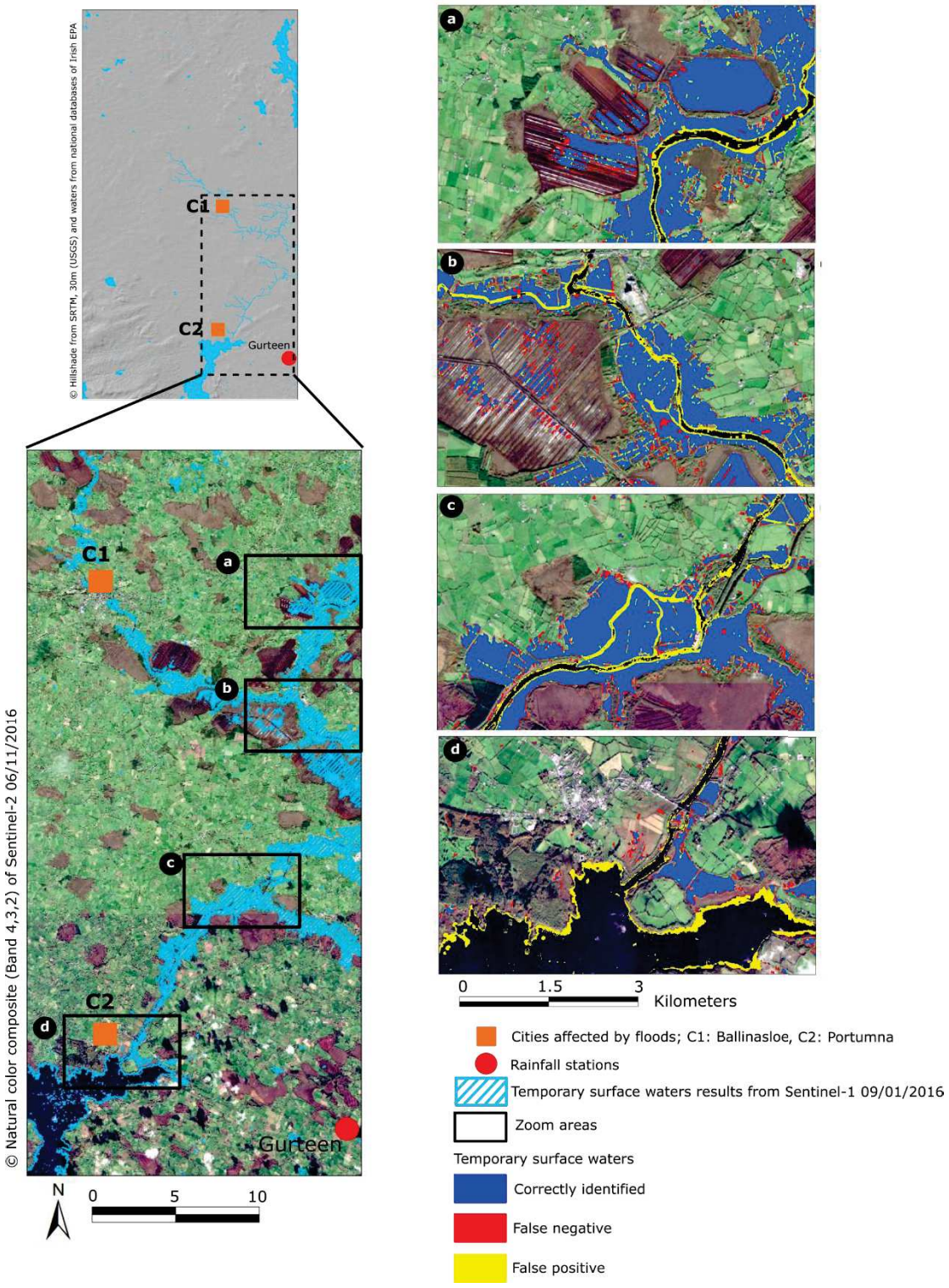

Figure 5. 9. Detection of the "temporary surface water" bodies in the Sentinel-1 image of 9 January 2016 and comparison to the flood map of Copernicus EMS, with details (zoom) on the Shannon River (sector a, b, c) and the north bank of Lough Dergh (sector d).

5.4 Discussion

Surface water dynamics can be monitored from the detection of "*temporary surface water*" from the time series images. These surfaces are extracted by applying the "*permanent surface water*" (detected in experiment 3) as a mask to posterior probability of Sentinel-1 time series. The remaining surfaces correspond to "*temporary surface water*" bodies (ca. 900 km2 over the study area). These areas are presented in a frequency map (Figure 5. 10a) which mapping the number of time a pixel is classified in "*temporary surface water*" bodies over the study area and for the complete time series. These areas are close to the main streams and located in the most flat areas of the region Figure 5. 10a). The pixels only classified once as "*temporary surface water*" bodies represents nearly 49% of the surfaces and can be excluded from "*temporary surface water*" bodies as they can be considered as noise or misclassification. The pixels with a frequency higher than 9 correspond to areas spatially close to the "*permanent surface water*" bodies and represent about 3% of the the surfaces. Therefore, the pixels classified at least 2 times and less than 9 times (Figure 5. 10b) are considered as the final "*temporary surface water*" maps.

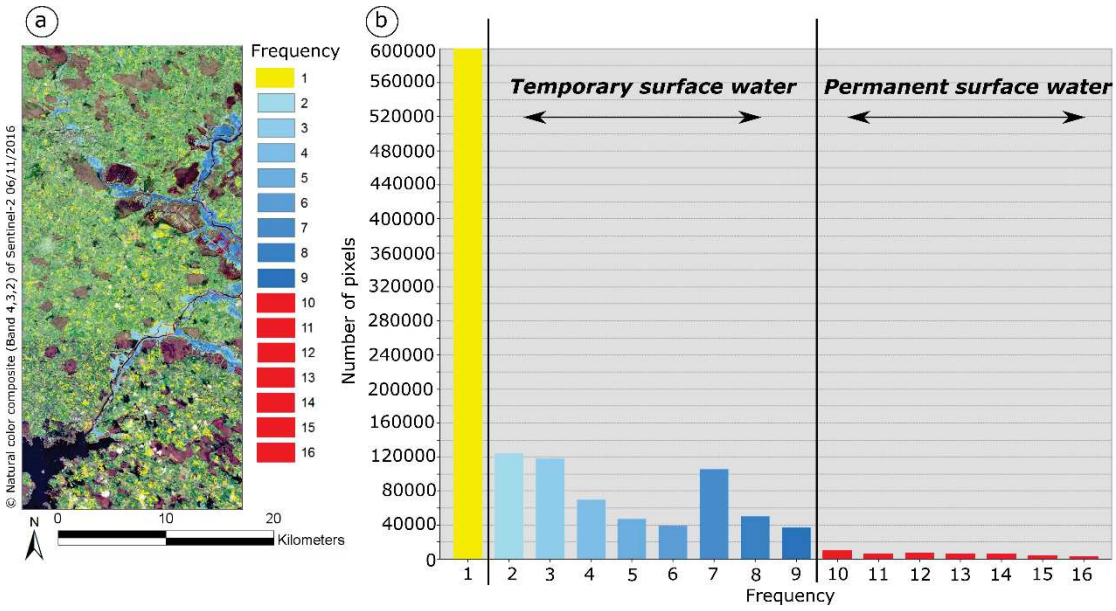

Figure 5. 10. Frequency map and histogram of "*temporary surface water*" bodies detected in the Sentinel-1 time series (16 images).

It is further possible to relate the detected *"temporary surface water"* bodies to the annual rainfall amounts. In December 2015, the largest amount of *"temporary surface*

water" bodies are observed over the one year period (Figure 5. 11) in relation to Storm Desmond (McCarthy et al., 2016). In January 2016, for lower amount of monthly rainfall, flooded areas are still observed because the water did not infiltrate in the soil or was evacuated by the drainage network. In Spring and Summer 2016, the surfaces of *"temporary surface water"* bodies decrease in relation to the decrease in rainfall. In May and June 2016, the detected water bodies seems to be overestimated probably because of higher noise in the Sentinel-1 images caused by strong wind and rough water surfaces. In Autumn 2016, only small surfaces of *"temporary surface water"* bodies are detected; the precipitation events of September 2016 did not cause flooding.

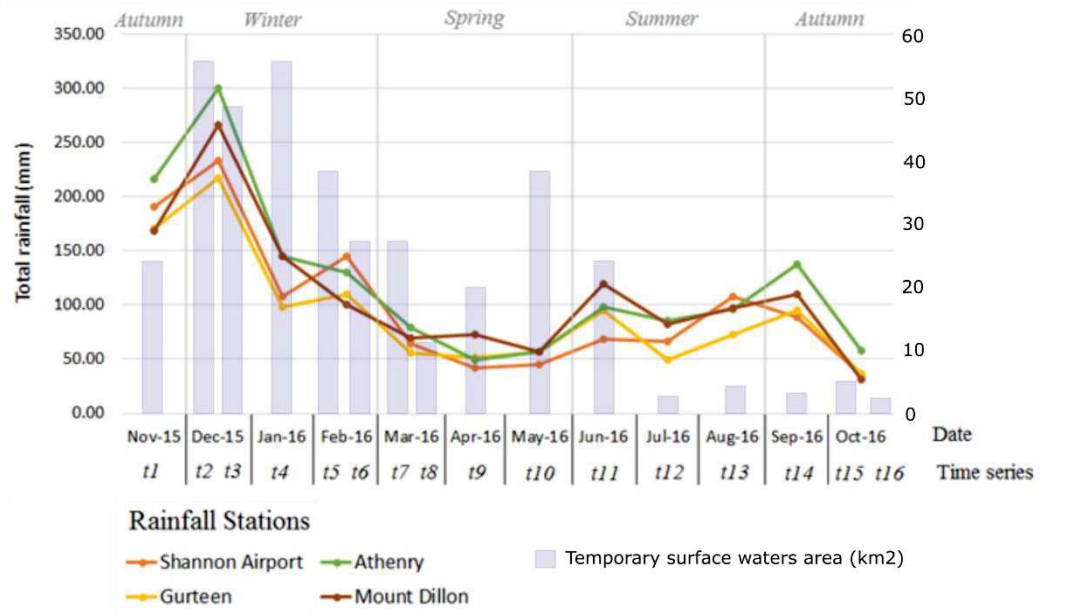

Figure 5. 11. Distribution of *"temporary surface water"* bodies per period and relation to the monthly rainfall amount for one hydrological year (November 2015 – October 2016).

The spatio-temporal dynamics of the *"temporary surface water"* bodies is further analyzed for the period November 2015 to April 2016 by interpretating the frequency value 2 to 4 (Figure 5. 12). The histogram of the possible pairwise combination (frequency 2) indicates that the maximum surfaces of flooded areas are observed for the period t2-t3 and t3-t4 (Figure 5. 12a); these flooded areas correspond spatially to local agricultural lands flooded during less than 4 weeks. The histogram of the possible combination of frequency 3 indicates that the maximum surfaces of flooded areas are observed for the period t2-t3-t4 (Figure 5. 12b); these flooded areas correspond spatially to larger agricultural lands flooded during less than 6 weeks. Finally, the histogram of

the possible combination of frequency 4 indicates that the maximum surfaces of flooded areas are observed for the period t2-t3-t4-t5 (Figure 5. 12c); these flooded areas correspond spatially to agricultural lands and wetlands flooded during more than 8 weeks.

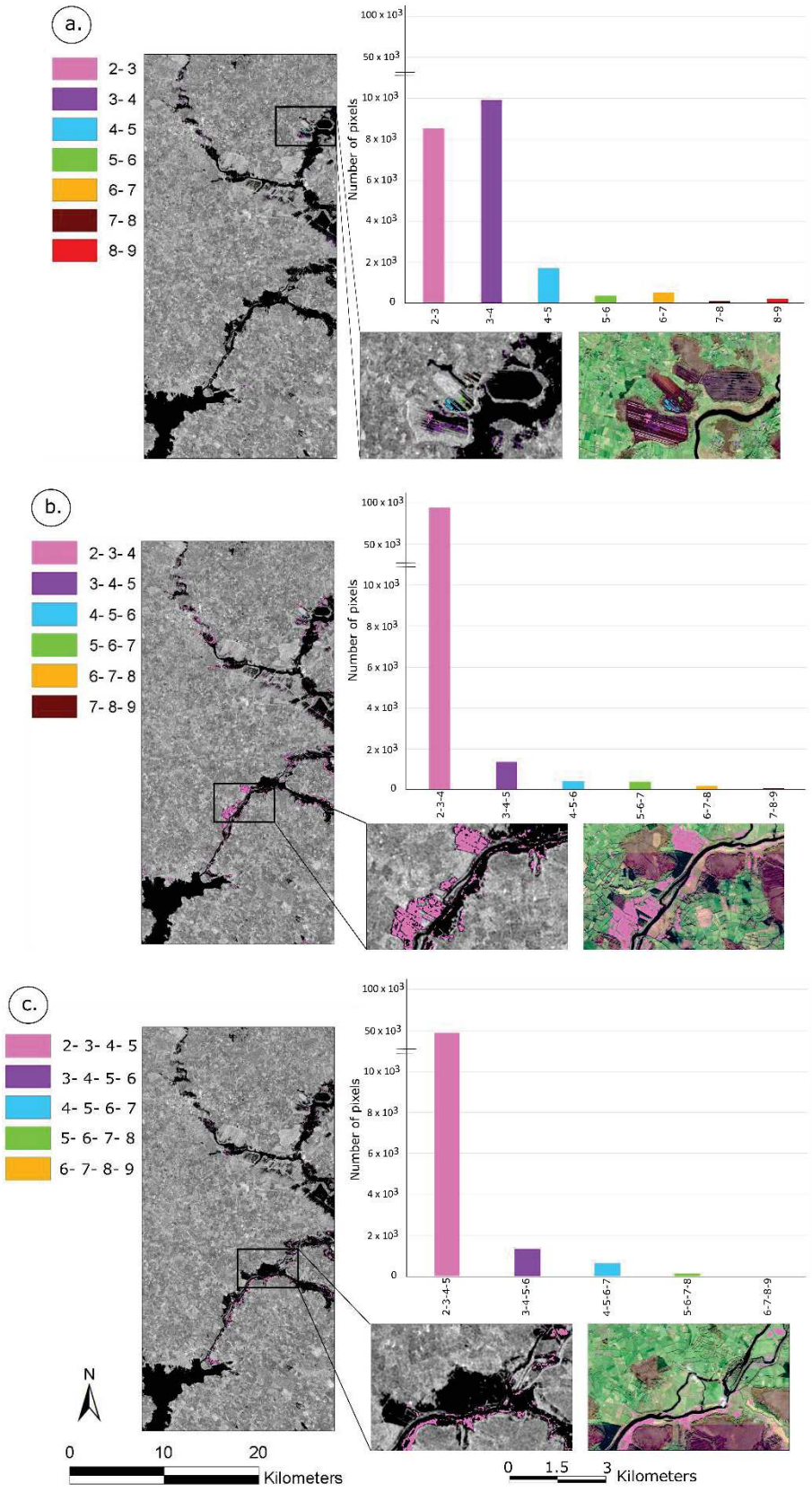

Figure 5. 12. Distribution and mapping of temporary surface water' pixels classified (a) twice, (b) third or (c) fourth during the flood period (from t2 to t9 e.g. Figure 5. 11).

The results show high similarity of permanent surface water with the Water & Wetness product using other fusion method. In this study, the methodology was specifically designed for the properties of Sentinel-1 and Sentinel-2 data. Since these data are freely available, it is possible to re-analyze other flooding events in order to estimate statistically the proportion of land being regularly flooded which will be useful for flood risk management, especially for large catchments, region or nation-wide analyses. Considering the results, the proposed method could be established as a permanent service solution for global surface water mapping. However, it is important to extend the observation period for example to 5 years in order to be able to better understand surface water behaviour.

5.5 Conclusions and perspectives

A methodology for combining surface waters detected from SAR (Sentinel-1) and optical (Sentinel-2) sensors is proposed using decision-level fusion rules. The methodology is applied over one hydrological year for the catchment of the Shannon river (Ireland) which has been severely impacted by flooding in Winter 2015/2016. The proposed methodology allows reducing the noise and increasing the detection level for time series of Sentinel-1 images, for multi-date Sentinel-2 images, and for the combination of both SAR and optical time series. Decision level rules are being tested for the particular case of surface water detection indicating that the Bayesian operator Sum is suitable for such application. Moreover, the analysis of image time series allows a better detection of both *"permanent surface water"* bodies (rivers and lakes) and *"temporary surface water"* bodies (flooded areas). It is further demonstrated that the fusion of SAR and optical time series increase the accuracy of the detection of the *"permanent surface water"* bodies. The proposed methodology is generic and does not require user interaction suggesting to be applicable for the monitoring of *"permanent surface water"* bodies over large areas and at high temporal frequency, with the possibility of using it as a permanent service if integrated on high performance computing centers. For the monitoring of *"temporary surface water"* bodies, the use of decision-level rules allows quantifying the probability of occurrence of inundated terrains at the pixel scale giving the possibility to understand the space and time

dynamics of the flooding. Such approach is of interest for improving flood risk management procedures.

This chapter has outlined the analysis in multi-source and multi temporal remote sensing data contribution for surface water mapping. Contribution of Sentinel-1 time series and Sentinel-2 multi-temporal imagery for mapping permanent water are analyzed through decision-level image fusion. The next chapter will presents another methods tested for surface water mapping and validation of proposed method for another thematic context.

Chapter 6

Another methods and validation on different thematic context

Contents

The previous chapter presented the contribution of multi-source and multi temporal remote sensing data for mapping surface water. This chapter will present another methods tested for surface water detection (Section 6.1) and two different experiments of massive processing to check the reproducibility of our proposed methods (Section 6.2).

6.1 Another methods

The objective of this section is to observe another methods in detecting surface water based on (1) the value of the SAR polarimetry (Sub-section 6.1.1) and (2) the fusion technique (Sub-section 6.1.2).

6.1.1 The value of SAR polarimetry for surface water mapping

In Chapter 1, we explained that SAR waves have polarization (horizontal and vertical). Different earth's surface objects will reflect SAR waves with different values of intensities. However, some objects, especially with anisotropic materials often reflect SAR waves with different polarizations and different intensities. Some target objects also can convert one polarization into another. For example, SAR sensor emits SAR wave with vertical polarization but target object reflect it to horizontal polarization, vice versa. Several images can be obtained from the same series of pulse by transmitting various types of polarizations and using receiving antennas with a specific polarization. Different combinations of polarization type can be used to synthesize color composite images which will be useful for Land Use and Land Cover classification (Chen and Wang, 2007). This technique is called SAR Polarimetry.

Equation 6.1 below explains about scattering matrix (S) of SAR. The matrix is used to identify the scattering behavior of target objects after interaction with electromagnetic waves. The matrix is represented by a combination of horizontal and vertical polarization of transmitted and received signals (Kumar, 2016).

$$S = \begin{bmatrix} S_{VV} & S_{VH} \\ S_{HV} & S_{HH} \end{bmatrix} \quad (6.1)$$

Where, HH is for horizontal transmit and horizontal receive, VV is for vertical transmit and vertical receive, HV is for horizontal transmit and vertical receive, and VH is for vertical transmit and horizontal receive. VV and HH polarization combinations are referred to like-polarized (co-polarization), because the transmitted and received state of polarizations are the same. HV and VH combinations are referred to cross-polarized due to the transmitted and received state of polarizations are orthogonal to one another (Woodhouse, 2005). Fully polarimetric data consists of all polarization combination (HH, HV, VV and VH). Yet, HV can be stated equal to VH, thus the effective complex scattering elements to build fully polarimetric data are HH, VV and HV (Kumar, 2016).

As mentioned in Chapter 3, **Sentinel-1 IW SLC mode available in this study only provides dual polarization data, VV and VH**. It is not fully polarimetric data, thus, the equation 6.1 becomes the equation 6.2 below (Ji and Wu, 2015).

$$S = \begin{bmatrix} S_{VV} & S_{VH} \\ S_{HV} & 0 \end{bmatrix} \quad (6.2)$$

where S_{HV} equal to $S_{VH,}$ thus, the matrix will become like below.

$$S = \begin{bmatrix} S_{VV} & S_{VH} \\ S_{VH} & 0 \end{bmatrix} \quad (6.3)$$

and the corresponding scattering vector is

$$k = [S_{VV} \quad 2S_{VH}]^T \quad (6.4)$$

SAR polarimetry can provide more information, thus it can upgrade object detection, extraction of edge, segmentation, classification, recognition and interpretation (Ji and Wu, 2015). Some references provide the usefulness of SAR polarimetry for monitoring surface water and explore its thematic classes (Irwin et al., 2018; Touzi et al., 2007). All our tests in Chapter 3 to 5 have been developed to highlight the interest of Sentinel 1 amplitude data (GRD images). Then, the objective here is to assess the capability of SAR polarimetry data for mapping different sub-classes of surface water.

First investigation tries to enhance the classification of surface water by using basic polarimetric method, using backscattering image from different polarizations (VV and VH), based on unsupervised classification. The second investigation explores features extracted from dual polarization decomposition process and performs unsupervised classification of dual polarizations data.

a. Classification using VV and VH polarizations

In the literature, amplitude information of dual polalimetric SAR imagery has been already used in a classical supervised classification scheme for land cover mapping (e.g., Abdikan et al., 2016). In this study, we decided to explore the interest of these data to enhance the water class (result of Chapter 4) and discovering several thematic classes (wetlands, etc). The method proposes an unsupervised classification scheme based on different cases of RGB combination of dual polarization (Figure 6. 1).

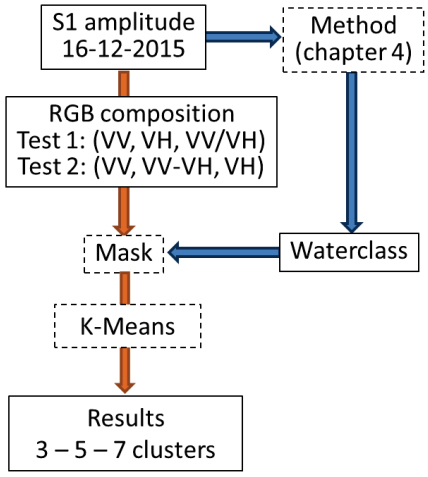

Figure 6. 1. Workflow of the first investigation.

In this first investigation, Sentinel-1 image on 16th December 2015 when floods happened in Ireland (Figure 3.2 – Zone A) is used. Backscattering image (sigma-nought) from VV and VH polarizations are then uses to build two different cases of RGB composition (Abdikan et al., 2016). Test 1 uses combination as follows:

- Red (R) : Sigma-nought VV (dB)
- Green (G) : Sigma-nought VH (dB)
- Blue (B) : Sigma-nought VV (dB) / Sigma-nought VH (dB)

While Test 2 utilizes combination as follows:

- Red (R) : Sigma-nought VV (dB)
- Green (G) : Sigma-nought VV (dB) - Sigma-nought VH (dB)
- Blue (B) : Sigma-nought VH (dB)

After building RGB images, we limit our study area as been explained in Chapter 3 (Figure 3.4). Then we used surface water areas resulted in Chapter 4 as a mask. We extract RGB images using the mask with the aim of focusing analysis in the surface water boundaries, (Figure 6. 2). Then we apply unsupervised classification based on K-Means in order to explore cluster and to reduce user intervention towards automatic processing. Classification results are produced with 3 until 7 clusters (Figure 6.3 and 6.4).

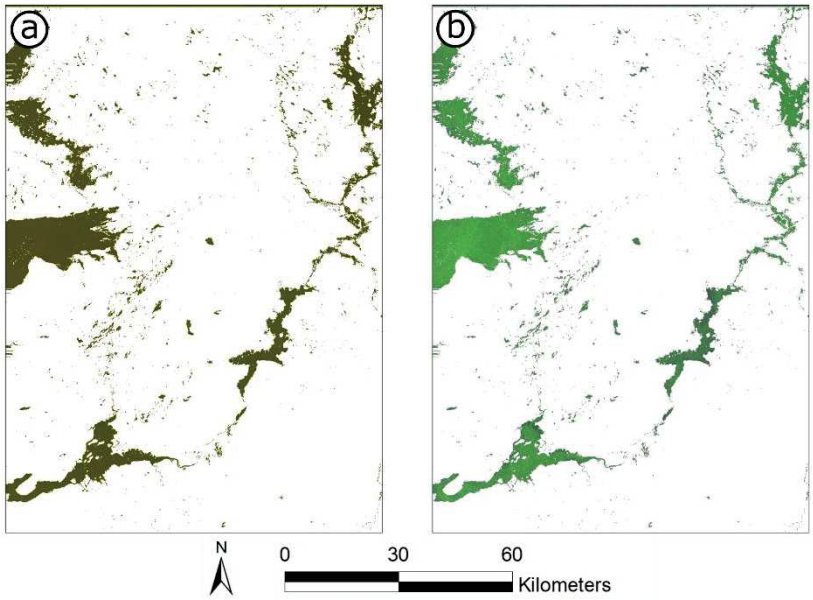

Figure 6. 2. RGB visualization of combinations from (a) Test 1 and (b) Test 2 in surface water boundaries.

The results are explored and assessed by visual interpretation. Figure 6. 3 show the results of classification with 3 clusters. In the area 1, there are red cluster and green cluster. In this area, based on reference data, red areas can represent intertidal flats, while green areas mean water bodies. However, red areas in different part of image scene, for example in northeast of scene, represent large lake which is water bodies. In addition, in area 2, red class did not represent intertidal flats but it represents bog or

wetlands. Another classification results with 5 and 7 clusters (Figure 6. 4) show a salt-and-pepper effect where it is not possible to identify several surface waters classes. . Test 2 also gives the same results (Figure 6. 5).

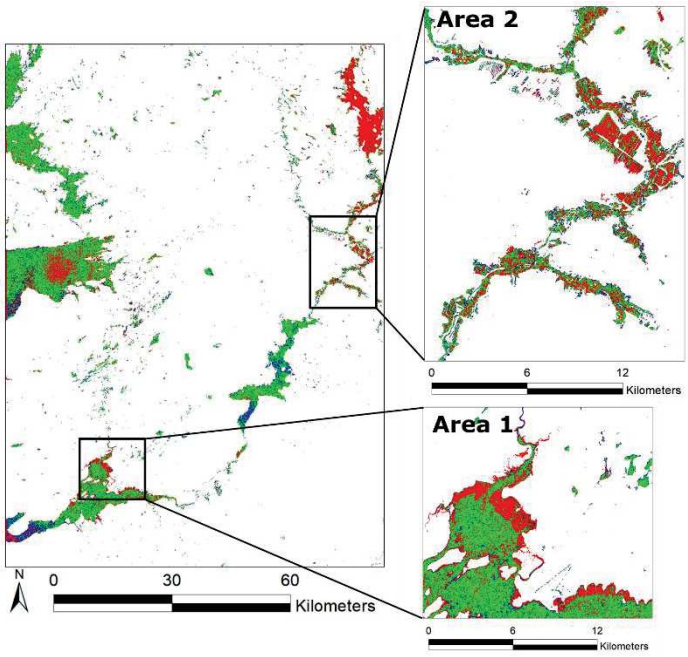

Figure 6. 3. Classification result of Test 1 with 3 clusters (red = cluster 1 / blue = cluster 2 / green = cluster 3).

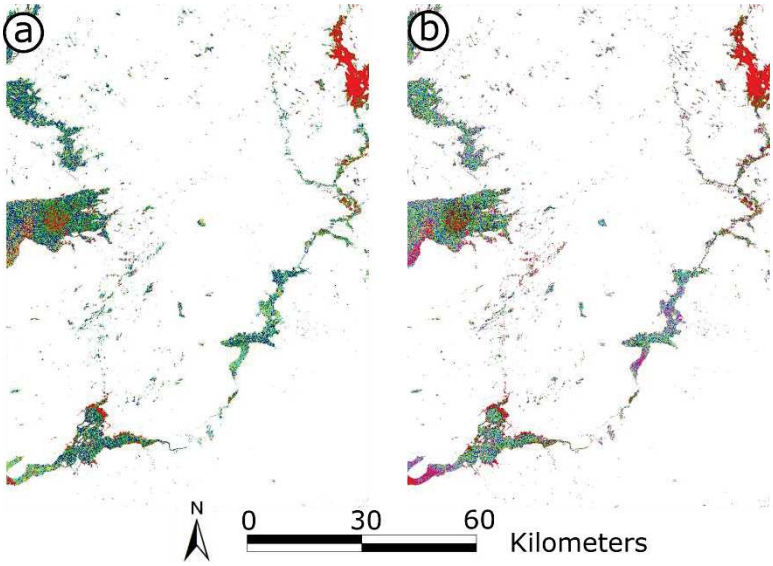

Figure 6. 4. Classification results of Test 1 with (a) 5 clusters and (b) 7 clusters.

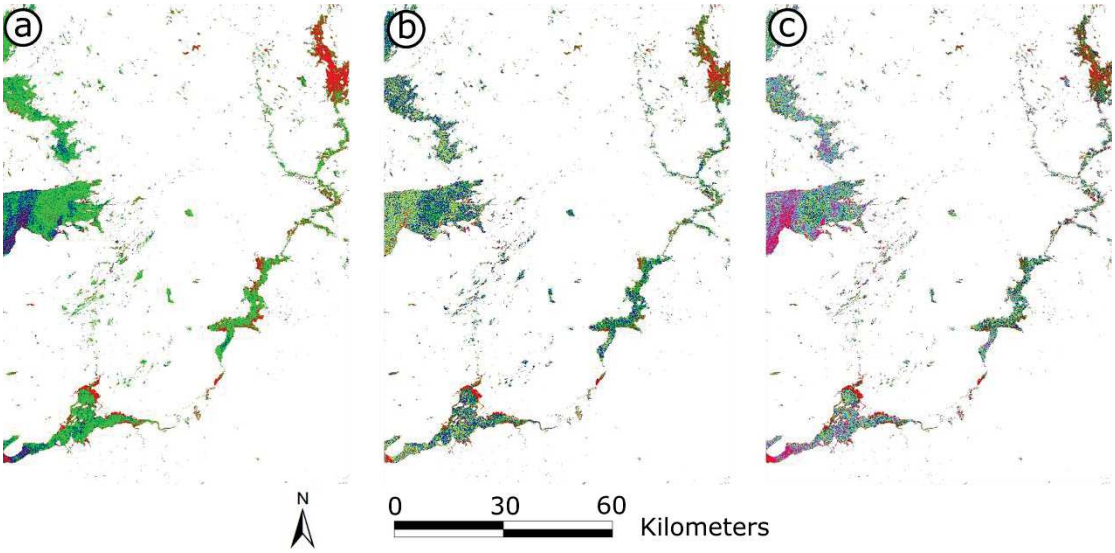

Figure 6. 5. Classification results of Test 2 with (a) 3 clusters, (b) 5 clusters and (b) 7 clusters.

In these results, pixels values of RGB images will depend on sigma-nought characteristics. Sigma-nought images are influenced by surface roughness. The study area covers a large area. Sometimes, in the south part, surface water consists of smooth water surface while in the north part, surface water consists of rough water surface. The different surface roughness can be caused by rain or wind in the north part. Thus, even in the north and south parts, surface water corresponds to lake (for example), the sigma-nought values will be different in both parts. This explanation clarifies why we get some classes (different colours) in the results but we can not interpret those classes into surface water thematic classes.

b. Applying H/Alpha dual decomposition and H-Alpha dual classification

In order to extract scattering mechanisms, target decomposition is an important method. This approach represents target scattering by several basic scattering mechanisms. The Sentinel Application Platform (SNAP) provides H/Alpha dual decomposition for Sentinel-1 dual polarization image. The H/Alpha decomposition is based on the Eigen decomposition of the coherency matrix. For a dual polarization SAR image, the coherency matrix of each pixel is 2x2 (T_{dual}), which is nonnegative definite and Hermitian. The eigenvalue decomposition of T_{dual} is shown below (Shan et al., 2011).

$$T_{dual} = \begin{bmatrix} T_{11} & T_{12} \\ T_{12}^{*} & T_{22} \end{bmatrix} = U \begin{bmatrix} \lambda_1 & \\ & \lambda_2 \end{bmatrix} U^{H} = \lambda_1 u_1 u_1^{H} + \lambda_2 u_2 u_2^{H} \quad (6.5)$$

where

$$U = \begin{bmatrix} u_{11} & u_{12} \\ u_{21} & u_{22} \end{bmatrix} = [u_1 \quad u_2] \quad \text{and} \quad u_i = e^{j\phi i} [\cos \alpha_i \quad \sin \alpha_i \, e^{j\delta_i}]^T \tag{6.6}$$

H denotes the conjugate transpose, and * denotes the conjugate. Then, the polarimetric entropy H and the scattering angle α can be derived as follows.

$$H = \sum_{i=1}^{2} P_i log_2 P_i \quad \text{and} \quad \sum_{i=1}^{2} P_i cos^{-1}(|u_{1i}|) \tag{6.7}$$

where

$$P_i = \lambda_i / \sum_{j=1}^{2} \lambda_j \tag{6.8}$$

Besides features exploration from decomposition process, terrain and land use classification is also the important applications in SAR polarimetry. The land classification algorithms based on the target scattering mechanisms have led to highly descriptive results about the physical properties of the Earth's surface.

In this part, second investigation is conducted using Sentinel-1 IW image on 09th January 2016, when floods happened in Ireland. The investigation uses Sentinel-1 IW SLC image because it needs both amplitude and phase information. This second investigation consists of two experiments:

(1) the first experiment explores features extracted from decomposition process;

(2) the second experiment performs classification using those features.

The objective is to observe features from H/Alpha dual decomposition and result from H-Alpha dual classification in detecting thematic classes of surface water.

In order to perform H/Alpha dual decomposition or H-Alpha dual classification, pre-processing steps including **deburst, apply orbit file and polarimetric speckle filtering** (Figure 6. 6) must be done. Sentinel-1 IW mode captures three sub-swaths. Each sub-swath consists of a series of bursts. In the SLC (Single Look Complex) level, each burst has been processed as a separate SLC image. Deburst process is applied in order to merging the sub-swaths and created wide area product. After deburst step,

apply orbit file is performed to solve problems in orbit information. Then, in order to clean up some of the speckle inherent in SAR images, polarimetric speckle filtering is applied. This filter can take advantage of all bands and preserve the complex information.

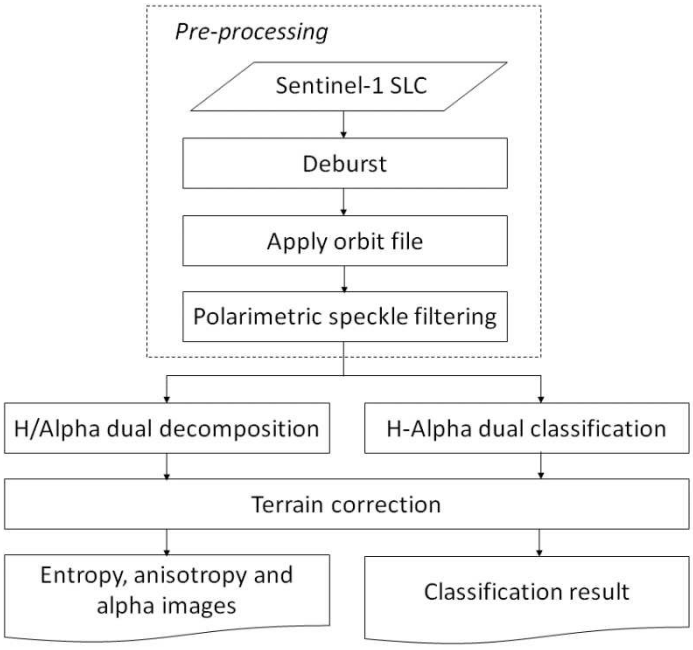

Figure 6. 6. Workflow of second investigation.

Polarimetric decomposition allows the separation of different scattering contributions and can be used to extract information about the scattering process. Using dual polarimetric data, only **H/Alpha dual decomposition** can be performed in SNAP software. This process is carried out after pre-processing steps. The entropy, anisotropy, and alpha images are the features resulted from this process after terrain correction (Figure 6. 7).

H/Alpha dual decomposition results show separation of surface waters from the other land cover type, especially in entropy and alpha image (Figure 6. 7). Same with the first investigation, we limit our study area as been explained in Chapter 3. However, we performed the limitation to the results due to the SNAP software used for this investigation needs the whole image scene for the process. Then, we focus only on surface waters boundaries by applying mask as the first investigation (Figure 6. 1).

Each feature resulted from H/Alpha dual decomposition does not represent different classes of surface waters (Figure 6. 8). Entropy and alpha images only present one

colour (blue). Anisotropy present some colours in the surface water boundaries. However, visual comparison with reference data (the national database of Ireland) show that those colours can not represent specific thematic classes of surface water. Compared with permanent and temporary surface water discussed in the Chapter 5, in the anisotropy image, permanent surface water will be represented with dominant red colour, while temporary surface water areas consist of several colours.

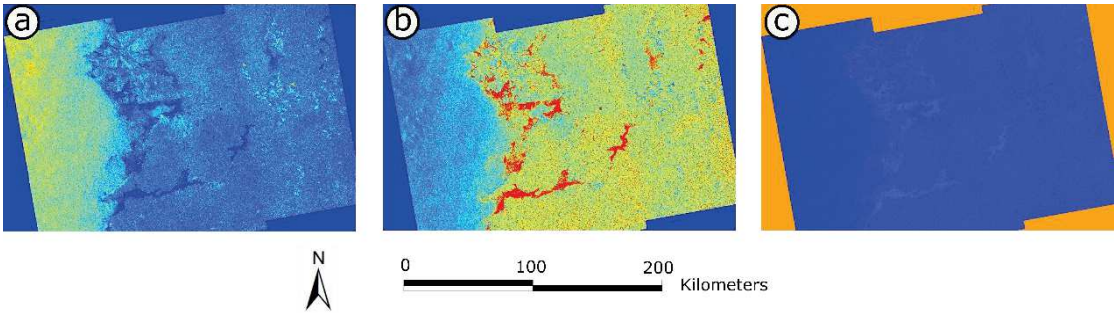

Figure 6. 7. Results of H/Alpha dual decomposition ; (a) Entropy, (b) Anisotropy, (c) Alpha.

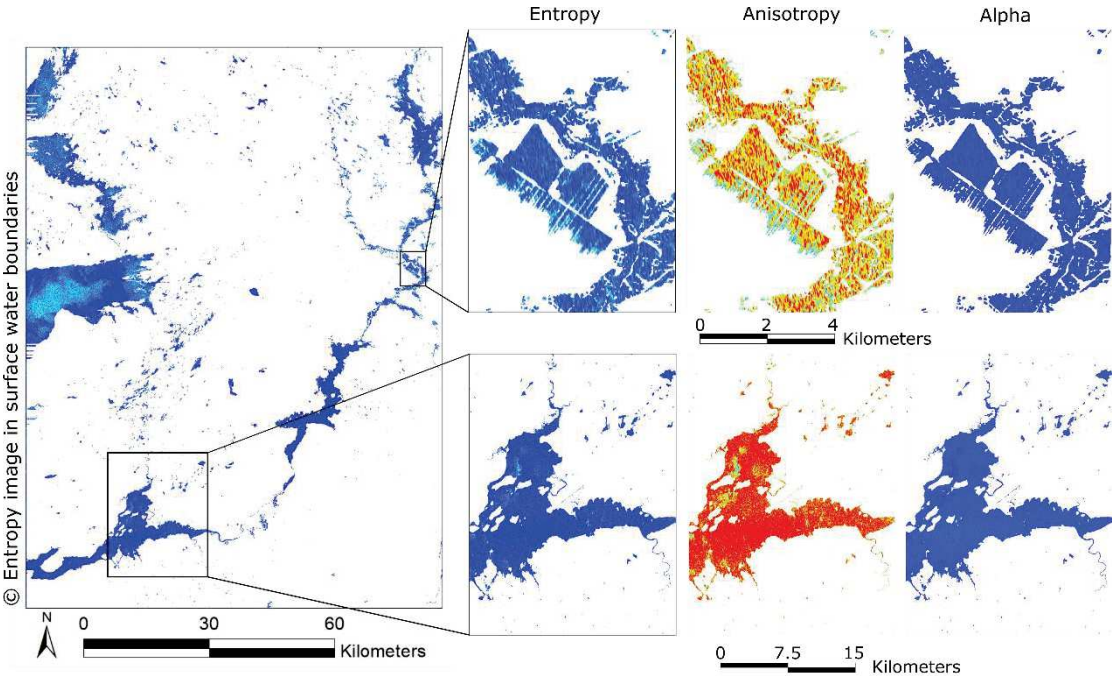

Figure 6. 8. Results of H/Alpha dual decomposition in surface waters boundaries (Zone A – Ireland).

A RGB color composition image with entropy in Red, anisotropy in Green, and alpha in Blue is built in order to explore surface waters (Figure 6. 9). Unfortunately, compared with reference data, the result also does not show different thematic classes of surface

waters. It can not distinguish between rivers, lakes and wetlands. The colors majority is red, but in some parts there are blue or green colors.

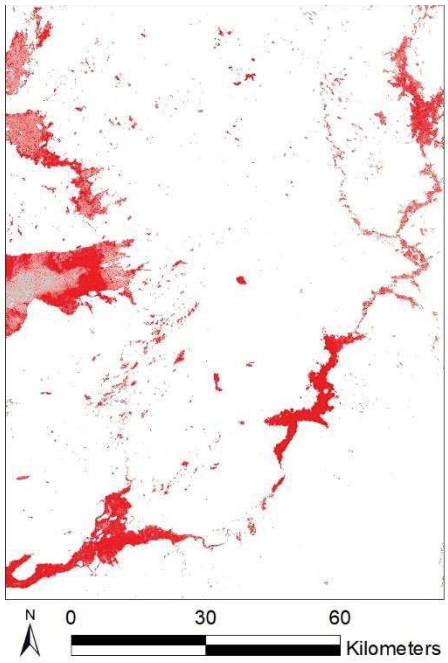

Figure 6. 9. RGB image of entropy, anisotropy and alpha in surface waters boundaries.

For terrain and land use classification, the **H-Alpha dual classification** is performed after pre-processing steps. The SNAP software used in this investigation only provides Whishart classifier for unsupervised classification of Sentinel-1 dual polarization data. Thus, the classification of dual polarimetric data uses a combination of entropy/alpha and unsupervised Whishart classifier. The unsupervised Wishart classification separates data into nine clusters corresponding to nine classes of different scattering mechanisms, using the zones defined in the H/Alpha plane. The Wishart classification will continue to compute the centers of the nine clusters, then reclassify the pixels based on their Wishart distances to cluster centers. This procedure will repeat several time until the user defined total number of iterations is reached (Lee et al., 2004).

The result (Figure 6. 10) indicated that H-Alpha dual classification is successfully classified land cover from Sentinel-1 SLC data. However, it does not show different classes of surface waters. It can only extracted surface waters from the other land cover type, but it cannot divide surface waters into different classes. This process needs Sentinel-1 SLC type as an input image which have larger size than Sentinel-1 GRD type.

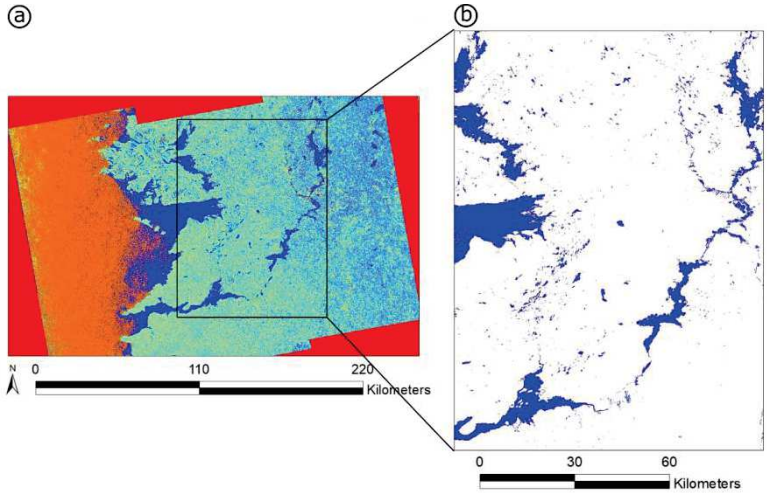

Figure 6. 10. Results of H-Alpha dual classification; (a) Classification result in all image scene, (b) Classification result in surface waters boundaries (zoom area).

Using reference map of Copernicus EMSR149, extracted surface water from the classification has almost the same accuracy assessment with surface water extraction from Chapter 4. However, the result from Chapter 4 has slightly better assessment (see Table 4.3). Overall accuracy in Chapter 4 is 98.68% (Table 6. 1) while the result from this classification has value of 98.32%. F-measure value in Chapter 4 is 0.92 while in here it has value of 0.90.

Table 6. 1. Accuracy assessment of extracted surface water from H-Alpha dual classification.

Overall Accuracy	**F-measure**	**True Positive Rate**	**False Positive Rate**	**Omission error**	**Commission error**
98.32%	0.90	85.29%	0.44%	14.71%	5.19%

The extent of surface water extracted from H-Alpha dual classification is presented with several zooms overlaying Sentinel-2 imagery in Figure 6. 11. The figure shows that false negatives occur mainly along the borders of surface water bodies, where most of the false positives are also located.

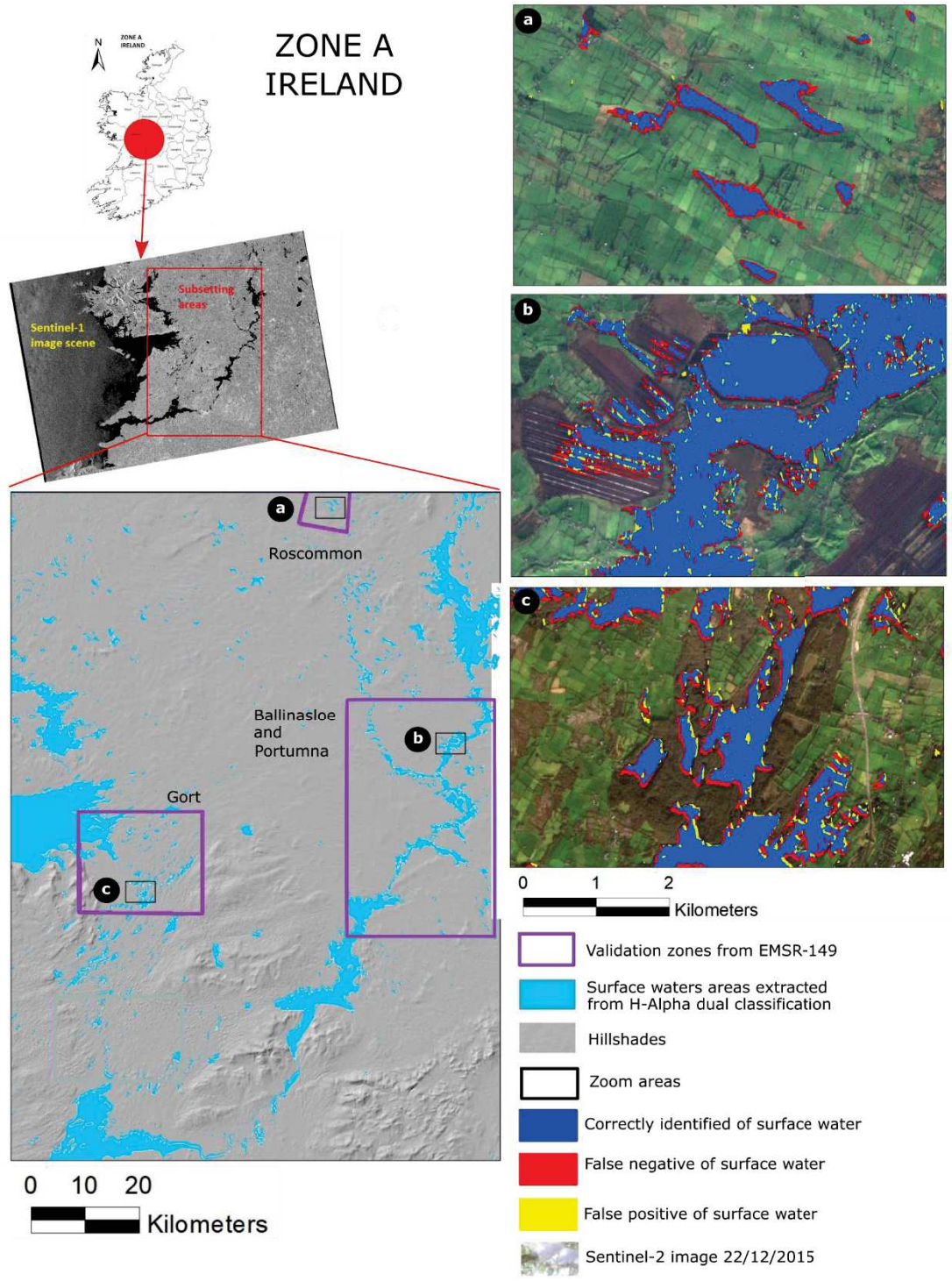

Figure 6. 11. Surface water extraction result from H-Alpha dual classification with several zoom areas overlaying Sentinel-2.

In conclusion, these tests could not show the interest of our investigations using dual polarization of SAR polarimetry methods, to map different surface waters thematic classes. The surface water extracted from H-Alpha dual classification has almost the

same accuracy values with surface water extraction from Chapter 4, with scarcely lower assessment.

6.1.2 The value of multi-source image fusion at feature level

In Chapter 2, we reminds that three levels of image fusion are existing: pixel-level, feature level and decision level. Classically in the literature, for surface water mapping, the use of optical and SAR fusion is in decision or feature levels. In Chapter 5, image fusion at decision level has been tested and assessed. In this sub-section, we investigate **image fusion at the feature level** where features are computed for each source separately and fed into the same classifer through a unique feature set. The classical supervised machine learning algorithm Random Forest has been chosen to classify surface water and to compare results with the proposed methods of Chapter 4.

Feature level of images fusion are carried out using **Principal Component Analysis (PCA)** method. PCA is a statistical technique which converts multivariate data sets from intercorrelation variables into a new uncorrelated linear combination data set of original variables. This classical technique is considered useful for image fusion by reducing multidimensional data to lower dimensions while retaining most of the information (Karamizadeh et al., 2013). Computation in PCA include the calculation of covariance or correlation matrix, eigenvalues, eigenvectors and production of PCs bands (Pohl and Van Genderen, 1998).

Random Forests (RF) are combination of tree predictors which each tree depends on random vector values taken independently and with the same distribution for all trees in the forest (Breiman, 2001). RF classification refers to a new approach that uses not only one, but many classifiers and their decisions are combined usually by plurality vote (Tian et al., 2016). RF classification are successfully applied in previous research for surface waters (e.g., Huang et al., 2018; Tian et al., 2016). Random Forest does not perform well when features are monotonic transformation of other features. Using PCA before performed RF classification can reduce the number of features and delete collinear features.

a. General methodology

The general methodology is described in Figure 6. 12. Classical features derived from Sentinel-1 GRD time series images (S1), Sentinel-2 multi-temporal images (S2) and Sentinel-1 SLC with polarimetry features (S1-pol) will be calculated from each data sources.

For Sentinel-1 GRD, time series imagery described in Chapter 5 are used again with sigma-nought VV as the feature. Since time series data consists of 16 images with different date, there will be 16 sigma-nought images as the features from this source. As for Sentinel-1 SLC, we will used polarimetry features which obtained from H/Alpha dual decomposition. The features are consisting of anisotropy, entropy and alpha images. The both images of Sentinel-1 SLC acquired on 16/12/2015 and 09/01/2016 when floods occurred are used for test. Thus, there are six features from this polarimetry source.

For Sentinel-2 data, the three multi-temporal images with low cloud cover uses in chapter 5 are tested. For each image, 8 features are extracted i.e., Band 2, 3, 4, 8, NDWI2 and textures images (correlation, dissimilarity and homogeneity). The four main bands are used due to their high spatial resolution (10 meter), as for NDWI2 are used as representation of water index used in previous chapter. Some textures images from Band 8 are used to consider also the spatial relationship of pixels. Correlation, dissimilarity and homogeneity are selected based on their low correlation with the other textures images of Sentinel-2. Consequently, there are total of 24 features from this source.

Based on these features, several tests are then performed which used four combination of sources as explained below (Figure 6. 12).

- Test 1: feature-level image fusion of S2 and S1, **40 features** in total.
- Test 2: feature-level image fusion of S2 and S1-pol, **30 features** in total.
- Test 3: feature-level image fusion of S1 and S1-pol, **22 features** in total.
- Test 4: feature-level image fusion of S2, S1 and S1-pol, **46 features** in total.

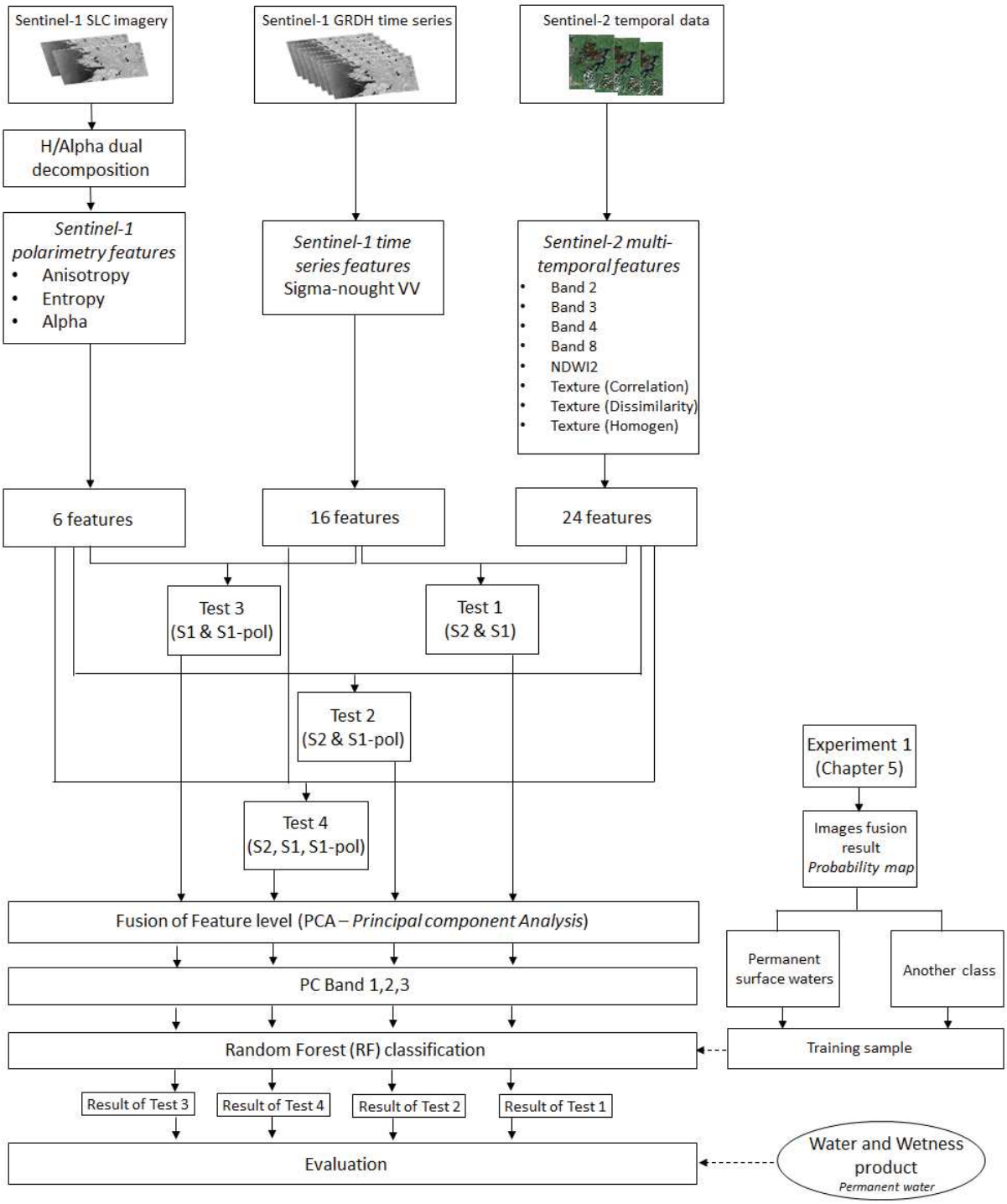

Figure 6. 12. Flowchart of processing steps in feature-level image fusion.

b. Selection of PCs bands

The second step consists to calculate the covariance matrix as the most common method to use in PCA with the majority of remote sensing datasets. An important issue in PCA

is to select the amount of the PCs bands which will be used for classification. Percentage of variance from PCs bands, their histograms and their cumulative values are used as criterias (Gniazdowski, 2017). The histograms showed percentage of variance, from largest to smallest, which the shape resembles a mountain slope. The amount of the extracted principal components can be selected from PCs bands located on the steep slope.

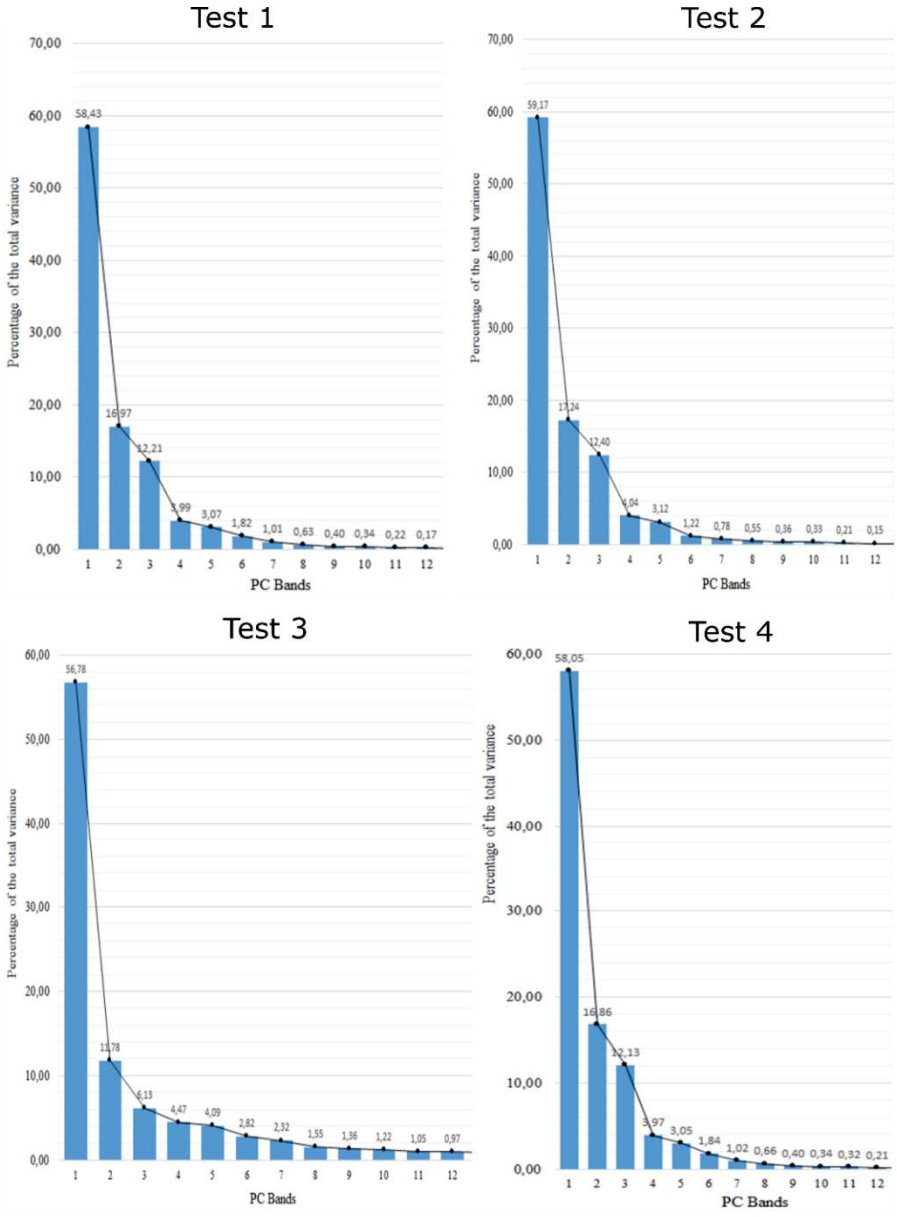

Figure 6. 13. Percentage of variance from each PC Bands in all tests.

Figure 6. 13 shows that PC Band 1 in all tests carry over 50% of the information. Cumulative percentage of variance from PCs Bands 1, 2 and 3 in all tests represented more than 70% of total variance. In addition, it can be seen from Figure 6. 13 that PCs

Bands 1, 2 and 3 are located in the steep slope in all tests, except test 3. PC Band 4 and the rest have shape like gentle slope. Therefore, **PCs Bands 1, 2 and 3** from the results of PCA **are selected to be used as input data in Random Forest** (RF) classification.

The contribution of features in selected PCs Bands is performed through the analysis of eigenvectors values.. The eigenvectors indicate the proportion of each input feature contributes to each PC band. In test 1, sigma-nought VV 08/06/2016 and 18/10/2016 have the biggest contribution in PCs Bands 1, 2 and 3 with high eigenvectors values. In test 2, entropy 16/12/2015 and anisotropy 09/01/2016 have greater impact than the other input features. For test 3, sigma-nought VV 08/05/2016, 30/10/2016 and 18/10/2016 have the biggest contribution. For the last test (test 4) which combined features from all sources, entropy 16/12/2015 and anisotropy 09/01/2016 have the biggest impact as in test 2.

If we look closely, in all tests, features from SAR data always have the biggest contribution. When combined with optical data (S2), features from S1 and S1-pol will give high contribution. In the test 3, when combination is from two types of SAR data, S1 with only amplitude values give higher contribution than S1-pol features. Yet, when all sources are combined, S1-pol features will give the biggest impact. The features contributions in PCs Bands 1, 2 and 3 will affected images results and give influence in outcome of classification.

c. Random Forest (RF) classification

For the third step, input data for RF classification are layer stacking of PCs Bands 1, 2 and 3 (multi-bands image with PC Band 1 in red channel, PC Band 2 in green channel and PC Band 3 in blue channel). Training samples for this RF are result of experiment 1 from Chapter 5 (Sentinel-1 time series image fusion result). The final results from each test are then assessed using Water and Wetness product.

Table 6. 2 shows quantitative evaluation results for test 1 until test 4. From the assessment, it can be seen that Test 3 with Sentinel-1 combination between features from Sentinel-1 GRD and Sentinel-1 SLC (polarimetry) give the best statistical result. Test 3 gives the highest overall accuracy and F-measure than the other tests.

Table 6. 2. Accuracy assessment for four tests in feature level images fusion.

Tests	Overall Accuracy	F-measure	True Positive Rate	False Positive Rate	Omission error	Commission error
Test 1 (S2 & S1)	98.09%	0.74	92.23%	1.73%	7.77%	38.69%
Test 2 (S2 & S1-pol)	97.63%	0.69	91.64%	2.19%	8.36%	44.52%
Test 3 (S1 & S1-pol)	99.28%	0.89	97.84%	0.67%	2.16%	18.76%
Test 4 (S2, S1, S1-pol)	97.09%	0.65	93.47%	2.80%	6.53%	50.22%

Compared with result of Experiment 3 (S1 & S2) in Chapter 5 (see Table 5.2), Test 1 in this investigation has lower values of accuracy assessment. Overall accuracy in Experiment 3 is 99.95% while Test 1 has value of 98.09%. F-measure value in Experiment 3 is 0.99 while Test 1 has value of 0.74. Overall, results from Chapter 5 have higher accuracy assessment than all results tests in this investigation.

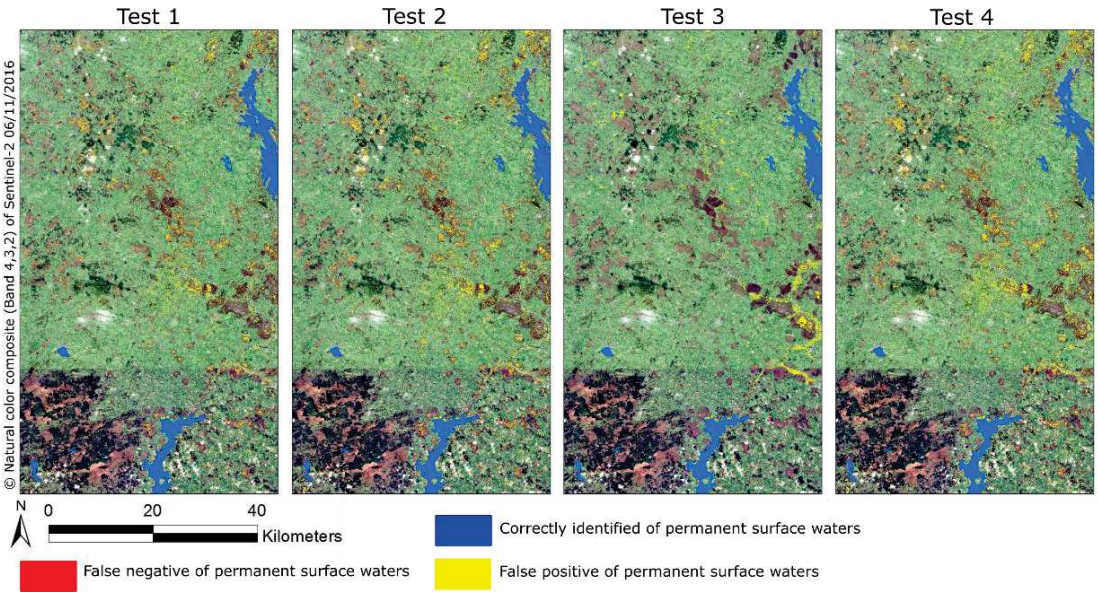

Figure 6. 14. Visualization results from all tests in feature-level image fusion.

Visual interpretation of results for all tests are represented in Figure 6. 14. The result from test 3 represents not only permanent surface water but also temporary surface water. Thus, there are many false positives appeared. It is due to classification input is PCs bands which represented variance in features. Floods areas in time series images give strong variance and captured by PCs bands. There is almost no false negative

appeared in all tests results. Only test 3 provided different extraction of water surfaces. In another tests, many false positives appeared outside floods or temporary area.

In test 1, PCs Bands 1, 2 and 3 have highest contribution from sigma-nought VV 08/06/2016 and 18/10/2016 which represent no-floods images. Therefore, result in test 1 does not extract temporary surface water. As been discussed before, there are roughness of the water surfaces caused by wind and turbulence effects, thus some errors are appeared cause false positives in the result. In test 2 and test 4, the highest contribution come from entropy and anisotropy images which detect water in wetland areas. Therefore the results show scattered false positives mostly in wetland areas.

From these analyzes, it can be concluded that multi-source image fusion at the feature-level can not give better result in mapping permanent surface water than image fusion at the decision-level. However, this method can give high overall accuracy with more than 97% and high F-measure values, about 0.7.

6.2 Validation on different thematic context through experiments of massive processing

6.2.1 Monitoring surface water in Grand-Est region, France

The purposes of this sub-section are to investigate the use of automatic mapping of surface water for spatio-temporal monitoring, to study the use of image fusion method proposed in Chapter 5 for mapping permanent surface water and to perform rapid mapping of temporary surface water for Zorn River flooding occurred during the winter 2018 (described in Chapter 3 – Part 3.1.2.2). Spatio-temporal monitoring in the Part a will apply method from Chapter 4 and map surface water as a whole. Part b and c will apply methods in Chapter 5 in mapping permanent and temporary surface water.

a. Spatiotemporal distribution of surface waters in Grand-Est

Using automatic mapping **method from Chapter 4**, eleven images of surface water are produced over short-time period (Table 3.4). The method is based on single data extraction (The Water-S1 method).

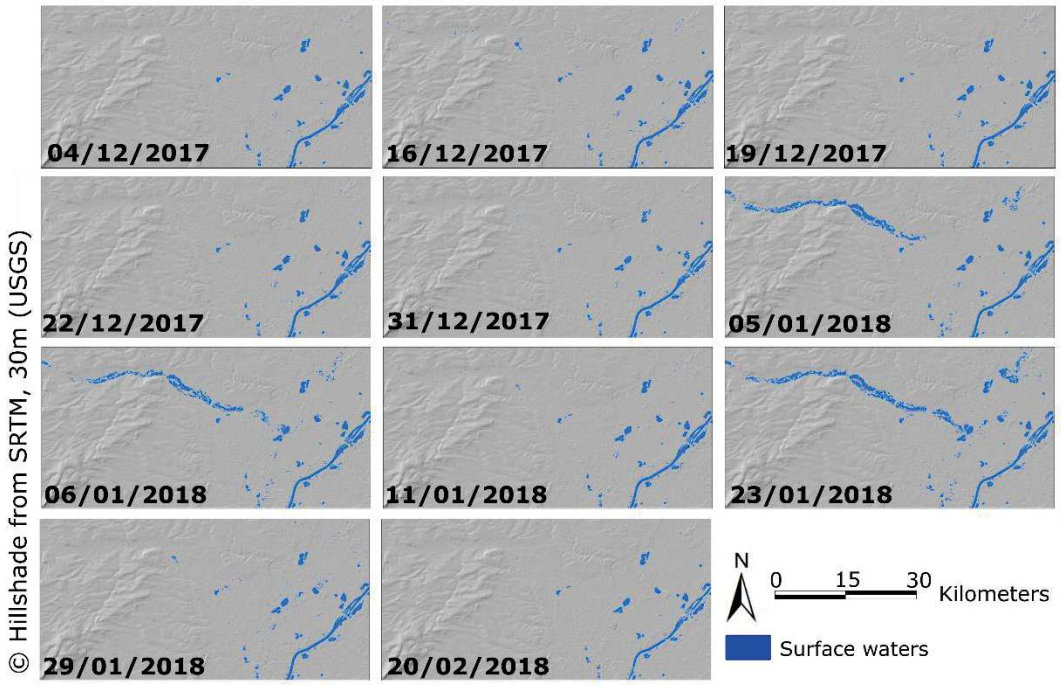

Figure 6. 15. Spatiotemporal distribution of surface waters based on automatic and rapid mapping extraction.

Figure 6. 15 represent spatiotemporal distribution of surface waters before, during and after floods events. In December 2017, water surfaces remain almost the same (Figure 6.18). There are no drastic changes occurred in this month. In 5th and 6th January 2018, there are surface waters appear in the north areas. Probably due to Storm Eleanor which caused inundation in those date along Zorn River. In, 11th January 2018, those floods disappear. Nevertheless, those areas along Zorn River (north areas in the figures) become flooded again on 23rd January 2018 with larger distribution of waters due to heavy precipitation (Sertit, 2018). Then, on 29th January 2018 and February, water surfaces become normal again. With short range interval observation, we can see more dynamic changes of water surfaces.

b. Large coverage mapping of permanent surface water using time series image fusion

In order to map permanent surface water in the study area, Sentinel-1 time series images fusion method in decision level using bayesian sum as presented **in Chapter 5** will be applied. In Chapter 5, time series images consist of data in one year period. However, to acquire permanent surface water, time series images are based on three months period. It is interesting to investigate if three months period is adapted and sufficient in determining permanent surface water areas.

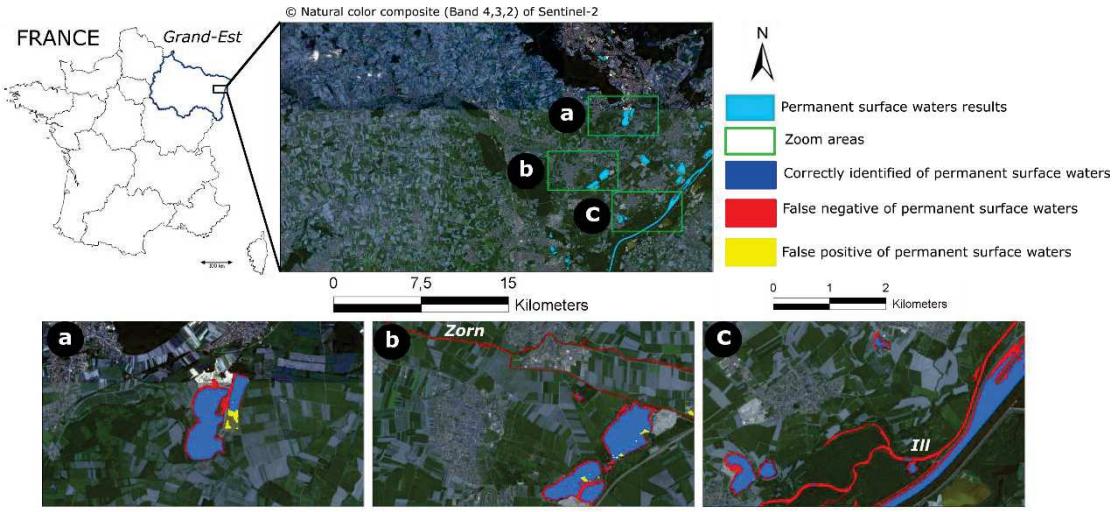

Figure 6. 16. Permanent surface water result from image fusion.

Quantitative evaluation is based on BDTopo IGN as reference data (Table 6. 3) and visual interpretation of results are presented in Figure 6. 16. Overall accuracy shows high value with more than 99% and F-measure provides value more than 0.7. Zorn River and Ill river are not detected due to their narrow width and the presence vegetation along their border which cover the signal, however Rhin River is successfully detected. In consequence, True Positive Rate only reaches about 60% and omission error reaches about 39%. However, there are almost no false positive and false negative appear, except in narrow rivers or border areas. Thus, the applied method using temporal image fusion allow value-added in acquiring permanent surface water in this case of short-term period. These results are consistent with those obtained on the case study of Italy and confirm that Sentinel-1 images are suitable for minimum surface of 1 ha (see Chapter 3).

Table 6. 3. Quantitative evaluation of permanent surface water result from Sentinel-1 time series image fusion.

Overall Accuracy	F-measure	True Positive Rate	False Positive Rate	Omission error	Commission error
99.31%	0.74	60.17%	0.02%	39.83%	2.20%

c. Rapid mapping of temporary surface water, case study: Zorn River flooding, Grand-Est

In this sub-section, temporary surface water is tried to be detected with focus on floods delineation. Using permanent surface water extracted in previous part (Part b of Sub-section 6.2.1) as mask, temporary surface water are extracted from each single date. This sub-section applied methods proposed **in Chapter 5**. Based on reference data, floods are detected on 23th January 2018, yet based observations in Part a of Sub-section 6.2.1, there are also floods in 5th and 6th January 2018. Thus, quantitative evaluations for floods areas are only performed for inundation result on 23th January 2018 (Table 6. 4) with flood map produced by ICUBE-SERTIT as reference data (see Chapter 3 – Part 3.1.2.2).

Table 6. 4 Quantitative evaluation of floods areas from Sentinel-1 single date image (23/01/2018).

Overall Accuracy	F-measure	True Positive Rate	False Positive Rate	Omission error	Commission error
98.76%	0.90	86.50%	0.43%	13.50%	6.91%

Even overall accuracy is lower than result of permanent surface water, the assessment from floods areas of 23th January 2018 results give better F-measure, True Positive Rate and omission error. In a qualitative point of view, with the visual interpretation in Figure 6. 17, floods along Zorn River are detected successfully with false positive and false negative appear only in the border area.

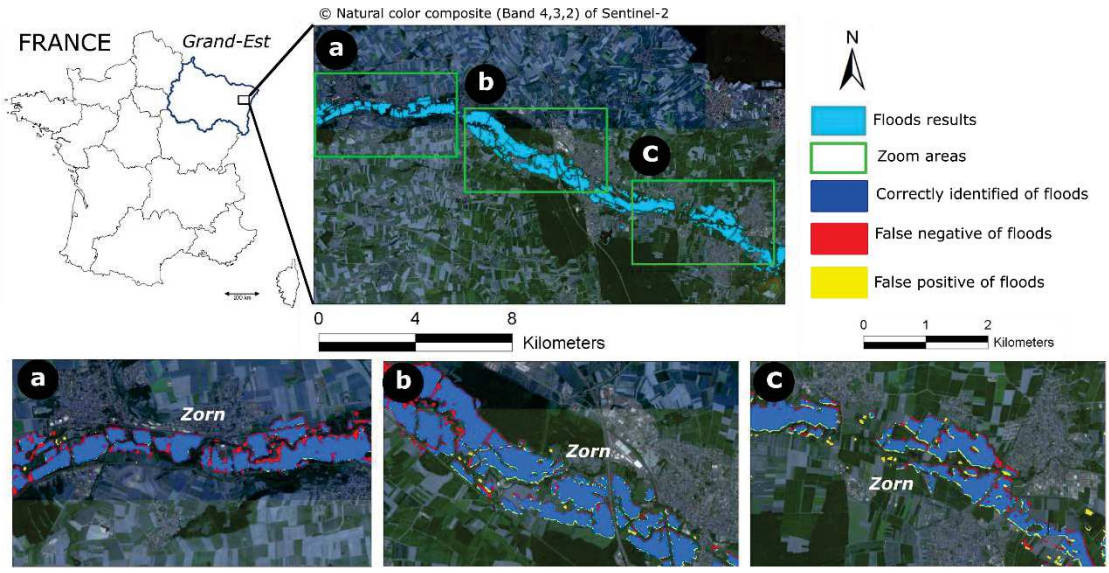

Figure 6. 17. Floods result from single date 23th January 2018.

A monitoring analysis of temporary surface water is presented in Figure 6.18. During the short-term period, temporary surface water areas normally not exceeding 400 ha. Two peaks of temporary surface water areas are observed in 5th and 6th January 2018, also 23rd January 2018, reached more than 900 ha.

For all the inundation period, flood reference map is only available for the 23rd January. Then to complete the visual assessment of this monitoring, we decide to collect data reference based on news media (Moreau, 2018) with floods photos. For instance Figure 6. 19 shows photographies taken on 5th and 6th January 2018 showing flooded road at the exit of Krautwiller and floods between Krautwiller and Wingersheim. This visual interpretation highlight the relevance of our extraction for small areas, next to the river.

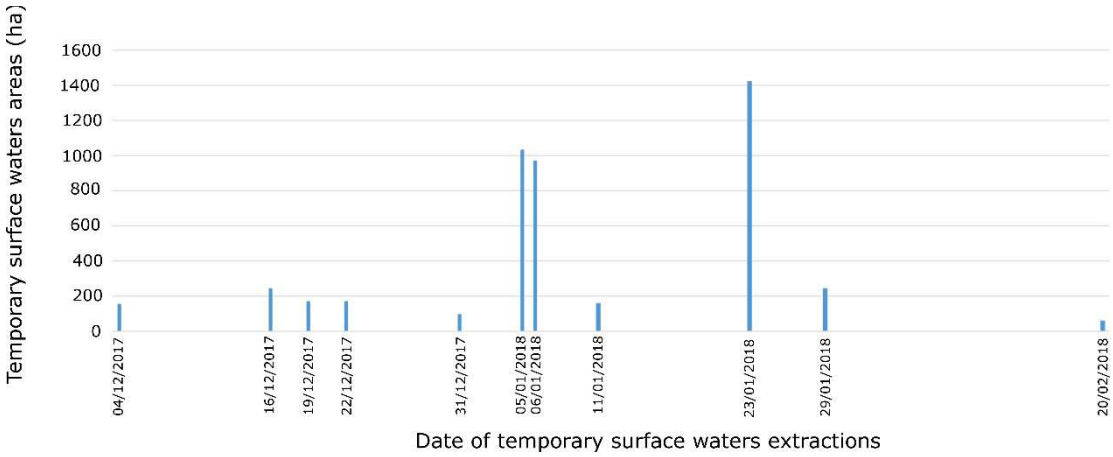

Figure 6. 18. Dynamic changes of temporary surface water areas (ha).

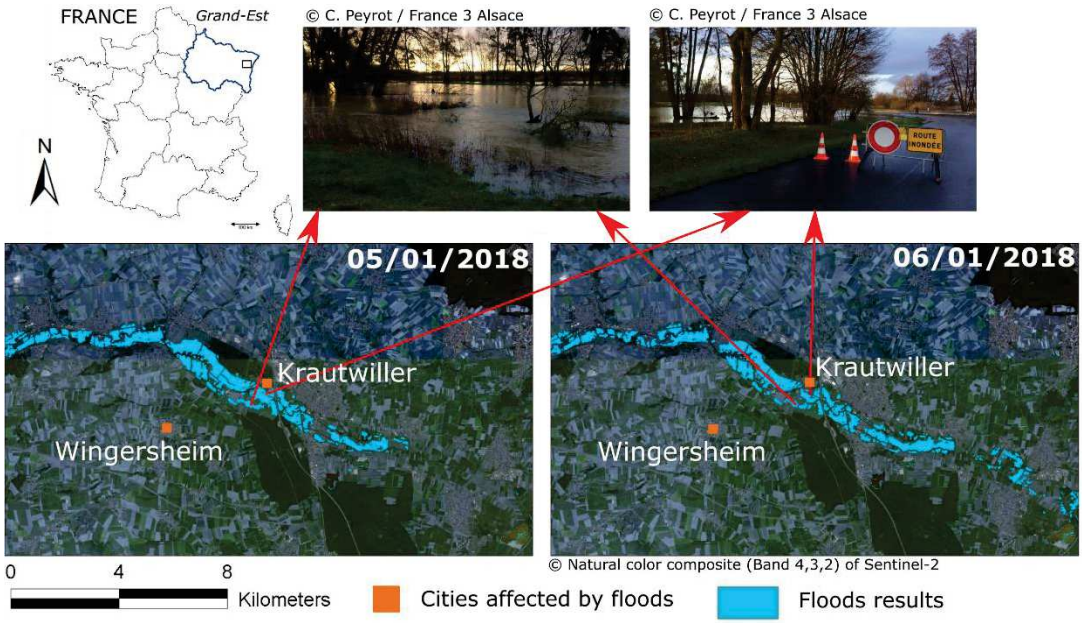

Figure 6. 19. Floods detection on 5th and 6th January 2018.

6.2.2 Monitoring Bengawan Solo River downstream area

In this sub-section, the main objective is to apply our proposed methods for surface waters monitoring in subwatershed of Bengawan Solo downstream, Indonesia. The purposes are thus (1) to study the use of image fusion in decision level method for mapping permanent surface waters; (2) to monitor irrigated croplands along Bengawan Solo River; and (3) to investigate the use of automatic and rapid mapping of surface water in extracting information about bankfull width for river discharge estimation.

a. Mapping permanent surface water of Bengawan Solo River, Indonesia

Twelve posterior probability maps of surface waters are generated over one year period (2017 – details in Chapter 3 – Part 3.1.2.2). Permanent surface water in the study area is obtained using Sentinel-1 time series image fusion in decision level with bayesian sum method as presented in Chapter 5. The result is then transformed into a binary image assigning all pixels with posterior probability of surface water greater than 0.9 as permanent surface water (Figure 6. 20). The accuracy assesment (Table 6. 5) is done

using surface waters classes of topography map from Indonesian Geospatial Information Agency (BIG, 2017).

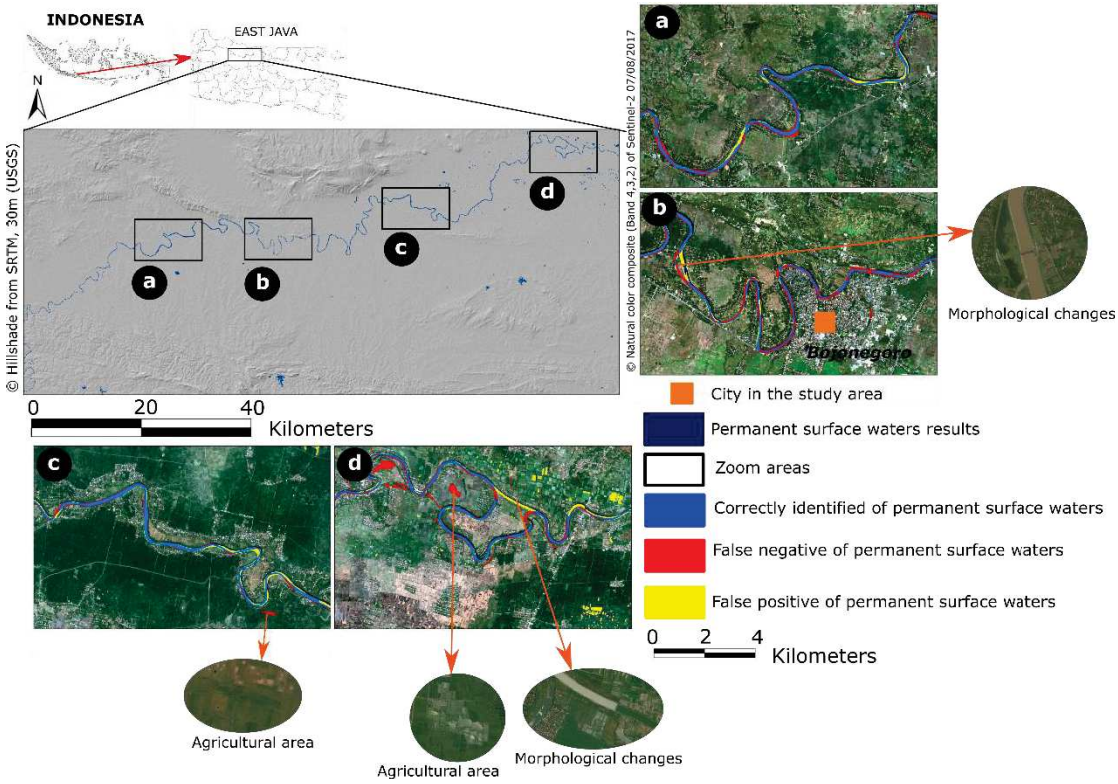

Figure 6. 20. Permanent surface water result of Bengawan Solo River, downstream area.

Overall accuracy shows high value with more than 97%, F-measure provides value 0.79, also very low False Positive Rate and commission error. Only omission error give value about 34% since the reference map was created at 1999. False positives and false negatives appeared in border area because of dynamical changes of waters in the river banks (Figure 6. 20a). Due to straightening, there are morphological changes in Bengawan Solo River which can be seen from false positive and false negative in Figure 6. 20b&d. Land use changes, for example in Figure 6. 20c&d, from small lake to agricultural area also created false negative. Some fishponds are also detected as permanent surface water in our result led to appearance of false positive (Figure 6. 20d). Based on accuracy assessment and visual interpretation, we can conclude that our proposed and automatic method extract successfully permanent surface water in Bengawan Solo downstream.

Table 6. 5. Quantitative evaluation of permanent surface water result in Bengawan Solo downstream from Sentinel-1 time series image fusion.

Overall Accuracy	F-measure	True Positive Rate	False Positive Rate	Omission error	Commission error
97.64%	0.79	65.91%	0.01%	34.08%	0.29%

b. Monitoring water variability in irrigation croplands areas

In this part, in order to monitor the water variability in irrigation cropland, temporary surface waters are detected. Using permanent surface water of previous part (a) as mask, temporary surface water can be extracted from each single date (12 images of Sentinel-1). This part applies methods proposed in Chapter 5. Temporary surface waters from one year period are presented as a frequency map in Figure 6. 21. This map show how many times temporary surface water pixels appear in the time period. Surfaces as river banks, fispond and irrigation croplands are successfully extracted.

Using irrigation croplands class from topography map of Indonesian Geospatial Information Agency as a mask (Figure 6. 22), temporary surface water can be focused only in the irrigation croplands area. The variation of water consists of frequency 1 until 11. The variability of water surfaces is presented in the graphic shown in Figure 6. 23. This figure shows that during rainy season (October - March), water in irrigation croplands has larger area than during dry season (April – September). Anomalies are only seen in April and October, probably due to change of season.

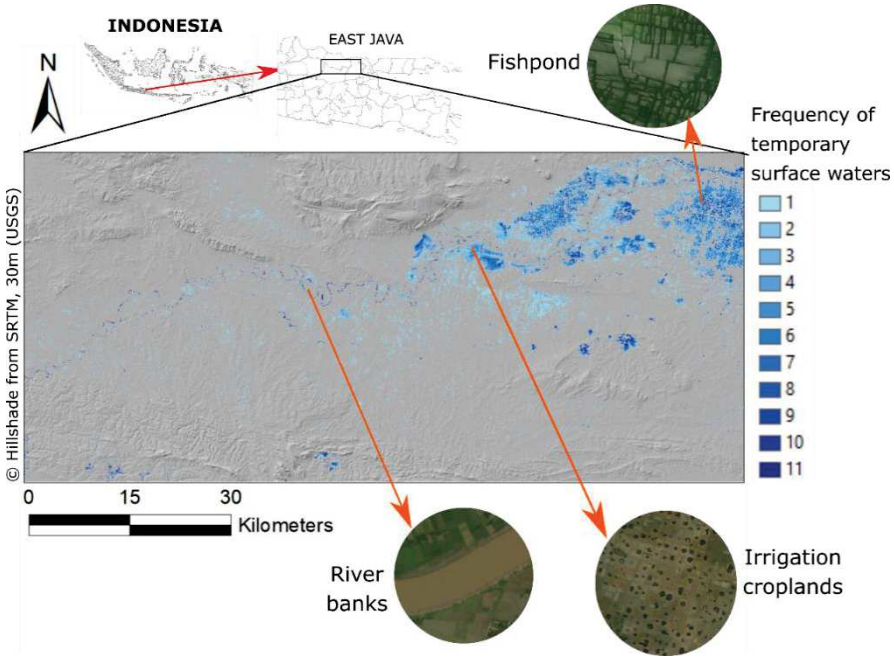

Figure 6. 21. Frequency map of temporary surface water from Sentinel-1 time series (12 images) in Bengawan Solo downstream.

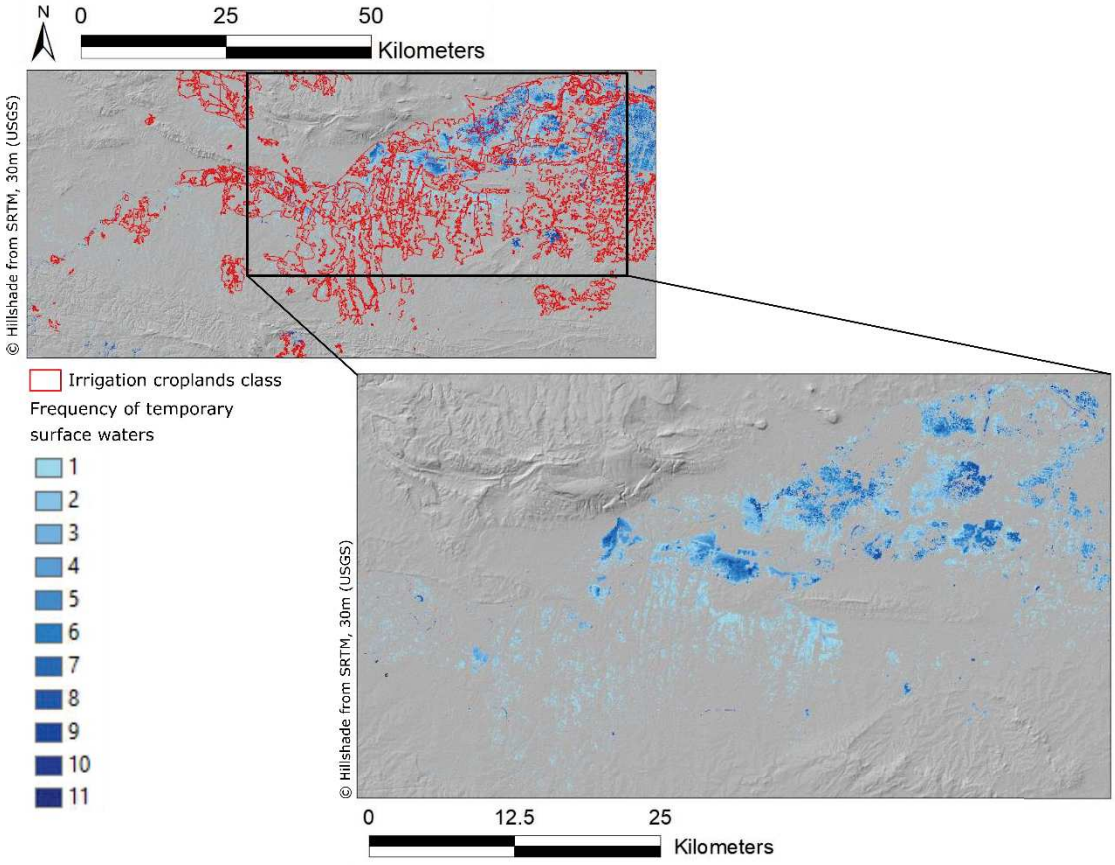

Figure 6. 22. Variability of water in irrigation croplands area as a frequency map.

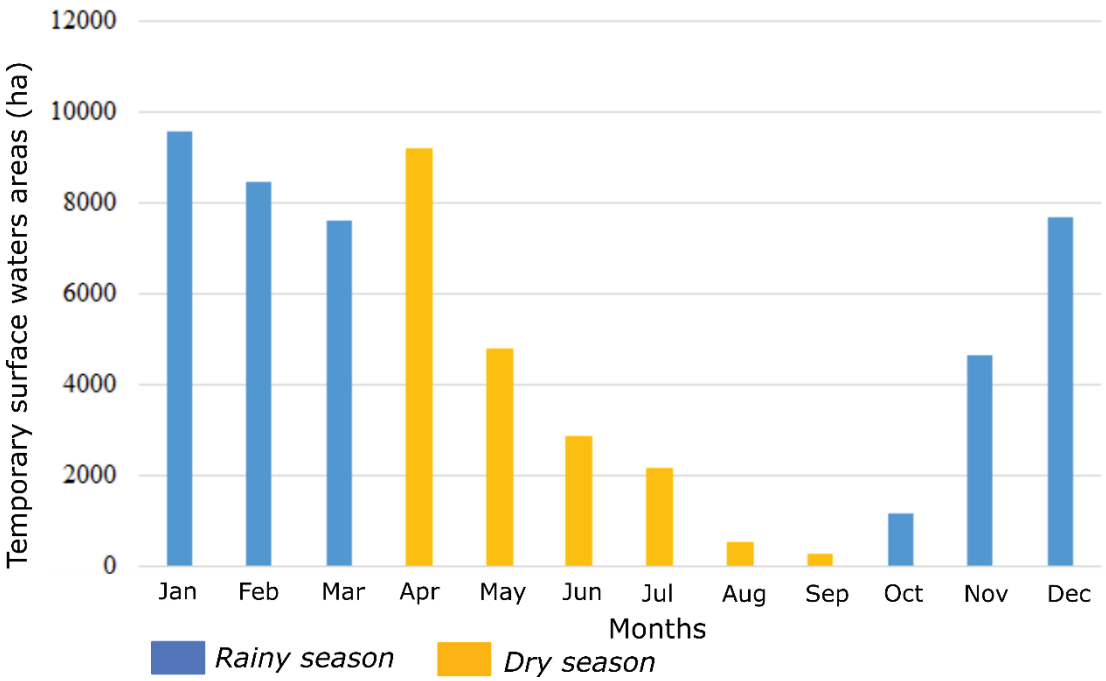

Figure 6. 23. Dynamic variation of water in the irrigation cropland indicated by area (ha).

First planting season in Indonesia commonly starts in November and ends in February (Wahyudi et al., 2014). The first planting season is identical with rainy season. In Figure 6. 23, water covers a large area in those periods. For second planting season on March until June, water existence also seems sufficient, over 2000 hectares. However, in the third planting season from July to October, water surfaces are low. Especially in August and September with water existence less than 1000 hectares. This monitoring of water variability in irrigation cropland can be useful for government as a basis for irrigation technique improvement. With enhancement of irrigation technique, it is expected to have larger water area in third planting season thus people can maintain or increase grain yield per unit area and volume of water.

c. River discharge estimation in one year period (2017)

One study related to river management is river discharge analysis. This approach allows to study the potential of drought or flooding. In the literature, river discharge can be estimate from satellite data, Sentinel-1 images, using equation 6.9 stated in (Bjerklie, 2007).

$$\text{River Discharge} = 0.24W^{1.64} \qquad (6.9)$$

Where *W* is bankfull width. Bankfull width is the measurement of the lateral extent of the water surface elevation perpendicular to the channel at bankfull depth (Washington State Department of Natural Resources, 2004). The equation is used due to Bengawan Solo river has morphology type of meandering river. Equation 6.9 is developed specifically for meandering river type (Bjerklie, 2007). Equation 6.9 is regression equation which obtained from relationship of width and streamflow as been stated by (Leopold and Maddock Jr., 1953).

Table 6. 6. In-situ measured data and Sentinel-1 estimation data of Bengawan Solo River discharge. *In-situ measured discharge of Bengawan Solo River from PUSDATARU Central Java Indonesia.

Month	In-situ measured discharge (m3/s)*	Discharge estimation from Sentinel-1 (m3/s)
Jan	335.66	354.63
Feb	300.29	507.42
Mar	201.70	261.64
Apr	202.68	281.10
May	186.63	212.23
Jun	65.32	214.51
Jul	30.52	202.94
Aug	17.03	183.19
Sep	32.15	142.57
Oct	35.21	252.95
Nov	65.13	264.66
Dec	156.45	244.08

Bankfull width can be obtained from Sentinel-1 IW GRD data. In this study, Bengawan Solo River are extracted in one year period (2017) from Sentinel-1 time series data using Water-S1 method proposed in Chapter 4. Bankfull width is then obtained using geometry calculation. After getting bankfull width, river discharge can be calculated using equation 6.9. The results are presented in Table 6. 6 and compared with in-situ

measured data from PUSDATARU Central Java Indonesia (PUSTADARU, 2017) (Figure 6. 24).

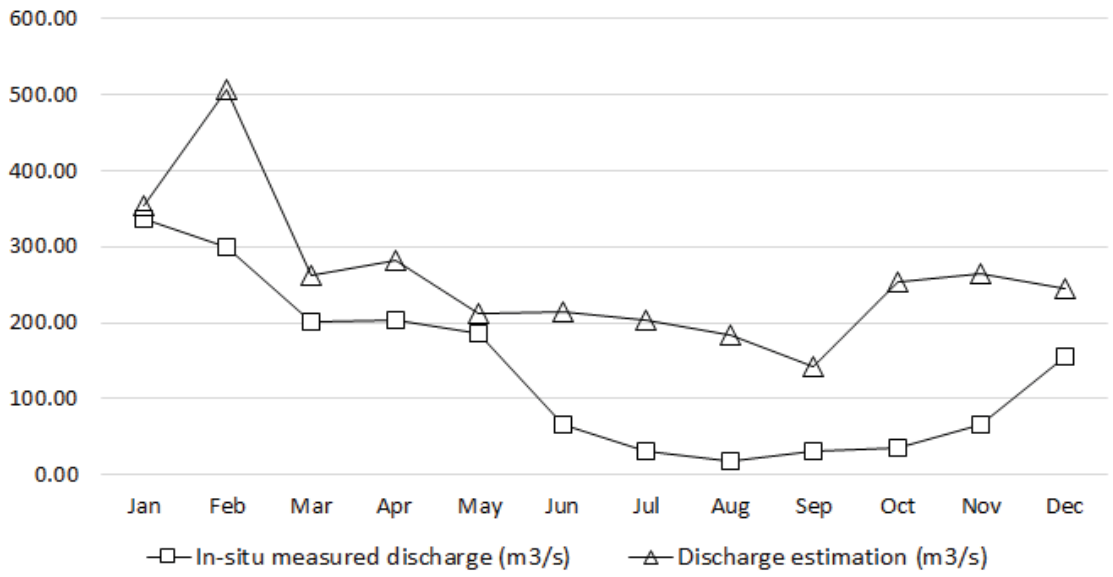

Figure 6. 24. Comparison between in-situ river discharge and estimation from Sentinel-1.

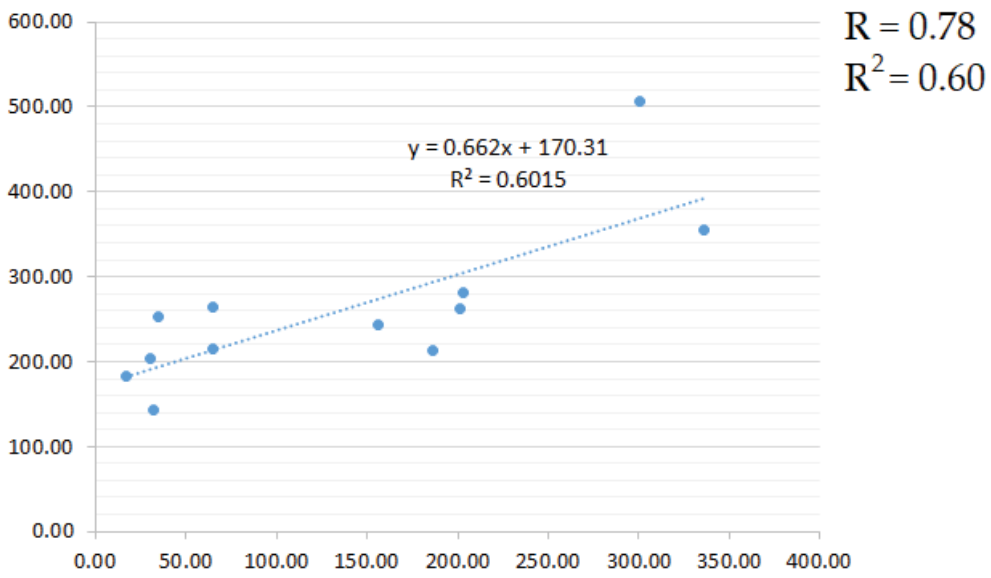

Figure 6. 25. Relationship between the satellite derived bankfull width and the in-situ measured discharge.

From Table 6. 6 and Figure 6. 24, discharge estimation from Sentinel-1 can predicted closely in some months such as December, January, March, April and May. In order to analyse relationship between in-situ measured discharge and discharge estimation

from Sentinel-1 data, coefficient of correlation (R) and coefficient of determination (R^2) were calculated (Figure 6. 25).

The coefficient of correlation can go between -1 and 1. Value 1 indicates that the two variables are moving in unison, while value 0 means not correlated. In this study, coefficient of correlation shows value 0.78 which indicates strong relationship between discharge estimation from Sentinel-1 data and in-situ measured discharge. In the other side, using linear regression, coefficient of determination shows value 0.60 or 60% which means 60% of the change in the total of in-situ measured discharge is associated with the change in discharge estimation.

Based on R^2, which provides value more than 50%, it shows the validations for the remotely-sensed discharge estimation equations with bankfull width as been presented in equation 6.9. Equation 6.9 is provided sufficient estimation for Bengawan Solo river discharge related to its meandering river type. However, there is another parameter which must be considered, such as dam. In the Bengawan Solo river, there are dams which make river have higher water levels than normal. Those affected water surfaces width and created larger width than bankfull width. Uncertainty appears due to difficulty in verifying whether the width obtained from satellite imageries corresponded to bankfull conditions or not (Andreadis et al., 2013). Those are explained why there are overestimation of river discharge in some months.

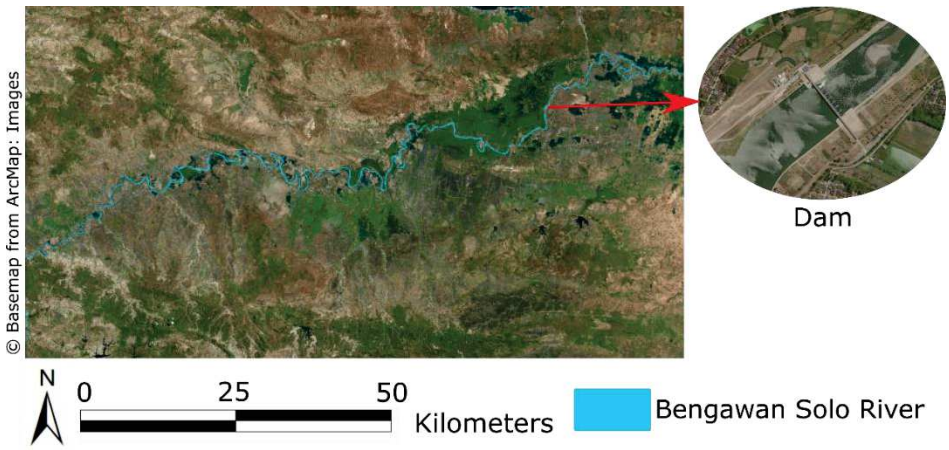

Figure 6. 26. Bengawan Solo River and its dam.

Another reason is limitation in Sentinel-1 resolution. Sentinel-1 data use in measuring bankfull width is limited by its spatial resolution, i.e., about 20 m. River bankfull width

error is fixed to the Sentinel-1 pixel size (Sichangi et al., 2016). Uncertainty in bankfull width calculation lead to inaccuracy of river discharge. This explains why in the dry season, when normally river has narrower river width produced larger discharge than in-situ measurement.

This chapter presented analysis of SAR polarimetry for surface water mapping. It also provided investigation of multi-source image fusion based on feature level. Moreover, it also presented massive processing for different case study: Grand-Est region, France and Bengawan Solo, Indonesia for validation of methods in different thematic context. The next chapter will provide general conclusions and perspectives.

Chapter 7

General conclusions and perspectives

Contents

This PhD thesis explores the single and combined use of Sentinel-1 and Sentinel-2 data either in mono-date image or multi-temporal image approach for surface water detection. We focused on the use of Sentinel-1 SAR data before combining it with Sentinel-2 optical data for complementary information. The technique includes automatic and rapid mapping of surface water from Sentinel-1 imagery. It also presented exploration of Satellite Image Time Series (SITS) and multi-source image fusion for improvements on surface water mapping.

7.1 Key findings

This study was guided by three research questions and three hypotheses. The answers of those questions are summarized in the sub-sections below.

7.1.1 What is the suitability and which methods are adapted and robust for an operational exploitation of Sentinel-1 data?

The suitability of Sentinel-1 for surface water mapping has been tested in Chapters 3 and 4. Spatial analysis showed that surface waters can be identified easily from Sentinel-1 imagery if they have an area of about 1 ha or more. We studied the polarization types of Sentinel-1 for surface water detection. VV polarization has better ability to discriminate between smooth open water area and land than VH polarization. Thus VV polarization is more adapted for surface water mapping. Investigation of features from Sentinel-1 data such as amplitude, intensity, sigma-nought, beta-nought and gamma showed sigma-nought as the optimal feature for surface water mapping. As SAR data, Sentinel-1 has speckle noise which can reduce image quality for interpretation. Analysis in some speckle filtering methods generated a conclusion that the Median filter with window size 5×5 pixels is the best approach to reduce speckle.

Several SAR-based water detection algorithms have been proposed in the literature. Among those methods, thresholding is the most commonly adopted method for SAR image analysis to discriminate water and non-water areas. There are many available

SAR-based water detection algorithms and automatic flood mapping services. Hence, while several semi-automatic and automatic tools already exist, there are, to the best of our knowledge, currently only a few scientific references which present a fully automatic water detection processor for surface water mapping from Sentinel-1 imagery. The method uses thresholding on individual pixels ignoring the correlation among neighboring pixels. Considering that individual pixels are not independent random variables but in the form of a random field, the potential to improve the accuracy of the flood extent maps exists. To this end, we presented an approach consisting of pixels modelling, probability map, and smoothness assumption in order to detect floods and surface waters.

We developed a modified SBA (Split Based Approach) method to enhance the focus on surface water areas rather than the whole image scene (Chapter 4). Finite Mixture Models are found to be suitable for the automatic modelling of surface waters and land classes. Using bilateral filtering for smooth labeling from a probability map led to more accurate results than using direct or empirical thresholding. HAND maps are used as terrain filters in order to remove potential false positives early on in the processing chain. Our results show that we were able to estimate floods and surface waters in three case studies with different spatial context with an average of F-measure about 0.8.

The proposed method is fully automatic in the sense that it does not require human or expert intervention in the processing. The method will focus on surface water areas and extract them automatically. The parameters to process the data are already in the system, thus people who use this method do not need to manually input them. The operational method is developed using the programming language R and only needs a short processing time. The time of processing is about 10 h per Sentinel-1 image, using a computer with multiple Intel Duo processors of 1.90 GHz and 32 GB RAM. Multiple images can be processed easily in parallel. Rapid mapping can hence be achieved in less than half a day after the image data is made publicly available. In manual processing, longer time is needed to determine parameters, enter them for each image and multiple images must be processed one by one. This proposed automatic method has the potential to be developed and performed for operational rapid mapping in other geographic regions due to: (1) the variable landscape characteristics at the investigated

sites and (2) the use of Sentinel-1 as free SAR data with wide area monitoring capabilities.

With our results, the suitability of Sentinel-1 for surface water mapping is verified. The adapted and robust methods for an operational exploitation of Sentinel-1 data have been proposed. The results are encouraging and constitute the first step to proposing operational image chain processing to help end-users quickly map flooding events or surface waters.

7.1.2 What is the contribution of Sentinel-1 time series?

The proposed methodology to explore the interest of Sentinel-1 time series in a processing chain has been developed in Chapter 5. This investigation is based on image fusion approach in decision-level with a Bayesian sum for the operator and gives relevant results to differentiate permanent and temporary surface water. Thus time series data can increase the detection level of surface water. The use of Satellite Image Time Series (SITS) can also reduce the noise qualitatively and quantitatively. Temporal data give variability of surface water areas during the long period of observation, thus can remove noises which only appear once or twice. Time series data also allow better understanding of temporary surface water in the context of space and time dynamics.

Validation of the proposed method in Chapter 6 shows that time series data can also provide new or complementary information on the behavior of surface water or their evolution on a short-time period. Permanent surface water can also be extracted over short-time period of observation. With our results, we conclude that time series data can improve surface water mapping through the reduction of noise and detection of permanent and temporary surface water (**Hypothesis 1**).

This proposed method based on time series data is a development from a previous automatic method in extracting surface water. With the help of the programming language Python, image fusion can be performed automatically. By using two computers that have the same specifications as sub-section 7.1.1, all processing can be carried out in about 3 days. For more rapid performance, more computers can be used because multiple images can be processed in parallel.

7.1.3 What is the contribution of multi-sensor data?

First, in Chapter 5, we have showed that the fully automatic method proposed in Chapter 4 can also be applied for Sentinel-2 imagery, with some modifications in pre-processing steps. The methods based on the NDWI2 water index or a times series of NDWI can give sufficient results. However, these methods with optical data are very dependent on the presence of cloud cover. Thus, it is more difficult to obtain time series data from this optical imagery, only multi-temporal images are available.

Furthermore, the complementarity of Sentinel-1 and Sentinel-2 has been explored. The methodology to combine multi-sensor (multi source) imagery (SAR − Sentinel-1 and optical − Sentinel-2) is proposed using decision-level image fusion. Compared with the use of mono-source time series data, the combination of Sentinel-1 and Sentinel-2 (multi-source) time series data can provide better accuracy in mapping permanent surface water.

For the monitoring of temporary surface water, the use of decision-level image fusion allows quantifying the probability of occurrence of flooded terrains at the pixel scale giving the possibility to understand the dynamics of the flooding. Some maps of temporary surface water can be helpful in giving new information for decision makers, for example in monitoring water variability in irrigation cropland. The monitoring can be useful as a basis for irrigation technique improvement (Chapter 6).

Another image fusion method in feature level followed by a Random Forest classification is also presented to compare and assess the best fusion approach. The result showed that decision-level image fusion give better performance than this approach.

We can conclude that fusion of SAR and optical time series can increase the accuracy of the detection and enhance the mapping of the permanent surface water. It is also useful for better understand the flood dynamics and useful for decision making through analysis of temporary surface water (**Hypothesis 2**).

Sentinel-1 SAR data in SLC mode can provide SAR polarimetry data. The investigations using those data showed that the separation of surface water areas from the other land cover can be done, but classification of surface water into different

thematic classes cannot be conducted. Compared with Sentinel-1 GRD, SAR polarimetry data are longer to process due to their big amount of data. Thus, for the purpose of surface water mapping, SAR polarimetry seems not to be a good idea to pursue. However, in order to identify surface water thematic classes, taking the other SAR polarimetry data into consideration at finer spatial resolutions or with full-polarization would be a good idea to explore.

The proposed methods are successfully applied for massive processing in different case studies. They can extract permanent surface water in the Grand-Est region, France and can perform rapid mapping of temporary surface water for the Zorn River flooding. Transposing the methods to the Bengawan Solo River in Indonesia, they can map permanent surface water with relevant and encouraging result. The methods can be applied also to monitor waters variability in irrigation croplands areas. Moreover, the methods can be used for getting river banks' full width information to estimate river discharge (**Hypothesis 3**).

The massive processing in the case study of Grand-Est, France is executed in about 3 days with 11 images as input. As for the case study of Bengawan Solo, Indonesia with 12 images of input, it needs more time for processing, about 5 days, due to its application for water variability in irrigation croplands and river discharge estimation. Those processing speed can be reached using two computers with multiple Intel Duo processors of 1.90 GHz and 32 GB RAM. More computers can be used to process multiple images in parallel for more rapid performance.

7.2 Perspectives

This PhD thesis opens many perspectives, some rather operational, others methodological or thematic. Some of these perspectives are explored in this section.

First, an automatic chain pocessing method for Sentinel-1 has been developped. Yet, there is a possibility to apply the method in other SAR data, for example ALOS-PALSAR 2 data from Kalideos Alsace. We applied the method in ALOS-PALSAR 2 before but we still need to observe the applicability result.

Second, the proposed methodology using a fusion of Sentinel-1 and Sentinel-2 image time series is generic. It does not require user interaction; suggesting that it is applicable for the monitoring of permanent surface water bodies over large areas and at high temporal frequency. It has the possibility to become a permanent service solution if integrated on high performance computing centers. In the case of temporary surface water, it can be explored more through detailed frequency map analysis for comprehensive understanding of the space and time dynamics. It is also possible to distinguish flooded and non-flooded area in the temporary surface water class using that analysis. Such approach is of interest for improving flood risk management procedures. Moreover, it is interesting to develop more the analysis so that the methods can adapt with the global use.

However, it is important to extend the observation period for example to 5 years in order to be able to learn surface water behaviour. More data and information can be collected from long time period, then time series analysis can be developed using trend analysis. The analysis can be useful to cover annual changes of surface water, seasonal monitoring and better understanding of surface water behavior through time. In order to obtain global product, we also need to apply or tests the method in arid regions because it is difficult to map water area due to water and water non-alike area in those regions, effect of backsacttering values.

Third, decision level image fusion with Bayesian sum operator can provide simple and rapid mapping. However, it will be interesting to analyze other methods beside fuzzy logic and Bayesian for image fusion. Besides the great many algorithms in the literature, there are also the deep learning algorithms that easily accommodate to different sources and missing data. Deep learning is a well-known method for massive data processing. Nowadays, it becomes a powerful, effective and flexible method to extract knowledge from data. It is not specific to data fusion, but it can accommodate data from different sources. However, a key point of this type of algorithm is the need of a large number of samples to train their network. The active learning approach arrives as a breakthrough in dealing with this issue. This approach can learn from a small number of examples to train their network, thus has a great potential in the image processing domain. Future research can include those methods (deep learning and active learning) for image fusion and compare with the results from this study.

Fourth, the operational system of automatic methods in this study are based on several free software and programming language. Future work is required to integrate all the processing, from pre-processing until post-processing, in one programming or create some plug-ins which can be placed in Sentinel Application Platform (SNAP). The integration will simplify and accelerate the image processing to produce maps of surface water.

Lastly, the results from our proposed method using Sentinel data can also become the data learning towards the launch of Surface Water Ocean Topography (SWOT) mission in the future. The mission is planned for launch in 2021 and provides shorter wavelength (Ka-band) than Sentinel-1. This mission intends to provide a major improvement in the availability of surface extent and storage change for surface water bodies such as lakes, reservoirs, wetlands, and rivers globally, also give information about water levels. Therefore, the use of SWOT and Sentinels mission can be expected for monitoring spatiotemporal variations of surface water and creating surface water database on a global scale.

Although the use of remote sensing data as operational source of information for surface water observations still requires development, the methods and tests proposed in this work are promising.

Bibliography

Abdikan, S., Sanli, F.B., Ustuner, M., Calò, F., 2016. Land Cover Mapping using Sentinel-1 SAR Data. ISPRS - International Archives of the Photogrammetry, Remote Sensing and Spatial Information Sciences, pp. 757–761. https://doi.org/10.5194/isprsarchives-XLI-B7-757-2016.

Acharya, T.D., Lee, D.H., Yang, I.T., Lee, J.K., 2016. Identification of Water Bodies in a Landsat 8 OLI Image Using a J48 Decision Tree. Sensors 16. https://doi.org/10.3390/s16071075

Aires, F., Prigent, C., Lehner, B., Yamazaki, D., Fluet, E., 2018. GIEMS-D3: A long-term, dynamical, high-spatial resolution inundation extent dataset at global scale, from multiple satellite observations. MWBS, Mapping Water Bodies conference, 27-28 March 2018, Frascati (Rome), Italy.

Anderson, J.R., Hardy, E.E., Roach, J.T., Witmer, R.E., 1976. A Land Use and Land Cover Classification System for use with Remote Sensor Data. Geological Survey Professional Paper 964, p. 41.

Andreadis, K.M., Schumann, G.J.-P., Pavelsky, T., 2013. A simple global river bankfull width and depth database: Data and Analysis Note. Water Resources Research 49, pp. 7164–7168. https://doi.org/10.1002/wrcr.20440.

Anna, A.N., Priyono, K.D., Priyana, Y., 2017. Analisis Potensi dan Kerawanan Banjir di DAS Bengawan Solo Hulu dan Tengah. The 5th Urecol Proceeding. UAD, Yogyakarta, Indonesia, p. 11.

Aurélien Willem, 2018. Les inondations de la Zorn : Krautwiller, Brumath et Mommenheim.

Baghdadi, N., Bernier, M., Gauthier, R., Neeson, I., 2001. Evaluation of C-band SAR data for wetlands mapping. International Journal of Remote Sensing 22, pp. 71–88. https://doi.org/10.1080/014311601750038857.

Banukumar, K., Panneerselvam, A., Aruchamy, S., Ganesh, A., 2011. A. Surface water mapping for Watershed management using Geospatial techniques. International Journal of Geomatics and Geosciences 2, pp. 289–299.

Bartsch, A., Trofaier, A.M., Hayman, G., Sabel, D., Schlaffer, S., Clark, D.B., Blyth, E., 2012. Detection of open water dynamics with ENVISAT ASAR in support of land surface modelling at high latitudes. Biogeosciences 9, pp. 703–714. https://doi.org/10.5194/bg-9-703-2012.

Bastviken, D., Tranvik, L.J., Downing, J.A., Crill, P.M., Enrich-Prast, A., 2011. Freshwater methane emissions offset the continental carbon sink. Science 331, p. 50.

Bazi, Y., Bruzzone, L., Melgani, F., 2007. Image thresholding based on the EM algorithm and the generalized Gaussian distribution. Pattern Recognition 40, pp. 619–634. https://doi.org/10.1016/j.patcog.2006.05.006.

Behnamian, A., Banks, S., White, L., Brisco, B., Millard, K., Pasher, J., Chen, Z., Duffe, J., Bourgeau-Chavez, L., Battaglia, M., 2017. Semi-Automated Surface Water Detection with Synthetic Aperture Radar Data: A Wetland Case Study. Remote Sens. 9, 1209. https://doi.org/10.3390/rs9121209.

Benaglia, T., Chauveau, D., Hunter, D., Young, D., 2009. mixtools: An R package for analyzing finite mixture models. Journal of Statistical Software 32, pp. 1–29.

Benediktsson, J.A., Cavallaro, G., Falco, N., Hedhli, I., Krylov, V.A., Moser, G., Serpico, S.B., Zerubia, J., 2018. Remote Sensing Data Fusion: Markov Models and Mathematical Morphology for Multisensor, Multiresolution, and Multiscale Image Classification. Math. Models Remote Sens. Image Process. pp. 277–323. https://doi.org/10.1007/978-3-319-66330-2_7.

BIG, 2013. Peta Rupabumi. Badan Informasi Geospatial (BIG) - Peta Rupabumi. http://www.big.go.id/peta-rupabumi/ (accessed 15 August 2018).

BIG, I.G.I.A., 2017. Indonesia Geospatial Portal. http://tanahair.indonesia.go.id/portal-web (accessed 05 October 2018).

Bioresita, F., Puissant, A., Stumpf, A., Malet, J.-P., 2018. A Method for Automatic and Rapid Mapping of Water Surfaces from Sentinel-1 Imagery. Remote Sensing 10, 217. https://doi.org/10.3390/rs10020217.

Bjerklie, D.M., 2007. Estimating the bankfull velocity and discharge for rivers using remotely sensed river morphology information. Journal of Hydrology 341, pp. 144–155. https://doi.org/10.1016/j.jhydrol.2007.04.011.

Blasco, F., Bellan, M.F., Chaudhury, M.U., 1992. Estimating the extent of floods in Bangladesh using SPOT data. Remote Sensing of Environment 39, pp. 167–178. https://doi.org/10.1016/0034-4257(92)90083-V.

Bourbigot, M., Johnsen, H., Piantanida, R., 2016. Sentinel-1 Product Specification (No. S1- RSMDA-52–7441). European Space Agency (ESA).

Bourgeau-Chavez, L.L., Riordan, K., Powell, R.B., Nowels, N.M. and M., 2009. Improving Wetland Characterization with Multi-Sensor, Multi-Temporal SAR and Optical/Infrared Data Fusion. Advances. Geoscience and Remote Sensing. https://doi.org/10.5772/8327

Bovolo, F., Bruzzone, L., 2007. A Split-Based Approach to Unsupervised Change Detection in Large-Size Multitemporal Images: Application to Tsunami-Damage Assessment. IEEE Transactions on Geoscience and Remote Sensing 45, pp. 1658–1670. https://doi.org/10.1109/TGRS.2007.895835.

Brakenridge, G.R., Anderson, E., 2006. MODIS-based flood detection, mapping, and measurement: the potential for operational hydrological applications. Proceedings of the NATO Advanced Research Workshop, Baile Felix – Oradea, Romania.

Breiman, L., 2001. Random Forests. Machine Learning 45, pp. 5–32. https://doi.org/10. 1023/A:1010933404324

British Geological Survey, Centre for Hydrology and Ecology, 2015. Hydrological Summary for United Kingdom.

Brönmark, C., Hansson, L.-A., 2002. Environmental issues in lakes and ponds: current state and perspectives. Environmental Conservation 29, pp. 290–306.

Buma, W., Lee, S.-I., Seo, J., 2018. Recent Surface Water Extent of Lake Chad from Multispectral Sensors and GRACE. Sensors 18, 2082. https://doi.org/10.3390/s18072082.

Calmant, S., Seyler, F., Cretaux, J.F., 2008. Monitoring continental surface waters by satellite altimetry. Surveys in Geophysics 29, pp. 247–269. https://doi.org /10.1007/s10712-008-9051-1.

Cazals, C., 2017. Apport des données Sentinel-1 pour la cartographie des milieux humides. Universite Paris-Est, Paris, France.

CCR, 2018. Retour sur les inondations de janvier et février 2018, Modélisation des dommages et évaluation des actions de prévention. CCR, France.

Chan, Y.K., Koo, V.C., 2008. An Introduction to Synthetic Aperture Radar (SAR). Progress In Electromagnetics Research B 2, pp. 27–60. https://doi.org /10.2528/PIERB07110101.

Chaouch, N., Temimi, M., Hagen, S., Weishampel, J., Medeiros, S., Khanbilvardi, R., 2012. A synergetic use of satellite imagery from SAR and optical sensors to improve coastal flood mapping in the Gulf of Mexico: Flood Mapping in the Gulf of Mexico using Satellite Imagery. Hydrological Processes 26, pp. 1617–1628. https://doi.org/10.1002/hyp.8268.

Chapman, B., McDonald, K., Shimada, M., Rosenqvist, A., Schroeder, R., Hess, L., 2015. Mapping Regional Inundation with Spaceborne L-Band SAR. Remote Sensing 7, pp. 5440–5470. https://doi.org/10.3390/rs70505440.

Chavez, P.S., 1991. Comparison of Three Different Methods to Merge Multiresolution and Multispectral Data:Landsat TM and SPOT Panchromatic. Photogramm. Eng. 9.

Chen, X.C., Khandelwal, A., Shi, S., Anderson, R., Blank, M., Boriah, S., Kumar, V., 2014. An Unsupervised Method to Monitor Surface Water Extent. The 4th International Workshop on Climate Informatics 2014, Boulder, Colorado.

Chen, Z., Wang, J., 2007. Multi-polarized SAR application to land use and land cover mapping in the mountainous Three Gorges Area, China. The Our Common Borders - Safety, Security, and the Environment Through Remote Sensing, Ottawa, Ontario, Canada.

Chengquan, H., DeVries, B., Wenli, H., Lang, M.W., Jones, J.W., Irena, F., 2018. Synergies of Landsat, Sentinel-2, and -1 for improved characterization of surface water dynamics. MWBS, Mapping Water Bodies from Space 2nd Conference, 27-28 March 2018, Frascati (Rome), Italy.

Chini, M., Hostache, R., Giustarini, L., Matgen, P., 2015. SAR-based flood mapping combining hierarchical split-based approach and change detection. The IEEE IGARSS 2015, Milan, Italy.

Clement, M.A., Kilsby, C.G., Moore, P., 2017. Multi-temporal synthetic aperture radar flood mapping using change detection: Multi-temporal SAR flood mapping using change detection. Journal of Flood Risk Management. https://doi.org /10.1111/jfr3.12303.

Conseil Général du Bas-Rhin, 2012. Le bassin versant de la Zorn.

Copernicus, 2016. Copernicus Emergency Management Service activated for floods in Northern Italy. http://copernicus.eu/news/copernicus-emergency-management-serviceactivated-floods-northern-italy (accessed 01 June 2017).

Copernicus, n.d. Copernicus Emergency Management Service – Mapping. http://copernicus.eu/news/copernicus-emergency-management-service-activated-floods-northern-italy (accessed 26 August 2016).

Copernicus, n.d. Water and Wetness Probability Index 2015. Copernicus Land Monitoring System Water and Wetness Probability Index 2015. https://land. copernicus.eu/pan-european/high-resolution-layers/water-wetness/expert-products/wetness-probabilityindex/2015/view (accessed 03 May 2018).

Crist, E.P., 1985. A TM Tasseled Cap equivalent transformation for reflectance factor data. Remote Sens. Environ. 17, pp. 301–306. https://doi.org/10.1016/0034-4257(85)90102-6.

Cwik, K., 2017. Flood Mapping with the Sentinel-1 Time-Series Data in Arid Areas (Master Thesis). Technical University of Munich, München, Deutschland.

Davranche, A., Lefebvre, G., Poulin, B., 2010. Wetland monitoring using classification trees and SPOT-5 seasonal time series. Remote Sensing of Environment 114, pp. 552–562. https://doi.org/10.1016/j.rse.2009.10.009.

De Jong, S.M., Van der Meer, F.D., 2004. Basics of Remote Sensing, in: Remote Sensing Image Analysis: Including the Spatial Domain. Springer, pp. 1–15.

De Roo, A., Van Der Knijff, J., Horritt, M., Schmuck, G., De Jong, S., 1999. Assessing Flood Damages of The 1997 Oder Flood and The 1995 Meuse Flood. The 2nd International Symposium on Operationalization of Remote Sensing, Enschede, The Netherlands.

Dechesne, C., Mallet, C., Le Bris, A., Gouet-Brunet, V., 2017. Semantic segmentation of forest stands of pure species combining airborne lidar data and very high resolution multispectral imagery. ISPRS J. Photogramm. Remote Sens. 126, pp. 129–145. https://doi.org/10.1016/j.isprsjprs.2017.02.011.

DeVries, B., Huang, C., Lang, M., Jones, J., Huang, W., Creed, I., Carroll, M., DeVries, B., Huang, C., Lang, M.W., Jones, J.W., Huang, W., Creed, I.F., Carroll, M.L., 2017. Automated Quantification of Surface Water Inundation in Wetlands Using Optical Satellite Imagery. Remote Sensing 9, 807. https://doi.org/10. 3390/rs9080807.

Direction de la climatologie, 2009. Statistiques climatiques de la France 1971-2000. Météo France, Toulouse.

Donchyts, G., Winsemius, H., Schellekens, J., Erickson, T., Gao, H., Savenije, H., van de Giesen, N., 2016. Global 30m Height Above the Nearest Drainage. The EGU General Assembly 2016, Vienna, Austria.

Dronova, I., Gong, P., Wang, L., Zhong, L., 2015. Mapping dynamic cover types in a large seasonally flooded wetland using extended principal component analysis and object-based classification. Remote Sens. Environ. 158, pp. 193–206.

Du, Y., Zhang, Y., Ling, F., Wang, Q., Li, W., Li, X., 2016. Water Bodies' Mapping from Sentinel-2 Imagery with Modified Normalized Difference Water Index at 10-m Spatial Resolution Produced by Sharpening the SWIR Band. Remote Sensing 8, 354. https://doi.org/10.3390/rs8040354.

Duggar, E.H., Li, Q., Van Praagh, A., 2016. Global Credit Strategy - Environmental Risks Understanding the Impact of Natural Disasters: Exposure to Direct Damages Across Countries (No. 1047662). Moody's Investors Service Sovereign and Supranational.

Duker, L., Bore, L., 2001. Biodiversity conservation of the world's lakes: A preliminary framework for identifying priorities, LakeNet Report Series. Anapolis, Maryland US.

eaufrance, 2018. Bulletin national de situation hydrologique. http://www.eaufrance.fr/docs/bsh/2018/02/precipitations.php (accessed 28 September 2018).

Éireann, M., 2015. Monthly Weather Bulletin 355.

Éireann, M., n.d. Met ÉireannThe Irish Meteorogical Service. Available Data – Met Éireann The Irish Meteorogical Service. URL https://www.met.ie/climate/ available-data (accessed 26 August 2016).

Engebretson, C., 2018. Landsat Thematic Mapper (TM) Level 1 (L1) Data Format Control Book (DFCB) Version 10.0.

EOSDIS, 2018. Remote Sensors | Earthdata. https://earthdata.nasa.gov/userresources /remote-sensors (accessed 07 August 2018).

EPA, I., n.d. EPA Ireland Catalogue - Geo Portal. https://gis.epa.ie/geonetwork/srv/eng/catalog.search#/home (accessed 23 October 2018).

EROS Center, 2018. Collection-1 Landsat Level-3 Dynamic Surface Water Extent (DWSE) Science Product. https://doi.org/10.5066/F7445KQK.

ESA, 2015. Sentinel-2 User Handbook.

ESA, 2014. Copernicus Open Access Hub. https://scihub.copernicus.eu/dhus/#/home (accessed 15 November 2015).

ESA, 2012. Sentinel-1 ESA's Radar Observatory Mission for GMES Operational Services. European Space Agency (ESA), Noordwijk, Netherlands.

ESA, n.d. RADAR and SAR Glossary. https://earth.esa.int/handbooks/asar/CNTR5-2.html (accessed 21 June 2018).

ESA, n.d. SENTINEL-2. ESA Sentinel Online Sentinel-2. https://sentinel.esa.int/web/sentinel/missions /sentinel-2 (accessed 26 August 2016).

Etherington-Smith, J., 2015. UK floods: Pictures of submerged Yorkshire as Britain battles worst flooding in 70 years. Int. Bus. Times.

eugenius, 2018. Regional Flood Monitoring with Sentinels Data.

euronews, 2016. Floods cause havoc and victims in northern Italy.

Evans, T.L., Costa, M., Telmer, K., Silva, T.S.F., 2010. Using ALOS/PALSAR and RADARSAT-2 to Map Land Cover and Seasonal Inundation in the Brazilian Pantanal. IEEE Journal of Selected Topics in Applied Earth Observations and Remote Sensing 3, pp. 560–575. https://doi.org/10.1109/JSTARS.2010.2089042.

Fauvel, M., Benediktsson, J.A., Chanussot, J., Sveinsson, J.R., 2007. Spectral and Spatial Classification of Hyperspectral Data Using SVMs and Morphological Profiles. Presented at the IGARSS 2007 - IEEE International Geoscience and Remote Sensing Symposium, Barcelona, Spain, p. 13.

Fawcett, T., 2006. An introduction to ROC analysis. Pattern Recognition Letters 27, pp. 861–874.

Feyisa, G.L., Meilby, H., Fensholt, R., Proud, S.R., 2014. Automated Water Extraction Index: A new technique for surface water mapping using Landsat imagery. Remote Sensing of Environment 140, pp. 23–35. https://doi.org/10.1016/j.rse.2013.08.029.

Fisher, A., Danaher, T., 2013. A Water Index for SPOT5 HRG Satellite Imagery, New South Wales, Australia, Determined by Linear Discriminant Analysis. Remote Sensing 5, pp. 5907–5925. https://doi.org/10.3390/rs5115907.

Fisher, A., Flood, N., Danaher, T., 2016. Comparing Landsat Water Index Methods for Automated Water Classification in Eastern Australia | Request PDF. Remote Sens. Environ. 175, 167–182.

Foumelis, M., 2015. ESA Sentinel-1 Toolbox Generation of SAR Backscattering Mosaics. Course Materials, 6th ESA Advanced Training Course on Land Remote Sensing, 14-18 September 2015, Bucharest, Romania.

Frazier, P.S., Page, K.J., 2000. Water body detection and delineation with Landsat TM data. Photogrammetric engineering and remote sensing 66, pp. 1461–1468.

Freeman, J.B., Dale, R., 2013. Assessing bimodality to detect the presence of a dual cognitive process. Behavior Research Methods 45, pp. 83–97. https://doi.org/10.3758/s13428-012-0225-x.

Gamba, P., 2014. Image and data fusion in remote sensing of urban areas: status issues and research trends. Int. J. Image Data Fusion 5, pp. 2–12. https://doi.org/10.1080/19479832.2013.848477.

Gautama, V.K., Gaurava, P.K., Murugana, P., Annaduraia, M., 2015. Assessment of Surface Water Dynamics in Bangalore using WRI, NDWI, MNDWI, Supervised Classification and K-T Transformation. Aquatic Procedia 4, pp. 739–746.

GCOS, 2011. Systematic observation requirements for satellite-based products for climate - 2011 updat - Supplemental details to the satellite-based component of the implementation plan for the global observing system for climate in support of the UNFCCC (2010 update). GCOS secretariat, WMO, Geneva.

Ghassemian, H., 2016. A Review of Remote Sensing Image Fusion Methods. Inf Fusion 32, pp. 75–89. https://doi.org/10.1016/j.inffus.2016.03.003.

Gniazdowski, Z., 2017. New Interpretation of Principal Components Analysis. Zeszyty Naukowe Warszawskiej Wyższej Szkoły Informatyki, pp. 43–65. https://doi.org/10.26348/znwwsi.16.43.

Gogtay, N., Thatte, U., 2017. Principles of Correlation Analysis. Journal of The Association of Physicians of India 65, pp. 78–81.

Gómez-Chova, L., Tuia, D., Moser, G., Camps-Valls, G., 2015. Multimodal Classification of Remote Sensing Images: A Review and Future Directions. Proc. IEEE 103, pp. 1560–1584. https://doi.org/10.1109/JPROC.2015.2449668.

Goyal, S., Wahla, R., 2015. A Review on Image Fusion. International Journal of Innovative Research in Computer and Communication Engineering 3, pp. 7582–7588. https://doi.org/10.15680/ IJIRCCE.2015. 030 8104.

Gstaiger, V., Huth, J., Gebhardt, S., Wehrmann, T., Kuenzer, C., 2012. Multi-sensoral and automated derivation of inundated areas using TerraSAR-X and ENVISAT ASAR data. Int. J. Remote Sens. 33, pp. 7291–7304. https://doi.org/10.1080/01431161.2012.700421.

Hahmann, T., Martinis, S., Twele, A., Roth, A., 2008. Extraction of water and flood areas from SAR data. The EUSAR 2008, 7th European Conference on Synthetic Aperture Radar, Graf-Zeppelin-Haus, Friedrichshafen, Germany.

Hartigan, J.A., Hartigan, P.M., 1985. The Dip Test of Unimodality. The Annals of Statistics 13, pp. 70–84. https://doi.org/10.1214/aos/1176346577.

Henry, J.-B., 2004. Systèmes d'information spatiaux pour la gestion du risque d'inondation de plaine. Universite Louis Pasteur, Strasbourg, France.

Henry, J.-B., Chastanet, P., Fellah, K., Desnos, Y.-L., 2006. Envisat multi-polarized ASAR data for flood mapping. Int. J. Remote Sens. 27, pp. 1921–1929. https://doi.org/10.1080/014311605004867 24.

Huang, C., Chen, Y., Zhang, S., Wu, J., 2018. Detecting, Extracting, and Monitoring Surface Water From Space Using Optical Sensors: A Review. Reviews of Geophysics 56, pp. 333–360. https://doi.org/10.1029/2018RG000598.

Huang, W., DeVries, B., Huang, C., Lang, M., Jones, J., Creed, I., Carroll, M., 2018. Automated Extraction of Surface Water Extent from Sentinel-1 Data. Remote Sensing 10, p. 797. https://doi.org/10.3390/rs10050797.

Huang, X., Xie, C., Fang, X., Zhang, L., 2015. Combining Pixel- and Object-Based Machine Learning for Identification of Water-Body Types From Urban High-Resolution Remote-Sensing Imagery. IEEE J. Sel. Top. Appl. Earth Obs. Remote Sens. 8, pp. 2097–2110. https://doi.org/10.1109/JSTARS.2015.2420713.

Huang, Y., Genderen, J.L. van, 1996. Evaluation of several speckle filtering techniques for ERS - 1&2 imagery. ISPRS 1996 : Vol. XXXI, Part B2. Vienna, pp. 164-169.

Huth, J., Ahrens, M., Klein, I., Gessner, U., Hoffmann, J., Künzer, C., 2015. WaMaPro – a user friendly tool for water surface derivation from SAR data and further products derived from optical data. The ESA Mapping Water Bodies from Space Conference 2015, Frascati, Italy.

IGN, 2017. Géoportail. https://www.geoportail.gouv.fr (accessed 15 August 2018).

IGN, 2014. BD TOPO Version 2.1 - Descriptif de Contenu. Institut Géographique National (IGN).

IGN, 2006. BD CARTHAGE Version 3.0 - Descriptif de contenu. Institut Géographique National (IGN).

Irwin, K., Braun, A., Fotopoulos, G., Roth, A., Wessel, B., 2018. Assessing Single-Polarization and Dual-Polarization TerraSAR-X Data for Surface Water Monitoring. Remote Sens. 10, p. 949. https://doi.org/10.3390/rs10060949.

Janssen, L.L.F., Huurneman, G.C. (Eds.), 2001. Principles of remote sensing: an introductory textbook, 2nd ed. ed, ITC educational textbook series. International Institute for Aerospace Survey and Earth Sciences (ITC), Enschede, The Netherlands.

Ji, K., Wu, Y., 2015. Scattering Mechanism Extraction by a Modified Cloude-Pottier Decomposition for Dual Polarization SAR. Remote Sensing 7, pp. 7447–7470. https://doi.org/10.3390/rs70607447

Jiang, H., Feng, M., Zhu, Y., Lu, N., Huang, J., Xiao, T., 2014. An Automated Method for Extracting Rivers and Lakes from Landsat Imagery. Remote Sensing 6, pp. 5067–5089. https://doi.org/10.3390/rs6065067.

Joshi, N., Baumann, M., Ehammer, A., Fensholt, R., Grogan, K., Hostert, P., Jepsen, M.R., Kuemmerle, T., Meyfroidt, P., Mitchard, E.T.A., Reiche, J., Ryan, C.M., Waske, B., 2016. A Review of the Application of Optical and Radar Remote Sensing Data Fusion to Land Use Mapping and Monitoring. Remote Sens. 8, p. 70. https://doi.org/10.3390/rs8010070.

Karamizadeh, S., Abdullah, S.M., Manaf, A.A., Zamani, M., Hooman, A., 2013. An Overview of Principal Component Analysis. J. Signal Inf. Process. 04, pp. 173–175. https://doi.org/10.4236/jsip.2013.43B031.

Kellndorfer, J.M., Pierce, L.E., Dobson, M.C., Ulaby, F.T., 1998. Toward consistent regional-to-global-scale vegetation characterization using orbital SAR systems. IEEE Transactions on Geoscience and Remote Sensing 36, pp. 1396–1411. https://doi.org/10.1109/36.718844.

Khand, K., Taghvaeian, S., Hassan-Esfahani, L., 2017. Mapping Annual Riparian Water Use Based on the Single-Satellite-Scene Approach. Remote Sens. 9, p. 832. https://doi.org/10.3390/rs9080832.

Kingsford, R.T., Thomas, R.F., Wong, P.S., Knowles, E., 1997. GIS Database for Wetlands of the Murray Darling Basin (Final report). Murray-Darling Basin Commission, National Parks and Wildlife Service, Sydney, Australia.

Kite, G., Pietroniro, A., 2000. Remote sensing of surface water, in: Remote Sensing in Hydrology and Water Management. Springer, Berlin, Germany, pp. 217–238.

Klemas, V., 2015. Remote Sensing of Floods and Flood-Prone Areas: An Overview. Journal of Coastal Research 31, pp. 1005–1013. https://doi.org/10.2112/JCOASTRES-D-14-00160.1

Kuenzer, C., Guo, H., Schlegel, I., Vo, Q.T., Xinwu, L., Dech, S., 2013. Varying Scale and Capability of Envisat ASAR-WSM, TerraSAR— Scansar and TerraSAR-X Stripmap Data to Assess Urban Flood Situations: A Case Study of the Mekong Delta in Can Tho Province. Remote Sensing 5, pp. 5122–5142.

Kumar, S., 2016. Advances in SAR Polarimetry. Presented at the SPIE APRS symposium, SPIE, New Delhi, India, p. 23.

Lang, M.W., Townsend, P.A., Kasischke, E.S., 2008. Influence of incidence angle on detecting flooded forests using C-HH synthetic aperture radar data. Remote Sens. Environ. 112, pp. 3898–3907. https://doi.org/10.1016/j.rse.2008.06.013.

Langanke, T., 2016. Copernicus Land Monitoring Service – High Resolution Layer Water and Wetness Product Specifications Document.

Lee, H., Yuan, T., Jung, H.C., Beighley, E., 2015. Mapping wetland water depths over the central Congo Basin using PALSAR ScanSAR, Envisat altimetry, and MODIS VCF data. Remote Sensing of Environment 159, pp. 70–79.

Lee, J.-S., Grunes, M.R., Pottier, E., Ferro-Famil, L., 2004. Unsupervised terrain classification preserving polarimetric scattering characteristics. IEEE Transactions on Geoscience and Remote Sensing 42, pp. 722–731. https://doi.org/10.1109/TGRS.2003.819883

Lee, J.-S., Pottier, E., 2009. Polarimetric Radar Imaging: From Basics to Applications.

Lehner, B., Döll, P., 2004. Development and validation of a global database of lakes, reservoirs and wetlands. Journal of Hydrology 296, pp. 1–22. https://doi.org/10.1016/j.jhydrol.2004.03.028

Leopold, L.B., Maddock Jr., T., 1953. The hydraulic geometry of stream channels and some physiographic implications (USGS Numbered Series No. 252), Professional Paper. Washington, D.C., USA.

Li, J., Chen, W., 2005. A rule-based method for mapping Canada's wetlands using optical, radar and DEM data. International Journal of Remote Sensing 26, pp. 5051–5069. https://doi.org/10.1080/01431160500166516.

Li, J., Wang, S., 2015. An automatic method for mapping inland surface waterbodies with Radarsat-2 imagery. Int. J. Remote Sens. 36, pp. 1367–1384. https://doi.org/10.1080/01431161.2015.1009653.

Liew, S.C., Saengtuksin, B., Kwoh, L.K., 2011. Mapping Water Quality of Coastal and Inland Waters Using High Resolution Worldview-2 Satellite Imagery, in: The GEOSS Era: Towards Operational Environmental Monitoring. Presented at the 34th International Symposium on Remote Sensing of Environment, ISPRS, Sydney, Australia.

Lillesand, T.M., Kiefer, R.W., Chipman, J.W., 2015. Concepts and Foundations of Remote Sensing, in: Remote Sensing and Image Interpretation. Wiley, United States of America, p. 736.

Liu, Z., Blasch, E., Bhatnagar, G., John, V., Wu, W., Blum, R.S., 2018. Fusing synergistic information from multi-sensor images: An overview from implementation to performance assessment. Information Fusion 42, pp. 127–145. https://doi.org/10.1016/j.inffus.2017.10.010.

Louis, J., Debaecker, V., Pflug, B., Main-Knorn, M., Bieniarz, J., Mueller-Wilm, U., Cadau, E., Gascon, F., 2016. Sentinel-2 Sen2Cor: l2A Processor for Users. Proceedings of the Living Planet Symposium. Presented at the ESA Living Planet Symposium, Prague, Czech Republic, p. 8.

Lunetta, R.S., Balogh, M.E., 1999. Application of Multi-Temporal Landsat 5 TM Imagery for Wetland Identification. Photogrammetric Engineering & Remote Sensing 65, pp. 1303–1310.

Mahapatra, P., Hanssen, R., 2011. Next ESA SAR Toolbox (NEST), in: Next ESA SAR Toolbox (NEST) A Cookbook. Presented at the Training Course on Active and Passive Microwave Remote Sensing, Delft University of Technology, Delft, The Netherlands.

Malnes, E., Guneriussen, T., Høgda, K.A., 2002. Mapping of flood-area by RADARSAT in Vannsjø, Norway. Proceedings of the 29th International Symposium on Remote Sensing of the Environment , Buenos Aires, Argentina.

Manjusree, P., Prasanna Kumar, L., Bhatt, C.M., Rao, G.S., Bhanumurthy, V., 2012. Optimization of threshold ranges for rapid flood inundation mapping by evaluating backscatter profiles of high incidence angle SAR images. International Journal of Disaster Risk Science 3, pp. 113–122. https://doi.org/10.1007/s13753-012-0011-5.

Marcus, W.A., Fonstad, M.A., 2008. Optical remote mapping of rivers at sub-meter resolutions and watershed extents. Earth Surface Processes and Landforms 33, pp. 4–24. https://doi.org/10.1002/esp.1637.

Markert, K.N., Chishtie, F., Anderson, E.R., Saah, D., Griffin, R.E., 2018. On the merging of optical and SAR satellite imagery for surface water mapping applications. Results in Physics 9, pp. 275–277. https://doi.org/10.1016/j.rinp.2018.02.054.

Martinez, J.M., Toan, T.L., 2007. Mapping of flood dynamics and spatial distribution of vegetation in the Amazon floodplain using multitemporal SAR data. Remote Sensing of Environment 108, pp. 209–223.

Martinis, S., 2017. Improving flood mapping in arid areas using Sentinel-1 time series data. 2017 IEEE International Geoscience Proceedings, pp. 193–196.

Martinis, S., 2010. Automatic near real-time flood detection in high resolution X-band synthetic aperture radar satellite data using context-based classification on irregular graphs. PhD Thesis, Fakultät für Geowissenschaften, Ludwig-Maximilians-Universität München, Germany.

Martinis, S., Kersten, J., Twele, A., 2015a. A fully automated TerraSAR-X based flood service. ISPRS Journal of Photogrammetry and Remote Sensing 104, pp. 203–212. https://doi.org/10.1016/j.isprsjprs.2014.07.014.

Martinis, S., Kuenzer, C., Wendleder, A., Huth, J., Twele, A., Roth, A., Dech, S., 2015b. Comparing four operational SAR-based water and flood detection approaches. International Journal of Remote Sensing 36, pp. 3519–3543.

Martinis, S., Twele, A., 2010. A Hierarchical Spatio-Temporal Markov Model for Improved Flood Mapping Using Multi-Temporal X-Band SAR Data. Remote Sensing 2, pp. 2240–2258. https://doi.org/10.3390/rs2092240.

Martinis, S., Twele, A., Voigt, S., 2011. Unsupervised Extraction of Flood-Induced Backscatter Changes in SAR Data Using Markov Image Modeling on Irregular Graphs. IEEE Transactions on Geoscience and Remote Sensing 49, pp. 251–263. https://doi.org/10.1109/TGRS.2010.2052816

Martinis, S., Twele, A., Voigt, S., 2009. Towards operational near real-time flood detection using a split-based automatic thresholding procedure on high resolution TerraSAR-X data. Natural Hazards and Earth System Sciences 9, pp. 303–314.

Matgen, P., Hostache, R., Schumann, G., Pfister, L., Hoffmann, L., Savenije, H.H.G., 2011. Towards an automated SAR-based flood monitoring system: Lessons learned from two case studies. Phys. Chem. Earth Parts ABC, Recent Advances in Mapping and Modelling Flood Processes in Lowland Areas 36, pp. 241–252. https://doi.org/10.1016/j.pce.2010.12.009

Matgen, P., Montanari, M., Hostache, R., Pfister, L., Hoffmann, L., Plaza, D., Pauwels, V.R.N., De Lannoy, G.J.M., De Keyser, R., Savenije, H.H.G., 2010. Towards the sequential assimilation of SAR-derived water stages into hydraulic models using the Particle Filter: proof of concept. Hydrology and Earth System Sciences 14, pp. 1773–1785. https://doi.org/10.5194/hess-14-1773-2010.

Matgen, P., Schumann, G., Henry, J.-B., Hoffmann, L., Pfister, L., 2007. Integration of SAR-derived river inundation areas, high-precision topographic data and a river flow model toward near real-time flood management. Int. J. Appl. Earth Obs. Geoinformation 9, pp. 247–263. https://doi.org/10.1016/j.jag.2006.03.003.

McCarthy, M., Spillane, S., Walsh, S., Kendon, M., 2016. The meteorology of the exceptional winter of 2015/2016 across the UK and Ireland. Weather 71, pp. 305–313. https://doi.org/10.1002/wea.2823

McFeeters, S.K., 1996. The use of the Normalized Difference Water Index (NDWI) in the delineation of open water features. International Journal of Remote Sensing 17, pp. 1425–1432.

Menne, B., Murray, V., 2013. Floods in the WHO European region: health effects and their prevention. World Health Organization, Regional Office for Europe, Copenhagen.

Mertz, C., 2018. Pluies Abondantes & Crues du 4 au 5 Janvier 2018.

Messager, M.L., Lehner, B., Grill, G., Nedeva, I., Schmitt, O., 2016. Estimating the volume and age of water stored in global lakes using a geo-statistical approach. Nature Communications 7, 13603. https://doi.org/10.1038/ncomms13603

Mitchell, A.L., Milne, A.K., Tapley, I., 2015. Towards an operational SAR monitoring system for monitoring environmental flows in the Macquarie Marshes. Wetlands Ecology and Management 23, pp. 61–77. https://doi.org/10.1007/s11273-014-9358-2

Montgomery, D.R., Dietrich, W.E., 1988. Where do channels begin?. Nature 336, pp. 232–234.

Moreau, C., 2018. PHOTOS. L'alerte orange est levée en Alsace, la décrue a commencé. France 3 Grand Est. https://france3-regions.francetvinfo.fr/grand-est/alsace/alsace-vigilance-orange-inondations-1395439.html (accessed 04 October 2018).

Morsy, S., Shaker, A., El-Rabbany, A., 2018. Using Multispectral Airborne LiDAR Data for Land/Water Discrimination: A Case Study at Lake Ontario, Canada. Appl. Sci. 8, p. 349. https://doi.org/10.3390/app8030349.

Moreira, A., Prats-Iraola, P., Younis, M., Krieger, G., Hajnsek, I., Papathanassiou, K.P., 2013. A tutorial on synthetic aperture radar. IEEE Geoscience and Remote Sensing Magazine 1, pp. 6–43. https://doi.org/10.1109/MGRS.2013.2248301.

Mueller, N., Lewis, A., Roberts, D., Ring, S., Melrose, R., Sixsmith, J., Lymburner, L., McIntyre, A., Tan, P., Curnow, S., Ip, A., 2016. Water observations from space: Mapping surface water from 25years of Landsat imagery across Australia. Remote Sensing of Environment 174, pp. 341–352. https://doi.org/10.1016/j.rse.2015.11.003.

Musa, Z.N., Popescu, I., Mynett, A., 2015. A review of applications of satellite SAR, optical, altimetry and DEM data for surface water modelling, mapping and parameter estimation. Hydrology and Earth System Sciences 19, pp. 3755–3769. https://doi.org/10.5194/hess-19-3755-2015.

Muster, S., Heim, B., Abnizova, A., Boike, J., 2013. Water Body Distributions Across Scales: A Remote Sensing Based Comparison of Three Arctic TundraWetlands. Remote Sensing 5, pp. 1498–1523. https://doi.org/10.3390/rs5041498.

NASA, n.d. MODIS Moderate Resolution Imaging Spectroradiometer – Data. MODIS web. https://modis.gsfc.nasa.gov/data/ (accessed 10 August 2018).

Nath, R.K., Deb, S.K., 2010. Water-Body Area Extraction from High Resolution Satellite Images-An Introduction, Review, and Comparison. International Journal of Image Processing (IJIP) 3, pp. 353–372.

National Directorate for Fire and Emergency Management, 2016. Report on Flooding December 4 2015 – January 13 2016. Department of Housing, Planning , Community and Local Government, Ireland.

Natural Resources Canada, 2008. Image Classification and Analysis. http://www.nrcan.gc.ca/node/9361 (accessed 13 August 2018).

NGA, N.G.-I.A., 2005. Documentation for the Shuttle Radar Topography Mission (SRTM) Water Body Data Files.

Nobre, A.D., Cuartas, L.A., Hodnett, M., Renno, C.D., Rodrigues, G., Silveira, A., Waterloo, M., Saleska, S., 2011. Height Above the Nearest Drainage – a hydrologically relevant new terrain model. Journal of Hydrology 404, pp. 13–29.

Ogilvie, A., Belaud, G., Massuel, S., Mulligan, M., Le Goulven, P., Calvez, R., 2018. Surface water monitoring in small water bodies: potential and limits of multi-sensor Landsat time series. Hydrology and Earth System Sciences Discussions, pp. 1–35. https://doi.org/10.5194/hess-2018-19.

O'Grady, D., Leblanc, M., Bass, A., 2014. The use of radar satellite data from multiple incidence angles improves surface water mapping. Remote Sensing of Environment 140, pp. 652–664. https://doi.org/10.1016/j.rse.2013.10.006.

Ottinger, M., Kuenzer, C., Liu, G., Wang, S., Dech, S., 2013. Monitoring land cover dynamics in the Yellow River Delta from 1995 to 2010 based on Landsat 5 TM. Applied Geography 44, pp. 53–68. https://doi.org/10.1016/j.apgeog.2013.07.003.

Overton, I.C., 2005. Modelling Floodplain Inundation on A Regulated River: Integrating GIS, Remote Sensing and Hydrological Models. River Res. Applic. 21, pp. 991–1001.

Palmer, S.C.J., Kutser, T., Hunter, P.D., 2015. Remote sensing of inland waters: Challenges, progress and future directions. Remote Sensing of Environment 157, pp. 1–8. https://doi.org/10.1016/j.rse.2014.09.021.

Pappenberger, F., Frodsham, K., Beven, K., Romanowicz, R., Matgen, P., 2007. Fuzzy set approach to calibrating distributed flood inundation models using remote sensing observations. Hydrology and Earth System Sciences Discussions 11, pp. 739–752.

Pekel, J.-F., Cottam, A., Gorelick, N., Belward, A.S., 2016. High-resolution mapping of global surface water and its long-term changes. Nature 540, pp. 418-422. https://doi.org/10.1038/nature20584

Pekel, J.-F., Vancutsem, C., Bastin, L., Clerici, M., Vanbogaert, E., Bartholomé, E., Defourny, P., 2014. A near real-time water surface detection method based on HSV transformation of MODIS multi-spectral time series data. Remote Sensing of Environment 140, pp. 704–716. https://doi.org/10.1016/j.rse.2013.10.008.

Perlman, H.A., 1998. Water science for schools (USGS Numbered Series No. 98–4086), Water-Resources Investigations Report. U.S. Dept. of the Interior, Geological Survey, Water Resources Division,.

Pierdicca, N., Pulvirenti, L., Chini, M., Guerriero, L., Candela, L., 2013. Observing floods from space: Experience gained from COSMO-SkyMed observations. Acta Astronautica 84, pp. 122–133. https://doi.org/10.1016/j.actaastro.2012.10.034.

Plank, S., Jüssi, M., Martinis, S., Twele, A., 2017. Mapping of flooded vegetation by means of polarimetric Sentinel-1 and ALOS-2/PALSAR-2 imagery. International Journal of Remote Sensing 38, pp. 3831–3850. https://doi.org/10.1080/01431161.2017.1306143

Pohl, C., Van Genderen, J.L., 1998. Review article Multisensor image fusion in remote sensing: Concepts, methods and applications. International Journal of Remote Sensing 19, pp. 823–854. https://doi.org/10.1080/014311698215748.

Pollak, S., 2016. Flooding crisis: Some roads reopening as waters recede. Ir. Times.

Pulvirenti, L., Chini, M., Marzano, F., Pierdicca, N., Mori, S., Guerriero, L., Boni, G., Candela, L., 2012. Detection of floods and heavy rain using Cosmo-SkyMed data: the event in Northwestern Italy of November 2011. Procedings of IEEE International Geoscience and Remote Sensing Symposium. Presented at the International Geoscience and Remote Sensing Symposium (IGARSS 2012), Munich, Germany, pp. 3026–3029.

PUSTADARU, C.J., 2017. Dinas Pekerjaan Umum Sumber Daya Air Dan Penataan Ruang Provinsi Jawa Tengah. http://pusdataru.jatengprov.go.id/ (accessed 05 October 2018).

Rahmawaty, M.A., 2015. Study of Bengawan Solo Watershed Vulnerability Based on Physical and Nonphysical Factors Using Multi Criteria Analysis (Case Study Lamongan Regency) (Master Thesis). Institut Teknologi Sepuluh Nopember, Surabaya, Indonesia.

Rast, M., Johannessen, J., Mauser, W., 2014. Review of Understanding of Earth's Hydrological Cycle: Observations, Theory and Modelling. Surveys in Geophysics Journal 35, pp. 491–513. https://doi.org/10.1007/s10712-014-9279-x.

Refice, A., D'Addabbo, A., Capolongo, D., 2017. Flood Monitoring through Remote Sensing. Springer.

Rennó, C.D., Nobre, A.D., Cuartas, L.A., Soares, J.V., Hodnett, M.G., Tomasella, J., Waterloo, M.J., 2008. HAND, a new terrain descriptor using SRTM-DEM: Mapping terra-firme rainforest environments in Amazonia. Remote Sensing of Environment 112, pp. 3469–3481. https://doi.org/10.1016/j.rse.2008.03.018.

Riffler, M., Moran, A., Dullek, B., Schleicher, C., Walli, A., Weichselbaum, J., 2018. Large-Scale Water and Wetness Detection using a Multi-Sensor and Multi-Temporal Approach.

Rokni, K., Ahmad, A., Selamat, A., Hazini, S., 2014. Water Feature Extraction and Change Detection Using Multitemporal Landsat Imagery. Remote Sensing 6, pp. 4173–4189. https://doi.org/10.3390/rs6054173.

Sarmap, 2009. Synthetic Aperture Radar and SARscape (The Earth Observation Information Gateway. SAR-Guidebook.pdf.

Saxena, N., Rathore, N., 2013. A Review on Speckle Noise Filtering Techniques for SAR Images. International Journal of Advanced Research in Computer Science and Electronics Engineering (IJARCSEE) 2, 5.

Schindler, K., 2012. an Overview and Comparison of Smooth Labeling Methods for Land-Cover Classification. IEEE Transactions on Geoscience and Remote Sensing 50, pp. 4534–4545.

Schlaffer, S., Hollaus, M., Wagner, W., Matgen, P., 2012. Flood delineation from synthetic aperture radar data with the help of a priori knowledge from historical acquisitions and digital elevation models in support of near-real-time flood mapping. Proceedings of SPIE, Earth Resources and Environmental Remote Sensing/GIS Applications III. Edinburgh, pp. 853813-1-853813–9.

Schlaffer, S., Matgen, P., Hollaus, M., Wagner, W., 2015. Flood detection from multi-temporal SAR data using harmonic analysis and change detection. International Journal of Applied Earth Observation and Geoinformation 38, pp. 15–24. https://doi.org/10.1016/j.jag.2014.12.001.

Schmitt, M., Zhu, X.X., 2016. Data Fusion and Remote Sensing: An ever-growing relationship. IEEE Geosci. Remote Sens. Mag. 4, pp. 6–23. https://doi.org/10.1109/MGRS.2016.2561021.

Schowengerdt, R.A., 2007. Remote Sensing: Models and Methods for Image Processing, Third edition. ed. Elsevier, Tucson, Arizona, United States of America.

Schreier, G. (Ed.), 1993. SAR Geocoding: Data and Systems. Wichmann, Karlsruhe.

Schumann, G., Di Baldassarre, G., Bates, P.D., 2009. The Utility of Spaceborne Radar to Render Flood Inundation Maps Based on Multialgorithm Ensembles. IEEE Transactions on Geoscience and Remote Sensing 47, pp. 2801–2807. https://doi.org/10.1109/TGRS.2009.2017937.

Schumann, G.J.-P., 2017. Remote Sensing of Floods. Oxford Research Encyclopedia of Natural Hazard Science. https://doi.org/10.1093/acrefore/9780199389407.013.265.

Schumann, G.J.-P., Moller, D.K., 2015. Microwave remote sensing of flood inundation. Physics and Chemistry of the Earth, Parts A/B/C 83–84, 84–95.

Sertit, iCUBE, 2018. Floods in Grand Est. Space serving the Earth. http://sertit.u-strasbg.fr/RMS/action.php?id=7615098111 (accessed 28 September 2018).

Shah, V., Choudhary, A., Tewari, K., 2011. River extraction from satellite image. IJCSI International Journal of Computer Science Issues 8.

Shan, Z., Wang, C., Zhang, H., Chen, J., 2011. H-α Decomposition and Alternative Parameters for Dual Polarization SAR Data. Progress In Electromagnetics Research Symposium Proceedings, Suzhou, China, pp. 1386–1890.

Sharma, R., Tateishi, R., Hara, K., Nguyen, L., 2015. Developing Superfine Water Index (SWI) for Global Water Cover Mapping Using MODIS Data. Remote Sensing 7, pp. 13807–13841. https://doi.org/10.3390/rs71013807.

Short, N., Brisco, B., Landry, R., Raymond, D., Van der Sanden, J., 2009. A Semi-automated tool for surface water mapping with RADARSAT-1. Canadian Journal of Remote Sensing 35, pp. 336–344.

Sichangi, A.W., Wang, L., Yang, K., Chen, D., Wang, Z., Li, X., Zhou, J., Liu, W., Kuria, D., 2016. Estimating continental river basin discharges using multiple remote sensing data sets. Remote Sensing of Environment 179, pp. 36–53. https://doi.org/10.1016/j.rse.2016.03.019.

Sidle, R.C., Ziegler, A.D., Vogler, J.B., 2007. Contemporary changes in open water surface area of Lake Inle, Myanmar. Sustainability Science 2, pp. 55–65. https://doi.org/10.1007/s11625-006-0020-7.

Simon, R.N., Tormos, T., Danis, P.A., 2014. Geographic object based image analysis using very high spatial and temporal resolution radar and optical imagery in tracking water level fluctuations in a freshwater reservoir. South-Eastern European Journal of Earth Observation and Geomatics 3, pp. 287–291.

Solbø, S., Solheim, I., 2005. Towards Operational Flood Mapping with Satellite SAR. Proc. of the 2004 Envisat & ERS Symposium, 6-10 September 2004, Salzburg, Austria, p. 8.

Srisuk, S., 2014. Bilateral filtering as a tool for image smoothing with edge preserving properties. The 2014 International Electrical Engineering Congress (IEECON), pp. 1–4. https://doi.org/10.1109/iEECON.2014.6925940.

Stewart, C., 2016. Exercise Sentinel-1 Processing, Course Materials. 8th ESA Training Course on Radar and Optical Remote Sensing, Cesis, Latvia, 5-9 September 2016.

Sulaeman, A., Suhartanto, E., 2017. Analisis Genangan Banjir akibat Luapan Bengawan Solo untuk Mendukung Peta Risiko Bencana Banjir di Kabupaten Bojonegoro. Jurnal Teknik Pengairan 8, pp. 146–157.

Sun, D., Yu, Y., Goldberg, M.D., 2011. Deriving Water Fraction and Flood Maps From MODIS Images Using a Decision Tree Approach. IEEE J. Sel. Top. Appl. Earth Obs. Remote Sens. 4, 814–825. https://doi.org/10.1109/JSTARS.2011.2125778.

Tarboton, D.G., Bras, R.L., Rodriguez-Iturbe, I., 1991. On the extraction of channel networks from digital elevation data. Hydrological Processes 5, pp. 81–100. https://doi.org/10.1002/hyp.3360050107.

Taylor, P.C., Mosiman, B.N., 2003. The Kansas Surface Water Database. Kansas Biological Survey Report 2003 #116 (Survey report No. 116). University of Kansas, Lawrence, Kansas.

The European Commission's Joint Research Centre, n.d. Global Surface Water - Data Access https://global-surface-water.appspot.com/download (accessed 03 June 2018).

Theia, 2018. Theia - Land Data Center. Muscate - Distribution Workshop. https://theia.cnes.fr/atdistrib/rocket/#/home (accessed 31 October 2018).

Tian, S., Zhang, X., Tian, J., Sun, Q., Tian, S., Zhang, X., Tian, J., Sun, Q., 2016. Random Forest Classification of Wetland Landcovers from Multi-Sensor Data in the Arid Region of Xinjiang, China. Remote Sensing 8, p. 954. https://doi.org/10.3390/rs8110954.

Torres, R., Snoeij, P., Geudtner, D., Bibby, D., Davidson, M., Attema, E., Potin, P., Rommen, B., Floury, N., Brown, M., Traver, I.N., Deghaye, P., Duesmann, B., Rosich, B., Miranda, N., Bruno, C., L'Abbate, M., Croci, R., Pietropaolo, A., Huchler, M., Rostan, F., 2012. GMES Sentinel-1 mission. Remote Sensing of Environment 120, pp. 9–24. https://doi.org/10.1016/j.rse.2011.05.028.

Touzi, R., Deschamps, A., Rother, G., 2007. Wetland characterization using polarimetric RADARSAT-2 capability. Can. J. Remote Sens. 33, p. 12.

Tranvik, L.J., Downing, J.A., Cotner, J.B., Loiselle, S.A., Striegl, R.G., Ballatore, T.J., Dillon, P., Finlay, K., Fortino, K., Knoll, L.B., Kortelainen, P.L., Kutser, T., Larsen, S., Laurion, I., Leech, D.M.,

McCallister, S.L., McKnight, D.M., Melack, J.M., Overholt, E., Porter, J.A., Prairie, Y., Renwick, W.H., Roland, F., Sherman, B.S., Schindler, D.W., Sobek, S., Tremblay, A., Vanni, M.J., Verschoor, A.M., Wachenfeldt, E.V., Weyhenmeyer, G.A., 2009. Lakes and reservoirs as regulators of carbon cycling and climate. Limonology & Oceanography 54, pp. 2298–2314. https://doi.org/10.4319/lo.2009.54.6_part_2.2298.

Tulbure, M.G., Broich, M., 2013. Spatiotemporal dynamic of surface water bodies using Landsat time-series data from 1999 to 2011. ISPRS Journal of Photogrammetry and Remote Sensing 79, pp. 44–52. https://doi.org/10.1016/j.isprsjprs.2013.01.010.

Twele, A., Cao, W., Plank, S., Martinis, S., 2016. Sentinel-1-based flood mapping: a fully automated processing chain. International Journal of Remote Sensing 37, pp. 2990–3004. https://doi.org/10.1080/01431161.2016.1192304

Twele, A., Martinis, S., Cao, W., Plank, S., 2015. Inundation mapping using C- and X-band SAR data: from algorithms to fully-automated flood services. The Mapping Water Bodies from Space (MWBS 2015), Frascati, Italy.

USGS, n.d. USGS Earth Explorer. http://earthexplorer.usgs.gov (accessed 15 November 2015).

van Rijsbergen, C.J., 1979. Information Retrieval, 2nd ed. London: Butterworths.

Van Zyl, J., Kim, Y., 2011. Synthetic Aperture Radar Polarimetry. John Wiley & Sons.

Van Zyl, J., Kim, Y., 2010. Synthetic Aperture Radars (SAR) Imaging Basics, in: Synthetic Aperture Radar Polarimetry, JPL Space Science and Technology Series. Jet Propulsion Laboratory - California Institute of Technology, California.

Verpoorter, C., Kutser, T., Tranvik, L.J., 2012. Automated Mapping of Water Bodies Using Landsat Multispectral Data. Limnol. Oceanogr. Methods 10, pp. 1037–1050. https://doi.org/10.4319/lom.2012.10.1037.

Voigt, S., Kemper, T., Riedlinger, T., Kiefl, R., Scholte, K., Mehl, H., 2007. Satellite Image Analysis for Disaster and Crisis-Management Support. IEEE Transactions on Geoscience and Remote Sensing 45, pp. 1520–1528. https://doi.org/10.1109/TGRS.2007.895830.

Wagner, E.G., Lanoix, J.N., 1959. Water Supply for Rural Areas and Small Communities. World Health Organization, Geneva.

Wahyudi, A., Anwar, N., Edijatno, 2014. Studi Optimasi Pola Tanam pada Daerah Irigasi Warujayeng Kertosono dengan Program Linier. Jurnal Teknik POMITS 3, pp. 30–35.

Wang, X., Ge, L., Li, X., 2012. Evaluation of Filters for Envisat ASAR Speckle Suppression in Pasture Area. ISPRS Annals of Photogrammetry, Remote Sensing and Spatial Information Sciences I–7, pp. 341–346. https://doi.org/10.5194/isprsannals-I-7-341-2012.

Wang, Y., Huang, F., Wei, Y., 2013. Water body extraction from LANDSAT ETM+ image using MNDWI and K-T transformation. The Geoinformatics 2013 21st International Conference, Henan University, Kaifeng, Henan, China.

Wang, Y., Ruan, R., She, Y., Yan, M., 2011. Extraction of Water Information based on RADARSAT SAR and Landsat ETM+. Procedia Environmental Sciences 10, pp. 2301–2306. https://doi.org/10.1016/j.proenv.2011.09.359

Warner, T., Bell, R., Singhroy, V., 1996. Local Incidence Angle Effects on X- and C-Band Radar Backscatter of Boreal Forest Communities. Canadian Journal of Remote Sensing 22, pp. 269–279. https://doi.org/10.1080/07038992.1996.10855182.

Washington State Department of Natural Resources, 2004. Channel Migration Zones and Bankfull Channel Features, in: Forest Practices Board Manual. Washington State Department of Natural Resources, pp. 1–69.

Wegner, J.D., Hnsch, R., Thiele, A., Soergel, U., 2011. Building detection from one orthophoto and high-resolution InSAR data using conditional random elds. IEEE J. Sel. Top. Appl. Earth Obs. Remote Sens. 4, pp. 83–91.

Wendl, C., Le Bris, A., Chehata, N., Puissant, A., Postadjian, T., 2018. Decision fusion of SPOT-6 and multitemporal Sentinel-2 images for urban area detection. Proceeding of The IEEE International Geoscience and Remote Sensing Symposium (IGARSS), Valencia, Spain.

Wendleder, A., Wessel, B., Roth, A., Breunig, M., Martin, K., Wagenbrenner, S., 2013. TanDEM-X Water Indication Mask: Generation and First Evaluation Results. IEEE Journal of Selected

Topics in Applied Earth Observations and Remote Sensing 6, pp. 171–179. https://doi.org/10.1109/JSTARS.2012.2210999

Westerhoff, R.S., Kleuskens, M.P.H., Winsemius, H.C., Huizinga, H.J., Brakenridge, G.R., Bishop, C., 2013. Automated global water mapping based on wide-swath orbital synthetic-aperture radar. Hydrology and Earth System Sciences 17, pp. 651–663. https://doi.org/10.5194/hess-17-651-2013.

Wetland Surveys Ireland, 2012. Map of Irish Wetlands. http://www.wetlandsurveysireland.com/wetlands/map-of-irish-wetlands--/map-of-irish-wetlands---map/index.html (accessed 29 July 2018).

Wetzel, R.G., 2001. Limnology: lake and river ecosystems, 3rd ed. Academic Press, San Diego.

Winter, T.C., Harvey, J.W., Franke, O.L., Alley, W.M., 1998. Ground Water and Surface Water A Single Resource. U.S. Geological Survey Circular 1139, Denver, Colorado.

Woodhouse, I.H., 2005. Introduction to Microwave Remote Sensing, 1st ed. Taylor & Francis.

WWF, n.d. Global Lakes and Wetlands Database. https://www.worldwildlife.org/pages/global-lakes-and-wetlands-database (accessed 01 June 2018).

Xia, J., Ming, Z., Iwasaki, A., 2018. Multiple Sources Data Fusion Via Deep Forest. Presented at the IGARSS 2018 - 2018 IEEE International Geoscience and Remote Sensing Symposium, Valencia, Spain.

Yamazaki, F., Shimakage, J., Liu, W., Nonaka, T., Sasagawa, T., 2013. Extraction of flooded areas due to the 2011 central Thailand flood using aster and TerraSAR-X data. Geoscience and Remote Sensing Symposium (IGARSS), 2013 IEEE International, pp. 707–710.

Yang, X., Zhao, S., Qin, X., Zhao, N., Liang, L., 2017. Mapping of Urban Surface Water Bodies from Sentinel-2 MSI Imagery at 10 m Resolution via NDWI-Based Image Sharpening. Remote Sensing 9, 596. https://doi.org/10.3390/rs9060596.

Yesou, H., Huber, C., Giraud, H., Studer, M., Haouet, S., Fraipont, P. de, Virelli, M., Desnos, Y.L., 2015. Mapping water bodies exploited multi-sensors and multi resolution optical and SAR data: gained experience from plain flood monitoring in Western Europe and Asia. Mapping Water Bodies from Space - MWBS 2015, 18-19 March 2015, Italy.

York Press, 2016. York floods 2015: How the devastating floods unfolded and how York rallied superbly. The Press.

Yuan, T., Lee, H., Jung, H., 2015. Toward Estimating Wetland Water Level Changes Based on Hydrological Sensitivity Analysis of PALSAR Backscattering Coefficients over Different Vegetation Fields. Remote Sensing 7, pp. 3153–3183. https://doi.org/10.3390/rs70303153.

Zadeh, L.A., 1976. A Fuzzy-Algorithmic Approach to the Definition of Complex or Imprecise Concepts. Systems Theory in the Social Sciences. Interdisciplinary Systems Research.

Zhang, F., Li, J., Zhang, B., Shen, Q., Ye, H., Wang, S., Lu, Z., 2018. A simple automated dynamic threshold extraction method for the classification of large water bodies from landsat-8 OLI water index images. Int. J. Remote Sens. 39, pp. 3429–3451. https://doi.org/10.1080/01431161.2018.1444292.

Zhao, L., Yang, J., Li, P., Zhang, L., 2014. Seasonal inundation monitoring and vegetation pattern mapping of the Erguna floodplain by means of a RADARSAT-2 fully polarimetric time series. Remote Sensing of Environment 152, pp. 426–440. https://doi.org/10.1016/j.rse.2014.06.026.

Zhou, Y., Dong, J., Xiao, X., Xiao, T., Yang, Z., Zhao, G., Zou, Z., Qin, Y., 2017. Open Surface Water Mapping Algorithms: A Comparison of Water-Related Spectral Indices and Sensors. Water 9, p. 256. https://doi.org/10.3390/w9040256.

Résumé long (français)

Exploitation de Series Temporelles d'Images Multi-Sources pour la Cartographie des Surfaces en Eau

Filsa BIORESITA

Thèse en Géographie / Géomatique

Université de Strasbourg

École Doctorale des Sciences de la Terre et de l'Environnement - ED413

Sous la direction de Anne PUISSANT

1. Introduction, problématique et objectifs

Les eaux de surface sont des ressources importantes pour la biosphère et l'anthroposphère. Elles favorisent la préservation des habitats, le développement de la biodiversité et le maintien des services écosystémiques en contrôlant le cycle des nutriments et le carbone à l'échelle mondiale. Elles sont essentielles à la vie quotidienne de l'homme, notamment pour l'irrigation, la consommation d'eau potable, la production hydro-électrique, etc. Par ailleurs, lors des inondations, elles peuvent présenter des dangers pour l'homme, les habitations et les infrastructures. La surveillance des changements dynamiques des eaux de surface a donc un rôle primordial pour guider les choix des gestionnaires dans le processus d'aide à la décision.

L'imagerie satellitaire constitue une source de données adaptée permettant de fournir des informations sur les eaux de surface. De nos jours, la télédétection satellitaire a connu une révolution avec le lancement des satellites Sentinel-1 (Radar) et Sentinel-2 (Optique) qui disposent d'une haute fréquence de revisite et d'une résolution spatiale moyenne à élevée. Ces données peuvent fournir des séries temporelles essentielles pour apporter davantage d'informations afin d'améliorer la capacité d'observation des eaux de surface. L'exploitation de telles données massives et multi-sources pose des défis en termes d'extraction de connaissances

et de processus de traitement d'images car les chaines de traitement doivent être le plus automatiques possibles.

Dans ce contexte, l'objectif de ce travail de thèse est de proposer de nouvelles approches permettant de cartographier l'extension spatiale des eaux de surface permanente et temporaire (inondations), en explorant l'utilisation unique et combinée des données Sentinel-1 et Sentinel-2. Afin d'atteindre cet objectif, ces problématiques liées à l'amélioration de la cartographie des eaux de surface sont synthétisées en trois questions :

- *Quelle est la pertinence et quelles méthodes sont adaptées et robustes pour une exploitation opérationnelle des données Sentinel-1 ?*
- *Quel est l'apport de la haute fréquence temporelle des images Sentinel-1 ?*
- *Que peuvent apporter les données multi-capteurs dans les méthodes automatiques ?*

Sur la base de ces problématiques, trois hypothèses sont émises :

1. Les séries temporelles d'images satellites peuvent améliorer la cartographie des eaux de surface.
2. Les images multi-capteurs sont utiles et pertinentes pour la cartographie et la surveillance des eaux de surface.
3. Les méthodes proposées sont génériques et peuvent être appliquées et adaptées à d'autres applications thématiques.

2. État de l'art

Cette partie a pour but d'examiner l'état de l'art des méthodes de cartographie des eaux de surface fondées par des méthodes de télédétection optique et radar et de présenter les produits existants des eaux de surface.

2.1 Télédétection optique pour la détection des eaux de surface

En cas de conditions météorologiques favorables, les images satellites « optiques » constituent la source d'information privilégiée pour la détection des eaux de surface en raison de leur facilité d'interprétation. L'imagerie optique peut fournir une bonne information sur la délimitation des surfaces en eaux lorsque les nuages, les arbres ou la végétation ne masquent pas la surface d'eau. Plusieurs méthodes ont été développées dans la littérature pour cartographier les eaux de surface avec des images optiques.

Le découpage de densité, la détection des contours, les méthodes de classification (non supervisées ou supervisées) et les méthodes décisionnelles sont fondées sur une rétro-diffusion faible de l'eau de surface. Le moyen facile et efficace de distinguer les zones en eau des zones terrestre consiste à utiliser des indices d'eau (par exemple : TCW, NDVI, NDWI, MNDWI et AWEI). Le seuillage est l'un des problèmes importants de la cartographie des eaux de surface. Des méthodes telles que le découpage de densité, la détection des contours et les indices d'eau sont appliquées par seuillage pour extraire l'eau de surface. La sélection des seuils est délicate et parfois difficile à généraliser en raison des caractéristiques différentes de l'eau de surface dans chaque image. Ainsi, un ajustement manuel du seuil est nécessaire pour obtenir des résultats plus précis. Il existe des méthodes d'extraction automatique de seuillage pour cartographier les eaux de surface.

Toutes les méthodes mentionnées ci-dessus utilisent généralement la réflectance des pixels pour extraire les eaux de surface. Cependant, avec des images à très haute résolution spatiale, les méthodes de classification dite 'orientée-objet' conviennent mieux.

Bien que le principe de l'extraction de l'eau de surface à partir des capteurs optiques soit assez simple, il est également important de rappeler que la qualité de l'extraction est dépendante de la qualité des images en termes de couverture nuageuses puisque les images optiques sont dépendantes des conditions atmosphériques. Dans ces conditions, plusieurs méthodes ont été développées dans la littérature à partir des images issues de capteurs actifs (images Radar à Synthèse d'Ouverture – RSO).

2.2 Télédétection RSO pour la détection des eaux de surface

La seuillage est aussi l'une des méthodes les plus couramment adoptées sur les images RSO pour distinguer les zones en eau des autres zones. L'approche est basée sur le retour faible des eaux de surface. Son avantage est représenté par l'efficacité du calcul qui pourrait le rendre approprié à des fins de cartographie rapide. Cependant, le choix de la valeur de seuil est un aspect critique car il dépend des paramètres environnementaux de la zone d'étude, ainsi que des paramètres du système.

Deux approches existent pour définir un seuil de détection de la surface de l'eau sur une image RSO : (i) la détermination manuelle peut être effectuée de manière empirique par interprétation visuelle de l'histogramme de l'image et par procédures d'essai et d'erreur, (ii) le seuillage automatique pour la cartographie des eaux de surface peut être basé sur plusieurs algorithmes (l'algorithme d'Otsu, *valley emphasis*, le seuillage automatique basé sur la modélisation statistique des histogrammes).

La plupart des études sus-mentionnées considèrent les pixels comme les plus petites composantes géométriques de données raster (à base de pixels). A très haute résolution spatiale, les objets de surface de la Terre sont généralement plus grands que la taille en pixels. Par conséquent, bien que les pixels représentent différentes propriétés spectrales, ils peuvent correspondre au même objet. La classification orientée objet sur ces images RSO s'est de plus en plus développée dans la cartographie des eaux de surface au cours des dernières années pour surmonter ce problème. Cette approche présente des avantages pour améliorer la classification en combinant des caractéristiques spectrales et des informations contextuelles. Cependant, cette méthode classe les éléments d'image par phase de segmentation à l'aide d'informations contextuelles limitées.

En conclusion, la plupart des méthodes de cartographie des eaux de surface basées sur des images optiques ou RSO à une seule date et proposée dans la littérature nécessitent une intervention considérable de la part de l'utilisateur. Cette intervention humaine n'est pas pratique pour la cartographie opérationnelle et n'est pas adaptée à la nouvelle génération de données optiques (Sentinel-2) et RSO (Sentinel-1), caractérisées par une résolution temporelle accrue. En effet, les informations contextuelles, telles que la corrélation entre les pixels voisins, doivent être prises en compte, étant donné que les pixels individuels ne sont pas des variables aléatoires indépendantes mais forment un champ aléatoire. Depuis quelques années, l'analyse d'images multi-temporelles a prouvé sa supériorité par rapport aux approches mono-temporelles afin d'extraire les eaux de surface et de surveiller ces surfaces.

2.3 Les données multi-temporelles et multi-sources pour la cartographie et la surveillance des eaux de surface

Les études utilisant des données multi-temporelles produisent de meilleurs résultats et sont plus largement plébiscitées que les approches mono-dates pour la cartographie des eaux de surface. Ce type d'approche ouvre la possibilité de surveiller les eaux de surface, de détecter les inondations, de détecter les changements et de classer les eaux de surface; par exemple, distinguer les eaux de surface permanentes et des eaux de surface temporaires (inondations). Avec la demande croissante de compréhension de la dynamiques des eaux de surface dans le monde, de multiples sources de données de télédétection avec des séries temporelles plus ou moins longues peuvent être utilisées à cette fin. Cependant, les études combinant une approche multi-temporelle et multi-source sont encore peu nombreuses.

L'utilisation des données multi-temporelles et multi-capteurs peuvent augmenter la précision de la cartographie des eaux de surface. La fusion d'images multi-sources a été largement étudiée dans le domaine de la télédétection. La fusion d'images peut être mise en œuvre à trois niveaux différents: (1) au niveau de pixel, (2) au niveau des attributs et (3) au niveau décisionnel. La fusion d'images au « niveau décisionnel » est couramment utilisée dans la littérature pour l'extraction des eaux de surface. Lorsque les images proviennent de plusieurs capteurs, la méthode la plus pertinente pour la fusion de données consiste à combiner les images avec les résultats des eaux de surface extraites individuellement pour chaque source d'image.

2.4 Les produits, outils et services existants pour la cartographie des eaux de surface

Il existe à l'heure actuelle un grand nombre des bases de données cartographiant les eaux de surface, telles que le produit *Global Surface Water* du *EC-Joint Research Centre*, le produit *SRTM Water Body* de la NGA, le produit *Global Lakes and Wetlands Database (GLWD)* de l'Université de Kassel (Allemagne) ou le produit *Water and Wetness* de EC-COPERNICUS.

Le nombre d'algorithmes de détection d'eau basés sur les images RSO et de services de cartographie automatique des inondations ont augmenté ces dernières années. Dans la plupart des cas, une certaine interaction de l'utilisateur est nécessaire pour la collecte, le prétraitement et l'intégration des données auxiliaires dans les « pipelines » de traitement. Le *NASA's Goddard's Office of Applied Science* propose un service mondial automatisé de cartographie des inondations et des eaux de surface (http://oas.gsfc.nasa.gov/floodmap/). Parmi les premiers services de RSO, le service *FAIRE (Fast Access to Imagery for Rapid Exploitation)* hébergé sur l'*ESA's Grid Processing on Demand system* (G-POD, http://gpod.eo.esa.int/) fournit un pré-traitement automatique des images RSO ainsi qu'un traitement de détection des changements qui peuvent être déclenché à la demande par un utilisateur via une interface web.

Des algorithmes automatiques pour la cartographie des eaux de surface à résolution moyenne existent également. Par exemple, *Fully Automatic Aqua Processing Service (FAAPS*) et *WaMaPro* ont implémenté le seuillage et le filtrage morphologique avec l'intervention de l'utilisateur. *RaMaFlood* a été développé pour la cartographie semi-automatique des étendues de crue en utilisant un algorithme interactif basé sur une méthode de classification orientée-objet. Le *TerraSAR-X Flood Service (TFS)* et le *TanDEM-X Water Indication Mask processor (TDX WAM)* sont des outils de détection de l'eau basés sur le traitement entièrement automatique des images TerraSAR-X et TanDEM-X. Le Centre Canadien Télédétection a mis au point l'outil de détection de l'eau *FnFCE (Forest non-Forest Class Extraction)* pour l'extraction automatisée des masses d'eau, mais cet outil ingère uniquement les images Radarsat.

Néanmoins, les bases de données existantes sur les eaux de surface sont pertinentes pour certaines applications mais ne répondent pas à tous les besoins actuels des communautés

scientifiques et de la gestion de l'eau. Par conséquent, le développement d'autres méthodes capables de traiter à la fois des données multi-sources (multi-cpateurs) et des séries temporelles afin de fournir une cartographie des eaux de surface permetant d'analyser leurs dynamiques reste un besoin d'actualité.

3. Site d'étude, données et prétraitement de Sentinel 1 & 2

3.1 Site d'étude et données

Sur la base de notre objectif de recherche principal, nous avons choisis trois zones de test en Irlande, en Angleterre et en Italie, afin de proposer une méthodologie opérationnelle et entièrement automatique pour extraire les eaux de surface et notamment le phénomène naturel des inondations. La sélection de ces zones d'étude repose également sur la disponibilité des données de référence. Concernant la première zone de test en Irlande, notre choix permettra également de cartographier les eaux de surface permanentes. Afin de valider notre méthodologie à différentes études de cas thématiques, nous avons également intégré plusieurs sites situés en France (Région Grand Est) et en Indonésie.

Le premier site est localisé en Irlande, et plus particulièrement dans les zones centrales de l'île. Lors de la tempête Desmond le 4 décembre 2015, il a été signalé à Keenagh Beg (comté de Mayo), de fortes précipitations avec une hauteur totale de 160,8 mm sur 24 h. La tempête a provoqué de graves inondations au cours de l'hiver 2015-2016, modifiant l'étendue géographique des fleuves pendant plusieurs jours. Des régions telles qu'Ennis, Gort, Roscommon, Ballinasloe et Portumna ont été gravement touchées. Nous avons utilisés quatre images des satellites européens d'Observation de la Terre « Sentinel-1 » IW GRD avec différentes dates :22/11/2015, 16/12/2015, 09/01/2016 et 14/02/2016. Ces images couvrent la zone d'étude avant, pendant et après le phénomène de crue.

Ce premier site est également intéressant pour tester notre méthodologie car (1) la densité des eaux de surface permanentes (par exemple, les lacs et les rivières) est élevée et (2) la variation de l'étendue spatiale du cours d'eau au cours de la saison est modérée en raison du climat tempéré océanique. Pour ces raisons, ce cas d'étude a été sélectionné pour répondre à nos deuxièmes grandes questions de recherche relatives aux potentialités des séries temporelles pour améliorer l'extraction permanente des informations concernant les eaux de surface, afin de surveiller les inondations. Les images temporelles de Sentinel-1 IW GRD (16 images) ont été utilisées pour cet objectif.

Pour l'analyse à partir des images multi-sources, trois images satellitaire de type « Sentinel 2 » sont disponibles avec une couverture nuageuse relativement faible (inférieure à 15%). Pour l'analyse de la polarimétrie RSO, le mode Sentinel-1 SLC a été utilisé pour les épisodes d'inondations (16/12/15 et 09/01/2015).

Le deuxième site a été sélectionné dans la région du Yorkshire en Angleterre suite aux fortes inondations survenues le 22 décembre 2015. En effet, environ trois semaines après la tempête Desmond de notre premier site, la tempête Eva s'est abattue sur cette zone avec de fortes précipitations (hauteur de 215 mm de précipitations sur 24 h). Suite à cet évènement, de vastes inondations ont été observées sur une grande partie du West Yorkshire, y compris dans la ville de Leeds. Pour étudier cet épisode, nous avons utilisé les images de « Sentinel-1 » IW GRD en date du 29/12/2015.

Un troisième site a été sélectionné en Italie suite à l'enregistrement de précipitations atteignant 200 mm en 12 heures le 21 novembre 2016, dans certaines régions du nord-ouest de l'Italie. Ces zones auraient été confrontées aux pires inondations de ces 20 dernières années. Nous avons utilisé pour l'étude de ce phénomène les images du 28/11/2016 issues Sentinel-1 IW GRD en date du 28/11/2016 (en période d'inondation).

Pour le choix de notre quatrième site d'étude, le passage de la tempête Eleanor avait déjà provoqué des précipitations importantes les 2 et 3 janvier 2018, affectant l'Irlande, le Royaume-Uni, la France, le Benelux, l'Allemagne, l'Autriche et la Suisse. Après la tempête, de fortes précipitations ont provoqué plusieurs inondations de grandes ampleurs en France, notamment dans la région du Grand-Est. L'un des principaux cours d'eau du Grand-Est, la Zorn, a été impacté par ces fortes précipitations, qui a provoqué un épisode de crue dans les zones environnantes. Cet épisode de crue dans le bassin versant de la Zorn a été enregistré le 23 janvier 2018, près des municipalités de Brumath, Hoerdt et Hochfelden. Pour cet épisode, nous avons eu recours à onze images de Sentinel-1 IW GRD enregistrées entre 2017 et 2018, à des intervalles de temps relativement cours compris entre un jour et vingt-deux jours pour l'intervalle le plus long.

Le dernier site d'étude se situe dans le bassin versant du fleuve de Bengawan Solo en Indonésie. Cette zone est située sur la partie occidentale de l'Ile de Java et couvre les districts de Bojonegoro, Tuban et Lamongan. Le fleuve Bengawan Solo est considéré comme le plus long et le plus grand fleuve de l'île de Java, en Indonésie. Cette rivière est considérée comme l'une des plus grandes ressources des eaux de cette partie de l'Indonésie. Toutefois, en observant son bilan hydrologique, on a observé de fortes variations en sur-abondance (épisodes de crues quasi annules) et déficit. Pour cette zone, nous avons utilisé douze images de type « Sentinel-1 IW GRD ». Ces images couvrent l'année 2017 avec une fréquence d'une image par mois.

Afin de formaliser et d'éprouver notre méthodologie, nous avons également eu recours à d'autres types de données, notamment pour explorer ou échantillonner les eaux de surface. Ces données proviennent de structure de référence nationale telle que *l'Institut Géographique National* pour la France ou l'*Environmental Protection Agency (EPA)* pour l'Irlande. Deux types de données ont été utilisés: (1) la base de données topographique nationale et (2) le modèle numérique de terrain (MNT), les données pluviométriques et les données in situ.

3.2 Prétraitement de Sentinel 1 & 2

L'objectif de cette partie est d'abord d'explorer le potentiel de l'image de type « Sentinel-1 » liée à la détection des eaux de surface. Dans ce contexte, nous avons effectué des évaluations pour explorer et définir:

a) <u>L'unité minimum de surface</u>
   Deux classes d'échantillons d'eaux de surface d'une superficie inférieure à 1 ha ont une valeur d'aire de répartition presque identique à celle de la classe d'échantillon terrestre. La classe des eaux de surface dont la superficie est supérieure ou égale à 1 ha est répartie séparément de la classe d'échantillons de terrain. Il sera donc difficile de détecter les eaux de surface inférieure à 1 ha avec la résolution spatiale des images de type « Sentinel-1 ».
b) <u>Le mode de polarisation optimal</u>
   Nous pouvons noter que le pourcentage de taux de faux négatifs pour la polarisation VH est très élevé par rapport à la polarisation VH. L'histogramme irrégulier de la polarisation VH a également tendance à rendre difficile la construction de modèles, ce

qui entraîne par la suite des erreurs dans les résultats d'extraction des eaux de surface. En conséquence, nous avons retenu la polarisation VV pour cette étude.

c) La caractéristique optimale

Le sigma-naught est choisi comme la caractéristique optimale parce que c'est la puissance renvoyée à l'antenne par le plan horizontal (sol). Cette condition est très appropriée avec le type de données Sentinel-1 utilisé dans cette étude (produits *GRD*). De plus, le sigma-naught est un produit calibré qui est meilleur que les produits non calibrés (en termes d'amplitude et d'intensité). De nombreuses études ont utilisé sigma-naught pour la cartographie des eaux de surface à partir de données RSO et ont décrit les fonctionnalités de cette fonction.

d) Influence du filtrage

Plus le valuer d'*ENL* (nombre de vues équivalent) est élevée pour un filtre et plus cela signifie que l'efficacité du lissage du bruit sur les zones homogènes est élevée. Plus l'indice de granularité est petit, moins il y a de bruit de granularité dans les images. Selon nos tests, la méthode fondée sur un filtre médian avec une fenêtre de 5x5 pixels a la valeur ENL la plus élevée et la valeur d'indice de granularité plus petite. Par conséquent, ce filtre sera utilisée comme méthode de filtrage dans cette étude.

Pour le pré-traitement des données d'amplitude Sentinel-1, la première étape consiste à appliquer des orbites Sentinel précises et à améliorer considérablement la précision de la géolocalisation. Dans la deuxième étape, nous transformons les images d'amplitude brutes en produits calibrées (sigma-naught) pour une utilisation quantitative des images RSO. Dans les troisième et quatrième étapes, afin de réduire le bruit, un filtre médian avec une taille de fenêtre de 5 × 5 pixels ont été utilisés. Ensuite, dans la cinquième étape, Une correction géomatrique est appliquée pour géocoder les images afin de résoudre la distorsion de la distance dans les images RSO.

Concernant les données de type « Sentinel-2 », nous appliquons un traitement afin de corriger les effets produits par les propriétés de l'atmosphère (sous forme de gaz et d'aérosols). Le résultat obtenu peut être utilisé pour extraire des informations spectrales précises des entités situées à la surface de la Terre. La deuxième étape est le masquage des nuages et des ombres. Ensuite, la troisième étape consiste à calculer un indice d'eau de surface (*NDWI2*).

4. Détection des eaux de surface à l'aide des données d'amplitude Sentinel-1

Ce chapitre présente une méthode « *Water-S1 »* développée pour le traitement automatique d'images Sentinel-1. Il est basé sur un article publié dans la revue Remote Sensing MDPI 2018, volume 10, numéro 2 : *A Method for Automatic and Rapid Mapping of Water Surfaces from Sentinel-1 Imagery*.

Plusieurs algorithmes de détection de l'eau basés sur l'image RSO ont été proposés dans la littérature. Parmi les méthodes, le seuillage est la méthode la plus couramment adoptée pour l'analyse d'image RSO afin de différencier les zones en eau des zones terrestres. Cependant, il est difficile de déterminer la valeur seuil optimale pour une scène / paysage, ce qui implique la nécessité d'une intervention de l'utilisateur.

Alors que plusieurs outils semi-automatiques et automatiques existent déjà, il n'existe, à notre connaissance, que très peu de références scientifiques présentant une méthode de détection qui soit entièrement automatique pour la cartographie des eaux de surface à partir d'images de Sentinel-1. Ces méthodes utilisent un seuillage sur des pixels « individuels » en ignorant la corrélation entre les pixels voisins. Étant donné que les pixels individuels ne sont pas des variables aléatoires indépendantes mais forment un champ aléatoire, le potentiel d'amélioration de la précision des cartes d'étendue d'inondation existe.

Les objectifs de cette partie sont donc (1) d'étudier l'utilisation du filtrage bilatéral en tant que méthode de *smooth labeling* pour définir automatiquement les seuils; (2) d'intégrer les informations hydrologiques / topographiques dans la détection à l'aide de l'indice topographique « *Height above nearest drainage (HAND)* »; et (3) d'évaluer quantitativement la précision de notre algorithme de détection de l'eau pour les données Sentinel-1.

La chaîne de traitement automatique est détaillée en présentant (i) le pré-traitement des données Sentinel-1, (ii) l'utilisation d'une méthode de tuilage (adaptée d'une méthode de fractionnement de l'espace) afin de se concentrer automatiquement sur les surfaces d'eau, (iii) la modélisation des classes avec un modèle de type Finite Mixture Models (FMMs) pour produire une carte de probabilité fondée sur les modèles de classes établis, (iv) le filtrage bilatéral de la classe et (v) le post-traitement final. La méthode est testée et validée sur trois zones d'étude affectées par des inondations (surfaces en eau temporaires) survenues dans la partie centrale de l'Irlande, dans le nord de l'Angleterre et dans le nord-ouest de l'Italie durant la période 2016-2017 (section 3.1).

Etant donné que le FMM est sensible aux valeurs initiales définies pour les écarts-types et aux probabilités de classes antérieures, nous examinons l'impact des variations des paramètres initiaux sur le modèle de classe final. L'influence des valeurs des paramètres FMM est évaluée pour l'image Sentinel-1 (9 janvier 2016). Cette analyse est réalisée pour trois tuiles dans la zone d'étude de l'Irlande, qui sont considérées comme étant représentatives de différentes proportions de surface d'eau et d'autres d'occupation du sol. Les résultats montrent que la tuile contenant de grandes quantités d'eau de surface convergent vers le même modèle de sortie stable, quelles que soient les valeurs initiales sélectionnées. À l'inverse, la tuile comprenant de très petites quantités d'eaux de surface tend à générer des solutions marginales avec des écarts-types supérieurs à 3 ou des probabilités antérieures pour la classe d'eau de surface supérieure à 0,5. Pour la tuile avec une proportion équilibrée de surfaces d'eau, le FMM converge vers une solution stable en dessous des écarts-types de 7 et des probabilités de classe d'eau de 0,7. Compte tenu des résultats de cette analyse, l'utilisation d'un écart type de 3 et d'une probabilité antérieure de 0,1 a été jugée suffisamment faible pour garantir la convergence du FMMs vers des solutions stables avec une bonne approximation des distributions bi-modales.

La taille de la fenêtre de filtrage et son influence sur les résultats sont également analysées. La sensibilité de la précision de la classification aux modifications de ces paramètres est évaluée de manière empirique pour la scène d'image Sentinel-1 enregistrée le 9 janvier 2016 dans la zone d'étude de Gort en Irlande. L'analyse montre qu'une taille de fenêtre de 5 × 5 pixels donne un résultat optimal. Par conséquent, pour toutes les expériences, la fenêtre de filtrage bilatéral a été fixée à 5 × 5 pixels. Il montre également que le filtrage bilatéral offre une précision globale supérieure par rapport aux cartes non filtrées. Ceci justifie clairement l'utilisation du filtre bilatéral comme méthode de lissage (*smooth labelling)* dans cette étude.

Par ailleurs, nous avons comparé deux scénarios de la chaîne de traitement basés sur l'utilisation de l'indice *HAND*. Dans le premier scénario, l'indice HAND est appliqué à l'étape

de prétraitement. Quant au deuxième scénario, l'indice HAND est utilisé comme dernière étape de post-traitement. D'après les résultats de l'évaluation des scénarios 1 et 2, il n'y a pas de différence significative entre les deux scénarios. Cependant, le scénario 1 donne des résultats d'évaluation légèrement meilleurs comparé au scénario 2.

Nous avons également efectué une analyse de sensibilité de la taille du tuilage. L'analyse a mis en évidence l'importance des zones d'eaux de surface pour déterminer la taille des tuiles. Cependant, par défaut une taille de tuile de 10 km donne des précisions globales élevées.

Pour tous les cas d'étude, les résultats ont montré une bonne estimation des eaux de surface avec une moyenne de *F-measure* d'environ 0,8. Cependant, des erreurs d'omissions sur les lits de rivière permanents sont observées quel que soit le site d'étude. Malgré tout, notre nouveau traitement automatique utilisant les données Sentinel-1 semble être efficace pour la cartographie des inondations et des surfaces d'eau. L'approche automatique testée pour les inondations en Irlande, en Angleterre et en Italie, suggère la production d'une cartographie opérationnelle (rapide) des inondations sur d'autres sites en dehors des zones d'étude présentées.

5. Détection des eaux de surface à l'aide de séries temporelles de données Sentinel-1 et Sentinel-2

Dans ce chapitre, une méthodologie pour la détection des eaux de surface combinant les séries temporelles de données Sentinel-1 et Sentinel-2 est proposée. Celle-ci utilise l'approche de fusion d'images au « niveau décisionnel » fondée sur la théorie bayésienne. La méthode est expérimentée pour les eaux de surfaces en Irlande. Elle fait l'objet d'une publication soumise et acceptée avec révision mineure dans la revue *International Journal of Remote Sensing*.

La détection des eaux de surface et le calcul de la probabilité d'occurrence sont effectués sur les images Sentinel-1 avec la méthode *Water-S1 (Chapitre 4)*. Une adaptation de la méthode *Water-S1* est utilisée pour le traitement des données optiques Sentinel-2. Les cartes d'occurrences obtenues pour les deux séries temporelles (Sentinel-1, Sentinel-2) sont combinées à l'aide de l'approche de fusion d'images au « niveau décisionnel ». Enfin, les résultats fusionnés sont évalués sur la cartographie des surfaces d'eau permanentes et pour les zones inondées temporairement pour les périodes correspondantes.

Dans la série temporelle Sentinel-1, durant la période d'inondation de l'hiver 2015/2016, des eaux de surface sont détectées dans la zone nord de *Lough Derg* jusqu'au 14 février 2016. L'extraction des eaux de surface en avril, juin et octobre 2016 présente certaines erreurs dues à la rugosité des surfaces d'eau provoquées par le vent et la turbulence. Dans l'image Sentinel-2 de décembre 2015, les eaux de surface sont clairement représentées dans la zone nord de Lough Derg. En raison de la présence d'une mince couche de cirrus, les zones d'eau de surface sont surestimées pour l'image Sentinel-2 de novembre 2016. Afin de résoudre ces problèmes, une technique fusion est appliquée.

Plusieurs méthodes de fusion au « niveau décisionnel » sont comparées (logique floue MIN, *Bayesian product, Bayesian sum*). Les probabilités d'occurrences d'eaux de surface sont calculées, d'une part, afin d'évaluer l'intérêt des séries temporelles pour améliorer la cartographie et, d'autre part, d'évaluer la complémentarité des résultats des capteurs RSO et optiques. Tous les calculs sont effectués au niveau des pixels en combinant les probabilités

d'occurrence de chaque test (test 1 = série temporelle des données Sentinelle-1, test 2 = série temporelle des données Sentinelle-2, test 3 = série temporelle des données Sentinelle 1 et Sentinelle -2).

La méthode fondée sur la logique floue MIN identifie uniquement les fractions de Lough; Le *Bayesian product* n'identifie pas le *Lough Derg* ni la rivière Shannon; Le *Bayesian sum* donne les meilleurs résultats avec l'identification de la rivière Shannon et de presque toute la superficie de Lough Derg. Cette méthode montre également la précision globale et la *F-measure* les plus élevées par rapport aux deux autres méthodes. En conséquence, l'opérateur de *Bayesian sum* est utilisé et appliqué aux autres tests (test 2 et test 3). En tenant compte de tous les paramètres utilisés pour l'évaluation de la précision, le meilleur résultat est obtenu avec la fusion des séries temporelles Sentinel-1 et Sentinel-2 (test 3).

L'eau de surface temporaire est extraite pour l'image Sentinel-1 du 09/01/2016 en appliquant la carte des eaux de surface permanentes résultant du test 3 comme un masque. Le résultat montre une précision globale élevée (> 98%), une *F-measure* (0,90) et un taux de vrai positif (86%); l'erreur d'omission est faible (13,9%). Par ailleurs la dynamique des eaux de surface peut être surveillée avec la méthode de fusion au « niveau décision » par le calcul de cartes de fréquence. La méthode est appliquée aux masses des eaux de surface temporaires identifiées dans la série temporelles Sentinel-1. La carte de fréquence représente le nombre de fois qu'un pixel est classé dans les masses d'eau de surface temporaire pour la série temporelles. Les pixels classés une seule fois peuvent être considérés comme du bruit ou une classification erronée. Les pixels de fréquence supérieure à 9 correspondent à des zones proches des masses des eaux de surface permanentes. Nous pouvons relier la carte de fréquence des eaux de surface temporaires aux quantités de précipitations annuelles. La dynamique spatio-temporelle de l'eau de surface temporaire peut être analysée plus en détail.

En conclusion, les résultats indiquent une réduction du bruit et une augmentation de la précision de la détection des eaux de surfaces permanentes. De plus, l'analyse des séries temporelles d'images permet un meilleur suivi des eaux de surface temporaires (inondations).

6. Les autres méthodes et validation sur différents contextes thématiques

Les autres méthodes de détection sont ensuite testées, telles que: (i) l'utilisation de la polarimétrie RSO pour la classification des eaux de surface et (ii) la fusion d'images au « niveau des attributs » pour la comparaison et l'évaluation de la meilleure approche de fusion. La validation des méthodes proposées sur différents contextes thématiques est ensuite présentée à travers deux expériences différentes de traitement massif de séries temporelles d'images Sentinel.

6.1 Intérêt de la polarimétrie RSO pour la cartographie des eaux de surface

Dans la littérature, les informations d'amplitude d'imagerie RSO en double polarimétrie ont déjà été utilisées dans un système de classification classique supervisé pour la cartographie de la couverture terrestre. Dans cette étude, nous avons décidé d'explorer l'intérêt de ces données pour améliorer l'extraction de cette classe « eau » et éventuellement découvrir d'autres classes thématiques (test 1). La méthode propose un système de classification non-supervisé basé sur

différents cas de combinaison RVB de double polarisation. Les résultats montrent certaines classes d'eau de surface (couleurs différentes), mais nous ne pouvons pas interpréter ces classes comme des classes thématiques d'eau de surface pertinentes.

Le deuxième test (test 2) est réalisée à l'aide de l'image Sentinel-1 IW du 9 janvier 2016, au moment des inondations en Irlande. l'étude utilise une image Sentinel-1 IW SLC car elle nécessite à la fois des informations d'amplitude et de phase. Ce deuxième test consiste en deux expériences:

(1) la première expérience explore les attributs extraits lors du processus de décomposition;
(2) la deuxième expérience effectue la classification en utilisant ces caractéristiques.

L'objectif est d'analyser les attributs de la décomposition double H/Alpha et le résultat de la classification double H-Alpha lors de la détection des classes thématiques d'eaux de surface.

Les résultats de la double décomposition H/Alpha montrent la séparation des eaux de surface de l'autre type d'occupation du sol, en particulier entre les images d'entropie et alpha. Chaque caractéristique résultant de la décomposition double H/Alpha ne représente pas différentes classes d'eaux de surface.

Dans un troisième test, nous avons effectué une classification des données polarimétriques doubles en utilisant une combinaison de classificateur H-Alpha et de classificateur de Whishart non-supervisé. Le résultat indique que la classification double H-Alpha (à partir de données Sentinel-1 SLC) permet une cartographie des différents mode d'occupation des sols . Cependant, cela ne permet pas de distinguer différentes classes d'eaux de surface.

En conclusion, ces tests n'ont pas permis de montrer l'intérêt de nos recherches utilisant la double polarisation des méthodes de polarimétrie RSO pour cartographier différentes classes thématiques des eaux de surface.

6.2 Intérêt de la fusion d'images multi-sources au « niveau des attributs »

Nous avons étudié la fusion d'images au « niveau des attributs », où les caractéristiques sont calculées séparément pour chaque source et introduites dans la même méthode de classification via un ensemble unique d'attributs. L'algorithme classique d'apprentissage automatique supervisé *Random Forest* a ensuite été choisi pour classer les eaux de surface. La fusion d'images au « niveau des attributs » est réalisé à l'aide de la méthode d'analyse en composantes principales (ACP).

Des attributs classiques dérivés des images de série temporelle Sentinel-1 GRD (S1), des images multitemporelles Sentinel-2 (S2) et de Sentinel-1 SLC (attributs de polarimétrie S1-pol) ont été calculés à partir de chaque source de données. Sur la base de ces attributs, plusieurs tests de fusion au niveau des attributs sont ensuite effectués en combinant les sources : :

- Test 1: calcul d'attributs dérivés de S2 et de S1
- Test 2: calcul d'attributs dérivés de S2 et de S1-pol
- Test 3: calcul d'attributs dérivés de S1 et S1-pol
- Test 4: calcul d'attributs dérivés de S2, S1 et S1-pol

Les résultats montrent que le test 3 donne le meilleur résultat avec une précision globale et une *F-measure* les plus élevées. L'analyse permet de conclure que la fusion d'images multi-sources au « niveau des attributs » ne peut pas donner de meilleurs résultats pour la cartographie de l'eau de surface permanente que la fusion d'images au « niveau décision ». Cependant, cette

méthode peut donner une précision globale élevée avec plus de 97% et des valeurs de *F-measure* élevées, environ 0,7.

6.3 Validation sur différents contextes thématiques

Cette partie présente deux applications thématiques des méthodes proposées sur des sites où les dynamiques des eaux de surface sont contrastées. La première application est effectuée sur la région Grand-Est (France), qui a subi un fort épisode d'inondations en janvier 2018. L'extension spatiale des inondations a été détectée avec une *F-measure* à 0,9 et des erreurs inférieures à 14 %.

La deuxième application est réalisée en aval de la rivière Solo (Java Oriental, Indonésie) où l'existence d'eau dans les cultures irriguées est déterminée. Le débit de la rivière est estimé à l'échelle annuelle avec un coefficient de corrélation de 0,78 indiquant une forte relation entre le débit estimé et le débit mesuré in-situ. À l'échelle de la saison, par exemple pour la saison sèche, les estimations de débit sont moins précises, principalement en raison de l'incertitude dans le calcul de la largeur. L'eau dans les cultures irriguées était faible de juillet à octobre, ce qui correspond à la troisième saison de plantation. Ce résultat suggère que la technique d'irrigation doit être améliorée pour obtenir une plus grande d'extension des surfaces d'eau pendant cette période de l'année, afin d'augmenter la production de rendement en grain.

7. Conclusion et perspectives

Grâce à nos résultats, les potentiel de Sentinel-1 à la cartographie des eaux de surface a été prouvé. Des méthodes adaptées et robustes pour une exploitation opérationnelle des données Sentinel-1 ont été proposées. Les résultats sont encourageants et constituent la première étape pour proposer un traitement opérationnel de la chaîne d'images afin d'aider les utilisateurs finaux à cartographier rapidement les inondations ou les eaux de surface permenantes.

L'utilisation de séries temporelles d'images satellitaires peut augmenter le niveau de détection des eaux de surface et réduire qualitativement et quantitativement le bruit. Les séries temporelles permettent également de mieux comprendre la dynamique spatio-temporellesdes eaux de surface temporaires. Les séries temporelles peuvent également fournir des informations nouvelles ou complémentaires sur le comportement des eaux de surface ou leur évolution sur une courte période.

Comparée à l'utilisation des données séries temporelles mono-capteur, la combinaison des données séries temporelles Sentinel-1 et Sentinel-2 (multi-capteurs) peut fournir une meilleure précision dans la cartographie des eaux de surface permanentes. Pour la surveillance des eaux de surface temporaires, l'utilisation de la fusion d'images au « niveau décisionnel » permet de quantifier la probabilité d'occurrence de terrains inondés à l'échelle du pixel, ce qui permet de comprendre la dynamique de l'inondation. Les cartes produites des eaux de surface temporaires peuvent être utiles pour fournir de nouvelles informations aux décideurs, par exemple pour surveiller la variabilité de l'eau dans les terres de cultures irriguées.

Les méthodes proposées sont appliquées avec succès à un traitement massif dans différentes études de cas. Elles peuvent extraire des eaux de surface permanentes dans la région du Grand-Est, France, et permettent d'effectuer une cartographie rapide des eaux de surface temporaires pour les inondations de la rivière Zorn. En transposant les méthodes au fleuve

Bengawan Solo en Indonésie, elles permettent de cartographier les eaux de surface permanentes avec des résultats pertinents et encourageants.

En résumé, cette thèse a permis de répondre à nos questionnements de départ et elle ouvre de nombreuses perspectives. Premièrement, les données Sentinel-1 conviennent à la cartographie des eaux de surface et leurs méthodes opérationnelles ont été développées. Cependant, il est possible d'appliquer la méthode à d'autres données RSO, par exemple les données ALOS-PALSAR 2 de Kalideos Alsace. Nous avons déjà appliqué la méthode dans ALOS-PALSAR 2, mais nous devons encore observer le résultat de l'applicabilité.

Deuxièmement, la méthodologie proposée utilisant une fusion des séries temporelles des images Sentinel-1 et Sentinel-2 est générique. Il ne nécessite pas d'interaction de l'utilisateur; suggérant qu'il est applicable pour la surveillance des masses d'eau de surface permanentes sur de vastes zones et à une fréquence temporelle élevée. Elle a la possibilité de devenir une solution de service permanente s'elle est intégrée à des Centres de Calcul Hautes erformances. Dans le cas des eaux de surface temporaires, il est possible d'explorer plus la carte des fréquences pour une compréhension globale de la dynamique spatio-temporelle. Cependant, il est important d'étendre la période d'observation par exemple à 5 ans pour pouvoir apprendre le comportement des eaux de surface. Pour obtenir un produit global, nous devons également appliquer ou tester la méthode dans les régions arides, car il est difficile de cartographier les surfaces en eau dans ces régions.

Troisièmement, la fusion d'images au « niveau décision » avec l'opérateur de *Bayesian sum* peut fournir une cartographie simple et rapide. Cependant, il sera intéressant d'analyser d'autres méthodes pour la fusion d'images. Il existe également des algorithmes d'apprentissage profonds (Deep Learning) qui s'adaptent facilement à différentes sources et aux données manquantes. Cependant, un élément clé de ce type d'algorithme est la nécessité d'un grand nombre d'échantillons d'apprentissage pour construire leur réseau. Les approches fondée sur un apprentissage actif constitue une avancée décisive dans la résolution de ce problème. Ce type d'approche peut tirer des enseignements d'un petit nombre d'exemples pour construire son modèle, ce qui présente donc un grand potentiel dans le domaine du traitement d'images. Les recherches futures peuvent inclure ces méthodes (apprentissage profonf et apprentissage actif) pour la fusion d'images et les comparer aux résultats de cette étude.

Bien que l'utilisation de données de télédétection comme outils opérationnels pour l'observation des eaux de surface (permanentes et temporaires) reste à finaliser, les résultats proposés dans cette thèse sont très prometteurs.

Filsa BIORESITA

EXPLOITATION DE SERIES TEMPORELLES D'IMAGES MULTI-SOURCES POUR LA CARTOGRAPHIE DES SURFACES EN EAU

Résumé

Les eaux de surface sont des ressources importantes pour la biosphère et l'anthroposphère. Elles favorisent la préservation des habitats, le développement de la biodiversité et le maintien des services écosystémiques en contrôlant le cycle des nutriments et le carbone à l'échelle mondiale. Elles sont essentielles à la vie quotidienne de l'homme, notamment pour l'irrigation, la consommation d'eau potable, la production hydro-électrique, etc. Par ailleurs, lors des inondations, elles peuvent présenter des dangers pour l'homme, les habitations et les infrastructures. La surveillance des changements dynamiques des eaux de surface a donc un rôle primordial pour guider les choix des gestionnaires dans le processus d'aide à la décision.

L'imagerie satellitaire constitue une source de données adaptée permettant de fournir des informations sur les eaux de surface. De nos jours, la télédétection satellitaire a connu une révolution avec le lancement des satellites Sentinel-1 (Radar) et Sentinel-2 (Optique) qui disposent d'une haute fréquence de revisite et d'une résolution spatiale moyenne à élevée. Ces données peuvent fournir des séries temporelles essentielles pour apporter davantage d'informations afin d'améliorer la capacité d'observation des eaux de surface. L'exploitation de telles données massives et multi-sources pose des défis en termes d'extraction de connaissances et de processus de traitement d'images car les chaines de traitement doivent être le plus automatiques possibles.

Dans ce contexte, l'objectif de ce travail de thèse est de proposer de nouvelles approches permettant de cartographier l'extension spatiales des eaux de surface et des inondations, en explorant l'utilisation unique et combinée des données Sentinel-1 et Sentinel-2.

Nous présentons une méthode Water-S1 qui est développée pour le traitement automatique d'image Sentinel-1. La méthode est testée et validée pour trois zones d'étude affectées par des inondations survenues dans la partie centrale de l'Irlande, dans le nord de l'Angleterre et dans le nord-ouest de l'Italie. Pour tous les cas d'étude, les résultats montrent une bonne estimation des eaux de surface avec une moyenne de F-measure d'environ 0,8. Cependant, des erreurs d'omissions sur les lits de rivière permanents sont observées quel que soit le site d'étude. Ainsi, de nouvelles améliorations de la chaîne de traitement pourraient inclure l'analyse de séries temporelles d'images Sentinel-1 afin d'améliorer la détection des eaux de surface permanentes localisées dans les lits de rivières.

Nous proposons une méthodologie pour la détection des eaux de surface en combinant les séries temporelles de données Sentinel-1 et Sentinel-2 basées sur l'approche de fusion d'images au « niveau décision » fondée sur la théorie bayésienne. La méthode est expérimentée pour les eaux de surfaces en Irlande. Les résultats indiquent une réduction du bruit et une augmentation de la précision de la détection des eaux de surfaces permanentes. De plus, l'analyse des séries temporelles d'images permet un meilleur suivi des eaux de surface temporaires.

Les autres méthodes de détection sont ensuite testées, telles que: (i) l'utilisation de la polarimétrie RSO pour la classification des eaux de surface et (ii) la fusion d'images au « niveau des attributs » pour la comparaison et l'évaluation de la meilleure approche de fusion. La validation des méthodes proposées sur différents contextes thématiques est ensuite présentée à travers deux expériences différentes de traitement massif.

Bien que l'utilisation de données de télédétection comme outils opérationnels pour l'observation des surfaces en eau (permanentes et temporaires) reste à finaliser, les résultats proposés dans cette thèse sont très prometteurs.

Mots-clés : surfaces en eau, Sentinel-1, Sentinel-2, traitement automatique, series temporelles, multi-source, fusion

Résumé en anglais

Surface waters are important resources for the biosphere and the anthroposphere. Surface waters preserve diverse habitat, support biodiversity and provide ecosystem service by controlling nutrient cycles and global carbon. Surface waters are essential for human's everyday life, such as for irrigation, drinking-water and/or the production of energy (power plants, hydro-electricity). Further, surface waters through flooding can pose hazards to human, settlements and infrastructures. Monitoring the dynamic changes of surface waters is crucial for decision making process and policy.

Remote sensing data can provide information on surface waters. Nowadays, satellite remote sensing has gone through a revolution with the launch of the Sentinel-1 SAR data and Sentinel-2 optical data with high revisit time at medium to high spatial resolution. Those data can provide time series and multi-source data which are essential in providing more information to upgrade ability in observing surface water. Analyzing such massive datasets is challenging in terms of knowledge extraction and processing as nearly fully automated processing chains are needed to enable systematic detection of water surfaces.

In this context, the objectives of the work are to propose new (e.g. fully automated) approaches for surface water detection and flood extents detection by exploring the single and combined used of Sentinel-1 and Sentinel-2 data.

We presents the Water-S1 method developed for Sentinel-1 image processing. The method is tested and validated on several flood events that occurred in Central Ireland, Northern England and Northwest Italy. For all test cases, the results show that surface water are estimated with an average F-measure about 0.8. However, omission of permanent river beds are observed for the three experiments. Thus, further improvements of the processing chain could include the analysis of SAR time-series to amplify the signal of permanent riverbeds through spatio-temporal averaging.

We propose a methodology for surface waters detection by combining Sentinel-1 and Sentinel-2 data time series based on image fusion approach in decision-level with a Bayesian sum for the operator. The method is experimented for surface water over Ireland. The proposed methodology allows reducing the noise and increasing the accuracy of the detection of the permanent surface water. Moreover, the analysis of image time series allows a better monitoring of temporary surface water.

Another methods are tested, such as: (i) the use of SAR polarimetry for surface water classification and (ii) feature-level image fusion for comparison and assessment of the best fusion approach. Validation of proposed methods on different thematic context is presented through two different experiments of massive processing.

Although the use of remote sensing data as operational source of information for surface water and flood observations still requires development, the methods and tests proposed in this PhD thesis are promising.

Keywords : surface waters, Sentinel-1, Sentinel-2, automated method, time series, multi-source, fusion